Dissertation zur Erlangung des Doktorgrades

der Fakultät für Chemie und Pharmazie

der Ludwig-Maximilians-Universität München

COLLAPSE DRIED PROTEIN POWDERS FOR NEEDLE-FREE BALLISTIC INJECTION

Enikö Elsa Etzl (geb. Kis)

aus Sathmar, Rumänien

2016

Für meine Familie

In Liebe und Dankbarkeit

ACKNOWLEDGEMENTS

LIST OF ABBREVIATIONS

AIDS	Acquired immunodeficiency syndrome
BLA	Biological licensing application
CDSN device	Convergent-divergent supersonic nozzle device
CLSM	Confocal laser scanning microscopy
CLSM	Confocal laser scanning microscopy
CPMP	Committee for Proprietary Medical Products
CST device	Contoured shock tube device
DSC	Differential scanning calorimetry
EMA	European Medicines Agency
EPI	Epidermal powder immunization
FITC	Fluorescein isothiocyanate
FNU	Formazine Nephelometric Units
FTIR	Fourier transformed infrared spectroscopy
GSK	Glaxo Smith Kline
HBV	Hepatits B virus
HIV	Human immunodeficiency virus
HMWA	High molecular weight aggregate
HPV	Human Papillomavirus vaccine
LWB	Lell's Foucault Accelerator
MTBE	*Tert*-butyl-methyl ether
NDA	New drug application
OVA	Albumin from chicken egg white (ovalbumin)
PAGE	Poly(acrylamide) gel electrophoreses
PBS	Phosphate-buffered saline
Ph. Eur.	European Pharmacopoeia
PMA	Pre-market approval
PMED	Particle mediated epidermal delivery
PSA	Primary secondary amine
rh-G-CSF	Recombinant human granulocyte stimulating factor
rh-IFN-α-2a	Recombinant-interferon- α-2a
rpm	Rounds per minute
SD	Standard deviation
SDS	Sodium dodecyl sulphate
SE-HPLC	Size exclusion high performance liquid chromatography
SEM	Scanning electron microscopy
SSA	Specific surface area
T_c	Collapse temperature
T_g	Glass transition temperature
T_g'	Glass transition temperature of the maximally freeze-concentrated solution
TRITC	Tetramethylrodamine isothiocyanate
WHO	World Health Organization
XRD	X-ray powder diffraction

x

TABLE OF CONTENTS

CHAPTER 1

GENERAL INTRODUCTION

1   NEEDLE-FREE VACCINATION TARGETING THE SKIN

The world health organization (WHO) recently reported that vaccination prevents estimated two to three million deaths every year in all age groups from infectious diseases as diphtheria, tetanus, pertussis and measles [1]. Hence, vaccination is still the most effective and cost efficient method to advert infectious diseases.

Vaccination dates back to the early success of the smallpox vaccine [2, 3]. Since then mass vaccination campaigns reduced significantly the incidence of many diseases, and herd immunity offers the protection of individuals who cannot be vaccinated. Recommendations for vaccination schedules are regularly outlined by public authorities. Future projects comprise the use of therapeutic vaccines in the treatment of non-curable diseases such as AIDS (acquired immunodeficiency syndrome), Alzheimer disease and cancer [4, 5]. A remarkable progress was achieved by the establishment of the Human Papillomavirus vaccine (HPV), Cervarix® (GSK) and Gardasil® (MSD), preventing cervical, vulvar and vaginal cancers [6-8].

There are many factors to consider for optimal vaccination, such as route of delivery, targeting of specialized immune cells and stimulation of humoral and cellular immunity [2]. Moreover, an ideal vaccine should be chemically stable, safe and effective and, in the best case, economical in order to facilitate a widespread use. The delivery of the vaccine should ideally be easy to handle, so that vaccine administration may be carried out after minimal operator training, already [9].

Despite of the progress made in research of new vaccination technologies, the conventional administration of vaccines is still mostly carried out by injecting a liquid vaccine formulation subcutaneously or intramuscularly using needles and syringes. However, this implicates also the risk of needle stick injuries and re-use of needles. Extensive cross-contamination with HIV (human immunodeficiency virus), HBV (Hepatitis B virus) and other blood borne diseases was reported to be a result of re-

use of needles particularly in developing countries. [10-14]. Furthermore, vaccination via needles and syringes is especially for children very stressful [15, 16]. Hence, needle-free delivery systems may therefore result in a better patient compliance [2].

Needle-free approaches for vaccine delivery have gained public interest in the last years as they offer a non-invasive alternative to conventional needle and syringe applications. The target areas for needle-free vaccine delivery are the oral, mucosal or dermal route. Especially the skin is a very attractive target area for vaccination as it comprises a dense network of immunocompetent cells and is easily accessible [17-23].

In addition to its mechanical barrier function, the skin is able to respond to foreign antigens and to regulate the nature and magnitude of the resulting immune responses, due to the presence of specialized antigen presenting cells, so called Langerhans cells [24-26], in the epidermis. Furthermore, the lack of vasculature and the low density of sensory nerve endings in the epidermal layer of the skin provide the opportunity for painless vaccine administration. The combination of a needle-free application together with the use of dry vaccine powders instead of a liquid vaccine formulation offer in addition the potential for enhanced stability and cold chain independent logistics [19, 27, 28]. The effectiveness of low doses of intradermal vaccines was shown to be comparable to full doses of conventional intramuscular vaccines [29-40].

The application of dry vaccine powders through the skin using needle-free powder injectors showed adequate immune responses in preclinical and clinical studies [41-43]. Despite of the demonstrated potential of needle-free powder injection systems using powdered vaccine formulations for immunization, they did not gained market approval for human use.

2   VACCINES

Vaccines are biological products which are applied to humans or animals in order to provide immunity to a certain disease. Live attenuated vaccines induce a strong cellular and antibody response and offer long term protection as they are non-pathogenic but possess all pathogenic features [44]. Examples for live attenuated vaccines are the measles, mumps and rubella vaccine [45].

Inactivated vaccines are regarded as safer as live attenuated vaccines as they cannot revert back to virulence [3-5]. However, they are also not as effective in comparison to live attenuated vaccines but provoke more inflammatory immune responses than subunit vaccines. An example for an inactivated vaccine is the Hepatitis A vaccine [46]

Subunit vaccines comprise one or more components of a pathogen, mostly recombinant peptides, proteins or polysaccharides. They are well defined and offer high purity and safety [47, 48]. One drawback of subunit vaccines is their low immunogenicity, and hence the need for co-administration of adjuvants. Examples for subunit vaccines are toxoid vaccines against diphtheria, tetanus, and pertussis. The subunit vaccine against hepatitis B that is composed of only the surface protein of the virus and the HPV vaccine, a virus like particle (VLP) composed of the viral major capsid protein [49].

3   ADJUVANTS

The administration of vaccines does not always lead to an effective immune response. Therefore, adjuvants are often necessary to enhance the specific immune responses towards the applied antigen [50]. They can also be used to reduce the amount of antigen or to improve the efficacy of vaccines [51, 52].

There are different approaches to classify adjuvants. One of the oldest goes back to Edelman [53]. According to him, adjuvants can be classified into three groups: (i) active immunostimulants, which increase the immune response to an antigen, (ii) carriers, consisting of immunogenic proteins and supporting T-cells and (iii) oily emulsions or liposomes, stimulating the immune response and serving as matrix for antigens. Other systems to classify adjuvants are according to their administration route, their origin, their mode of action [54] or certain physicochemical properties [50, 55-58].

Alum based compounds are the most commonly used adjuvants approved for human use [59, 60].

One of the most potent known adjuvants is Freund's complete adjuvant, consisting of an emulsion of water and mineral oil containing killed mycobacteria [61]. However, due to severe local reactions only Freund's incomplete adjuvant, without added mycobacteria, is approved for human use [62, 63].

Further examples for oil in water emulsions are MF59 (based on squalene) [64, 65] and AS03 (based on squalene and α-tocopherol) [66, 67], which are both approved for human use in influenza vaccines.

Currently adjuvants for mucosal immunization are in the focus of vaccine development, enabling the uptake of antigen through mucosal routes. Alum salts failed to enhance specific immune response when administered by the oral or nasal route [68]. However, Maa *et al.* showed that alum adjuvanted vaccines were well tolerated and immunogenic after the administration via the skin (by epidermal powder immunization) in a guinea pig model [69]. Bacterial derivatives like cholera toxin, the B subunit of cholera toxin, diphtheria toxoid or tetanus toxoid were shown to be highly effective mucosal adjuvants [3, 48, 70-77]. Diphtheria toxoid was also explored via epidermal powder injection in mice and showed promising results [75]. Synthetic or inactivated delivery systems, including synthetic polymeric particles [78, 79], alginates, gelatin, liposomes and ISCOMS, are another group of adjuvants suitable for the mucosal route [47, 50, 80, 81].

However, the efficacy of adjuvants and also the likelihood of side-effects depend on the route of administration [82], and hence, have to be taken into consideration.

4 DRY VACCINE FORMULATIONS

4.1 DRY POWDER VACCINE FORMULATIONS

Efficient vaccination using ballistic needle-free devices implicate the development of dry vaccine formulations. The development of solid-state or dry vaccine formulations is a feasible approach to achieve room temperature stability of the formulations [83, 84].

Powdered vaccine formulations provide enhanced stability of the vaccine. They are less dependent on cold-chains and therefore particularly desirable for vaccination programs in the developing world, offering higher stability and facilitated storage conditions [28, 85].

Vaccine particles intended for intradermal injection have to exhibit certain characteristics in order to be delivered to the target area by ballistic acceleration. The sizes of the particles, as well as their density determine significantly the velocity of particles upon acceleration as well as the particle distribution and penetration depth into the skin. Particles based on sugar formulations need a particle size of about 20 to 70 µm in order to penetrate into the skin, as they have to compensate their low density, which is in general of about 1.5 g/cm³ or lower [75, 86-88]. However, the size of the particles is also a limiting factor for intradermal injection, as particles larger than 100 µm can cause pain and bleeding at the site of injection [89].

A sugar excipient formulation composed of trehalose, mannitol and different polymers (dextran, polyvinylpyrrolidone, hydroxyethylstarch or polyethylene glycol) for the formation of particles by spray freeze-drying or spray drying was extensively studied for its suitability for intradermal injection [90-95]. It was shown that sugar particles were successfully delivered into the skin using a powder injection device, and were retrieved mostly in the extracellular space of the epidermis [87]. A cheap and easy manufacturing process of vaccine loaded sugar particles, a high loading capacity of the sugar matrix with antigen, as well as the possibility to store the formulation at room temperature are major advantages of this approach. Preclinical and clinical studies showed an adequate immune response after injection of vaccine loaded

powders into the skin [41-43]; however, local site reactions like erythema, petechiae, oedema and skin discoloration were prominent at the site of injection [89].

4.2 PARTICULATE SYSTEMS AS CARRIERS FOR VACCINES

Apart from sugar based vaccine formulations, other particulate systems were evaluated as carrier particles for vaccines intended for intradermal injection like silica nanoparticles embedded in sugar microparticles [96], agarose beads [91], aluminium salts [69, 92] and gold particles [87, 97, 98].

The use of gold particles has been extensively studied for the delivery of DNA vaccines using a supersonic particle injection device. As particle penetration into the skin is a function of size, density and velocity, gold particles with a particle size of 1 to 3 µm can be delivered successfully to the skin by ballistic approaches and are mainly deposited intracellularly [98]. Thereby, immunocompetent cells in the epidermal layers of the skin can be efficiently targeted [87, 97, 99]. However, it was also reported that cell death can occur due to the direct impact of the gold particles due to stress and shock waves within the tissue [100, 101]. By using this technology, only a low amount of DNA vaccine is necessary to transfect the cells with a high transfection efficiency [97, 102, 103]. Limitations of this system are given by the amount of DNA that can be precipitated on the particle surface and hence, in some cases, the need of multiple shots at multiple delivery sites in order to deliver the require payload [87, 104, 105]. From an economical view of sight, the use of gold particles may be too costly for mass vaccination campaigns. It was observed in preclinical vaccination studies, that DNA vaccine coated on gold microparticles was able to elicit antibody responses, however, this was only achieved with the highest dose levels [98, 104, 106].

5 DRYING TECHNIQUES FOR THE GENERATION OF VACCINE POWDER FORMULATIONS

Drying techniques such as spray drying, spray freeze drying and air drying (desiccation) have been explored to create particles suitable for epidermal powder immunization using a supersonic device developed by PowderJect Technologies [42, 69, 85, 90-95].

Furthermore, other technologies like supercritical fluid drying were used for the generation of stable vaccine products. For example microparticulate powder formulations containing diphtheria toxoid for pulmonary vaccination and inhalable powders of live attenuated measles virus vaccine were generated using this technology [107, 108].

Freeze drying is a gentle method to create a porous cake by preserving the stability of sensitive vaccine products [84, 109-112]. By applying this method a subsequent particle formation, e.g. milling, is required in order to generate particles in the appropriate size range suitable for ballistic powder injection [41, 85].

The controlled collapse of lyophilizates [113, 114] as well as products obtained by vacuum foam drying [27] offer sugar matrices with a highly reduced surface area in comparison to conventional lyophilizates. A reduced surface area of the sugar matrix implicates a dense and mechanical robust cake, which is a vital prerequisite for ballistic injection of vaccine powders [115]. Hence, these techniques, combined with a second particle formation step, are of interest for the generation of particles suitable for ballistic powder delivery.

5.1 FREEZE-DRYING AND COLLAPSE FREEZE DRYING

Freeze drying is a preferred method to convert vaccines into the solid state. In brief, the fluid formulation is frozen and subsequently dried by the removal of water by sublimation, directly from the solid state to gas under reduced pressure [111, 116, 117]. After removal of all water, the biopharmaceutical compound is embedded in a dry sugar glass, with a glass transition temperature depending on the excipients used. The obtained product is a highly porous cake with a high specific surface area which can easily be reconstituted, offering stability advantages [28, 85]. The choice of stabilizers determines decisively the preservation of vaccine quality during freezing, drying and subsequent storage [110, 116].

7

A controlled collapse of the lyophilizates due to a modified lyophilization cycle performed by Schersch *et al.* was shown to result in a highly dense sugar matrix, comprising a low specific surface area whilst the stability of the incorporated biopharmaceuticals was preserved [113]. In addition, enhanced protein stability during storage could be shown by applying the collapse freeze-drying cycle [118]. Thus, by combining the process with a subsequent milling step, and, if required, a sieving step, collapse freeze-drying offers a promising option to generate powder particles with desirable characteristics for ballistic injection.

Whilst jet-milling of pharmaceutical powders is already commonly used for the preparation of inhaled biopharmaceuticals [119], only little is known about milling of biopharmaceuticals intended for intradermal application [85]. Though, Chen *et al.* proved evidence of immunogenicity in mice of a recombinant envelope protein rgp120 (rgp120), a human immunodeficiency virus (HIV) component, when administered by epidermal powder immunization after manually grinding of the powder formulation with a pestle and mortar [41]. Another pulverization method, cryo-milling, will be explored in detail in this thesis.

5.2 SPRAY FREEZE DRYING

Spray freeze drying is technological process to produce pharmaceutical powders of small and large scale particles or powders. Spray freeze drying is a two-step process combining the atomisation of a liquid formulation into a cloud of small droplets and subsequent lyophilization. In the first step, a liquid formulation containing antigens and excipients is atomized through a high frequency ultrasonic nozzle to generate fine liquid droplets that are flash frozen in liquid nitrogen. In a second step, the frozen droplets are lyophilizated, generating a dry powder formulation [93, 95, 120]. Spray freeze drying offers an extremely rapid vitrification process due to the enormous surface area for heat transfer generated during the atomization in the spraying process and the direct contact of the liquid droplets with the freezing medium. Using this process, it is also possible to produce particles with adjustable sizes due to variations in process parameters [85]. The dry particles obtained by spray freeze-drying are suitable for epidermal powder immunization as shown by Dean *et al.* with a trivalent influenza vaccine embedded in an excipient solution composed of mannitol, trehalose and dextran [89]. Similarly, Hepatitis B antigens in a

formulation based on trehalose were successfully spray freeze-dried and showed excellent stability without a loss of vaccine potency in accelerated stability studies [83, 91].

5.3   SPRAY DRYING

Spray drying is a drying method suitable to convert biopharmaceuticals into a dry and solid state. A liquid sugar formulation containing a biopharmaceutical is atomized in the hot air of a spray dryer into a cloud of small droplets. The droplet surface is moisture saturated and water evaporates in an endothermic process so that the droplet temperature remains significantly lower than the hot air temperature. The sugar concentration of the droplet increases during evaporation of the water and the droplet temperature begins to rise. At a certain concentration the sugar becomes solid. Water molecules evaporate under conditions that the solution is in thermodynamic equilibrium. If the evaporation rate of the water is fast enough, the sugar has no sufficient time to crystallize and turns into a dry amorphous glassy state [121, 122].

Oxygen sensitive materials and solvents require drying with nitrogen gas. The incorporation of the biopharmaceutical into a glassy sugar matrix protects it from degradation during the spray drying process. However, heat denaturation can occur if process parameters are not well chosen. The biopharmaceutical is rapidly vitrified by using a large liquid-gas interface at elevated temperature and rapid moisture removal. The air-water interfacial stress and the shear stress induced by the atomisation can lead to degradation of the biopharmaceutical. The addition of surface-active agents reduces the interfacial stress induced by the spray drying process and improves the stability of the biopharmaceutical [85]. An example of stable vaccine powder formulations generated by spray drying is an influenza subunit vaccine powder stabilized using the oligosaccharide inulin. The obtained particles were spherical and smooth with an average particle size of 3 μm and maintained the antigen's immunogenicity *in vivo* [28].

5.4   DESICCATION/AIR DRYING

The process of drying using a hygroscopic substance in a sealed desiccator is called desiccation. A small amount of material is dried on a shelf above a drying agent like silica gel or anhydrous caustic soda. The process is carried out at room temperature and takes several hours [28]. Desiccation is very time consuming method incorporating a high risk of sugar crystallization and phase separation and subsequent denaturation of the biopharmaceutical.

Chen *et al.* prepared a split vaccine powder formulation by air drying. The vaccine was desiccated in a trehalose solution overnight using an N_2 purge. Whether the integrity of the vaccine compound in the dry product was affected, was not investigated, however the performed immunization studies were successful [41, 123].

5.5   VACUUM DRYING

Vacuum drying describes the process of drying at a certain pressure and constant temperature so that the boiling point of water is lowered below the sample temperature [124, 125]. The constant addition of heat prevents the sample to cool from heat loss by evaporation of the water. The sugar solution is saturated at a certain point, so that it starts to precipitate simultaneously with the evaporation of the water molecules, when the solution is in thermodynamic equilibrium. [28].

5.6   VACUUM FOAM DRYING

Vacuum foam drying is based on the principle of evaporation under vacuum at low temperatures. It is a suitable method to stabilize therapeutic biomolecules which are stable at moderate temperatures and pressures [126].

Vacuum foam drying can be performed by using a freeze-dryer. A solution or suspension of a biopharmaceutical is supplemented with protective additives, in general sugars. The solution is transformed into foam by boiling under vacuum above the freezing point. Thereby foam is generated consisting of thin films of material of which water can be efficiently removed at an elevated temperature. The final solid product is amorphous and shows enhanced storage stabilities [27, 127].

5.7 SUPERCRITICAL FLUID DRYING

Supercritical fluid drying is, as spray drying and spray freeze-drying, a method capable to produce powders in the µm-range. Supercritical fluids are characterized by a temperature and a pressure above their critical points [128]. The fluid possesses unique thermo-physical properties, being able to penetrate substances like a gas and dissolve materials like a liquid. In pharmaceutical industry supercritical-CO_2 is used as standard. In the concept of this technique, the supercritical fluid is used as an antisolvent for the biopharmaceutical and as a water extraction medium [129, 130].

The process is divided into three parts. In the first step, water is extracted by the supercritical fluid out of the protein solution followed by an increase in concentration. In the second part, proteins and other constituents precipitate due to the increasing concentration and the dissolution of the supercritical fluid in the solution. In the last part supercritical fluid extracts the remaining solvent forming dry protein particles. Another method for supercritical fluid drying is by spraying the formulation in a supercritical fluid. The supercritical fluid is dissolved at high pressure in the solution containing the biopharmaceutical and other excipients and sprayed to atmospheric conditions. The supercritical fluid is used as propellant agent during the spray drying process at a low temperature. The atomization process is thereby enhanced and the duration of the drying process is shortened [129, 131]. Retention of the viral activity of a measles vaccine virus, live attenuated, formulated with trehalose was reported after supercritical fluid drying using a bubble-dryer process without the use of an organic solvent [108, 132].

6   DEVICES FOR INTRADERMAL VACCINATION

The conventional use of needles and syringes commonly fail to target the immunocompetent cells in the epidermal layer of the skin, as due to the length of the needle and the applied standard technique only deeper subcutaneous or muscle tissue can be reached [133, 134]. The urgent need for devices to facilitate correct and accurate intradermal administration is attempted by the development of a variety of delivery systems [9]. Ballistic approaches were successfully proven in clinical trials in humans [89] and initiate the development of needle-free ballistic injection devices.

A detailed review of delivery devices for intradermal vaccination [135] highlighting the pros and cons of the different systems was compiled within this thesis and can be found in the appendix.

7 OBJECTIVES OF THE THESIS

The precise delivery of vaccine particles into the skin using a needle-free ballistic approach is crucial for vaccination efficiency. This depends firstly on particle characteristics and secondly on the performance of the ballistic device. The overall aim of this thesis was the preparation of dry powder vaccine formulations suitable for needle-free ballistic injections and the development of an appropriate delivery technology in cooperation with Dr. Lell (Pyroglobe GmbH, Hettenshausen, Germany).

Appropriate particle characteristics of dry powder vaccine formulations for ballistic injection implicate a particle size in the range of 20-70 µm, a narrow particle size distribution and a highly dense and robust particle structure, as these preconditions are mandatory to achieve sufficient impact during ballistic injection and to breach the epidermal layers of the skin. Furthermore the incorporated vaccine has to exhibit stability throughout the shelf-life of the product.

The aim was to achieve these goals by a two-step process of collapse freeze-drying and cryo-milling for the preparation of antigen loaded powder particles.

It is known from previous work of our group that the application of an aggressive freeze-drying cycle leads to a controlled collapse and thereby a substantial reduction of the specific surface area of the sugar matrix, whilst protein stability can be preserved. It was anticipated that collapse freeze-drying leads to highly dense and robust particles. Thus, the first major objective was to investigate the effect of collapse freeze-drying and cryo-milling on particle morphology and stability of the model antigen ovalbumin and to benchmark the process with a conventional moderate freeze-drying cycle (chapter 3).

A second major aim of this thesis was the systematic investigation and optimization of the cryo-milling process for the production of vaccine loaded powder particles, allowing a scale up of the milling process in a partially sterile environment appropriate for industrial standards. The influence of different adjustable milling parameters on particle morphology and protein stability as well as the applicability of the cryo-milling process on other model proteins will be outlined in chapter 4.

It was assumed in literature that higher molecular weight polymers would be essential to generate mechanical robust particles by spray-freeze-drying, though, the benefit of polymers as stabilizers in freeze-dried formulations is controversy discussed.

A thorough formulation screening and storage stability for the model antigen ovalbumin after collapse freeze-drying and cryo-milling as well as an assessment of the effect of polymers on physico-chemical particle characteristics and antigen stability will be outlined in chapter 5.

The interface between powder particles and the device surface plays an important role for the proper delivery of particles into the skin and thus has a decisive impact on the efficacy of the vaccination procedure. The adhesion of particles on membranes, representing the device surface, by the use of oily adjuvants as well as the stability of vaccine particles in combination with selected adjuvants will be explored in chapter 6.

The effectiveness of ballistic particle injection depends decisively on the performance of the delivery device and the device-target interaction. The final pivotal aim of this thesis was to investigate a novel principle of particle acceleration to deliver vaccine loaded powder particles by a needle-free approach into the skin. The development of a method to measure the velocity of particles, a thorough investigation of the relationship of particle parameters like size and density as well as proof of concept of particle delivery in *ex-vivo* excised pig skin will be given in chapter 7.

8 REFERENCES

[1]   WHO. Global Immunization Data. 2015 [cited 13.02.2016]; Available from: http://www.who.int/immunization/monitoring_surveillance/Global_Immunization_Data.pdf?ua=1

[2]   Babiuk S, Baca-Estrada M, Babiuk LA, Ewen C, Foldvari M. Cutaneous vaccination: the skin as an immunologically active tissue and the challenge of antigen delivery. Journal of Controlled Release 2000;66(2-3):199-214.

[3]   Glenn GM, Kenney RT, Ellingsworth LR, Frech SA, Hammond SA, Zoeteweij JP. Transcutaneous immunization and immunostimulant strategies: capitalizing on the immunocompetence of the skin. Expert Review of Vaccines 2003;2(2):253-67.

[4]   Henderson RA, Mossman S, Nairn N, Cheever MA. Cancer vaccines and immunotherapies: emerging perspectives. Vaccine 2005;23(17-18):2359-62.

[5]   Moingeon P. Cancer vaccines. Vaccine 2001;19(11-12):1305-26.

[6]   Tovar JM, Bazaldua OV. New quadrivalent HPV vaccine developments. Postgraduate medicine 2008;120(4):14-6.

[7]   Paul KT. "Saving lives": Adapting and adopting Human Papilloma Virus (HPV) vaccination in Austria. Social Science & Medicine 2016.

[8]   Beavis AL, Levinson KL. Preventing Cervical Cancer in the United States: Barriers and Resolutions for HPV Vaccination. Frontiers in Oncology 2016;6:19.

[9]   Kim Y-C, Jarrahian C, Zehrung D, Mitragotri S, Prausnitz MR. Delivery systems for intradermal vaccination. Current Topics in Microbiology and Immunology 2012(351):77-112.

[10]   Kermode M. Unsafe injections in low-income country health settings: need for injection safety promotion to prevent the spread of blood-borne viruses. Health promotion international 2004;19(1):95-103.

[11]   Ford P, Furness G. Needle-free vaccine delivery to become the global norm? Target World Drug Delivery News 2003(19):7-9.

[12]   Collins CH, Kennedy DA. Needlestick injuries and infections: an overview. European Journal of Parenteral Sciences 2002;7(2):45-8.

[13]   Rosenstock L. Needlestick injuries among healthcare workers. Centers for Disease Control and Prevention 2000;<http://www.cdc.gov/washington/testimorry/ps062200.htm> (2000).

[14]   WHO. Saftey of Injections:Global Facts and Figures. World Health Organization, Geneva: World Health Organization, 2004.

[15]   Nir Y, Paz A, Sabo E. Fear of injections in young adults: prevalence and associations. American Journal of Tropical Medicine and Hygiene 2003;68:341-4.

[16]   Breau LM. Facial expression of children receiving immunizations: a principle components analysis of the child facial coding system. Clinical Journal of Pain 2001;17:178-86.

[17]   Banchereau J, Steinman RM. Dendritic cells and the control of immunity. Nature 1998;392(6673):245-52.

[18]   Toebak MJ, Gibbs S, Bruynzeel DP, Scheper RJ, Rustemeyer T. Dendritic cells: biology of the skin. Contact Dermatitis 2009;60(1):2-20.

[19]   Amorij J-P, Hinrichs WLJ, Frijlink HW, Wilschut JC, Huckriede A. Needle-free influenza vaccination. Lancet Infectious Diseases 2010;10(10):699-711.

[20]   Nicolas J-Fo, Guy B. Intradermal, epidermal and transcutaneous vaccination: from immunology to clinical practice. Expert Review of Vaccines 2008;7(8):1201-14.

[21]   Bal SM, Ding Z, van Riet E, Jiskoot W, Bouwstra JA. Advances in transcutaneous vaccine delivery: Do all ways lead to Rome? Journal of Controlled Release 2010;148(3):266-82.

[22]   Engelke L, Winter G, Hook S, Engert J. Recent insights into cutaneous immunization: How to vaccinate via the skin. Vaccine 2015;33(37):4663-74.

[23]   Karande P, Mitragotri S. Transcutaneous immunization: an overview of advantages, disease targets, vaccines, and delivery technologies. Annual Review of Chemical and Biomolecular Engineering 2010;1:175-201.

[24]   Bos J.D. The skin as an organ of immunity. Clinical and Experimental Immunology 1997;107:3-5.

[25]   Jakob T, Udey MC. Epidermal Langerhans cells: from neurons to nature's adjuvants. Advances in Dermatology 1998;14:209-58; discussion 59.

[26]   Udey M. Cadherins and Langerhans cell immunobiology. Clinical and Experimental Immunology 1997;107:6-8.

[27]   Abdul-Fattah A, Truong-Le V, Yee L, Pan E, Ao Y, Kalonia D, et al. Drying-Induced Variations in Physico-Chemical Properties of Amorphous Pharmaceuticals and Their Impact on Stability II: Stability of a Vaccine. Pharmaceutical Research 2007;24(4):715-27.

[28]   Amorij JP, Huckriede A, Wilschut J, Frijlink H, Hinrichs W. Development of Stable Influenza Vaccine Powder Formulations: Challenges and Possibilities. Pharmaceutical Research 2008;25(6):1256-73.

[29]   Sugimura T, Ito Y, Tananari Y, Ozaki Y, Maeno Y, Yamaoka T, et al. Improved antibody responses in infants less than 1 year old using intradermal influenza vaccination. Vaccine 2008;26(22):2700-5.

[30]   Künzi V, Klap JM, Seiberling MK, Herzog C, Hartmann K, Kürsteiner O, et al. Immunogenicity and safety of low dose virosomal adjuvanted influenza vaccine administered intradermally compared to intramuscular full dose administration. Vaccine 2009;27(27):3561-7.

[31]   Chiu SS, Peiris JSM, Chan KH, Wong WHS, Lau YL. Immunogenicity and Safety of Intradermal Influenza Immunization at a Reduced Dose in Healthy Children. Pediatrics 2007;119(6):1076-82.

[32]   Belshe RB, Newman FK, Cannon J, Duane C, Treanor J, Van Hoecke C, et al. Serum Antibody Responses after Intradermal Vaccination against Influenza. The New England Journal of Medicine 2004;351(22):2286-94.

[33]   Kenney RT, Frech SA, Muenz LR, Villar CP, Glenn GM. Dose sparing with intradermal injection of influenza vaccine. The New England Journal of Medicine 2004;351(22):2295-301.

[34]   Auewarakul P, Kositanont U, Sornsathapornkul P, Tothong P, Kanyok R, Thongcharoen P. Antibody responses after dose-sparing intradermal influenza vaccination. Vaccine 2007;25(4):659-63.

[35]   Jo YM, Song JY, Hwang IS, Lee J, Oh SC, Kim JS, et al. Dose sparing strategy with intradermal influenza vaccination in patients with solid cancer. Journal of Medical Virology 2009;81(4):722-7.

[36]   Belshe RB, Newman FK, Wilkins K, Graham IL, Babusis E, Ewell M, et al. Comparative immunogenicity of trivalent influenza vaccine administered by intradermal or intramuscular route in healthy adults. Vaccine 2007;25(37-38):6755-63.

[37]   Van Damme P, Oosterhuis-Kafeja F, Van der Wielen M, Almagor Y, Sharon O, Levin Y. Safety and efficacy of a novel microneedle device for dose sparing intradermal influenza vaccination in healthy adults. Vaccine 2009;27(3):454-9.

[38]   Charest AF, McDougall J, Goldstein MB. A Randomized Comparison of Intradermal and Intramuscular Vaccination Against Hepatitis B Virus in Incident Chronic Hemodialysis Patients. American Journal of Kidney Diseases 2000;36(5):976-82.

[39]   Egemen A, Aksit S, Kurugöl Z, Erensoy S, Bilgiç A, Akilli M. Low-dose intradermal versus intramuscular administration of recombinant hepatitis B vaccine: a comparison of immunogenicity in infants and preschool children. Vaccine 1998;16(16):1511-5.

[40]   Zehrung D, Jarrahian C, Wales A. Intradermal delivery for vaccine dose sparing: overview of current issues. Vaccine 2013;31(34):3392-5.

[41]   Chen D, Endres RL, Erickson CA, Weis KF, McGregor MW, Kawaoka Y, et al. Epidermal immunization by a needle-free powder delivery technology: Immunogenicity of influenza vaccine and protection in mice. Nature Medicine 2000;6(10):1187-90.

[42]   Chen D, Zuleger C, Chu Q, Maa YF, Osorio J, Payne LG. Epidermal Powder Immunization with a Recombinant HIV gp120 Targets Langerhans Cells and Induces Enhanced Immune Responses. AIDS Research and Human Retroviruses 2002;18(10):715-22.

[43]   Osorio JE, Zuleger CL, Burger M, Chu Q, Payne LG, Chen D. Immune responses to hepatitis B surface antigen following epidermal powder immunization. Immunology and Cell Biology 2003;81(1):52-8.

[44]   Clem AS. Fundamentals of Vaccine Immunology. Journal of Global Infectious Diseases 2011;3(1):73.

[45]   Ravanfar P, Satyaprakash A, Creed R, Mendoza N. Existing antiviral vaccines. Dermatologic Therapy 2009;22(2):110-28.

[46]   Bovier PA. Recent advances with a virosomal hepatitis A vaccine. Expert Opinion on Biological Therapy 2008;8(8):1177-85.

[47]   Eriksson K, Holmgren J. Recent advances in mucosal vaccines and adjuvants. Current Opinion in Immunology 2002;14(5):666-72.

[48]   Scharton-Kersten T, Yu J-m, Vassell R, O'Hagan D, Alving CR, Glenn GM. Transcutaneous immunization with bacterial ADP-ribosylating exotoxins, subunits, and unrelated adjuvants. Infection and Immunity 2000;68(9):5306-13.

[49]   Roy P, Noad R. Virus-like particle as a vaccine delivery system. Myths and facts. Human Vaccines 2008;4(1):5-12.

[50]   Petrovsky N, Aguilar JC. Vaccine adjuvants: current state and future trends. Immunology and Cell Biology 2004;82(5):488-96.

[51]   McElrath MJ. Selection of potent immunological adjuvants for vaccine construction. Seminars in Cancer Biology; 1995: Elsevier; 1995. p. 375-85.

[52]   Marx PA, Compans RW, Gettie A, Staas JK, Gilley RM, Mulligan MJ, et al. Protection against vaginal SIV transmission with microencapsulated vaccine. Science 1993;260(5112):1323-7.

[53]   Edelman R. Vaccine adjuvants. Review of Infectious Diseases 1980;2(3):370-83.

[54]   Temizoz B, Kuroda E, Ishii KJ. Vaccine adjuvants as potential cancer immunotherapeutics. International Immunology 2016:015.

[55]   Aguilar J, Rodriguez E. Vaccine adjuvants revisited. Vaccine 2007;25(19):3752-62.

[56]   Cox JC, Coulter AR. Adjuvants—a classification and review of their modes of action. Vaccine 1997;15(3):248-56.

[57]   Gupta RK, Siber GR. Adjuvants for human vaccines - current status, problems and future prospects. Vaccine 1995;13(14):1263-76.

[58]   O'Hagan DT. New Generation Vaccine Adjuvants. eLS: John Wiley & Sons, Ltd, 2001.

[59]   Vogel FR, Powell MF, Alving CR. A compendium of vaccine adjuvants and excipients. Vaccine design: the subunit and adjuvant approach 1995;6:141-228.

[60]   Gupta A, Chaphalkar SR. Vaccine Adjuvants: The Current Necessity of Life. Shiraz E-Medical Journal 2015;16(7).

[61]   Freund J, Casals J, Hosmer EP. Sensitization and Antibody Formation after Injection of Tubercle Bacilli and Paraffin Oil. Experimental Biology and Medicine 1937;37(3):509-13.

[62]   Stuart-Harris C. Adjuvant influenza vaccines. Bulletin of the World Health Organization 1969;41(3-4-5):615.

[63]   Salerno EP, Shea SM, Olson WC, Petroni GR, Smolkin ME, McSkimming C, et al. Activation, dysfunction and retention of T cells in vaccine sites after injection of incomplete Freund's adjuvant, with or without peptide. Cancer Immunology, Immunotherapy 2013;62(7):1149-59.

[64]   O'Hagan DT. MF59 is a safe and potent vaccine adjuvant that enhances protection against influenza virus infection. Expert Review of Vaccines 2007;6(5):699-710.

[65]   O'Hagan DT, Ott GS, Nest GV, Rappuoli R, Giudice GD. The history of MF59® adjuvant: a phoenix that arose from the ashes. Expert Review of Vaccines 2013;12(1):13-30.

[66]   Garçon N, Vaughn DW, Didierlaurent AM. Development and evaluation of AS03, an Adjuvant System containing α-tocopherol and squalene in an oil-in-water emulsion. Expert Review of Vaccines 2012;11(3):349-66.

[67]   Morel S, Didierlaurent A, Bourguignon P, Delhaye S, Baras B, Jacob V, et al. Adjuvant System AS03 containing α-tocopherol modulates innate immune response and leads to improved adaptive immunity. Vaccine 2011;29(13):2461-73.

[68]   Alpar H, Bowen J, Brown M. Effectiveness of liposomes as adjuvants of orally and nasally administered tetanus toxoid. International Journal of Pharmaceutics 1992;88(1):335-44.

[69]   Maa Y-F, Shu C, Ameri M, Zuleger C, Che J, Osorio JE, et al. Optimization of an Alum-Adsorbed Vaccine Powder Formulation for Epidermal Powder Immunization. Pharmaceutical Research 2003;20:969-77.

[70]   Belyakov IM. Transcutaneous immunization induces mucosal CTLs and protective immunity by migration of primed skin dendritic cells. J Clin Invest 2004;113:998-1007. The Journal of Allergy and Clinical Immunology 2004;114(3):712.

[71]   Gockel CM, Bao S, Beagley KW. Transcutaneous immunization induces mucosal and systemic immunity: a potent method for targeting immunity to the female reproductive tract. Molecular Immunology 2000;37(9):537-44.

[72]   Glenn GM, Taylor DN, Li X, Frankel S, Montemarano A, Alving CR. Transcutaneous immunization: A human vaccine delivery strategy using a patch. Nature Medicine 2000;6(12):1403-6.

[73]   Scharton-Kersten T, M. Glenn G, Vassell R, Yu J-m, Walwender D, R. Alving C. Principles of transcutaneous immunization using cholera toxin as an adjuvant. Vaccine 1999;17(Supplement 2):S37-S43.

[74]   Kenney RT, Yu J, Guebre-Xabier M, Frech SA, Lambert A, Heller BA, et al. Induction of Protective Immunity against Lethal Anthrax Challenge with a Patch. The Journal of Infectious Diseases 2004;190(4):774-82.

[75]   Chen D, Erickson CA, Endres RL, Periwal SB, Chu Q, Shu C, et al. Adjuvantation of epidermal powder immunization. Vaccine 2001;19(20-22):2908-17.

[76]   Glenn GM, Rao M, Matyas GR, Alving CR. Skin immunization made possible by cholera toxin. Nature 1998;391(6670):851-2.

[77]   Hammond SA, Walwender D, Alving CR, Glenn GM. Transcutaneous immunization: T cell responses and boosting of existing immunity. Vaccine 2001;19(17):2701-7.

[78]   Eldridge JH, Staas JK, Meulbroek JA, McGhee JR, Tice TR, Gilley RM. Biodegradable microspheres as a vaccine delivery system. Molecular Immunology 1991;28(3):287-94.

[79]   Eldridge JH, Staas J, Meulbroek J, Tice T, Gilley R. Biodegradable and biocompatible poly (DL-lactide-co-glycolide) microspheres as an adjuvant for staphylococcal enterotoxin B toxoid which enhances the level of toxin-neutralizing antibodies. Infection and Immunity 1991;59(9):2978-86.

[80]   Po ALW, Rogers E, Shepphard M, Scott E. Delivery systems for non-parenteral vaccines. Advanced Drug Delivery Reviews 1995;18(1):101-9.

[81]   Yuki Y, Kiyono H. New generation of mucosal adjuvants for the induction of protective immunity. Reviews in Medical Virology 2003;13(5):293-310.

[82]   Neutra MR, Pringault E, Kraehenbuhl J-P. Antigen sampling across epithelial barriers and induction of mucosal immune responses. Annual Review of Immunology 1996;14(1):275-300.

[83]   Chen D, Maa Y-F, Haynes JR. Needle-free epidermal powder immunization. Expert Review of Vaccines 2002;1(3):265-76.

[84]   Brandau DT, Jones LS, Wiethoff CM, Rexroad J, Middaugh CR. Thermal stability of vaccines. Journal of Pharmaceutical Sciences 2003;92(2):218-31.

[85]   Maa Y-F, Prestrelski SJ. Biopharmaceutical powders: particle formation and formulation considerations. Current Pharmaceutical Biotechnology 2000;1(3):283-302.

[86]   Hardy MP, Kendall MAF. Mucosal deformation from an impinging transonic gas jet and the ballistic impact of microparticles. Physics in Medicine and Biology 2005;50(19):4567.

[87]   Dean HJ. Epidermal delivery of protein and DNA vaccines. Expert Opinion on Drug Delivery 2005;2(2):227-36.

[88]   Truong N, Liu Y, Kendall M. Gas and Particle Dynamics of a Contoured Shock Tube for Pre-clinical Microparticle Drug Delivery. Shock Waves 2006;15(3):149-64.

[89]   Dean HJ, Chen D. Epidermal powder immunization against influenza. Vaccine 2004;23(5):681-6.

[90]   Maa Y-F, Ameri M, Shu C, Payne LG, Chen D. Influenza vaccine powder formulation development: spray-freeze-drying and stability evaluation. Journal of Pharmaceutical Sciences 2004;93(7):1912-23.

[91]   Maa Y-F, Ameri M, Shu C, Zuleger CL, Che J, Osorio JE, et al. Hepatitis-B Surface Antigen (HBsAg) Powder Formulation: Process and Stability Assessment. Current Drug Delivery 2007;4:57-67.

[92]   Maa Y-F, Zhao L, Payne LG, Chen D. Stabilization of alum-adjuvanted vaccine dry powder formulations: Mechanism and application. Journal of Pharmaceutical Sciences 2002;92(2):319-32.

[93]   Sonner C, Maa Y-F, Lee G. Spray-freeze-drying for protein powder preparation: Particle characterization and a case study with trypsinogen stability. Journal of Pharmaceutical Sciences 2002;91(10):2122-39.

[94]   Rochelle C, Lee G. Dextran or hydroxyethyl starch in spray-freeze-dried trehalose/mannitol microparticles intended as ballistic particulate carriers for proteins. Journal of Pharmaceutical Sciences 2007;96(9):2296-309.

[95]   Schiffter H, Condliffe J, Vonhoff S. Spray-freeze-drying of nanosuspensions: the manufacture of insulin particles for needle-free ballistic powder delivery. Journal of the Royal Society Interface 2010;7(Suppl 4):S483-S500.

[96]   Deng Y, Mathaes R, Winter G, Engert J. Encapsulation of antigen-loaded silica nanoparticles into microparticles for intradermal powder injection. European Journal of Pharmaceutical Sciences 2014;63:154-66.

[97]   Fuller DH, Loudon P, Schmaljohn C. Preclinical and clinical progress of particle-mediated DNA vaccines for infectious diseases. Methods 2006;40(1):86-97.

[98]   Chen D, Weis KF, Chu Q, Erickson C, Endres R, Lively CR, et al. Epidermal Powder Immunization Induces both Cytotoxic T-Lymphocyte and Antibody Responses to Protein Antigens of Influenza and Hepatitis B Viruses. Journal of Virology 2001;75(23):11630-40.

[99]   Lesinski GB, Smithson SL, Srivastava N, Chen D, Widera G, Westerink MAJ. A DNA vaccine encoding a peptide mimic of Streptococcus pneumoniae serotype 4 capsular polysaccharide induces specific anti-carbohydrate antibodies in Balb/c mice. Vaccine 2001;19(13-14):1717-26.

[100]   Kendall MAF. Needle-Free Vaccine Injection. Drug Delivery: Springer Berlin Heidelberg, 2010: 193-219.

[101]   Raju PA, McSloy N, Truong NK, Kendall MAF. Assessment of epidermal cell viability by near infrared multi-photon microscopy following ballistic delivery of gold micro-particles. Vaccine 2006;24(21):4644-7.

[102]   Lebre F, Borchard G, de Lima M, Borges O. Progress Towards a Needle-Free Hepatitis B Vaccine. Pharmaceutical Research 2010:1-27.

[103]   Eisenbraun MD, Fuller DH, Haynes JR. Examination of parameters affecting the elicitation of humoral immune responses by particle bombardment-mediated genetic immunization. DNA and Cell Biology 1993;12(9):791-7.

[104]   Roy MJ, Wu MS, Barr LJ, Fuller JT, Tussey LG, Speller S, et al. Induction of antigen-specific CD8+ T cells, T helper cells, and protective levels of antibody in humans by particle-mediated administration of a hepatitis B virus DNA vaccine. Vaccine 2000;19(7-8):764-78.

[105]   Tacket CO, Roy MJ, Widera G, Swain WF, Broome S, Edelman R. Phase 1 safety and immune response studies of a DNA vaccine encoding hepatitis B surface antigen delivered by a gene delivery device. Vaccine 1999;17(22):2826-9.

[106]   Rottinghaus ST, Poland GA, Jacobson RM, Barr LJ, Roy MJ. Hepatitis B DNA vaccine induces protective antibody responses in human non-responders to conventional vaccination. Vaccine 2003;21(31):4604-8.

[107]   Amidi M, Pellikaan HC, Hirschberg H, de Boer AH, Crommelin DJA, Hennink WE, et al. Diphtheria toxoid-containing microparticulate powder formulations for pulmonary vaccination: Preparation, characterization and evaluation in guinea pigs. Vaccine 2007;25(37-38):6818-29.

[108]   Burger JL, Cape SP, Braun CS, McAdams DH, Best JA, Bhagwat P, et al. Stabilizing Formulations for Inhalable Powders of Live-Attenuated Measles Virus Vaccine. Journal of Aerosol Medicine and Pulmonary Drug Delivery 2008;21(1):25-34.

[109]   Amorij J, Meulenaar J, Hinrichs W, Stegmann T, Huckriede A, Coenen F, et al. Rational design of an influenza subunit vaccine powder with sugar glass technology: preventing conformational changes of haemagglutinin during freezing and freeze-drying. Vaccine 2007;25(35):6447-57.

[110]   Carpenter J, Pikal M, Chang B, Randolph T. Rational Design of Stable Lyophilized Protein Formulations: Some Practical Advice. Pharmaceutical Research 1997;14(8):969-75.

[111]   Wang W. Lyophilization and development of solid protein pharmaceuticals. International Journal of Pharmaceutics 2000;203(1-2):1-60.

[112]   Carpenter JF, Chang BS. Lyophilization of protein pharmaceuticals. Biotechnology and Biopharmaceutical Manufacturing, Processing, and Preservation 1996;2:199-264.

[113]   Schersch K, Betz O, Garidel P, Muehlau S, Bassarab S, Winter G. Systematic investigation of the effect of lyophilizate collapse on pharmaceutically relevant proteins I: Stability after freeze-drying. Journal of Pharmaceutical Sciences 2010;99(5):2256-78.

[114]   Bosch T. Aggressive Freeze-Drying: a fast and suitable method to stabilize biopharmaceuticals: München, Ludwig-Maximilians-Universität, Diss. ; 2014.

[115]   Ziegler A, Simon S, Lee G. Comminution of carbohydrate and protein microparticles on firing in a ballistic powder injector. Journal of Pharmaceutical Sciences 2010;99(12):4917-27.

[116]   Tang X, Pikal M. Design of Freeze-Drying Processes for Pharmaceuticals: Practical Advice. Pharmaceutical Research 2004;21(2):191-200.

[117]   Pikal MJ. Freeze drying. Encyclopedia of Pharmaceutical Technology, Marcel Dekker, New York 2002;1299:1326.

[118]   Schersch K, Betz O, Garidel P, Muehlau S, Bassarab S, Winter G. Systematic investigation of the effect of lyophilizate collapse on pharmaceutically relevant proteins, part 2: Stability during storage at elevated temperatures. Journal of Pharmaceutical Sciences 2012;101(7):2288-306.

[119]   Shoyele SA, Cawthorne S. Particle engineering techniques for inhaled biopharmaceuticals. Advanced Drug Delivery Reviews 2006;58(9):1009-29.

[120]   Mumenthaler M, Leuenberger H. Atmospheric spray-freeze drying: a suitable alternative in freeze-drying technology. International Journal of Pharmaceutics 1991;72(2):97-110.

[121]   Maa Y-F, Nguyen P-AT, Hsu SW. Spray-drying of air–liquid interface sensitive recombinant human growth hormone. Journal of Pharmaceutical Sciences 1998;87(2):152-9.

[122]   Vehring R. Pharmaceutical particle engineering via spray drying. Pharmaceutical Research 2008;25(5):999-1022.

[123]   Chen D, Endres RL, Erickson CA, Maa Y-F, Payne LG. Epidermal powder immunization using non-toxic bacterial enterotoxin adjuvants with influenza vaccine augments protective immunity. Vaccine 2002;20(21-22):2671-9.

[124]   Mattern M, Winter G, Rudolph R, Lee G. Formulation of proteins in vacuum-dried glasses. I: Improved vacuum-drying of sugars using crystallising amino acids. European Journal of Pharmaceutics and Biopharmaceutics 1997;44(2):177-85.

[125]   Mattern M, Winter G, Kohnert U, Lee G. Formulation of Proteins in Vacuum-Dried Glasses. II. Process and Storage Stability in Sugar-Free Amino Acid Systems. Pharmaceutical Development and Technology 1999;4(2):199-208.

[126]   Abdul-Fattah AM, Truong-Le V, Yee L, Nguyen L, Kalonia DS, Cicerone MT, et al. Drying-induced variations in physico-chemical properties of amorphous pharmaceuticals and their impact on stability (I): Stability of a monoclonal antibody. Journal of Pharmaceutical Sciences 2007;96(8):1983-2008.

[127]   Pisal S, Wawde G, Salvankar S, Lade S, Kadam S. Vacuum foam drying for preservation of LaSota virus: Effect of additives. AAPS PharmSciTech 2006;7(3):E30-E7.

[128]   Koushik K, Kompella UB. Preparation of Drug Delivery Systems Using Supercritical Fluid Technology. Critical Reviews in Therapeutic Drug Carier Systems 2001;18(2):28.

[129]   Jovanović N, Bouchard A, Hofland GW, Witkamp G-J, Crommelin DJA, Jiskoot W. Stabilization of Proteins in Dry Powder Formulations Using Supercritical Fluid Technology. Pharmaceutical Research 2004;21(11):1955-69.

[130]   Jung J, Perrut M. Particle design using supercritical fluids: literature and patent survey. The Journal of Supercritical Fluids 2001;20(3):179-219.

[131]   Jovanović N, Bouchard A, Hofland GW, Witkamp G-J, Crommelin DJ, Jiskoot W. Distinct effects of sucrose and trehalose on protein stability during supercritical fluid drying and freeze-drying. European Journal of Pharmaceutical Sciences 2006;27(4):336-45.

[132]   Cape SP, Villa JA, Huang ET, Yang T-H, Carpenter JF, Sievers RE. Preparation of active proteins, vaccines and pharmaceuticals as fine powders using supercritical or near-critical fluids. Pharmaceutical Research 2008;25(9):1967-90.

[133]   Combadière B, Mahé B. Particle-based vaccines for transcutaneous vaccination. Comparative Immunology Microbiology and Infectious Diseases 2008;31(2-3):293-315.

[134]   Kendall M. Engineering of needle-free physical methods to target epidermal cells for DNA vaccination. Vaccine 2006;24(21):4651-6.

[135]   Kis EE, Winter G, Myschik J. Devices for intradermal vaccination. Vaccine 2012;30(3):523-38.

CHAPTER 2

MATERIALS AND METHODS

1 MATERIALS

1.1 OVALBUMIN

Albumin from chicken egg white (ovalbumin, grade V) was obtained from Sigma-Aldrich Chemie GmbH, Steinheim, Germany. Ovalbumin, derived from chicken egg white, is a glycoprotein which comprises 386 amino acids. The sequence includes six cysteines with a single disulfide bond between Cys74 and Cys121. It has a molecular weight of 44,287 Da (by calculation, data provided by the manufacturer Sigma-Aldrich) and features a net negative surface charge. Ovalbumin is a member of the serpin superfamily, however, without having any protease activity [1, 2]. It is commonly used as immunological model in *in vivo* and *in vitro* studies since specific monoclonal antibodies against different epitopes of OVA have been developed [3].

1.2 RH-G-CSF

Recombinant human granulocyte-colony stimulating factor (rh-G-CSF) was formulated in a 10 mM sodium acetate buffer at pH 4.0. The concentration of rh-G-CSF in the bulk drug substance was 4.04 mg/mL. The bulk solution contained 0.004 % polysorbate 20. The physiological role of rh-G-CSF is the stimulation of the proliferation and differentiation of neutrophilic immature cells to neutrophilic granulocytes. The rh-G-CSF molecule has two disulfide bonds between amino acids 36 and 42 and between amino acids 64 and 74, respectively. It belongs to the family of the four-helix bundle cytokines with four α-helices ranged in an up-up and down-down structure. Rh-G-CSF derives from *E. coli* and is not glycosylated [4, 5]. A high aggregation and self-association

tendency of the liquid formulation is a result of the fact that the major part of the rh-G-CSF molecule consists of hydrophobic regions [6, 7]. The molecular weight of rh-G-CSF is about 18,816 Da [8].

1.3   RH-INTERFERON-A-2A

Rh-IFN α-2a (rh-IFN α-2a) was provided at a concentration of 1.5 mg/mL and contained 25 mM acetate buffer (pH 5.0) and 120 mM sodium chloride at pH 5. The protein consists of 166 amino acids and is not glycosylated with a molecular weight of 19,241 Da. It has two disulfide bonds, one between amino acids 1 and 98, and the second between amino acids 29 and 138. The tertiary structure of the all-helical protein is arranged by five α-helices [9].

1.4   OILY ADJUVANTS AND ADHESIVES

Table 2.1: Excipients used for the preparation of oily adjuvants and for the use as adhesive

Excipient	Description	Supplier
Squalene	≥98%	Sigma Aldrich Chemie GmbH (Steinheim, Germany)
Squalane	≥99%	VWR International GmbH (Darmstadt, Germany)
Polysorbate 80	Ph.Eur.	Sigma Aldrich Chemie GmbH (Steinheim, Germany)
Span® 85	Ph.Eur.	VWR International GmbH (Darmstadt, Germany)
Paraffin oil	Ph.Eur.	Sigma Aldrich Chemie GmbH (Steinheim, Germany)
Freund's incomplete adjuvant		Sigma Aldrich Chemie GmbH (Steinheim, Germany)
Miglyol®812		VWR International GmbH (Darmstadt, Germany)
Silicon oil AP 100		Sigma Aldrich Chemie GmbH (Steinheim, Germany)
Polyisobutylene	Mw~1,000,000	Acino Pharma GmbH (Miesbach, Germany)
Polyethylene glycol 400		Sigma Aldrich Chemie GmbH (Steinheim, Germany)
Castor oil	Ph.Eur.	VWR International GmbH (Darmstadt, Germany)

For the preparation of the mixture of the oily components of MF59 1500 µl squalene were vortexed with 150 µl polysorbate 80 and with 150 µl Span 85 in an Eppendorf tube for 10 seconds.

1.5 FURTHER CHEMICALS, REAGENTS AND MATERIALS

Table 2.2: Chemicals and reagents used for analytical purposes

Excipient	Description	Supplier
Acetic acid	100%	VWR International GmbH (Darmstadt, Germany)
Sodium acetate	≥99%	Sigma Aldrich Chemie GmbH (Steinheim, Germany)
5α-Cholestane	≥97%	Sigma Aldrich Chemie GmbH (Steinheim, Germany)
Tert-butyl-methyl-ether	99.8%	Sigma Aldrich Chemie GmbH (Steinheim, Germany)
Sodium hydroxide	50%	Merck KGaA (Darmstadt, Germany)
Sudan red	Ph.Eur.	Sigma Aldrich Chemie GmbH (Steinheim, Germany)
Hydranal Methanol dry	Riedel-de Haën, ≤0.01% water	Sigma Aldrich Chemie GmbH (Steinheim, Germany)
Hydranal Formamide dry	Riedel-de Haën, ≤0.02% water	Sigma Aldrich Chemie GmbH (Steinheim, Germany)
Hydranal Water Standard 1.00	Riedel-de Haën, 0.1% water	Sigma Aldrich Chemie GmbH (Steinheim, Germany)
Hydranal Coulomat AG	Riedel-de Haën	Sigma Aldrich Chemie GmbH (Steinheim, Germany)
N-trimethylsilylimidazole	p.A.	Macherey Nagel (Düren, Germany)
N-methyl-N-trimethylsilyltrifluoroacetamide	p.A.	Macherey Nagel (Düren, Germany)
Primary secondary amine (PSA)	particle size 40 µm	Varian (Harbor City, USA)
Na_2SO_4		Sigma Aldrich Chemie GmbH (Steinheim, Germany)

Table 2.3: Particles used for ballistic acceleration studies

Particle	Description	Supplier
Fluorescein isothiocyanate (FITC) labelled polystyrene particles	Density 1.1 g/cm^3; size 40 µm	microparticles GmbH (Berlin, Germany)
Blue dyed polystyrene particles	Density 1.1 g/cm^3; 20 µm; 40 µm and 60 µm.	microparticles GmbH (Berlin, Germany)
Glass spheres	Density 2.5 g/cm^3; size 20-40 µm; 40-63 µm; 63-70 µm; 600 µm; 900 µm	microparticles GmbH (Berlin, Germany)
Hollow glass spheres	Density 1.1 g/cm^3; size 11 µm	microparticles GmbH (Berlin, Germany)
Hollow glass spheres	Density 0.6 g/cm$^{3;}$ size 18 µm	microparticles GmbH (Berlin, Germany)

1.6 FREEZE-DRYING EXCIPIENTS

Table 2.4: Excipients used for freeze-drying experiments

Excipient	Description	Supplier
D(+)-trehalose dihydrate	Ph.Eur.	VWR International GmbH (Darmstadt, Germany)
Mannitol	Ph.Eur.	VWR International GmbH (Darmstadt, Germany)
Dextran from *Leuconostoc spp.* (Mr~70,000)		Sigma Aldrich Chemie GmbH (Steinheim, Germany)
Dextran from *Leuconostoc spp.* (Mr~40,000)		Sigma Aldrich Chemie GmbH (Steinheim, Germany)
Dextran from *Leuconostoc spp.* (Mr~ 6,000)		Sigma Aldrich Chemie GmbH (Steinheim, Germany)
Phenylalanine	≥99%	Sigma Aldrich Chemie GmbH (Steinheim, Germany)
Hydroxyethylstarch (Mr~70,000)		Serumwerk Bernburg (Bernburg, Germany)
Sodium dihydrogen phosphate dihydrate	p.A.	VWR International GmbH (Darmstadt, Germany)
di-Sodium hydrogen phosphate	p.A.	VWR International GmbH (Darmstadt, Germany)
Sodium chloride	p.A.	VWR International GmbH (Darmstadt, Germany)

2 METHODS

2.1 PREPARATION OF FORMULATIONS

The formulations contained trehalose or a combination of trehalose and mannitol (at a weight ratio of 1:1), or a ternary combination of trehalose, mannitol and dextran (at a weight ratio of 3:3:4). The total solid content of the formulations varied from 15% to 35% (w/w) [10, 11].

In terms of a large scale formulation screening, as described in chapter 5, a combination of trehalose, mannitol and hydroxyethylstarch (weight ratio 3:3:4) or a secondary combination of trehalose and phenylalanine (weight ratio 9.5:0.5) was used, if not stated otherwise.

The excipients were dissolved in phosphate buffer (pH 7.0, 10 mM phosphate, 50 mM ionic strength adjusted with sodium chloride). Ovalbumin was adjusted to a final protein concentration of 2.5% (w/w) in each formulation. Phosphate buffer was chosen as it has been reported to stabilize ovalbumin [12, 13].

Rh-G-CSF was formulated in a 20 mM sodium acetate buffer, pH 4.0, with 0.004% polysorbate and 15% (w/w) trehalose-mannitol (weight ratio 1:1) and a final protein concentration of 2.5% (w/w).

Rh-IFN α-2a was formulated in a 25 mM sodium acetate buffer (pH 4.2), containing 120 mM sodium chloride with 15% (w/w) trehalose-mannitol (weight ratio 1:1) and a final protein concentration of 2.5% (w/w).

Prior to freeze-drying, all formulations were filtered through a 0.2 μm PVDF syringe filter unit (Pall GmbH, Dreieich, Germany). The filters were pre-flushed with 5 mL buffer prior to use.

2.2 DIALYSIS

Prior to usage the rh-G-CSF bulk solution was dialyzed against 20 mM acetate buffer at pH 4 or pH 3.7, respectively, in a volumetric ratio of 1:50 at room temperature. Dialysis

was carried out using a CelluSepT1® dialysis membrane with a molecular weight cut-off of 3,500 Da (Orange Scientific, Braine-l'Alleud, Belgium).

The rh-IFN α-2a bulk solution was excessively dialyzed against 25 mM acetate buffer at pH 4.2 containing 120 mM sodium chloride. Dialysis was performed at room temperature in a volumetric ratio of 1:50 using a CelluSepT1® dialysis membrane with a molecular weight cut-off of 3,500 Da (Orange Scientific, Braine-l'Alleud, Belgium).

2.3   VISCOSITY MEASUREMENTS

A Physica MCR 100 rotational rheometer (Anton Paar, Graz, Austria) was used to measure the viscosity of the liquid formulations of 15 to 35% (w/w). One mL of each liquid was pipetted directly onto the plate of the rheometer and the temperature of the sample was adjusted to 25°C. The dimensions of the cone (CP50-1) were 50 mm diameter and a 1° angle. Thirty data points were collected over ten seconds at shear rates ranging from 1 to 100 s^{-1}.

2.4   FREEZE-DRYING

One mL aliquots of the filtered solutions were filled into 2 R blow back vials glass type I from Schott (Schott, Mainz, Germany) resulting in a fill height of approximately 1.5 cm and partially stoppered with cross-linked high molecular weight polydimethylsiloxane-coated rubber-lyophilization stoppers (B2-44, West, Eschweiler, Germany).

Freeze-drying was performed using a Christ Epsilon 2-6D freeze dryer (Christ, Osterode am Harz, Germany). Two different freeze-drying protocols were applied, which were developed according to literature [14].

2.4.1 MODERATE FREEZE-DRYING CYCLE

The moderate freeze-drying cycle (moderate FD cycle) was conducted at -40 and -20°C during primary drying and followed by 20 and 35°C during secondary drying at a

chamber pressure of 0.03 mbar. A detailed freeze-drying protocol is given in table 2.6. The product temperature approached the shelf temperature and the final product temperature reached 32°C.

Table 2.5: Conventional freeze-drying cycle

Process Step	Time [min]	Temperature [°C]	Pressure [mbar]
Loading	0	20	1113
Ramp	90	-50	1113
Freezing	120	-50	113
Vacuum ramp	1	-50	0.03
Ramp	30	-40	0.03
Primary drying	1800	-40	0.03
Ramp	200	-20	0.03
Secondary drying	600	20	0.03
Ramp	80	35	0.03
Secondary drying	300	35	0.03
End	30	5	0.03

2.4.2 COLLAPSE FREEZE-DRYING CYCLE

An aggressive freeze drying cycle (collapse FD cycle) was applied in order to produce collapsed lyophilizates. Primary as well as secondary drying were performed at a shelf temperature of 45°C and at a chamber pressure of 1.98 and 0.03 mbar, respectively. A detailed freeze-drying protocol is given in table 2.6. The product temperature as well as the shelf temperature were monitored and the product temperature approached the shelf temperature after approximately ten hours, which indicates the endpoint of primary drying [15].

Table 2.6: Collapse freeze-drying cycle

Process Step	Time [min]	Temperature [°C]	Pressure [mbar]
Loading	0	20	1113
Ramp	90	-50	1113
Freezing	120	-50	1113
Preparing	30	-40	1113
Ramp	1	-40	1.98
Primary drying	20	-40	1.98
Ramp	120	45	1,98
Secondary drying	1440	45	1,98
Ramp	1200	45	0.03
Secondary drying	120	20	0.03
End	15	5	0.03

Regarding a conventional freeze-drying cycle, the degree of super-cooling influences the cake structure and thereby the sublimation rates as well as other product parameters like specific surface area and residual moisture [16, 17]. However, in the case of the aggressive freeze-drying cycle used in this study, the cake structure is re-built during the drying process as the collapse temperature of the formulations is exceeded [18]. The rather long secondary drying time was chosen to assure low residual moisture of the product as the collapse leads to a very small specific surface area of the sugar matrix which makes it more difficult to remove the absorbed water. The process has the potential to be even further optimized; however, this was not the focus of this study.

2.5 SAMPLE PROCESSING AFTER FREEZE-DRYING

2.5.1 CRYO-MILLING SWING MILL RETSCH

Milling was performed in a swing mill MM301 (Retsch Technology, Haan, Germany). Eight lyophilizate cakes, obtained from one-milliliter aliquots of the solutions for freeze-drying, were filled in 5 mL high grade steel grinding beakers together with two stainless steel balls, dipped in liquid nitrogen for at least 2 minutes until a product temperature

below -130°C was reached and milled for 10 seconds or 30 seconds, at a frequency of 30 s^{-1}.

2.5.2 CRYO-MILLING CRYO-MILL RETSCH

Cryo-milling was performed semi-automatically using a cryo-mill (Retsch Technology, Haan, Germany). Three lyophilizate cakes, obtained from 6-mililiter aliquots of the solutions for freeze-drying, were filled in a 5 mL steel grinding beaker together with two stainless steel balls and mounted in the grinding station. Several parameters were adjusted using the semi-automatic program of the cryo-mill such as pre-cooling time, milling frequency, milling time and number and duration of the milling cycles. During the sequence pre-cooling, the stainless steel beaker was continuously flushed with liquid nitrogen, whilst the beaker was moving with a frequency of 5 s^{-1}. After a pre-cooling time of 10 min, the product temperature was below -130°C. If not stated otherwise, milling was performed for 15 seconds at a frequency of 25 s^{-1}.

2.5.3 TEXTURE ANALYZER

The rigidity of collapse freeze-dried cakes was examined using a Texture Analyzer XTPlus (Stable Mircosystems, UK). Therefore a cylindrical piston (4 mm in diameter) was moved with 1 mm/s into the sample. The maximally force (in N/s) to break the lyohilisate cake was recorded.

2.6 ACCELERATED STABILITY TESTING AND STORAGE STABILITY

2.6.1 STORAGE STABILITY OF THE FORMULATIONS

Samples, comprised of lyophilizates or powder consisting of cryo-milled lyophilizates, were stored at 2-8°C for 12 months in 2R blow back vials type I from Schott (Mainz, Germany) stoppered with B2-44 lyophilization stoppers (West, Eschweiler, Germany). Vials as well as stoppers were washed and dried for at least 7 hours in a vacuum dryer VTS-2 (Memmert, Schwabach, Germany) at 0.1 mbar and 60°C.

After the 12 months storage interval, the samples were analyzed for protein aggregation and changes in particle morphology.

2.6.2 STORAGE STABILITY OF SAMPLES WITH OILY ADJUVANTS AND ADHESIVES

Samples were prepared by bedding approximately 50 mg of protein powder formulation on a 10 µl thin film comprised of the adhesive or composition of the oily adjuvant (list of adhesives and composition of the oily adjuvant see section 1.4.) on the surface of a 2R glass vial. The samples were stoppered with B2-44 lyophilization stoppers (West, Eschweiler, Germany) and were stored at 2-8°C, 25°C and 40°C for a time period of 12 weeks. Vials as well as stoppers were washed and dried for at least 7 hours in a vacuum dryer VTS-2 (Memmert, Schwabach, Germany) at 0.1 mbar and 60°C.

After a storage interval of 2, 4, 8 and 12 weeks the samples were analyzed for protein aggregation, changes in particle morphology and chemical stability of the oily adjuvants.

2.7 CHARACTERIZATION OF PROTEIN STABILITY

2.7.1 SIZE-EXCLUSION CHROMATOGRAPHY

SE-HPLC for was performed on a summit HPLC system (Dionex GmbH, Idstein, Germany), equipped with an UVD 170 U detector (Dionex GmbH, Idstein, Germany) using a TSK gel G3000SW$_{XL}$ column (Tosoh Bioscience, Stuttgart, Germany). Samples were reconstituted in mobile phase and centrifuged at 10,000 rpm for 10 min (neo lab 16/18, Hermle Labortechnik GmbH, Wehingen, Germany) prior to injection, in order to remove insoluble aggregates. The analytics were performed at a flow rate of 0.5 mL/min with UV-detection at 280 nm. Injection volume was 40 µl. At least two samples of each formulation was analyzed and injected twice.

The running buffer for ovalbumin was composed of 0.05 M sodium phosphate and 0.15 M sodium chloride, adjusted to pH 7.2 with sodium hydroxide. For rh-G-CSF a 0.1 M sodium phosphate at pH 7.0 running buffer was used. The running buffer for rh-IFN α-2a consisted of 0.12 M disodium hydrogenphosphate dihydrate, 0.02 M sodium

dihydrogenphosphate and 4g/L sodium chloride, adjusted to pH 5.0 with hydrochloric acid.

The peak areas of the chromatograms were integrated using the data acquisition program Chromeleon version 6.60 (Dionex GmbH, Idstein, Germany). Sample recovery was determined using a calibration curve of five known concentrations of the analyzed protein of the respective formulation. The content in % of soluble oligomers, dimers, monomer and fragments was calculated by dividing the partial area under the curve (AUC) of each species by the total AUC. Additionally, the amount of remaining monomer was evaluated from the area under the monomer peak compared with that of the respective liquid formulation prior to lyophilization.

2.7.2 LIGHT OBSCURATION PARTICLE ANALYSIS

Number and distribution of particles was analyzed by light obscuration using a SVSS-C40 apparatus (PAMAS GmbH, Rutesheim, Germany). The system was flushed six times with 1.0 mL highly purified water with a fill and ejection rate of 10 mL/min, until less than 10 particles $\geq$ 1 µm/mL were detected. In order to decrease the viscosity of the samples to an appropriate level, 1 mL of the liquid formulation, which was prepared prior to freeze-drying, was diluted with 1 mL buffer. We have tested the effect of dilution on particle counting and found no effect within the precision of the method. 150 mg of the lyophilizate cake or powder samples were reconstituted in 2000 µl buffer, resulting in a protein concentration according to the liquid formulation. Prior to measurement, the system was flushed with 0.3 mL of sample followed by three injections at a volume of 0.3 mL per injection. Particles larger than or equal to 1 µm are presented as cumulative counts per mL calculated from the mean value of three injections.

2.7.3 TURBIDITY

A NEPHLA turbidimeter (Dr. Lange, Düsseldorf, Germany) was used in order to determine the turbidity of protein formulations in formazine nephelometric units (FNU). Turbidity was measured by 90° light scattering at λ=860 nm according to the method

described in the European Pharmacopoeia (method 2.2.1). About 1 mL of the liquid formulation (pre-lyohilization solution) was diluted 1:1 with formulation buffer prior to measurement. Likewise, 150 mg of the lyophilizate cake or powder formulation, respectively, was dissolved in 2 mL formulation buffer prior measurement. Each value represents the average of at least two measurements.

2.7.4 TRANSMISSION FOURIER TRANSFORM INFRARED (FTIR) SPECTROSCOPY

The conformational stability of the proteins was analyzed by FTIR spectroscopy using a Tensor 27 FTIR spectrometer (Bruker Optics, Ettlingen, Germany) equipped with a calcium fluoride flow through cell (Aquaspec 1110 M, Bruker Optics, Ettlingen, Germany) with 6.5 μm path length and a nitrogen-cooled photovoltaic MCT detector. 120 scans were performed per measurement at a resolution of 4 cm^{-1}. Each sample was injected at least twice. Data analysis was performed by using Opus software Version 6.5. For relative comparison of the different samples, the obtained spectra of the amid I region was background subtracted, vector normalized and the second derivative was calculated.

2.7.5 SODIUM DODECYL SULPHATE POLYACRYLAMIDE GEL ELECTROPHORESIS (SDS-PAGE)

The aggregation and fragmentation of the protein formulations was determined by non-reducing denaturing SDS-PAGE. The protein solutions were diluted in a pH 6.8 tris-buffer, containing 2% SDS and 2% glycerine. Prior to loading 20 μl of the samples into the gel wells (NuPAGE© Pre-Cast 10% Bis-Tris gels 1 mm; Invitrogen, Groningen, The Netherlands), the samples were denatured at 90°C for 30 min. A molecular weight standard (Mark 12 Unstained Standard, Invitrogen, Karlsruhe, Germany) was added to each gel in order to determine the molecular weight of the detected bands. Electrophoresis was performed using an XCell II Mini cell system (Novex, San Diego, CA, USA) in a constant current mode of 30 mA in a tris-glycerine/SDS running buffer (MES running buffer; Invitrogen, Groningen, The Netherlands) for approximately 40 min. The gels were stained with a silver staining kit (SilverXpress©, Invitrogen, Karlsruhe,

Germany) or by applying Coomassie staining (Imperial© protein stain solution, Thermo Fisher, Rockford, IL, USA).

2.7.6 UV-SPECTROSCOPY

UV-measurements for the determination of protein concentrations were carried out on an Agilent 8453 UV-VIS spectrophotometer (Agilent Technologies Deutschland GmbH, Böblingen, Germany) equipped with a Peltier temperature controller.

OVA concentration was determined at λ = 280 nm using a UV extinction coefficient ε = 0.700 mL*mg^{-1}*cm^{-1}. Rh-G-CSF concentration was determined using a UV extinction coefficient ε = 0.815 mL*mg^{-1}*cm^{-1} and rh-IFN α-2a using a UV extinction coefficient ε = 0.924 mL*mg^{-1}*cm^{-1}, respectively, at λ = 280 nm.

2.8 CHARACTERIZATION OF LYOPHILIZATE AND POWDER CHARACTERISTICS

2.8.1 X-RAY POWDER DIFFRACTION

The morphology of the freeze-dried and ground products was analyzed using a X-ray diffractometer XRD 3000 TT (Seifert, Ahrenburg, Germany) equipped with a copper anode (λ= 154.17 pm, 40 kV, 30 mA). Samples were scanned between 5° and 40° 2-Theta at steps of 0.05° 2-Theta and a duration of two seconds per step.

2.8.2 KARL-FISCHER TITRATION

Residual moisture content was determined by direct methanol extraction using a Karl Fischer coulometric titrator (652-KF Coulometer, Metrohm, Filderstadt, Germany). Ten to 20 mg of the samples was weighed accurately in a vial. The samples were weighed in a controlled low humidity environment using a glove box which was flushed with nitrogen until less than 10% RH was reached. The vial was sealed with a flange and 1 mL dry methanol (Hydranal® Methanol dry, Fluka, Steinheim, Germany) was added by injection. To enhance the water extraction, the samples were placed into an

ultrasonic water bath for 10 min. 200 µl aliquots of the samples were injected into the reaction vessel of the titrator. The performance of the system was validated by the analysis of water standards (Hydranal® water standard 0.1, Riedel-de-Haën, Sigma Aldrich, Steinheim, Germany) at the beginning and the end of the measurement. Three blank measurements containing dry methanol were performed at the beginning and the end of the analysis.

2.8.3 DIFFERENTIAL SCANNING CALORIMETRY

Physicochemical characteristics of the samples were evaluated by differential scanning calorimetry using a DSC 204 Phoenix® (Netzsch, Selb, Germany). For the determination of the glass transition temperature of the maximally freeze-concentrated solution (Tg') approximately 20 µl were weighed into aluminum crucibles. The aluminum crucibles containing the sample as well as an empty reference pan were cold-sealed. The samples were cooled to -70°C with a scan rate of 5 K/min and subsequently heated to +20°C with a scan rate of 10 K/min.

Approximately 10 - 20 mg lyohilizate cakes as well as powdered formulations were weighed into aluminum crucibles and cold-sealed in a dry atmosphere. Therefore the preparation of the samples was conducted in a glove box which was flushed with dry nitrogen. Tg of the samples was determined in a first scan by cooling the samples to -20°C and subsequently heating to +100°C with a scan rate of 10K/min, respectively. In a second scan, the samples were cooled to -20°C and subsequently heated to +200°C with a scan rate of 10K/min, respectively. The heat scans were analyzed for thermal events.

2.8.4 SPECIFIC SURFACE AREA MEASUREMENT

Specific surface area measurements were performed with krypton 4.8 using an Autosorb-1MP analyzer (Quantachrome, Odelzhausen, Germany). Samples were degassed under vacuum for at least three hours at 20°C before each measurement. Krypton adsorption at 77K was measured at eleven points over a relative pressure

range of 0.05 to 0.3. The Brunauer Emmett and Teller (BET) equation was used to fit the data and calculate the SSA. Therefore at least five measurement points were used. The correlation coefficient of the fit was at least 0.9975 and hence in line with the recommendation of the European Pharmacopoeia.

2.8.5 DENSITY MEASUREMENT

True density, defined as the density of the material excluding pores and interparticle spaces, was measured using an AccuPyc 1330 helium pycnometer (Micrometrics GmbH, Aachen, Germany) at a sample volume unit of 0.718507 cm³. Prior to analysis 10 cleaning cycles were performed using analytical grade helium. Approximately 300-350 mg of the sample was analyzed and the true density was calculated as an average of six measurements.

Powder tap density was measured according to the method of the European Pharmacopoeia (7.0/2.9.34.) using a 10 mL volumetric flask.

2.8.6 SCANNING ELECTRON MICROSCOPY

The morphology of the freeze-dried cakes and ground powders was examined on a scanning electron microscope (Jeol JSM-6500F, Ebersberg, Germany). Samples were attached to a self-adhesive carbon tape (Bal-tec GmbH, Witten, Germany) before sputtering them under vacuum with a thin layer of carbon (MED 020, Bal-tec GmbH, Witten, Germany).

2.8.7 MOISTURE SORPTION ANALYSIS

Water sorption of the samples in dependence of relative humidity was analyzed using an IGASorp Moisture Sorption Analyzer (Hiden Analytical, Warrington, UK). Approximately 5-10 mg of sample was sequentially exposed to 0-90% relative humidity in 10% relative humidity steps. The temperature was held constant at 25°C during the measurement. Measurements were repeated three times for each formulation.

2.8.8 PARTICLE SIZE ANALYSIS BY STATIC LIGHT DIFFRACTION

Particle size distribution of the ground powders was measured by laser light diffraction using a Horiba LA-950 (Retsch Technology, Haan, Germany). Samples were dispersed in isooctane at a concentration to achieve 90-70% transmittance of the LD laser and 90-80 % transmittance of the LED laser. Background alignment was performed with pure isooctane before addition of the samples. Particle size distribution was calculated as an average of 6 measurements applying the Fraunhofer theory and characterized with median diameter and span of the volume distribution.

Alternatively, particle size distribution was determined with a He-Ne laser beam equipped laser light diffraction using a Mastersizer X (Malvern, Herrenberg, Germany). Approximately 5 mg of the dried-powder was dispersed in 10 mL Miglyol 812 and pumped into the sample cell by using the small-volume-presentation-unit. Background alignment was performed with pure Miglyol 812 before the powder-dispersion was added. Particle size was evaluated by applying the Fraunhofer theory using a polydisperse mode.

2.8.9 DIGITAL MICROSCOPY

For the visualization of glass and polystyrene particles digital microscopy was performed using the Keyence VHX-500F (Keyence Corporation, Osaka, Japan). The employed magnification was 100 x 50 or 100 x 500.

2.9 CHARACTERIZATION OF OILY ADJUVANTS

2.9.1 ACCELERATED STABILITY TESTING OF OILY ADJUVANTS

In order to investigate if the oily adjuvants were sensitive towards stress conditions during storage at elevated temperatures, the samples were subjected to different accelerated stress conditions. Chemical stress was applied by incubation of the samples with 1 mL 30% hydrogen peroxide or 1 N sodium hydroxide for a time period of 24 hours. UV-light stress was applied in a SUNTEST CPS (Heraeus, Original Hanau,

Germany) at 54 W/m^2 by a Xenon lamp for a time period of 7 days. As UV-light stress caused also heat and thus resulted in increased sample temperatures of 35°C, as a reference samples were additionally exposed to heat stress at 35°C whilst being protected from light by an aluminum cover, respectively.

2.9.2 GAS CHROMATOGRAPHY AND MASS SPECTROMETRY

Gas chromatography and mass spectrometry was accomplished in cooperation with Dr. Christoph Müller (Department Pharmaceutical Chemistry, Munich).

Gas chromatography was performed using a Varian 3800 gas chromatograph connected with a Varian 1177 injector with split/splitless option (Darmstadt, Germany) and a Varian FactorFour$^{TM\ VF}$- 5 ms capillary column (30 m x 0.25 mm inner diameter, 0.25 μm film thickness), in order to quantify and detect changes in the quality of oily adjuvants. One μl of the pre-processed samples was injected with an inlet temperature of 250°C (split 1:25).

Quantification of the oily adjuvant components squalane, squalene and the oily components of MF59 was performed using a Varian Iontrap 2200. After a solvent delay of 8 min the MS scanned from 8-14 min at 50-450 m/z. Data analysis and instrument control was performed with Varian Workstation 6.9 SP 1 software as described by Mueller *et al.* [19].

Quantification of the oily substances paraffin and Freund's incomplete adjuvant was performed by gas chromatography connected with a flame-ionization detector (GC–FID). Analysis was accomplished in cooperation with Dr. Florian Plößl (ZInstSanBW, Munich). Gas chromatography was performed using an Agilent Hewlett Packard 6890 gas chromatograph (Böblingen, Germany), equipped with a split/splitless injector, a flame-ionization detector (FID) and connected to an Agilent 19091J-413 HP-5 5% Phenyl-Methyl-Siloxane capillary column (30 m x 0.32 mm inner diameter, 0.25 μm film thickness). One μl of the pre-processed samples was injected with an inlet temperature of 250°C (split 1:15). Data analysis and instrument control was performed with Agilent ChemStation software.

The method for recovery of the oily substances was validated using a calibration curve of the solutions at 5 different concentrations ranging from 40 – 70 µg/mL. Three individual samples of each concentration were injected 6 times each.

Samples contained approximately 10 mg of the oily substance and 50 mg of OVA loaded powder particles (a trehalose/mannitol formulation with 25 µg/mg OVA). For the extraction of the oily substance 1 mL purified water was added to the sample in order to reconstitute the protein-sugar matrix. One mL of *tert*-butyl-methyl ether (MTBE) containing an internal standard (10 mg/mL 5α-cholestan) was added and the mixture was vortexed for 10 seconds. For the separation of the organic upper layer, the sample was centrifuged at 10,000 rpm for 10 min. After a second solvent extraction step with 1 mL MTBE an aliquot of 1500 µl of the two combined organic upper layers was transferred to another Eppendorf cap containing 40 mg of a mixture of PSA/Na_2SO_4 (1:7). After another mixing and centrifugation step an aliquot of the organic phase was diluted (1:100) with MTBE

Samples containing the oily adjuvant substance as single component (without a protein-sugar matrix) were mixed directly with 1 mL MTBE containing 10 mg/mL 5α-cholestan and 1 mL MTBE. The mixture was diluted 1:100 with MTBE.

2.9.3 REPROCESSING OF SAMPLES WITH OILY ADJUVANTS FOR FURTHER ANALYSIS OF PROTEIN SUGAR MATRIX

Prior to the analysis of the protein formulation for protein stability, the oily substances had to be separated from the protein sugar matrix as the oily adjuvants were shown to interfere with the established analytical methods. Therefore, 1 mL of MTBE was pipetted into the vial containing the sample, vortexed for 10 seconds and transferred subsequently into an Eppendorf cap. The suspension was then centrifuged for 10 seconds at 10000 rpm. The powder pellet was retained for two further washing steps with MTBE, whereas the supernatant was discarded. The powder pellet was dried in a vacuum chamber at 25 mbar for at least four hours at 25°C prior to analysis.

2.10 TESTING OF THE ADHESIVE STRENGTH AT THE INTERFACE BETWEEN PARTICLES AND DEVICE SURFACE

2.10.1 PREPARATION OF THE SAMPLES

Membranes, consisting of metal or plastic material, were covered with a thin film (approximately 10 μL/cm^2) of adhesive and dipped in a bed of particles. The excess of particles was tapped off. The adhesion force of the particles onto the adhesives covered membranes was scrutinized using either a jolting volumeter or a custom made drop apparatus.

2.10.2 JOLTING VOLUMETER

Membranes, prepared as described above, were fixed on the inner surface of a petri dish and were attached headfirst to a jolting volumeter. The particle covered side was turned downwards. The border of the petri-dish served as a spacer to the surface of the jolting volumeter. The mass of remaining particles and adhesive on the membranes after 10, 20, 50, 100 and 500 beats performed by the jolting volumeter was determined gravimetrically.

2.10.3 CUSTOM MADE DROP APPARATUS

A piece of membrane coated with adhesive and particles as described before was fixed in a metal clam and dropped from one meter height using a custom made drop apparatus, charged with 382 g weight, as described by Stabenau *et al.*[20]. By the impact onto two distance pieces at the bottom of the drop apparatus, the metal clam was stopped abruptly from free-falling by a beat. The experiment was repeated 10 times with three replicates. The remained particles and adhesive mass on the membrane was determined gravimetrically.

2.11 BALLISTIC ACCELERATION OF PARTICLES

2.11.1 LELL'S FOUCAULT ACCELERATOR

The Lell's Foucault accelerator is a custom made surrogate accelerator for ballistic acceleration of particles. The repulsive force to accelerate particles is generated by a magnetic field in an electromagnetical coil. Thus a turbulent electrical current is induced in a carrier membrane. Dependent on the pre-selected voltage of the capacitor bank, different particle velocities can be generated. Further approaches for the ballistic acceleration of particles using different actuator mechanisms is described in detail in chapter 7.

2.11.2 VELOCITY MEASUREMENT USING HIGH SPEED CAMERAS

The velocity of particles accelerated by ballistic approaches was measured using two synchronized Flash Cam PCO cameras. The distance of the flight of the particle cloud or single particles was calibrated using a scale. The velocity of the particles was calculated as a quotient of the flight distance and the time frame between the two synchronized cameras.

2.11.3 CONFOCAL LASER SCANNING MICROSCOPY (CLSM)

For the analysis of the penetration depth of fluorescein isothiocyanate (FITC) labelled polystyrene particles in pig skin after ballistic injection a confocal scanning laser microscope (Zeiss LSM 510 Meta Invert Laser Scan Microscope, Carl Zeiss Microscope Systems, Jena, Germany) equipped with an Argon and a HeNe1 laser for excitation was used. 3D images of the samples were obtained using a Z-stacking mode of Zeiss LSM Image Browser software as described by Deng *et al.*[21].

3. REFERENCES

[1]   Huntington JA, Stein PE. Structure and properties of ovalbumin. Journal of Chromatography B: Biomedical Sciences and Applications 2001;756(1–2):189-98.

[2]   Weijers M, Broersen K, Barneveld PA, Cohen Stuart MA, Hamer RJ, De Jongh HHJ, et al. Net Charge Affects Morphology and Visual Properties of Ovalbumin Aggregates. Biomacromolecules 2008;9(11):3165-72.

[3]   Barnden MJ, Allison J, Heath WR, Carbone FR. Defective TCR expression in transgenic mice constructed using cDNA-based [agr]- and [bgr]-chain genes under the control of heterologous regulatory elements. Immunology and Cell Biology 1998;76(1):34-40.

[4]   Brems DN. The kinetics of G-CSF folding. Protein Science 2002;11(10):2504-11.

[5]   Kolvenbach CG, Narhi LO, Philo JS, Li T, Zhang MEI, Arakawa T. Granulocyte-colony stimulating factor maintains a thermally stable, compact, partially folded structure at pH 2. The Journal of Peptide Research 1997;50(4):310-8.

[6]   Rajan RS, Li T, Aras M, Sloey C, Sutherland W, Arai H, et al. Modulation of protein aggregation by polyethylene glycol conjugation: GCSF as a case study. Protein Science 2006;15(5):1063-75.

[7]   Raso SW, Abel J, Barnes JM, Maloney KM, Pipes G, Treuheit MJ, et al. Aggregation of granulocyte-colony stimulating factor in vitro involves a conformationally altered monomeric state. Protein Science 2005;14(9):2246-57.

[8]   Serno T, Härtl E, Besheer A, Miller R, Winter G. The role of polysorbate 80 and HPβCD at the air-water interface of IgG solutions. Pharmaceutical Research 2013;30(1):117-30.

[9]   Klaus W, Gsell B, Labhardt AM, Wipf B, Senn H. The three-dimensional high resolution structure of human interferon α-2a determined by heteronuclear NMR spectroscopy in solution. Journal of Molecular Biology 1997;274(4):661-75.

[10]   Sonner C, Maa Y-F, Lee G. Spray-freeze-drying for protein powder preparation: Particle characterization and a case study with trypsinogen stability. Journal of Pharmaceutical Sciences 2002;91(10):2122-39.

[11]   Schiffter H, Condliffe J, Vonhoff S. Spray-freeze-drying of nanosuspensions: the manufacture of insulin particles for needle-free ballistic powder delivery. Journal of the Royal Society Interface 2010;7(Suppl 4):S483-S500.

[12]   de Groot J, de Jongh HHJ. The presence of heat-stable conformers of ovalbumin affects properties of thermally formed aggregates. Protein Engineering 2003;16(12):1035-40.

[13]   Bajaj H, Sharma VK, Badkar A, Zeng D, Nema S, Kalonia DS. Protein structural conformation and not second virial coefficient relates to long-term irreversible aggregation of a monoclonal antibody and ovalbumin in solution. Pharmaceutical Research 2006;23(6):1382-94.

[14]   Schersch K, Betz O, Garidel P, Muehlau S, Bassarab S, Winter G. Systematic investigation of the effect of lyophilizate collapse on pharmaceutically relevant proteins, part 2: Stability during storage at elevated temperatures. Journal of Pharmaceutical Sciences 2012;101(7):2288-306.

[15]   Tang X, Pikal M. Design of Freeze-Drying Processes for Pharmaceuticals: Practical Advice. Pharmaceutical Research 2004;21(2):191-200.

[16]   Rambhatla S, Ramot R, Bhugra C, Pikal MJ. Heat and mass transfer scale-up issues during freeze drying: II. Control and characterization of the degree of supercooling. AAPS PharmSciTech 2004;5(4):54-62.

[17]   Konstantinidis AK, Kuu W, Otten L, Nail SL, Sever RR. Controlled nucleation in freeze-drying: Effects on pore size in the dried product layer, mass transfer resistance, and primary drying rate. Journal of Pharmaceutical Sciences 2011;100(8):3453-70.

[18]   Schersch K, Betz O, Garidel P, Muehlau S, Bassarab S, Winter G. Systematic investigation of the effect of lyophilizate collapse on pharmaceutically relevant proteins I: Stability after freeze-drying. Journal of Pharmaceutical Sciences 2010;99(5):2256-78.

[19]   Müller C, Staudacher V, Krauss J, Giera M, Bracher F. A convenient cellular assay for the identification of the molecular target of ergosterol biosynthesis inhibitors and quantification of their effects on total ergosterol biosynthesis. Steroids 2013;78(5):483-93.

[20]   Stabenau A. Trocknung und Stabilisierung von Proteinen mittels Warmlufttrocknung und Applikation von Mikrotropfen: München, Ludwig-Maximilians-Universität, Diss. ; 2003.

[21]   Deng Y, Winter G, Myschik J. Preparation and validation of a skin model for the evaluation of intradermal powder injection devices. European Journal of Pharmaceutics and Biopharmaceutics 2012;81(2):360-8.

CHAPTER 3

TOWARD INTRADERMAL VACCINATION: PREPARATION OF POWDER FORMULATIONS BY COLLAPSE FREEZE-DRYING

All experiments presented here were performed by Elsa Etzl, the paper was written by Elsa Etzl. The following chapter would not have been possible without the scientific guidance of my supervisors Gerhard Winter and Julia Engert. Gerhard Winter and Julia Engert are thanked for critical discussion of the experimental layout and for help with the preparation of the manuscript. Julia Engert submitted the manuscript to the Journal.

1   INTRODUCTION

Vaccination is an effective tool to control and eliminate infectious diseases, preventing two to three million deaths each year [1]. However, the administration of liquid vaccines using conventional needles and syringes holds the risk of needle-stick injuries and thereby the transmission of blood-borne diseases. In addition, the administration requires well trained health care personnel [2]. Emerging needle-free injection technologies such as the intradermal powder injection, which is the main focus of our study and is one very specific approach in the area of upcoming needle-free technologies, offer the potential to overcome these issues and furthermore allow the effective targeting of immunocompetent cells in the epidermal or dermal layers of the skin [3, 4]. The use of dried particles for powder injection provides enhanced stability for vaccines and may offer a superior long term stability of the vaccine in comparison to liquid formulations [4]. Particularly with regard to mass vaccination programs in developing countries, the use of dried vaccine particles may permit independency of a cold chain, thereby facilitating the distribution of vaccines.

In order to be suitable for the intradermal delivery, the dried vaccine particles have to fulfill several requirements. Particle characteristics like size, density, shape and morphology have a great influence on the penetration depth of the particles. Particularly a high rigidity of the particles, which is attributed to the particle surface structure and to particle porosity, prevents fragmentation of the particles during acceleration and penetration [5].

Different processes can be used to generate dry vaccine particles for intradermal injection like spray drying, spray freeze-drying, freeze-drying, spray coating or simply desiccation [6-11]. Applying freeze-drying or desiccation requires a subsequent milling step in order to generate particles in the desired size ranges [6, 12]. The use of sugars as excipients to stabilize the vaccine during the preparation process implicates a rather low density of the particles (~700-1200 kg/m³) [13, 14]. Therefore, an appropriate size of the particles of 20 to 70 µm is needed to achieve appropriate physical characteristics for the intradermal injection process [7, 12]. Several approaches have been reported in literature to increase the tap density of the particles. The group of Costantino *et al.* showed that a high solid content of the liquid formulation is necessary to obtain particles

of high density, when particles are produced by spray-freeze-drying [15]. The group of Maa *et al.* stated that the formulation composition as well as the solid content of the formulation have an influence on the resulting particle morphology and tap density of the particles [6]. Similar results were obtained by the group of Schiffter *et al.* [11]. They were able to increase the density of sugar particles prepared by spray-freeze-drying by increasing the solid content of the spraying solution and by the formulation composition. The addition of the polymer dextran in a ternary mixture with mannitol and trehalose and 35% (w/w) led to shrinkage of the particles. The tap density of the powder was maximized to 0.72 g/cm³ using this approach. However, high molecular weight polymers like dextran might lead to phase-separation and have a poor protein stabilizing effect [10]. Also the increase of the total solid content of the formulation was limited to 35% (w/w) due to the high viscosity of the formulation which also complicates several manufacturing steps [6, 16].

Besides the physical characteristics, the particles also have to maintain physical and chemical integrity of the incorporated vaccine in addition to a high loading capacity of the vaccine antigen [17], as only a limited amount of powder can be injected into the skin. Particles based on sugar matrices also bear the potential for the incorporation of substructures like nanoparticulate carriers, which are preferentially internalized by the Langerhans cells [18].

In this study we investigated the development of protein loaded powder particles that fulfill the requirements for intradermal injection. Two different formulations, based on trehalose and a ternary combination of trehalose, mannitol and dextran with total solid contents ranging from 15% to 35% (w/w) were investigated. The ternary mixture of trehalose, mannitol and dextran was chosen as it was found in literature to be appropriate to generate high density spray-freeze-dried particles with appropriate characteristics for intradermal injection [10].

Ovalbumin was chosen as model antigen. Powder particles for intradermal powder injection were prepared by freeze-drying and subsequent cryo-milling. An aggressive freeze drying cycle was applied similar to the method published by Schersch *et al.*, leading to a controlled collapse of the sugar matrix [19, 20]. Most importantly, using an

aggressive freeze-drying-cycle a much more dense structure of the freeze dried cake can be obtained.

We investigated the effect of collapse freeze-drying on particle morphology and protein quality in comparison to a conventional moderate freeze-drying cycle. We scrutinized the effect of formulation composition as well as the total solid content of the formulation. Samples were analyzed after the cryo-milling process for particle size, density, specific surface area and residual moisture as well as protein stability. Long term storage stability at 2-8°C and 50°C was also investigated.

2   FORMULATION PREPARATION AND LYOPHILIZATION PROCESS

In this study we explored the possibility to combine the approach of collapse freeze-drying with a subsequent cryo-milling-step of the lyophilizates. A controlled collapse of a sugar matrix, induced by an aggressive freeze-drying cycle, offers the potential to generate collapsed lyophilizates with a dense matrix structure and reduced surface porosity without having negative effects on protein stability [20].

Regarding a conventional freeze-drying cycle, the degree of super-cooling influences the cake structure and thereby the sublimation rates as well as other product parameters like specific surface area and residual moisture [21, 22]. However, in the case of the aggressive freeze-drying cycle used in this study, the cake structure is re-built during the drying process as the collapse temperature of the formulations is exceeded [19].

The subsequent cryo-milling of the lyophilizates generates particles in the desired size range with high density and appropriate properties for intradermal injection. A second objective was to investigate the role of formulation composition and the total solid content of the formulation on particle density, and on particle morphology by applying the collapse freeze-drying cycle. Two different formulations based on trehalose and a ternary combination of trehalose, mannitol and dextran were prepared with 15%, 25% and 35% (w/w) total solids content.

Table 3.1: Viscosity of the liquid formulations obtained at a shear rate of 100 (1/s).

formulation composition	viscosity [mPa*s] at shear rate 100 [1/s]
trehalose 15% (w/w) solid content	1.95 ± 0.25
trehalose 25% (w/w) solid content	2.24 ± 0.29
trehalose 35% (w/w) solid content	3.19 ± 0.51
trehalose/mannitol/dextran 15% (w/w) solid content	4.10 ± 0.62
trehalose/mannitol/dextran 25% (w/w) solid content	11.15 ± 0.13
trehalose/mannitol/dextran 35% (w/w) solid content	35.50 ± 2.63

The preparation of the liquid formulation was complicated with increasing solid contents of the formulation by the viscosity of the formulations. Table 3.1 shows that the viscosity of the formulations, which all show Newtonian behavior, increased drastically with increasing solid content. The trehalose/mannitol/dextran formulation at 15% (w/w) showed a higher viscosity (4.10 ± 0.62 mPa*s) than the trehalose formulation with 35% (w/w) (3.19 ± 0.51 mPa*s). The viscosity of the trehalose/mannitol/dextran formulation increased up to 35.50 ± 2.63 mPa*s at 35% (w/w), leading to difficulties during the filtration of the liquid formulation as it required high pressure forces. Freeze-drying was performed using a conventional, moderate freeze-drying cycle and an aggressive freeze-drying cycle.

The macroscopic appearance of the freeze-dried cakes was investigated by visual inspection. Collapse-drying of the formulations resulted in completely collapsed cakes, exhibiting a foam-like structure, whereas formulations freeze-dried after the moderate freeze-drying protocol resulted in elegant, porous, non-collapsed cakes (figure 3.1).
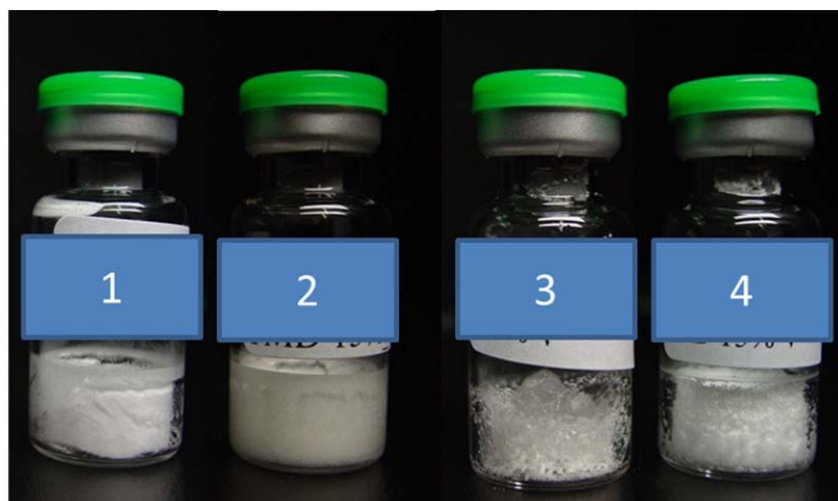
Figure 3.1: Macroscopic appearance of lyophilizates after moderate and collapse freeze-drying: (1) moderate freeze-dried trehalose lyophilizate, (2) moderate freeze-dried trehalose/mannitol/dextran lyophilizate, (3) collapse freeze-dried trehalose lyophilizate and (4) collapse freeze-dried trehalose/mannitol/dextran lyophilizate.
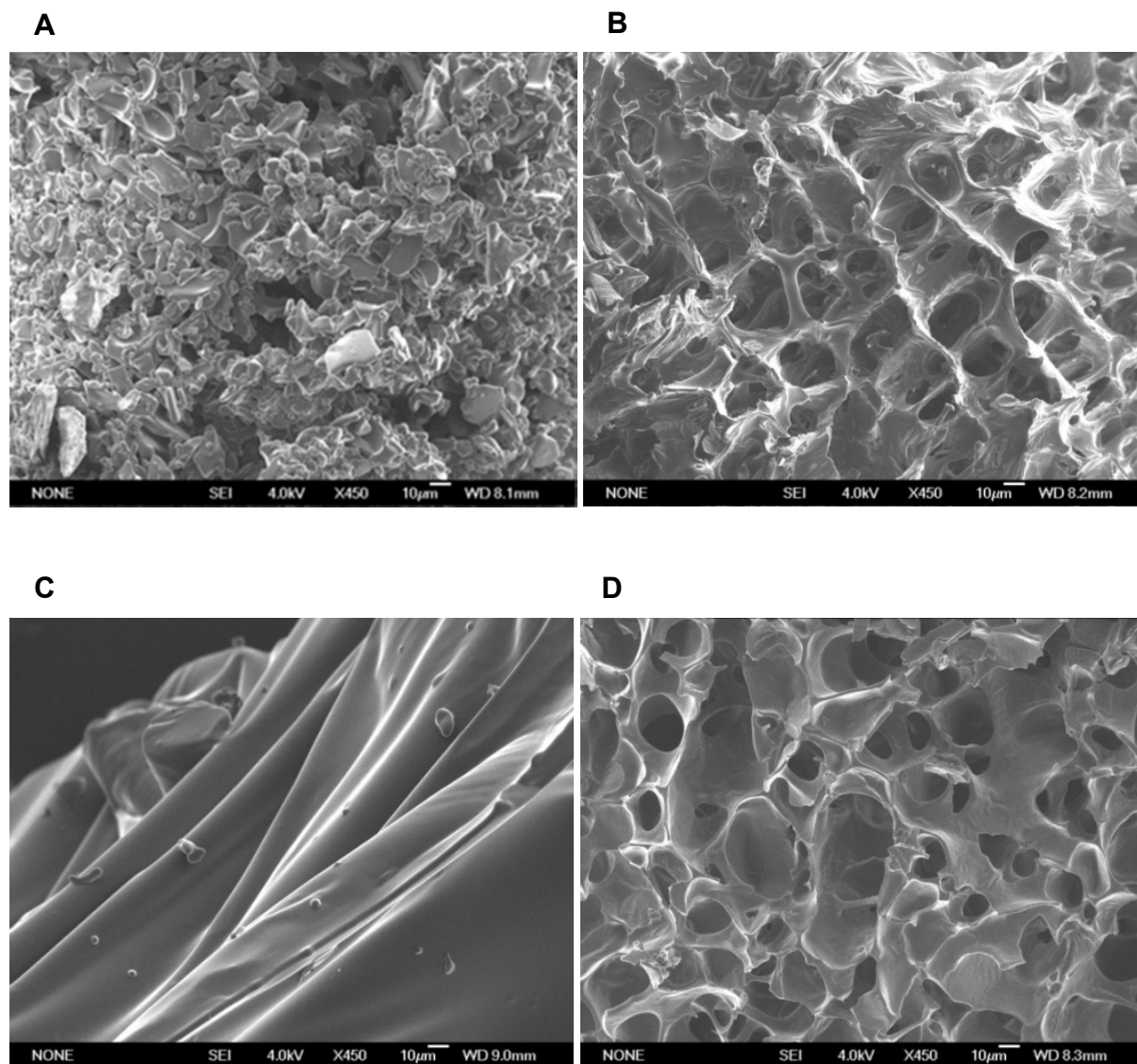
Figure 3.2: Scanning electron micrographs of lyophilizate cakes after moderate and collapse freeze-drying. Magnification 450x. (A) Moderate freeze-dried trehalose lyophilizate, (B) moderate freeze-dried trehalose/mannitol/dextran lyophilizate, (C) collapse freeze-dried trehalose lyophilizate and (D) collapse freeze-dried trehalose/mannitol/dextran lyophilizate.

However, trehalose based lyophilizates underwent slightly partially collapse in form of slight cake shrinkage even after application of the moderate freeze-drying protocol. Scanning electron micrographs showed a very smooth and dense matrix structure of the collapse freeze-dried trehalose lyophilizates, whilst moderate freeze-dried trehalose lyophilizates revealed a more porous cake structure, as commonly described in

literature (figure 3.2). Morphological differences between collapse-dried and moderate freeze-dried lyophilizates were less pronounced in trehalose/mannitol/dextran formulations.

The impact of formulation composition and the freeze-drying process on the morphology of the lyophilizates was also analyzed by X-ray powder diffraction.
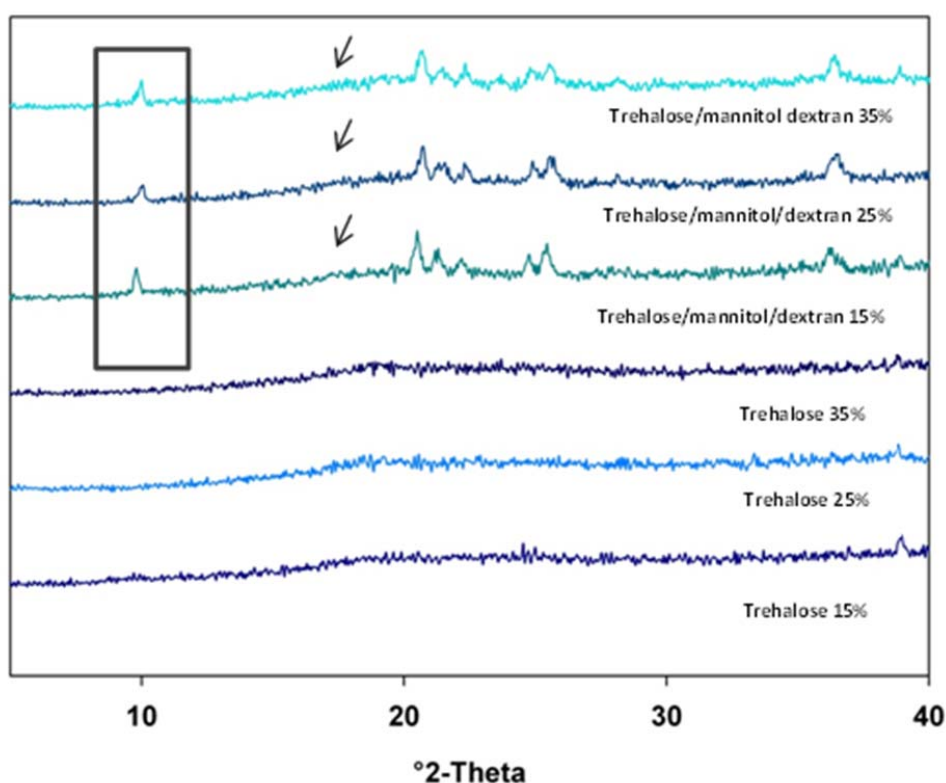
Figure 3.3: Exemplary XRD patterns of cryo-milled lyophilizates after collapse freeze-drying. The morphological pattern did not change also after 12 months of storage at 2-8°C. Peaks at 9.7°2-Theta (emphasized with a frame) in combination with the absence of peaks at 17.9°2-Theta (indicated by arrows) are characteristic for the δ-modification of mannitol.

Formulations based on trehalose formed an amorphous sugar matrix during freeze-drying, whilst the ternary formulation of trehalose, mannitol and dextran showed a partly crystalline structure due to the bulking agent mannitol. Mannitol crystallized into the δ-modification during freeze-drying as confirmed by the characteristic XRD-patterns. The

δ-modification of mannitol is characterized by peaks at 9.7 °2-Theta, whilst no peaks are apparent at 17.9 °2-Theta (figure 3.3).

Despite the reduced drying time, the residual moisture content of the collapse freeze-dried lyophilizates was comparable to the residual moisture content of moderate freeze-dried lyophilizates (figure 3.4).
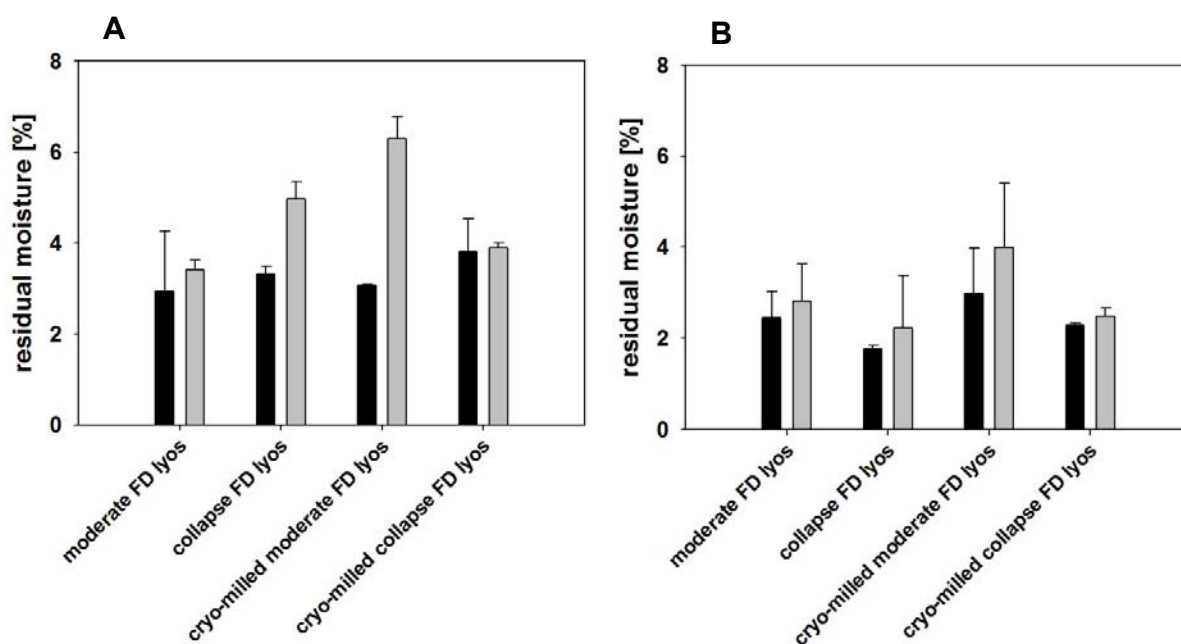
Figure 3.4: Residual moisture levels of moderate and collapse freeze-dried lyophilizates before and after cryo-milling and after 12 months storage at 2-8°C. (A) Trehalose formulations with 15% (w/w) at the beginning of the study (black bars) and after 12 months storage at 2-8°C (grey bars). (B) Trehalose/mannitol/dextran formulations with 15% (w/w) at the beginning of the study (black bars) and after 12 months storage at 2-8°C (grey bars).

The residual moisture level of moderate freeze-dried trehalose lyophilizates was approximately 2.9%, whereas the residual moisture level of collapse freeze-dried trehalose lyophilizates was 3.3%. Moderate freeze-dried trehalose/mannitol/dextran formulations had residual moisture levels of 2.5%, whilst collapse freeze-drying of this composition resulted in 1.8% residual moisture. In general, formulations containing a mixture of trehalose, mannitol and dextran had lower residual moisture levels in comparison to trehalose formulations. This can be attributed to the content of the crystalline bulking agent mannitol in the formulation.

3   INFLUENCE OF THE CRYO-MILLING PROCESS ON PARTICLE MORPHOLOGY

In order to generate particles suitable for intradermal injection, the lyophilizates had to be further processed by milling. In general, milling applies mechanical stress to the product, which is turned into heat and surface energy and is associated with newly created particle surfaces [23]. Cryo-milling involves a cooling step of the lyophilizates by the use of liquid nitrogen and thereby decreases the product temperature to -130°C prior to the milling process. This step makes the lyophilizates brittle and in addition absorbs most of the heat that is created during the milling process. Cryo-milling was performed using a swing mill MM301 (Retsch Technology, Haan, Germany) as described in Chapter 2.

In our study, cryo-milling of the lyophilizates resulted in irregularly shaped particles as observed by scanning electron microscopy (figure 3.5). Particles based on trehalose showed a very smooth surface, whereas trehalose/mannitol/dextran particles were square edgily shaped.

The median volume diameter of the cryo-milled particles varied between 23.2 ± 2.2 μm and 25.8 ± 1.9 μm for the moderate freeze-dried trehalose formulations and between 25.7 ± 0.9 μm and 31.4 ± 4.2 μm for the collapse freeze-dried trehalose formulations (table 3.2). The span of the volume distribution indicates a narrow particle size distribution.

Lyophilizates consisting of the ternary combination of trehalose/mannitol and dextran resulted in slightly larger particles, what might be due to a higher rigidity of the cakes. As the rigidity of collapse freeze dried trehalose/mannitol/dextran lyophilizates with 35% (w/w) exceeded the rigidity of the other formulations, it was necessary to adjust the cryo-milling protocol in order to result in comparable particle sizes. For these formulations the total milling time was set to 30 seconds instead of 10 seconds. A comparable particle size of the different formulations was in the main focus of the project as this allows us to compare the specific surface area of the particles among each other. The specific surface area of the particles served as a parameter for the extent of collapse and is related to highly dense, robust and most likely stable particles.

Subsequent experiments showed that the prolongation of the milling time to 30 seconds did not decrease further the particle size of trehalose lyophilizates (data not shown).

A

B

C

D
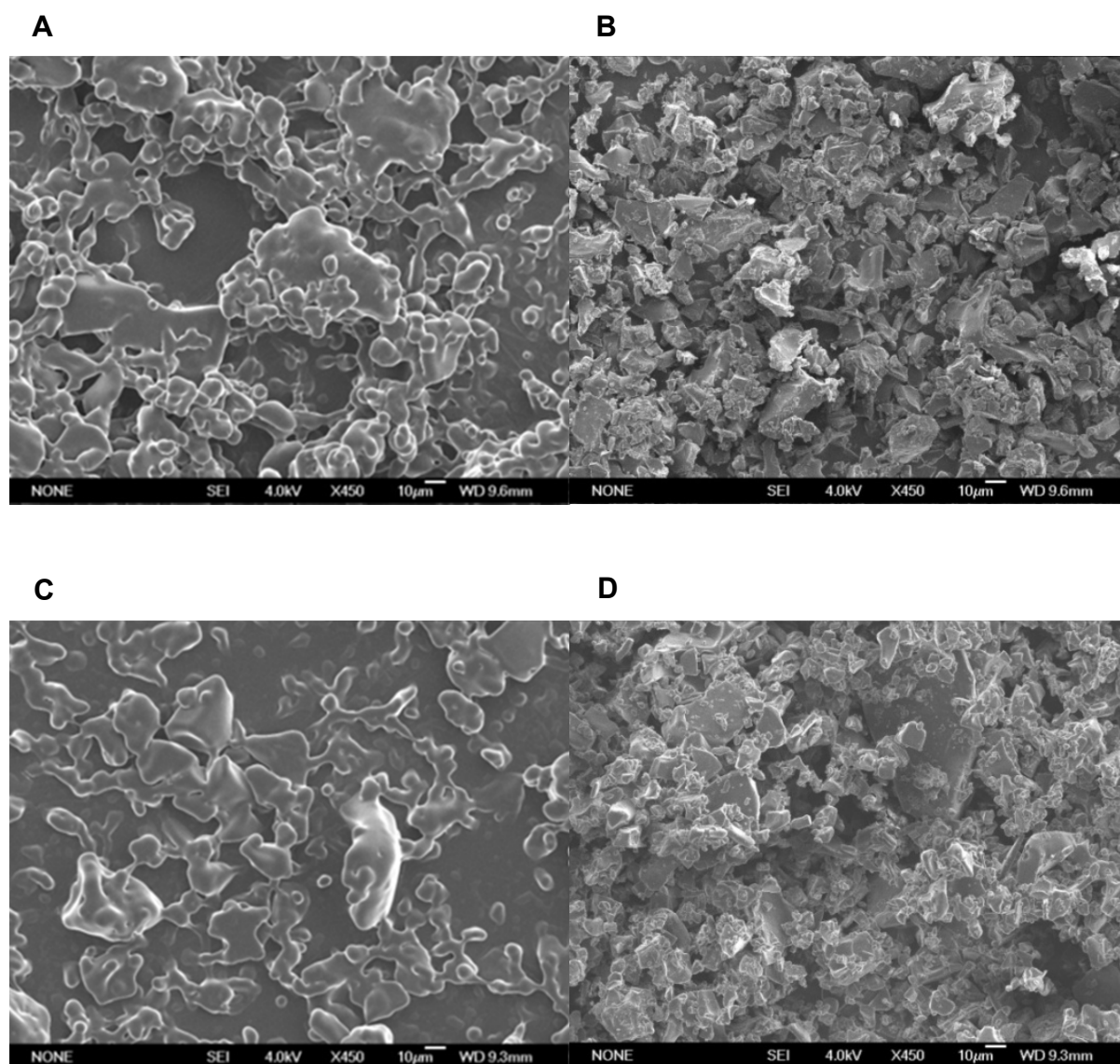
Figure 3.5: Scanning electron micrographs of cryo-milled particles after moderate and collapse freeze-drying. Magnification 450x. (A) Moderate freeze-dried trehalose particles, (B) moderate freeze-dried trehalose/mannitol/dextran particles, (C) collapse freeze-dried trehalose particles and (D) collapse freeze-dried trehalose/mannitol/dextran particles.

Table 3.2: Particle size distribution of cryo-milled powders calculated as an average of 6 measurements and characterized with median diameter and span of the volume distribution.

cryo-milled powders	median particle size [µm]			
	collapse freeze-dried	span	moderate freeze-dried	span
trehalose 15% (w/w) solid content	27.0 ± 4.3	3.0 ± 2.1	23.2 ± 2.2	6.7 ± 3.0
trehalose 25% (w/w) solid content	25.7 ± 0.9	1.6 ± 0.1	24.8 ± 2.7	2.8 ± 1.1
trehalose 35% (w/w) solid content	31.4 ± 4.2	3.1 ± 0.6	25.8 ± 1.9	3.0 ± 1.4
trehalose/mannitol/dextran 15% (w/w) solid content	42.9 ± 8.0	3.8 ± 1.6	33.2 ± 0.6	3.1 ± 1.4
trehalose/mannitol/dextran 25% (w/w) solid content	39.0 ± 2.5	3.0 ± 0.3	37.0 ± 1.9	2.4 ± 0.1
trehalose/mannitol/dextran 35% (w/w) solid content	23.5 ± 1.2 *	4.5 ± 0.0	47.2 ± 4.9	3.6 ± 0.4

* Collapse freeze-dried trehalose/mannitol/dextran lyophilizates with 35% (w/w) were milled for 30 seconds, whereas all other lyophilizates were milled for 10 seconds.

XRD-analysis of the particles showed, that cryo-milling did not change the crystallinity of the formulations. Formulations based on trehalose remained amorphous and also the crystalline structure of trehalose/mannitol/dextran formulations was not altered (figure 3.3).

Cryo-milling did only slightly increase the residual moisture levels of the lyophilizates (figure 3.4). However, a distinct increase in the residual moisture levels of cryo-milled moderate freeze-dried trehalose particles was observed after storage at 2-8°C for 12 months. This will be discussed more in detail in section 5.

In summary, cryo-milling was found to be appropriate to generate particles in the desired size range without altering particle morphology or strongly increasing the residual moisture level of the particles. The influence of the cryo-milling process on protein stability will be discussed in section 5.

4 INFLUENCE OF THE COLLAPSED MATRIX STRUCTURE ON PARTICLE MORPHOLOGY

The moisture sorption properties of pharmaceutical formulations have an impact on their storage stability [24]. We expected a reduction of the moisture uptake of particles due to the reduction of their specific surface area when prepared by the collapse-freeze-drying process. However, collapse freeze-dried particles showed only small differences in their vapor-adsorption curves in comparison to moderately freeze-dried particles (figure 3.6).
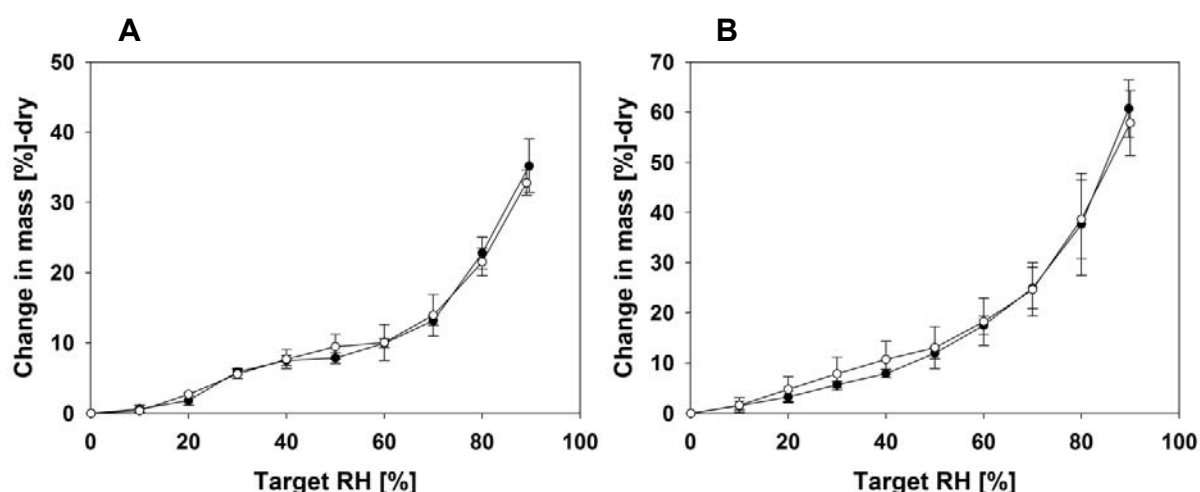
Figure 3.6: Moisture sorption properties of moderate and collapse freeze-dried cryo-milled lyophilizates after exposure to 0-90% relative humidity. The temperature was constantly held at 25°C during the measurement. (A) Collapse freeze-dried trehalose particles (filled circle) and moderate freeze-dried trehalose (open circle). (C) Collapse freeze-dried trehalose/mannitol/dextran particles (filled circle) and moderate freeze-dried trehalose/mannitol/dextran particles (open circle).

Trehalose particles showed less water vapor uptake above 50% relative humidity than trehalose/mannitol/dextran formulations. This may be attributed to the hygroscopic characteristic of the polymer dextran, as it is capable to sorb 10-20% moisture at 50% relative humidity [25].

It is reported in literature that a high density of the particles is required, with a tap density ≥ 0.5 g/cm³ for effective skin penetration [6]. In our study, we achieved high powder tap densities by applying the collapse freeze-drying cycle. Trehalose

formulations reached a tap density of 0.739 g/cm³ and trehalose/mannitol/dextran formulations 0.771 g/cm³ (table 3.3), respectively. The tap density of collapse dried powder particles was increased in comparison to moderate freeze dried particles (table 3.3). With rising solid content of the formulation, a further increase in tap density up to 0.903 g/cm³ was observed.

Table 3.3: True and tap density values for collapse and moderate freeze-dried lyophilizates after cryo-milling. Hausner factor was calculated from the quotient of tap and bulk density.

formulation composition	true density [g/cm³]		tap density [g/cm³]	
	collapse freeze-dried	moderate freeze-dried	collapse freeze-dried	moderate freeze-dried
trehalose 15% (w/w) solid content	1.532 ± 0.002	1.528 ± 0.001	0.739 ± 0.023	0.671 ± 0.031
trehalose 25% (w/w) solid content	1.521 ± 0.002	1.528 ± 0.001	0.806 ± 0.024	0.671 ± 0.020
trehalose 35% (w/w) solid content	1.517 ± 0.001	1.532 ± 0.001	0.878 ± 0.007	0.705 ± 0.028
trehalose/mannitol/dextran 15% (w/w) solid content	1.492 ± 0.002	1.511 ± 0.002	0.771 ± 0.005	0.654 ± 0.002
trehalose/mannitol/dextran 25% (w/w) solid content	1.489 ± 0.003	1.509 ± 0.002	0.869 ± 0.002	0.716 ± 0.026
trehalose/mannitol/dextran 35% (w/w) solid content	1.494 ± 0.002	1.507 ± 0.001	0.903 ± 0.030	0.739 ± 0.033

The true density of the formulations is not much influenced by the kind of freeze-drying cycle or the solid content of the formulation, but by the composition of the formulation. Formulations based on trehalose have a slightly higher true density (1.517 – 1.532 g/cm³) as formulations based on the ternary composition of trehalose, mannitol and dextran (1.489 – 1.511 g/cm³) (table 3.3).

The specific surface area (SSA) is an important parameter to characterize the structure of dried matrices. Compared to the true density of the formulations, it allows a more accurate differentiation of the densification of the sugar matrix due to the kind of the applied freeze-drying cycle. The collapse of the sugar matrix led to a strong reduction of the specific surface area of the lyophilizates.
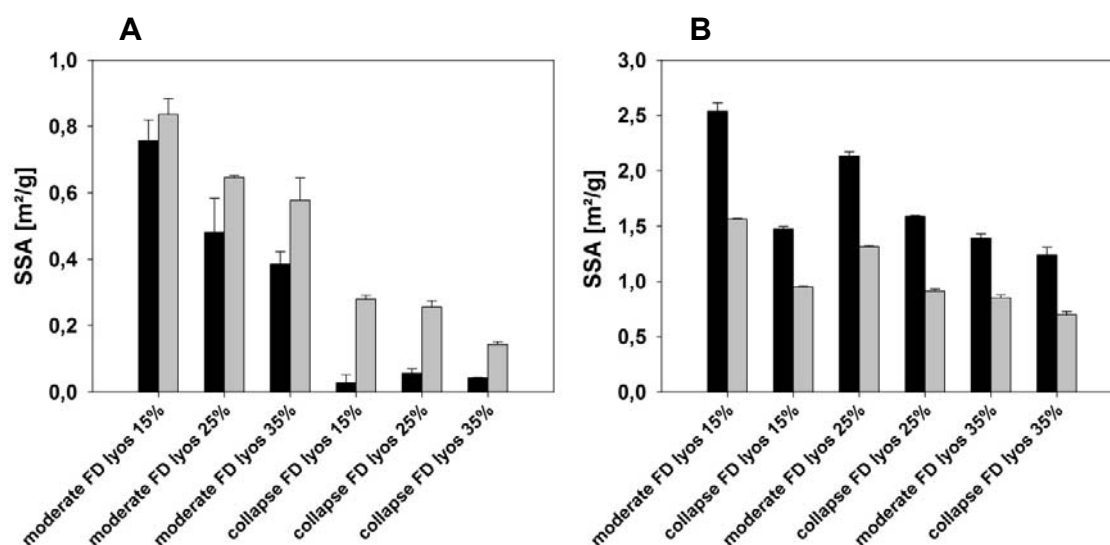
Figure 3.7: Specific surface area (SSA) of (A) trehalose (black bars) and trehalose/mannitol/dextran formulations (grey bars) generated by moderate and collapse freeze-drying as determined by BET gas adsorption. (B) SSA of the cryo-milled powder particles. Trehalose formulations are indicated with black bars and trehalose/mannitol/dextran formulations are indicated with grey bars.

Collapse freeze-dried trehalose lyophilizates (15% (w/w)) showed a SSA of 0.028 ± 0.025 m²/g, moderate freeze-dried lyophilizates of 0.757 ± 0.062 m²/g (figure 3.7 A). The SSA of trehalose/mannitol/dextran lyophilizates was reduced from 0.836 ± 0.048 m²/g to 0.279 ± 0.012 m²/g. Hence, the collapse of the sugar matrix resulted in a reduction of the SSA of trehalose lyophilizates down to 3.7 % and in trehalose/mannitol/dextran formulations down to 33%. Abdul Fattah and colleagues obtained comparable results in an amorphous sugar matrix applying foam drying [26]. Furthermore, Abdul Fattah *et al.* were able to show that the reduced surface area of the lyophilizates, which was obtained by foam drying, increased the stability of the incorporated vaccine. Similar stabilization trends were also obtained investigating spray-freeze-dried BSA particles stabilized with trehalose or mannitol. Costantino *et al.* correlated the specific surface area of the particles with the monomer loss of BSA and thereby demonstrated a stabilizing effect on the protein by reduction of the SSA [15].

Expectedly, cryo-milling resulted in an increase of the SSA in all formulations (figure 3.7 B) due to the formation of small particles in the range of 23.24 to 65.60 µm size. The

relatively smaller SSA of the particles after collapse drying of the sugar matrix was maintained also after the cryo-milling process compared to moderate dried particles.

The SSA of moderate freeze-dried cryo-milled powders was also lower for formulations with higher solid content [6]. Notably, this effect was less pronounced in collapse freeze-dried cryo-milled powders.

Besides the economic advantages of the collapse freeze-drying process, we were able to obtain powder particles with a small surface area. A small surface area is related to highly dense, robust and most likely stable particles. During intradermal injection, particles are accelerated to high velocities, even above the sonic barrier. Therefore particles have to be robust and require a highly dense structure, so that they are able to breach the outermost barrier of the skin, the stratum corneum.

5 PROTEIN STABILITY AFTER CRYO-MILLING AND STORAGE

The protein stability of ovalbumin was assessed by size exclusion chromatography and light obscuration. Regarding the results obtained by size exclusion chromatography, the freeze-drying process and also the cryo-milling process had no influence on the stability of ovalbumin (table 3.4).

Table 3.4: Recovery of soluble monomer [%] of ovalbumin of moderate and collapse freeze-dried samples with 15% (w/w) as determined by size-exclusion chromatography.

	after lyophilisation	after cryo-milling	after 12 months storage
trehalose collapse freeze-dried	100.15 ± 0.02	100.55 ± 0.14	100.61 ± 0.42
trehalose moderate freeze-dried	100.10 ± 0.01	100.02 ± 0.14	101.24 ± 0.05
trehalose/mannitol/dextran collapse freeze-dried	99.99 ± 0.08	99.81 ± 0.19	100.22 ± 0.22
trehalose/mannitol/dextran moderate freeze-dried	100.01 ± 0.01	100.05 ± 0.07	100.52 ± 0.10

There was no change in the recovery of soluble monomer of ovalbumin, neither after the moderate nor after the collapse freeze-drying cycle (table 3.4). These results confirm the findings of Schersch *et al.*, that an aggressive freeze-drying cycle, leading to a collapse of the sugar matrix, does not result in a detrimental effect on protein stability [20]. Also the cryo-milling process did not influence monomer recovery. All powder formulations remained stable during storage at 2-8°C for 12 months.

However, an additional stability study at elevated temperature (50°C) over a time period of 12 weeks showed a negative influence of formulations containing dextran on the stability of ovalbumin. Though none of the glass transition temperatures of the formulations was lower than the storage temperature, a slight increase of higher molecular weight aggregate species was observed after 12 weeks of storage at 50°C in trehalose/mannitol/dextran (70 kDa) formulations. No change in the recovery for soluble aggregates was found in trehalose formulations (figure 3.8).
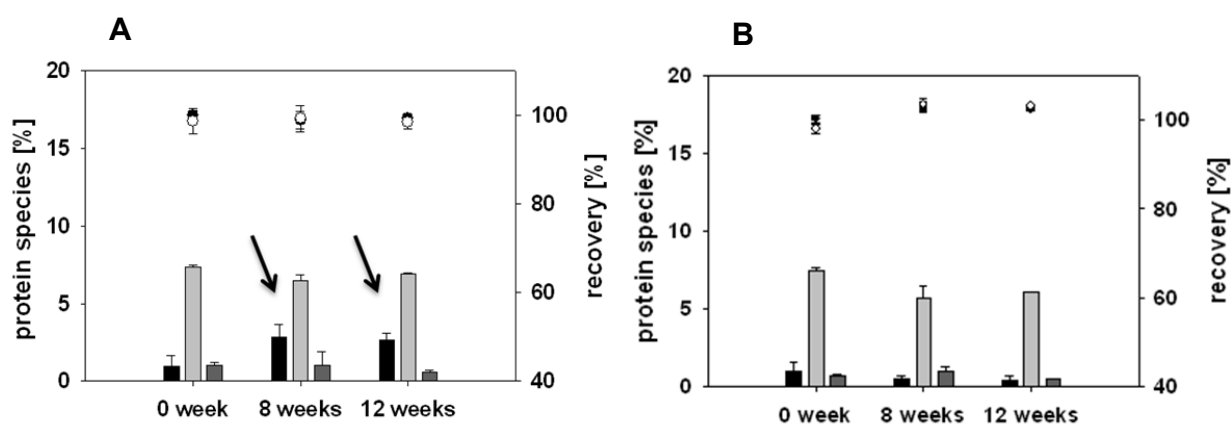
Figure 3.8: Recovery of ovalbumin protein species [%] in trehalose/mannitol/dextran formulations (A) and trehalose formulations (B) as determined by size-exclusion chromatography after 0, 8 and 12 weeks of storage at 50°C. Higher molecular weight aggregates (black bars), dimers (grey bars), fragments (dark grey bars). Recovery of soluble monomer [%] (filled circle), total protein recovery [%] (open circle). The increase of higher molecular weight aggregates after 8 and 12 weeks of storage at 50°C are indicated with black arrows.

Formulations containing the polymer dextran seem to be detrimental for protein integrity during storage at elevated temperatures. These results are also supported by light obscuration and turbidity measurements (data not shown). A destabilizing effect of higher molecular weight polymers on bovine liver catalase during spray freeze-drying was also observed by Rochelle *et al.* [10]. Whilst the addition of polymers into spray-freeze-dried formulations is necessary to obtain appropriate particle morphology and density for intradermal injection, this need can also be fulfilled by applying collapse freeze-drying and subsequent cryo-milling.

The formation of insoluble aggregates in the liquid formulations as well as in the reconstituted lyophilizates and cryo-milled powders was assessed by light obscuration. The increase in particle count can be attributed to the formation of protein aggregates; no increase in particle counts was determined in cryo-milled placebo lyophilizates, excluding that abrasion had created particulate matter (data not shown). The cumulative particle counts > 1 μm of the samples increased after freeze-drying in comparison to the

particle counts in the liquid formulation before drying. This was observed in both moderate and collapse freeze-dried formulations. However, collapse freeze-dried trehalose formulations showed only a small increase in particle counts > 1 µm in comparison to the moderate freeze-drying cycle (figure 3.9 A). Trehalose/mannitol/dextran formulations showed already in the liquid formulation higher particle counts than trehalose formulations. An increase in particles > 10 µm was observed in moderate freeze-dried samples, whereas no increase in the particle count > 10 µm was visible in collapse freeze-dried lyophilizates (figure 3.9 B).
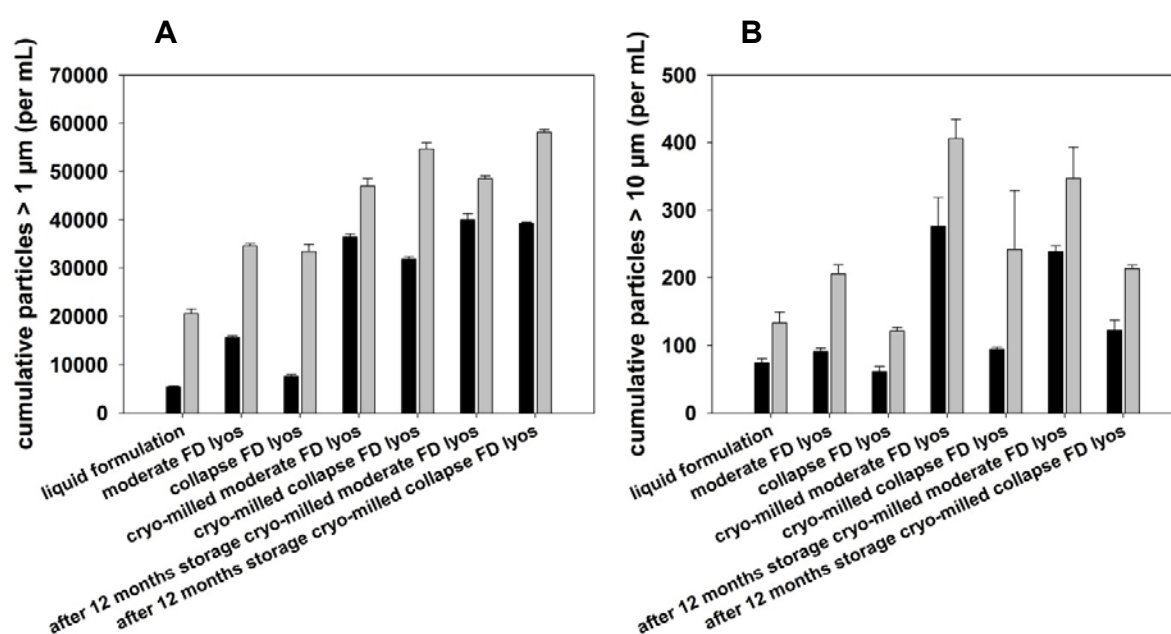
Figure 3.9: Cumulative particle counts (A) > 1 µm per ml and (B) > 10 µm per ml in trehalose (black bars) and trehalose/mannitol/dextran formulations (grey bars) with 15% (w/w) as measured by light obscuration.

After cryo-milling, the cumulative particle count > 1 µm increased in both formulations independent of the kind of freeze-drying process (figure 3.9 A). Though regarding the cumulative particle counts > 10, cryo-milling resulted in higher particle counts in moderate freeze-dried lyophilizates (figure 3.9 B) in comparison to collapse freeze-dried lyophilizates. Collapse freeze-drying shows herein a superior protein stabilizing effect in

comparison to moderate freeze-drying. Trehalose/mannitol/dextran formulations showed after each processing step a generally higher particle count than trehalose formulations. The particle count did not further increase after storage at 2-8°C for 12 months. Neither the secondary structure, nor the tertiary structure, nor the activity of ovalbumin were assessed in this study. Therefore, we cannot predict if the collapse might induce any changes or inactivation even without the formation of aggregates.

After 12 months storage at 2-8°C the residual moisture content increased in cryo-milled moderate freeze-dried trehalose particles (figure 3.4). This was not the case for cryo-milled collapse freeze-dried trehalose particles. Also an increase in the residual moisture level of collapse freeze-dried trehalose lyophilizates was observed. All other lyophilizates and milled powder particles showed just a slight increase in their residual moisture levels after storage. It was reported in literature that moisture transfer from stoppers or the vapors permeability of stoppers have to be taken into count as possible causes for moisture increase of lyophilizates during storage [27-30]. Generally, an increase in moisture levels during storage is related to an adverse effect on protein stability [31-33]; however, this could not be confirmed in this study for ovalbumin in trehalose formulations during storage at 2-8°C for 12 months.

XRD-analysis showed that storage over 12 months at 2-8°C did not influence the amorphous structure and crystallinity of the trehalose or trehalose/mannitol/dextran formulations (figure 3.3).

We were able to show that collapse freeze-drying and subsequent cryo-milling of the lyophilizates generated dense particles with a low specific surface area, independent of the formulation composition or the total solid content of the formulation. Furthermore protein stability of the model antigen ovalbumin could be preserved in trehalose based formulations over a storage period of 12 months at 2-8°C and 50°C (figure 3.8). Further investigations in order to see if this process is also applicable to other model proteins will be discussed in chapter 4.

6 SUMMARY AND CONCLUSION

We established a process to generate particles suitable for intradermal injection by combining the collapse-freeze-drying process with subsequent cryo-milling of the lyophilizates. Collapse freeze-drying provides lyophilizates with a very dense matrix structure and low specific surface area. Subsequent cryo-milling of the cakes was found to be an appropriate method to generate particles in the desired size range and with a narrow size distribution without having a negative influence on the stability of ovalbumin. Particles of high density were generated by applying this approach, independent of the formulations composition or the solid content of the formulation. The collapse freeze-drying process is, in comparison to a standard lyophilization process, a rather fast drying-process, reducing costs by saving drying time and can be easily combined with a subsequent cryo-milling step.

7 REFERENCES

[1] WHO. Saftey of Injections:Global Facts and Figures. World Health Organization, Geneva: World Health Organization, 2004.

[2] Kermode M. Unsafe injections in low-income country health settings: need for injection safety promotion to prevent the spread of blood-borne viruses. Health promotion international 2004;19(1):95-103.

[3] Mitragotri S. Immunization without needles. Nature Reviews Immunology 2005;5(12):905-16.

[4] Chen D, Maa Y-F, Haynes JR. Needle-free epidermal powder immunization. Expert Review of Vaccines 2002;1(3):265-76.

[5] Ziegler A, Simon S, Lee G. Comminution of carbohydrate and protein microparticles on firing in a ballistic powder injector. Journal of Pharmaceutical Sciences 2010;99(12):4917-27.

[6] Maa Y-F, Ameri M, Shu C, Payne LG, Chen D. Influenza vaccine powder formulation development: spray-freeze-drying and stability evaluation. Journal of Pharmaceutical Sciences 2004;93(7):1912-23.

[7] Maa Y-F, Ameri M, Shu C, Zuleger CL, Che J, Osorio JE, et al. Hepatitis-B Surface Antigen (HBsAg) Powder Formulation: Process and Stability Assessment. Current Drug Delivery 2007;4:57-67.

[8] Maa Y-F, Zhao L, Payne LG, Chen D. Stabilization of alum-adjuvanted vaccine dry powder formulations: Mechanism and application. Journal of Pharmaceutical Sciences 2002;92(2):319-32.

[9] Sonner C, Maa Y-F, Lee G. Spray-freeze-drying for protein powder preparation: Particle characterization and a case study with trypsinogen stability. Journal of Pharmaceutical Sciences 2002;91(10):2122-39.

[10] Rochelle C, Lee G. Dextran or hydroxyethyl starch in spray-freeze-dried trehalose/mannitol microparticles intended as ballistic particulate carriers for proteins. Journal of Pharmaceutical Sciences 2007;96(9):2296-309.

[11] Schiffter H, Condliffe J, Vonhoff S. Spray-freeze-drying of nanosuspensions: the manufacture of insulin particles for needle-free ballistic powder delivery. Journal of the Royal Society Interface 2010;7(Suppl 4):S483-S500.

[12] Chen D, Endres RL, Erickson CA, Weis KF, McGregor MW, Kawaoka Y, et al. Epidermal immunization by a needle-free powder delivery technology: Immunogenicity of influenza vaccine and protection in mice. Nature Medicine 2000;6(10):1187-90.

[13] Hardy MP, Kendall MAF. Mucosal deformation from an impinging transonic gas jet and the ballistic impact of microparticles. Physics in Medicine and Biology 2005;50(19):4567.

[14] Chen D, Erickson CA, Endres RL, Periwal SB, Chu Q, Shu C, et al. Adjuvantation of epidermal powder immunization. Vaccine 2001;19(20-22):2908-17.

[15] Costantino H, R. , Laleh F, Chichih W, Karen GC, Kai G, Stephen EZ, et al. Protein spray freeze drying. 2. Effect of formulation variables on particle size and stability. Journal of Pharmaceutical Sciences 2002;91(2):388-95.

[16] Shire SJ, Shahrokh Z, Liu J. Challenges in the development of high protein concentration formulations. Journal of Pharmaceutical Sciences 2004;93(6):1390-402.

[17] Amorij J-P, Hinrichs WLJ, Frijlink HW, Wilschut JC, Huckriede A. Needle-free influenza vaccination. Lancet Infectious Diseases 2010;10(10):699-711.

[18] Noh Y-W, Jang Y-S, Ahn K-J, Lim YT, Chung BH. Simultaneous in vivo tracking of dendritic cells and priming of an antigen-specific immune response. Biomaterials 2011;32(26):6254-63.

[19] Schersch K, Betz O, Garidel P, Muehlau S, Bassarab S, Winter G. Systematic investigation of the effect of lyophilizate collapse on pharmaceutically relevant proteins I: Stability after freeze-drying. Journal of Pharmaceutical Sciences 2010;99(5):2256-78.

[20] Schersch K, Betz O, Garidel P, Muehlau S, Bassarab S, Winter G. Systematic investigation of the effect of lyophilizate collapse on pharmaceutically relevant proteins, part 2: Stability during storage at elevated temperatures. Journal of Pharmaceutical Sciences 2012;101(7):2288-306.

[21] Rambhatla S, Ramot R, Bhugra C, Pikal MJ. Heat and mass transfer scale-up issues during freeze drying: II. Control and characterization of the degree of supercooling. AAPS PharmSciTech 2004;5(4):54-62.

[22] Konstantinidis AK, Kuu W, Otten L, Nail SL, Sever RR. Controlled nucleation in freeze-drying: Effects on pore size in the dried product layer, mass transfer resistance, and primary drying rate. Journal of Pharmaceutical Sciences 2011;100(8):3453-70.

[23] Maa Y-F, Prestrelski SJ. Biopharmaceutical powders: particle formation and formulation considerations. Current Pharmaceutical Biotechnology 2000;1(3):283-302.

[24] Strickland W. Study of water vapor sorption by pharmaceutical powders. Journal of Pharmaceutical Sciences 1962;51(4):310-4.

[25] Fakes MG, Dali MV, Haby TA, Morris KR, Varia SA, Serajuddin AT. Moisture sorption behavior of selected bulking agents used in lyophilized products. PDA Journal of Pharmaceutical Science and Technology 2000;54(2):144-9.

[26] Abdul-Fattah A, Truong-Le V, Yee L, Pan E, Ao Y, Kalonia D, et al. Drying-Induced Variations in Physico-Chemical Properties of Amorphous Pharmaceuticals and Their Impact on Stability II: Stability of a Vaccine. Pharmaceutical Research 2007;24(4):715-27.

[27] Jennings TA. Managing the Risk of Residual Moisture on Lyophilized Products from Elastomer Closures. Journal of Process Analytical Chemistry 2008;10(2):44-9.

[28] House J, Mariner J. Stabilization of rinderpest vaccine by modification of the lyophilization process. Developments in Biological Standardization 1995;87:235-44.

[29] Earle J, Bennett P, Larson KA, Shaw R. The effects of stopper drying on moisture levels of Haemophilus influenzae conjugate vaccine. Developments in Biological Standardization 1991;74:203-10.

[30] Lueckel B, Helk B, Bodmer D, Leuenberger H. Effects of formulation and process variables on the aggregation of freeze-dried interleukin-6 (IL-6) after lyophilization and on storage. Pharmaceutical Development and Technology 1998;3(3):337-46.

[31] Liu WR, Langer R, Klibanov AM. Moisture induced aggregation of lyophilized proteins in the solid state. Biotechnology and Bioengineering 1991;37(2):177-84.

[32] Costantino HR, Langer R, Klibanov AM. Moisture-induced aggregation of lyophilized insulin. Pharmaceutical Research 1994;11(1):21-9.

[33] Roos Y, Karel M. Plasticizing effect of water on thermal behavior and crystallization of amorphous food models. Journal of Food Science 1991;56(1):38-43.

CHAPTER 4

EVALUATION OF A CRYO-MILLING PROCESS FOR PARTICLE PROCESSING

Within this chapter, the work related to section 2.2 - 2.4 includes results from the "Advanced Practical Course A" with the title "Scale-up and optimization of the manufacturing process of collapse freeze-dried and cryo-milled particles" by Josefine F. Pott, LMU Munich, 2011. The results within section 2.2 – 2.4 are expressed in figures 4.1 – 4.7, which were reproduced in a modified form. The "Advanced Practical Course A" has been planned, structured and carried out under my direct supervision. The results obtained and the conclusions drawn have been discussed under my supervision.

1 INTRODUCTION

The main challenge for the preparation of dry powder vaccine formulations for needle-free ballistic injection is firstly the production of the powders with reproducible particle size and distribution as well as the ability of the formulation to stabilize the incorporated vaccine. Secondly, an appropriate delivery technology is crucial for the application of the powdered formulation at the target site, the superficial layers of the skin, in order to elicit an adequate immune response.

As discussed in Chapter 3, the preparation of powdered formulations by collapse-freeze drying and subsequent cryo-milling generated particles with a narrow particle size distribution of 25-50 µm, comprising a dense matrix structure and low specific surface area of the particles. A size range of 20-70 µm of the particles is mandatory to achieve sufficient impact during ballistic injection to breach the epidermal layers of the skin [1-4], as sugar particles have to compensate their generally low density by their size.

By applying the above described process it was possible to preserve protein stability of the model protein ovalbumin. However, cryo-milling was performed using a swing mill, whereat the milling beakers were dipped manually into liquid nitrogen prior to the milling process. Thus the process is limited to a laboratory scale.

The aim of the following work was to systematically investigate and optimize a cryo-milling process for the production of vaccine loaded powder particles for intradermal ballistic delivery by using a semi-automated approach of a cryo-mill, allowing the development of a sterile production process, one crucial requirement to scale-up the process to industrial standards. Within this system the milling beakers are flushed continuously with liquid nitrogen prior to the automated milling-process. Further insight in different adjustable parameters like milling frequency, milling time and time of pre-cooling with liquid nitrogen was taken. The influence of the different milling parameters on particle size, microscopic appearance and residual moisture of the powders as well as on the stability of the model vaccine ovalbumin was assessed. Furthermore, the applicability of the cryo-milling process on other model protein was investigated.

2 DEVELOPMENT OF A CRYO-MILLING PROCESS

2.1 SELECTION OF DIFFERENT FORMULATIONS FOR THE EVALUATION OF THE CRYO-MILLING PROCESS

Three different formulations were selected for the evaluation of the cyro-milling process: a formulation based on trehalose (T), a combination of trehalose and the amino acid phenylalanine (TP) at a weight ratio of (9.5:0.5) and a ternary mixture of trehalose, mannitol and dextran (TMD) at a weight ratio of (3:3:4), respectively. Dextran had an average molecular weight of 70 kDA. All formulations contained 2.5% (w/w) ovalbumin and had a total solid content of 15% (w/w). The formulations were freeze-dried applying a collapse freeze-drying cycle according to the protocol described in chapter 2 [5]. This approach allowed for a collapse of the sugar matrix and the generation a high density structure of the freeze dried cake.

The ternary mixture of trehalose, mannitol and dextran was selected as it is known from literature to be appropriate to generate high density particles with appropriate characteristics for ballistic injection [6-9]. As already described in chapter 3, trehalose/mannitol/dextran formulation preserved, despite of the collapse-freeze drying cycle, a macroscopically elegant cake structure.

The formulation based on trehalose was chosen, as it showed superior morphological characteristics for ballistic injection and as it was able to preserve protein stability of ovalbumin for a time period of 12 months at 2-8°C and 50°C [10].

Generally, collapse freeze-drying of formulations based on trehalose results in macroscopic collapse of the matrix structure. By contrast, the addition of amino acids in lyophilizate formulations prevents the macroscopic collapse of amorphous lyoprotectants. Phenylalanine does not only act as cryoprotactant by exerting preferential exclusion from the protein/water interface [11], but also forms a network structure, on which amorphous trehalose can attach during lyophilization [12, 13].

The impact of these different cake structures on the rigidity of the lyophilizates and hence the impact of the formulation on the resulting particle size and distribution of the powders after cryo-milling was investigated.

2.2 MACROSCOPIC APPEARANCE AND RIGIDITY OF THE LYOPHILIZATES

Figure 4.1 depicts the macroscopic appearance of the lyophilizates after collapse-freeze drying. Formulations containing a ternary mixture of trehalose/mannitol/dextran were slightly shrunken, however, maintained an elegant cake structure. Trehalose/phenylalanine formulations showed a partially collapsed structure to a higher extent as trehalose/mannitol/dextran formulations. Formulations based on trehalose were foam-like shaped.

Figure 4.1: Macroscopic appearance of the lyophilizates after collapse freeze drying. (A) trehalose/mannitol/dextran (B) trehalose/phenylalanine (C) trehalose.

The rigidity of collapse freeze-dried cakes provides an indication on the resistance of the formulation during milling and was examined using a texture analyzer. Therefore a cylindrical piston was moved with 1 mm/s into the sample as described in chapter 2.

The required force to deform or break through the lyophilizate cake was monitored. A high rigidity (breaking force 30.4 N ± 2.8) of the freeze-dried cake was observed in formulations containing a combination of trehalose, mannitol and dextran (figure 4.2).
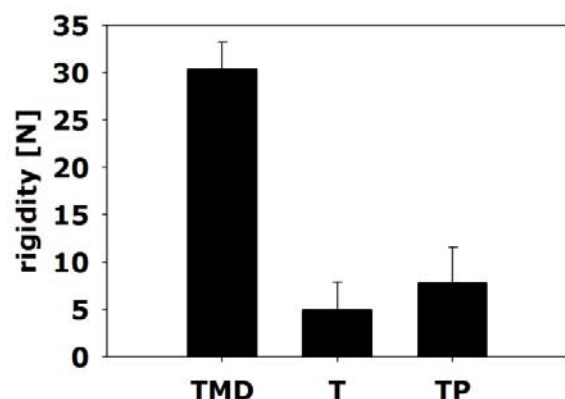
Figure 4.2: Rigidity of the lyophilizates determined by indentation using a texture analyzer.

Lower rigidity (4.9 N ± 2.9) of the freeze-dried cake was observed in formulations containing trehalose or a combination of trehalose and phenylalanine (7.8 N ± 3.8).

Thus, as the rigidity of the freeze-dried cakes were comparable, formulations containing trehalose were chosen representatively for trehalose and trehalose/phenylalanine formulations for the subsequent investigation of the milling parameters.

2.3 INFLUENCE OF THE MILLING PARAMETERS PRE-COOLING TIME AND MILLING FREQUENCY ON THE POWDERED PRODUCT

First, the influence of pre-cooling time and milling frequency on the resulting particle size after cryo-milling was analyzed. Stainless-steel milling beakers, containing the milling load of 1.0 g and a milling ball of 1 cm diameter, were flushed during the pre-cooling phase continuously with liquid nitrogen. A pre-cooling time of 5 and 10 min was explored and compared to milling without pre-cooling. A subsequent milling step was performed for 30 seconds at 25 Hz using a milling load of 1.0 g. The temperature of the milling load was measured directly after milling. These experiments were performed exemplarily with trehalose-formulations. The resulting particle size distribution of the powders was measured by laser light diffraction as described in chapter 2. Particle size distribution was calculated as an average of 6 measurements applying the Fraunhofer

theory and characterized with median diameter and span of the volume distribution. Each sample was measured at least in triplicates.
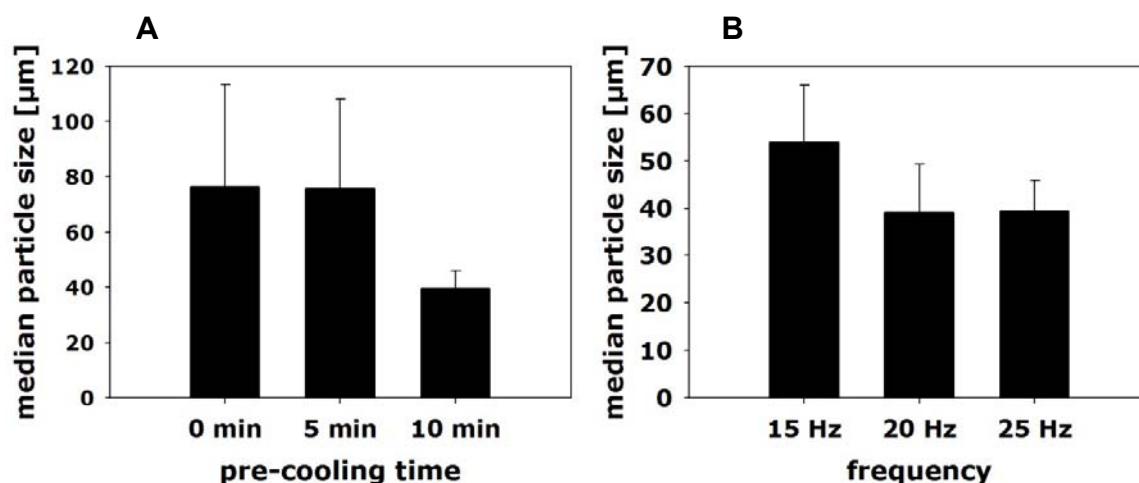
Figure 4.3: (A) Median particle size of trehalose powders after 0, 5 and 10 minutes of pre-cooling of the grinding beaker and (B) at 15, 20 and 25 Hz milling frequency.

The pre-cooling time prior milling affected particle size and distribution of the powder as well as the homogeneity of the milled product. Milling without pre-cooling of the sample at room temperature (20°C) resulted in a mean particle size of 76.45 µm ± 36.9 µm and a span of 3.59 ± 1.17 (figure 4.3). The friction forces, which were caused by the milling process, created heat which in turn induced a melt together of the particles as pointed out in the scanning electron micrographs (figure 4.4).

Generally, heat caused by friction forces during milling might not only induces a local melting of the particles but also exceed the glass transition temperature of the formulation [14] and hence potentially destabilize the incorporated protein [15].
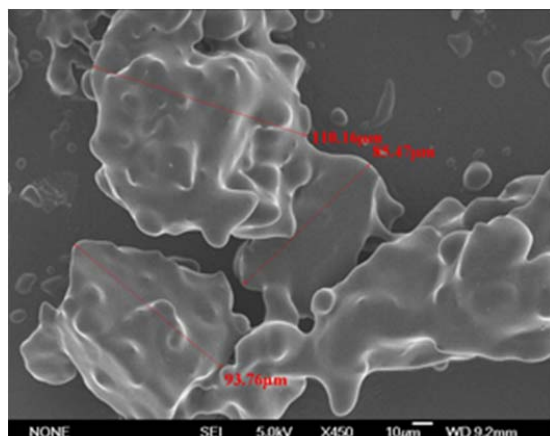
Figure 4.4: Scanning electron micrographs of trehalose powder particles after milling without pre-cooling of the sample for 30 seconds at 25 Hz and a milling load of 1.0 g. Magnification 450x.

This observation was also confirmed in experiments performed by Garmise *et al.* Milling of an influenza vaccine formulation based on lactose or trehalose intended for nasal delivery at room temperature using a micro-ball mill required milling times larger than 15 min up to 2 hours in order to result in the required particle size of 45-125 µm [16, 17]. The milling load of the freeze-dried cakes was 200 mg. Higher velocity during milling resulted in larger flakes, suggesting melting and recrystallization of the formulation components [17], supporting our observations. Similar observations were made by Maa *et al.* after compressing, manually grounding and sieving of a lyophilizate containing a Hepatitis-B vaccine and a ternary formulation of trehalose, mannitol and dextran (~ 10 kDa). The potency recovery of the Hepatitis-B vaccine was quite low with 20-30%, indicating a destabilizing effect of the process steps. Furthermore, manually grinding and sieving of the powder resulted in a broad particle size distribution and a low yield of particles in the desired size range of 25-30 µm [8].

After a pre-cooling time of 5 minutes the temperature of the powdered product decreased to -52°C. However, this did not influence the mean particle size or distribution of the powder, which remained 75.70 µm ± 32.38 µm in size with a span of 2.91 ± 0.29. A pre-cooling time of 10 minutes resulted in a maximal low product temperature of -136°C. Thus, the low product temperature created brittle cakes and

uniform powder particle size of 39.47 µm ± 6.45 µm and a narrow size distribution (span 3.20 ± 1.43). Applying this approach, cryo-milling generally resulted in non-spherical solid particles.

The choice of a maximal milling frequency of 25 Hz reduced the required milling time (figure 4.3B). By controlling the temperature of the milling load, the potential to reduce vaccine potency can be minimized whereas milling speed (frequency) and milling time can be optimized.

These conditions, 10 min pre-cooling and 25 Hz milling frequency, maximized the production of appropriately sized particles and were chosen for the following production conditions.

2.4 INFLUENCE OF MILLING TIME ON THE MEDIAN PARTICLE SIZE OF THE POWDERS

For trehalose formulations a milling time of 15 seconds at 25 Hz was sufficient to obtain particles in the desired size range of 41.95 µm ± 8.73 µm (span 3.07 ± 0.58). Longer milling times lead to particle agglomeration (figure 4.5).
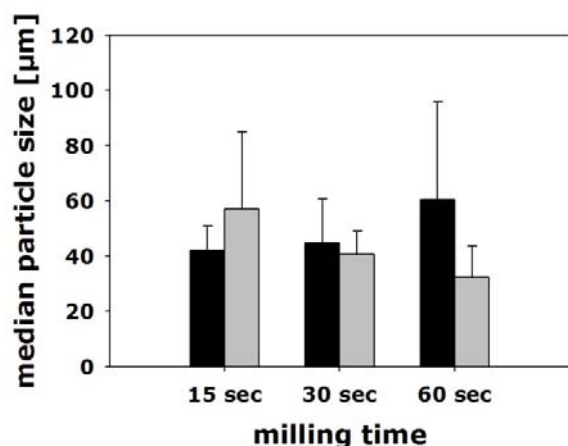
Figure 4.5: Median particle sizes of trehalose powders (black bars) and trehalose/ mannitol/dextran powders (grey bars) after 15, 30 and 60 seconds of milling.

Formulations containing a ternary formulation of trehalose/mannitol and dextran required longer milling times. 30 seconds of milling at a frequency of 25 Hz were

appropriate to generate particles in the desired size range of 40.57 µm ± 8.32 µm (span 3.03 ± 0.77).

Figure 4.6A depicts exemplarily particle sizing results of a trehalose/mannitol/dextran formulation after 10 min of pre-cooling using a milling load of 1 g and a milling time of 30 seconds at 25 Hz. Figure 4.6B depicts particle sizing results of a trehalose formulation cryo-milled using the same conditions though after a milling time of 15 seconds.
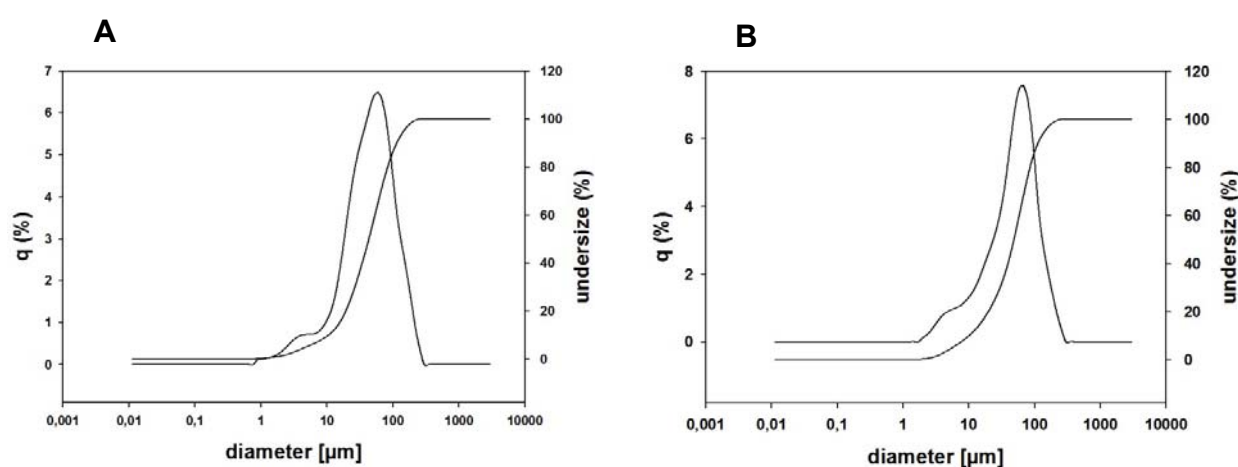
Figure 4.6: Median particle sizes of trehalose powder (A) after a pre-cooling time of 10 minutes and 15 seconds of milling at 25 Hz. Median particle size trehalose: 43.22 µm; span 2.42; D (v, 0.1) 10.49 µm; D (v, 0.9) 115.02 µm. (B) Trehalose/mannitol/dextran powder after a pre-cooling time of 10 minutes and 30 seconds of milling at 25 Hz. Median particle size trehalose/mannitol/dextran: 48.66 µm; span 2.11; D (v, 0.1) 10.17 µm; D (v, 0.9) 112.85 µm.

Particle size distribution of the powders could be confirmed by scanning electron microscopy (figure 4.7.). Cryo-milling of trehalose/mannitol/dextran formulations resulted in irregularly square-edged shaped particles, whereas cryo-milled trehalose particles exhibited a smooth surface structure. In contrast, common methods for protein powder preparation as spray drying or spray freeze-drying generally result in spherical particles with very smooth surfaces and a porous inner particle structure [4, 18, 19].
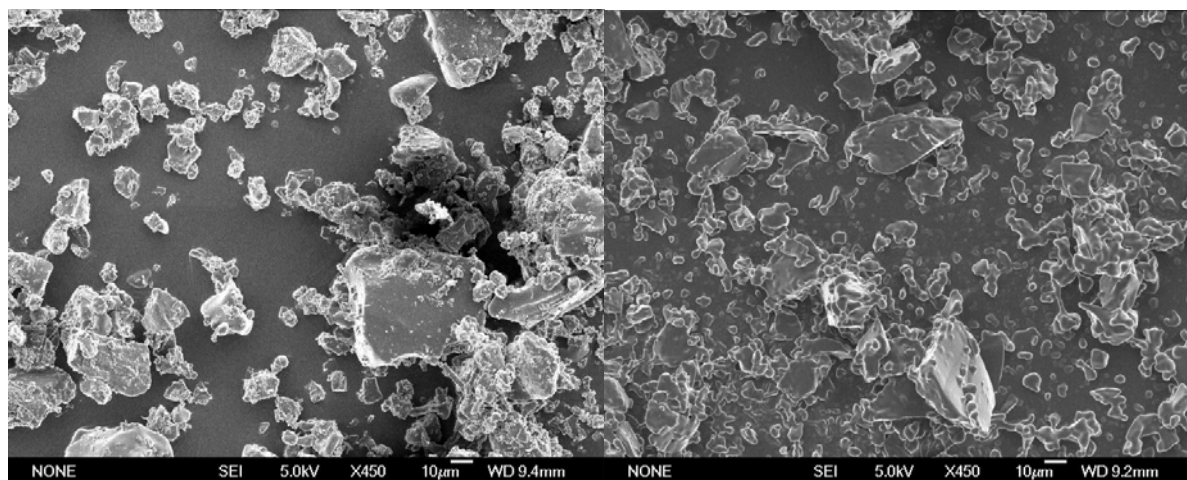
Figure 4.7: (A) Scanning electron micrographs of trehalose/mannitol/dextran powders and (B) trehalose powders after cryo-milling after 30 seconds and 15 seconds of milling, respectively. Magnification 450x.

However, a porous inner particle structure indicates a low mechanical stability of powders [20] as well as a low density. As these properties are unfavourable for ballistic injection of the powders, cryo-milling of freeze-dried lyophilizates provide an important option for this purpose.

2.5 INFLUENCE OF CRYO-MILLING ON RESIDUAL MOISTURE LEVELS AND PROTEIN STABILITY

Residual moisture content of the formulations was determined directly after lyophilization and subsequently after cryo-milling. Initial residual moisture levels of trehalose/mannitol/dextran lyophilizate cakes were 1.51% ± 0.07%, whereas trehalose lyophilizate cakes showed higher residual moister levels with 4.34% ± 0.16%. The presence of phenylalanine in trehalose/phenylalanine lyophilizates reduced the initial residual moisture level of the lyophilizate cake to 2.34% ± 0.24%. Cryo-milling using the semi-automated cryo-mill did only slightly increase the residual moisture levels of the lyophilizate cakes (figure 4.8). This confirms also the findings using a non-automated cryo-milling set-up as described in chapter 3.
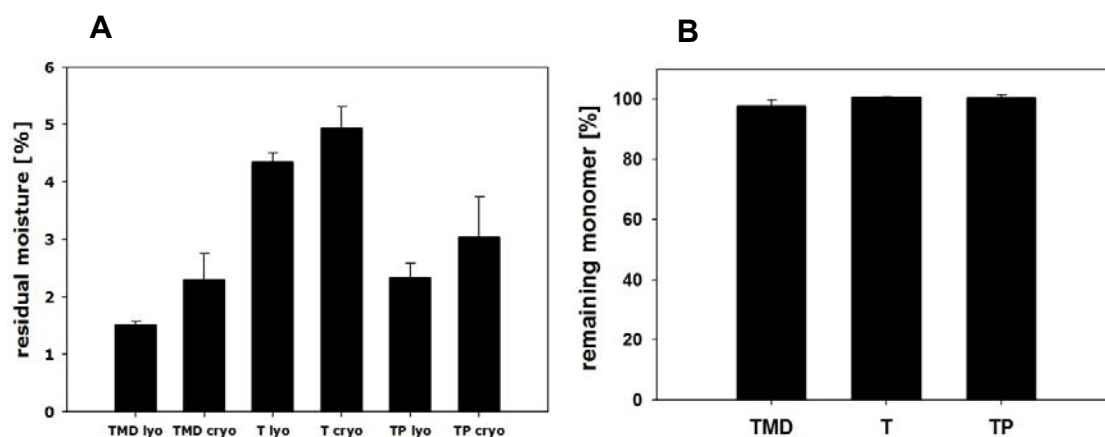
Figure 4.8: (A) Residual moisture content of trehalose (T), trehalose/phenylalanine (TP) and trehalose/mannitol/dextran (TMD) lyophilizates prior to the milling process and after cryo-milling. (B) Recovery of soluble monomer [%] of ovalbumin after cryo-milling, as compared to the amount of monomer present in the solution prior to freeze-drying as determined by size-exclusion chromatography.

The influence of the cryo-milling process on protein stability was investigated by size exclusion chromatography. No significant changes in the recovery of the soluble monomer of ovalbumin were observed (figure 4.8) directly after the cryo-milling process, thus confirming the results using a non-automated cryo-milling set-up [10]. The performance of cryo-milled powders during storage at elevated temperatures is discussed in chapter 5.

2.6   DEVELOPMENT OF A STERILE PRODUCTION PROCESS FOR CRYO-MILLED POWDERS

A sterile production process was developed to produce low endotoxin cryo-milled powders. All primary packaging materials, vials, stoppers as well as additional equipment like spatulas, beaker glasses and grinding beakers were sterilized either by heat sterilization at 160°C for two hours or by steam pressure sterilization at 120°C for 15 min.
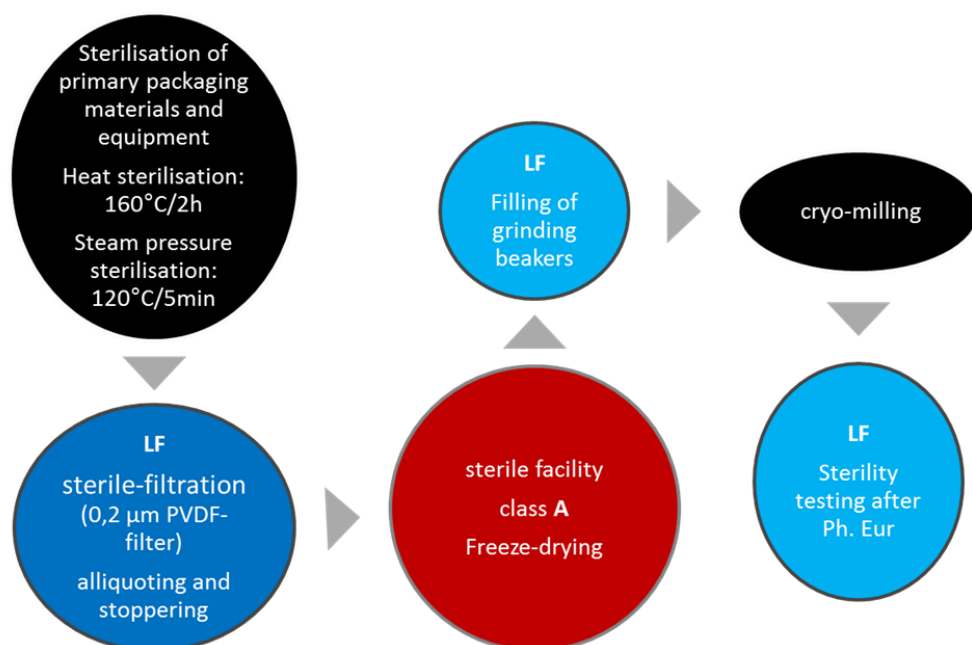
Figure 4.9: Process flow chart of the sterile production process for cryo-milled powders.

All excipients were dissolved in buffer and filtered under the laminar air flow using 0.2 µm PVDF filters into sterile 50 ml tubes. The liquid formulation was filled into lyophilization vials and stoppered completely before taking them out of the laminar air flow. The stoppered vials were transferred under appropriate conditions into the clean room class A of the sterile facility. The vials were opened and partially stoppered again before loading them into the freeze-dryer. After freeze-drying the vials were stoppered completely and transferred out of the sterile facility into the laminar air flow. The freeze-dried cakes were filled into the grinding beaker of the cryo-mill and closed properly. Cryo-milling was conducted under non-sterile conditions. After the milling process the grinding was transferred into the laminar air flow and the powder was filled into sterile glass beakers.

Sterility tests of the powders were performed according to the European Pharmacopoeia [21] using the membrane filter test. All powders were sterile according to pharmacopoeia, confirming the possibility to use the semi-automated cryo-mill process for the production of powders suitable for parenteral administration.

3 APPLICABILITY OF THE CRYO-MILLING PROCESS TO THE MODEL PROTEINS RH-GCSF AND RH-IFN A-2A

Formulations containing ovalbumin were shown to be stable after cryo-milling. Rh-G-CSF and rh-IFN-α-2a were chosen as model proteins to investigate the applicability of the cryo-milling process to different proteins in addition to the already thoroughly scrutinized model antigen ovalbumin. Both proteins are known to be prone towards aggregation, particularly if the proteins are subjected to heat [22], an extensive air-water interface or agitation [23-25]. However, little is known about the effect of milling or cryo-milling of the lyophilizates on protein aggregation.

Rh-G-CSF was dialyzed using a 0.02 M acetate buffer pH 4.0, and formulated with 0.004% polysorbate and 15% (w/w) trehalose/mannitol in a weight ratio of 1:1. Rh-IFN-α-2a was formulated in a 0.025 M acetate buffer pH 5.0, containing 0.12 M sodium chloride and 15% (w/w) trehalose/mannitol in a weight ratio of 1:1. Ovalbumin was dissolved in phosphate buffer (pH 7.0, 10 mM phosphate, 50 mM ionic strength adjusted with sodium chloride) and formulated with 15% (w/w) trehalose/mannitol in a weight ratio of 1:1. The final protein content of all formulations was 2.5% (w/w).
Lyophilization was performed applying the collapse cycle as described in chapter 2. Cryo-milling was carried out after a pre-cooling time of 10 min at 25 Hz for 15 seconds. A trehalose/mannitol formulation containing ovalbumin (15% solid content, 2.5% protein content) served as a reference.

Size exclusion chromatography showed a significant decrease of 6 to 7% of the total protein recovery of rh-IFN-α-2a after freeze-drying, indicating an increase of insoluble aggregates (table 4.1). No changes in the recovery of the monomer species were observed. This is also in line with the results obtained by Sharma *et al.*, showing the formation of insoluble aggregates of vacuum dried rh-IFN-α-2a formulations along with the absence of soluble aggregates [26]. Interestingly, the total protein content of rh-IFN-α-2a formulations did not change after the cryo-milling process in comparison to the total protein content after collapse freeze-drying.

Rh-G-CSF formulations showed a slight increase in dimer species of 1.67% after collapse freeze-drying accompanied by an equal decrease in monomer species. The formation of dimers in rh-G-CSF formulations was already observed after collapse freeze-drying and did not change after cryo-milling. This reflects the sensitivity of rh-G-CSF towards surface-induced stress at air-water interfaces, which was also a stress vector during cryo-milling [23, 24].

Formulations containing ovalbumin showed no significant differences in protein recovery or the pattern of protein species after collapse freeze-drying or after cryo-milling. Only a slight increase in the content of higher molecular weight species could be observed, however the changes were not significant.

Table 4.1: Protein recovery and pattern of the protein species as determined by size-exclusion chromatography.

		higher molecular weight aggregate [%]	dimer [%]	monomer [%]	fragments [%]	relative recovery* [%]
Rh-IFN-α-2a	liquid formulation			100.00 ± 0.00		99.45 ± 1.76
	lyophilizate			100.00 ± 0.00		93.00 ± 2.90
	cryo-milled powder			100.00 ± 0.00		93.90 ± 0.86
G-CSF	liquid formulation			100.00 ± 0.00		99.28 ± 1.30
	lyophilizate		1.67 ± 0.14	98.33 ± 0.14		100.64 ± 0.36
	cryo-milled powder		1.57 ± 0.69	98.43 ± 0.69		99.71 ± 0.97
OVA	liquid formulation	1.86 ± 0.61	7.59 ± 0.13	89.90 ± 0.60	0.65 ± 0.08	101.84 ± 0.78
	lyophilizate	1.63 ± 0.24	7.82 ± 0.01	89.90 ± 0.28	0.66 ± 0.03	99.76 ± 0.33
	cryo-milled powder	2.17 ± 0.28	7.96 ± 0.04	89.13 ± 0.37	0.74 ± 0.05	98.86 ± 0.38

*Relative recovery of the total protein content = area under the curve after cryo-milling/area under the curve at t_0 (liquid formulation) x 100.

Rh-IFN-α-2a lyophilizates showed a strong increase in turbidity after lyophilization up to turbidity levels of 5.7 ± 0.07 NFU (figure 4.10 A). This was in accordance with the results obtained by size exclusion chromatography.
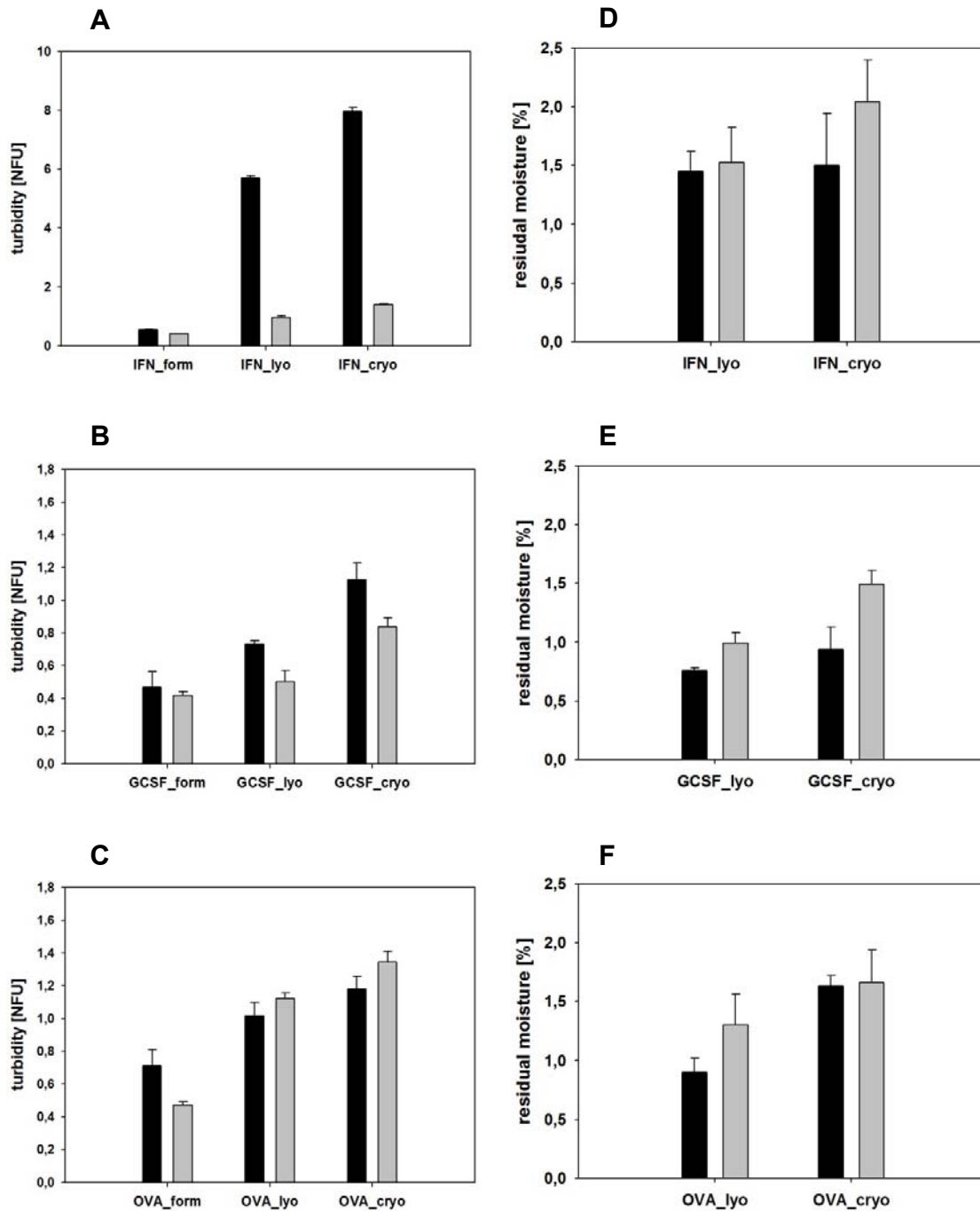
Figure 4.10: Turbidity of rh-IFN-α-2a-formulations (A), rh-G-CSF-formulations (B), and ovalbumin-formulations (C). The liquid formulation is abbreviated as "form", lyophilizate is abbreviated as "lyo" and cryo-milled powders are abbreviated as "cryo". Residual moisture levels after lyophilization and cryo-milling of rh-IFN-α-2a-formulations (D) rh-G-CSF-formulations (E) and OVA formulations (F). Formulations containing protein (black bars) and placebo formulations (grey bars).

The turbidity of rh-IFN-α-2a further increased after the cryo-milling process up to 7.96 ± 0.14 NFU indicating a destabilization of the protein.

A slight increase in turbidity of rh-G-CSF formulations was observed after collapse freeze-drying and cryo-milling in comparison to placebo samples (containing only excipients) (figure 4.9 B).

Rh-G- CSF lyophilizates exhibited a turbidity level of 0.73 ± 0.02 FNU whereas the corresponding placebo lyophilizates showed a turbidity level of 0.50 ± 0.07 FNU. After cryo-milling rh-G-CSF powders had a turbidity level of 1.13 ± 0.10 FNU in comparison to the corresponding placebo powders with 0.84 ± 0.05 FNU.

Similarly, the turbidity of ovalbumin formulations increased after the cryo-milling process, however to an extent comparable to the increase of placebo formulations (containing only excipients) after the milling process (figure 4.10C). This indicates that insoluble particles were formed in the course of the cryo-milling process due to the formation of particles built up of excipients (as observed in the placebo samples as control samples) rather that due to the formation of protein aggregates.

The residual moisture levels of all formulation increased just slightly after cryo-milling with 0.05% in rh-IFN-α-2a formulations, 0.17% in rh-G-CSF formulations and 0.73% in ovalbumin formulations (figure 4.10 D-F). All cryo-milled protein powders showed acceptable residual moisture levels with less than 1.6%. Placebo formulations showed already after collapse freeze-drying a slightly higher residual moisture level compared to formulations containing protein.

Figure 4.11 A-C shows the cumulative particle counts of rh-G-CSF formulations measured by light obscuration. The cryo-milling process caused particles larger than 1, 10 and 25 µm per mL in rh-G-CSF formulations as well as in the corresponding placebo formulations. Only the cumulative particle count larger than 10 µm per mL was significantly higher than in the placebo formulations. However, particle counts > 10 µm were below 400 counts per containment, which is well in line with the specified limits of the European Pharmacopoeia (Ph. Eur.), requiring less than 6000 particles per containment in this size range.
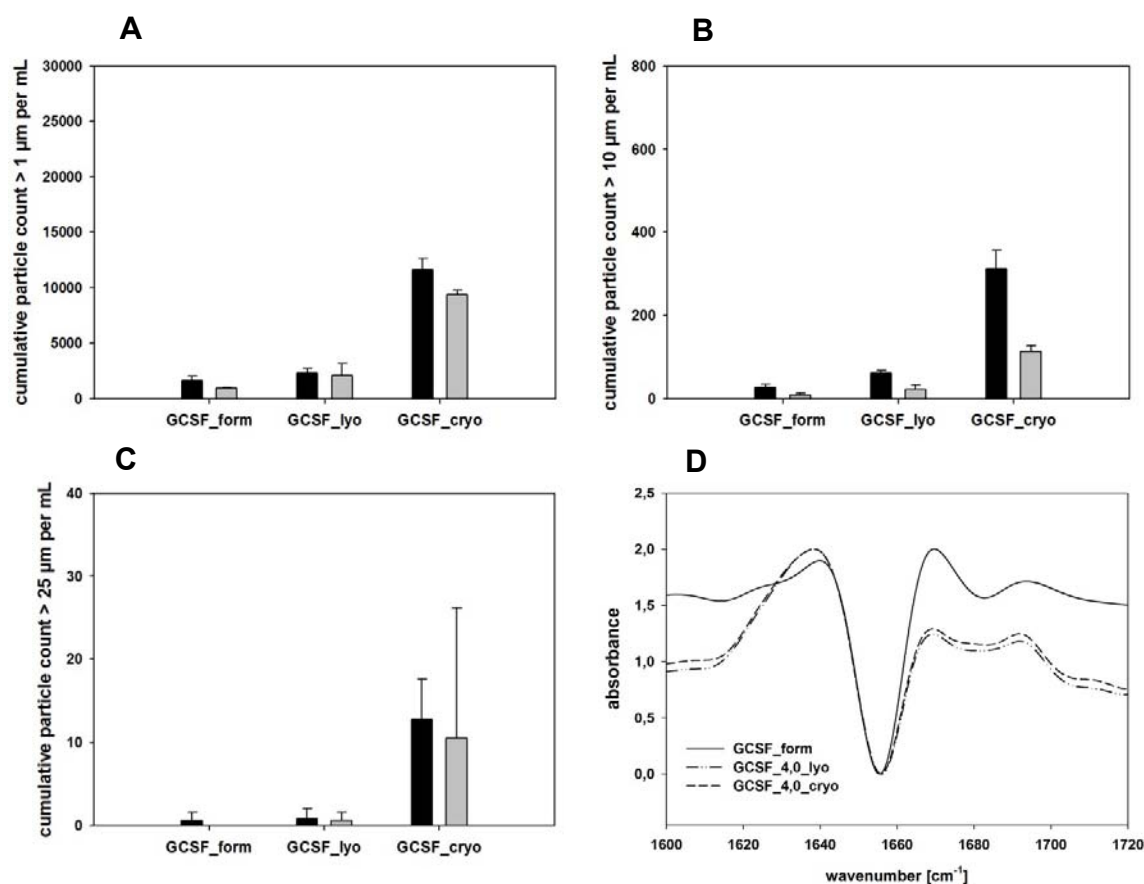
Figure 4.11: (A-C) Cumulative particle counts > 1, 10 and 25 μm of rh-G-CSF formulations as determined by light obscuration. (D) Second derivative amid I FTIR-spectra of rh-G-CSF formulations. Formulations containing protein (black bars) and placebo formulations (grey bars).

In order to assess the conformational stability of rh-G-CSF after lyophilization and cryo-milling, FTIR spectra of the liquid formulation, the lyophilizate and the cryo-milled powder were obtained. The lyophilizate as well as the cryo-milled powder had to be reconstituted in purified water prior to analysis. Since particle-free solutions are required for the recording of the spectra in the IR-transmission cell, the samples were centrifuged and only the remaining supernatant was analyzed. The FTIR spectra of the amid I bands of the rh-G-CSF formulations depicted in figure 4.11B were background corrected against the respective placebo formulation and vector-normalized. The α-helical band at 1656 cm^{-1} showed no changes in its intensity after lyophilization and cryo-milling indicating the preservation of the native secondary structure of rh-G-CSF

after both process steps. Baseline slopes and shifts in the intensity of the spectra in the region of 1600 – 1630 cm^{-1} and 1670 – 1720 cm^{-1} were observed after lyophilization and cryo-milling, however, the formation of new bands, which might be attributed to intermolecular ß-sheet formations, could not be observed [27-29]. It is known from literature that FTIR spectra of freeze-dried proteins often show band broadening and shifts in the band positions and intensities of amide I spectra due to the removal of water and hence environmental changes [30, 31], but are not consequently based on disturbances in the secondary structure of the protein.

Minor perturbations in the conformational stability of rh-G-CSF occurred after collapse freeze-drying; however, no relevant changes in the spectra were observed after the cryo-milling process in comparison to the spectra obtained after collapse freeze-drying.

Figure 4.12 A-C depicts the cumulative particle counts of rh-IFN-α-2a-formulations formulations measured by light obscuration. Cumulative particle counts larger than 1 and 10 µm per mL increased significantly after lyophilization and were further reduplicated after the cryo-milling process (figure 4.12 A and B). These results are in accordance with the findings of size exclusion chromatography and turbidity analysis. Only a small increase in particles larger than 25 µm per mL was observed.

The FTIR spectra of the amid I bands of reconstituted rh-IFN-α-2a formulations depicted in figure 4.12 D were background corrected against the respective placebo formulation and vector-normalized. The intense peak in the rh-IFN-α-2a formulations at 1654 cm^{-1}, the typical feature of an α-helix band [29], did show only a marginal shift to 1658 cm^{-1} indicating, that the secondary structure of the protein could be preserved.
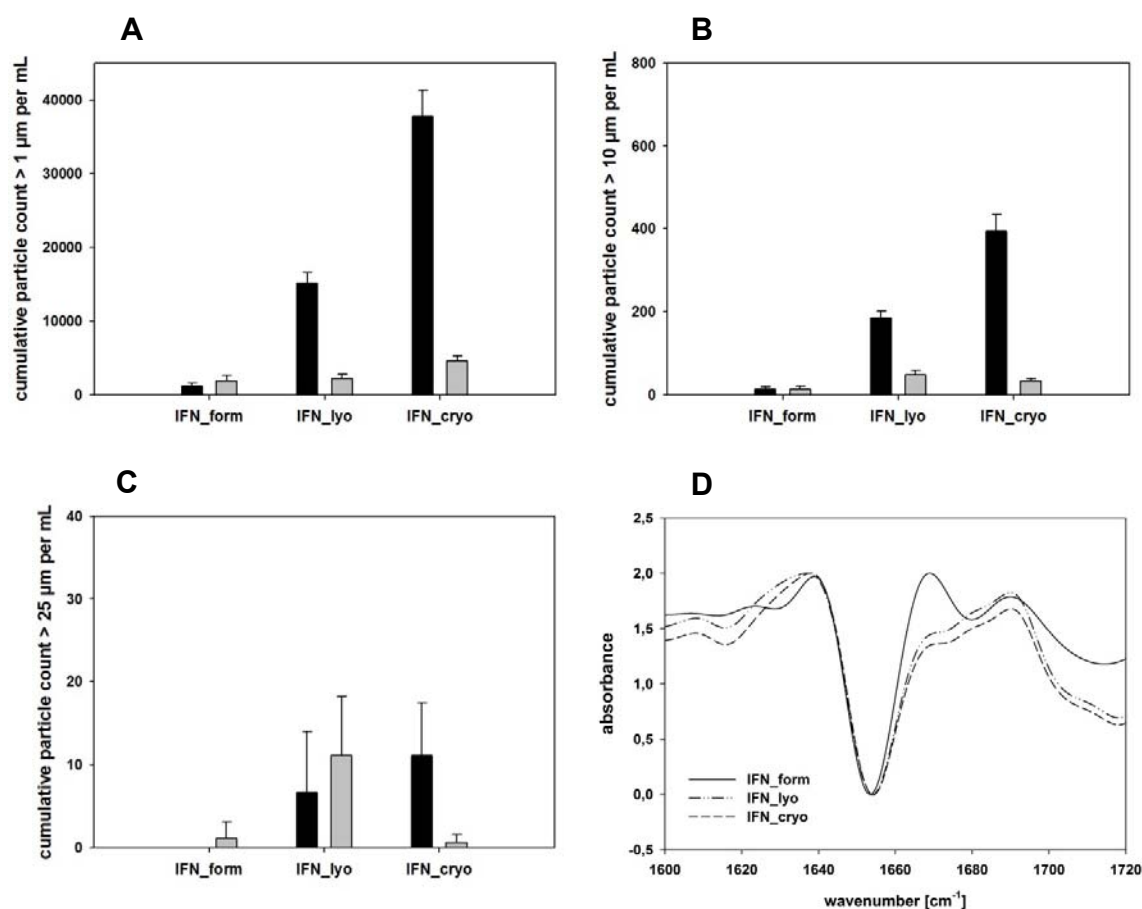
Figure 4.12: (A-C) Cumulative particle counts > 1, 10 and 25 µm of rh-IFN-α-2a-formulations as determined by light obscuration. (D) Second derivative amid I FTIR-spectra of rh-IFN-α-2a-formulations. Formulations containing protein (black bars) and placebo formulations (grey bars).

Similarly to the observations in rh-G-CSF formulations, baseline slopes and shifts in the intensity of the spectra in the region of 1600 – 1630 cm^{-1} and 1665 – 1720 cm^{-1} were observed after lyophilization and cryo-milling of rh-IFN-α-2a formulations. However, only slight differences in the spectra of rh-IFN-α-2a lyophilizates or cryo-milled powders could be detected. In addition to the results obtained by size exclusion chromatography, turbidity and light obscuration, it can be concluded, that aggregation of rh-IFN-α-2a does not take place via an intermediate formation of soluble aggregates but directly by the formation of larger, insoluble aggregates. This is clearly in contrast to the findings of Sharma *et al.* demonstrating the stabilization of rh-IFN-α-2a in a trehalose-mannitol formulation after vacuum drying [26].

87

Also ovalbumin formulations showed an increase in cumulative particle counts > 1, 10 and 25 µm (figure 4.13A-C). This is clearly in contradiction to the results obtained by turbidity measurements (figure 4.10C) and size exclusion chromatography (table 4.1).
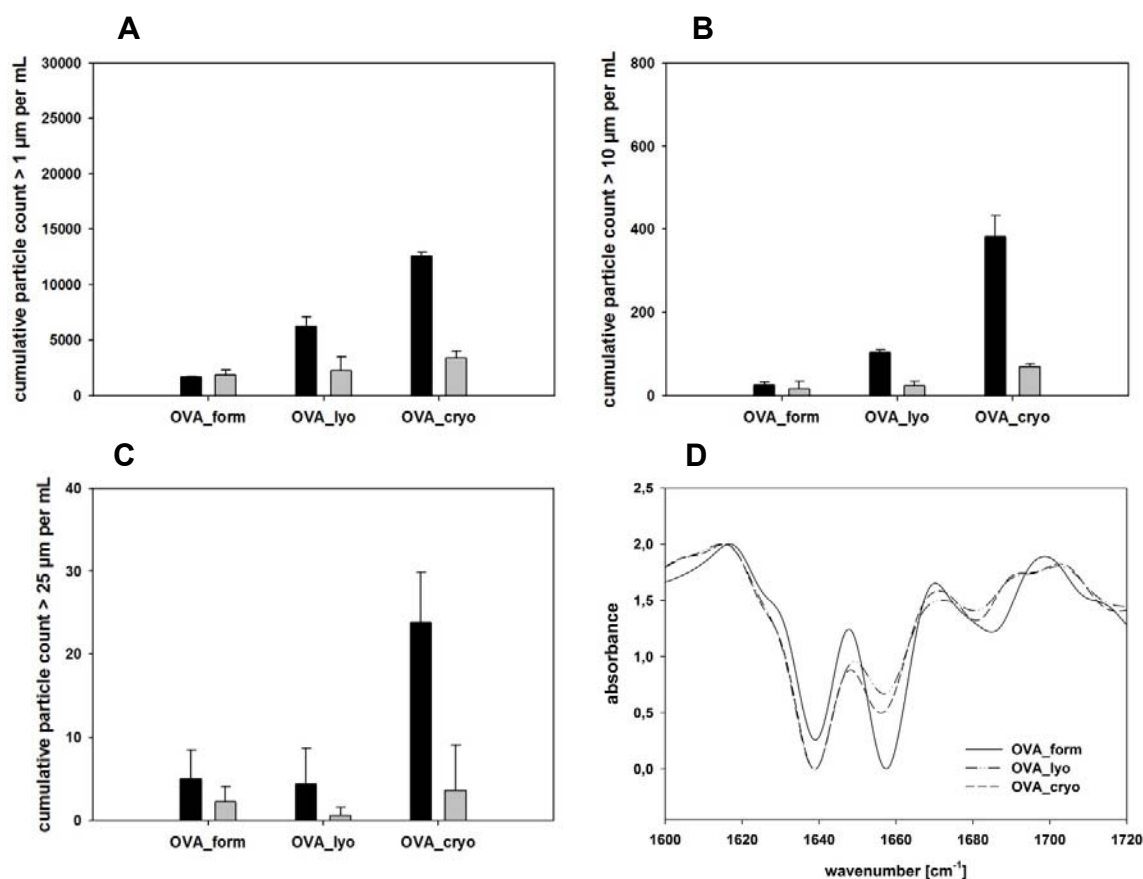
Figure 4.13: (A-C) Cumulative particle counts > 1, 10 and 25 µm of OVA-formulations as determined by light obscuration. (D) Second derivative amid I FTIR-spectra OVA-formulations. Formulations containing protein (black bars) and placebo formulations (grey bars).

FTIR spectra of ovalbumin formulations showed a decrease in the α-helical region after freeze-drying (figure 4.13D), thus pointing out changes in the secondary structure of the protein. However, these structural changes remained comparable after the cryo-milling

process. Long-term storage stability of ovalbumin in collapse freeze-dried and cryo-milled trehalose/mannitol formulations will be scrutinized in chapter 5 of this thesis.

4   SUMMARY AND CONCLUSION

A systematic investigation of different milling parameters using a semi-automated cryo-mill was explored as well as the development of a sterile production process for cryo-milled powders. The sterile production process opens up the possibility to upscale cryo-milling to industrial standards.

Optimal parameters regarding the cryo-milling process were evaluated for formulations with discriminant differences regarding the rigidity of the lyophilizates. Pre-cooling of the product loaded milling beakers was determined to be necessary to prevent local melting of the particles during milling. Thus, the optimized parameters allowed a fast, efficient and gentle milling process resulting in the target size range of the particles. The majority of the particles were in the size range of 20 to 70 μm. Only a small amount of the particles were larger than 100 μm. However, regarding the ballistic intradermal injection process, it might be necessary to separate particles > 100 μm from the powders, as it is known from literature, that large particles can harm the skin and provoke pain and bleeding at the injection site [32]. Depending on the delivery device used, it might also be necessary to separate the fine particle fraction < 20 μm as the fine particle fraction might not be able to penetrate into the epidermal layers of the skin. Residual moisture levels of the powders were only marginal affected by the cryo-milling process. Furthermore a sterile production process was set up, where the cryo-milling step could be performed outside the sterile facility.

The applicability of the cryo-milling process for another two model proteins, rh-G-CSF and rh-IFN - α-2a in a trehalose/mannitol formulation was investigated and compared to ovalbumin formulations as a reference. Collapse freeze-drying of rh-G-CSF formulations resulted only in a slight increase of soluble dimer species and moreover, the recovery of soluble dimer species did not change after cryo-milling in comparison to the lyophilizates. Turbidity levels, light obscuration as well as the FTIR-spectra of cryo-milled rh-G-CSF formulations showed only slight perturbations of the protein.

Rh-IFN-α-2a formulations were not stable after collapse freeze-drying, what was reflected in the formation of insoluble aggregates. Aggregation of rh-IFN-α-2a was also

observed after cryo-milling. This is in accordance with the results obtained by Sharma *et al.*, observing aggregation of rh-IFN-α-2a formulations after vacuum drying [26]. Similarly, Mohl *et al.* showed that trehalose was not effective to stabilize rh-IFN-α-2a in a freeze-dried formulation, which was subsequently incorporated in a lipid carrier system. In contrast to that, the addition of hydroxypropyl-β-cyclodextrin as stabilizing excipient during freeze-drying, was successful to retain up to 95% of the native form of rh-IFN-α-2a after freeze-drying and release of the protein of the lipid carrier system.

Ovalbumin formulations showed no significant differences in protein recovery or the pattern of protein species after the collapse freeze-drying cycle or after the cryo-milling process as determined by size exclusion chromatography. This was also confirmed by turbidity measurements. However, light obscuration and FTIR analysis indicated perturbations in protein stability. Stability of cryo-milled ovalbumin powders at elevated temperatures will be evaluated and discussed in chapter 5.

In summary the applicability of the cryo-milling process to other proteins was shown for rh-GSCF, however, not for rh-IFN-α-2a. As the stabilizing excipient plays a key role in the preservation of the protein integrity rather than the cryo-milling process itself, stability after cryo-milling has to be evaluated for each protein or antigen individually. The effect of formulation composition on ovalbumin in cryo-milled powders during storage will be scrutinized in chapter 5 of this thesis.

Comprehensively, cryo-milling was shown to be a rapid and adjustable process, enabling sterile manufacturing of powder particles. However, the described manufacturing process for powder particles comprises at least two steps: (1) collapse freeze-drying, (2) cryo-milling and optionally a third one, (3) sieving. Based on the overall growing interest on intradermal vaccination the competitiveness of this two or three step process to other manufacturing processes, like spray-drying or spray-freeze-drying, as well as the up-scaleability to industrial standards have still to be proven.

5 REFERENCES

[1]   Hardy MP, Kendall MAF. Mucosal deformation from an impinging transonic gas jet and the ballistic impact of microparticles. Physics in Medicine and Biology 2005;50(19):4567.

[2]   Chen D, Erickson CA, Endres RL, Periwal SB, Chu Q, Shu C, et al. Adjuvantation of epidermal powder immunization. Vaccine 2001;19(20-22):2908-17.

[3]   Dean HJ, Fuller D, Osorio JE. Powder and particle-mediated approaches for delivery of DNA and protein vaccines into the epidermis. Comparative Immunology, Microbiology and Infectious Diseases 2003;26(5-6):373-88.

[4]   Maa Y-F, Ameri M, Shu C, Payne LG, Chen D. Influenza vaccine powder formulation development: spray-freeze-drying and stability evaluation. Journal of Pharmaceutical Sciences 2004;93(7):1912-23.

[5]   Schersch K, Betz O, Garidel P, Muehlau S, Bassarab S, Winter G. Systematic investigation of the effect of lyophilizate collapse on pharmaceutically relevant proteins I: Stability after freeze-drying. Journal of Pharmaceutical Sciences 2010;99(5):2256-78.

[6]   Rochelle C, Lee G. Dextran or hydroxyethyl starch in spray-freeze-dried trehalose/mannitol microparticles intended as ballistic particulate carriers for proteins. Journal of Pharmaceutical Sciences 2007;96(9):2296-309.

[7]   Sonner C, Maa Y-F, Lee G. Spray-freeze-drying for protein powder preparation: Particle characterization and a case study with trypsinogen stability. Journal of Pharmaceutical Sciences 2002;91(10):2122-39.

[8]   Maa Y-F, Ameri M, Shu C, Zuleger CL, Che J, Osorio JE, et al. Hepatitis-B Surface Antigen (HBsAg) Powder Formulation: Process and Stability Assessment. Current Drug Delivery 2007;4:57-67.

[9]   Schiffter H, Condliffe J, Vonhoff S. Spray-freeze-drying of nanosuspensions: the manufacture of insulin particles for needle-free ballistic powder delivery. Journal of the Royal Society Interface 2010;7(Suppl 4):S483-S500.

[10]   Etzl EE, Winter G, Engert J. Toward intradermal vaccination: preparation of powder formulations by collapse freeze-drying. Pharmaceutical Development and Technology 2014;19(2):213-22.

[11]   Carpenter JF, Arakawa T, Crowe JH. Interactions of stabilizing additives with proteins during freeze-thawing and freeze-drying. Developments in Biological Standardization 1992;74:225-38; .

[12]   Mattern M, Winter G, Kohnert U, Lee G. Formulation of Proteins in Vacuum-Dried Glasses. II. Process and Storage Stability in Sugar-Free Amino Acid Systems. Pharmaceutical Development and Technology 1999;4(2):199-208.

[13]   Mattern M, Winter G, Rudolph R, Lee G. Formulation of proteins in vacuum-dried glasses. I: Improved vacuum-drying of sugars using crystallising amino acids. European Journal of Pharmaceutics and Biopharmaceutics 1997;44(2):177-85.

[14]   Descamps M, Willart JF, Dudognon E, Caron V. Transformation of pharmaceutical compounds upon milling and comilling: The role of Tg. Journal of Pharmaceutical Sciences 2007;96(5):1398-407.

[15]   Maa Y-F, Prestrelski SJ. Biopharmaceutical powders: particle formation and formulation considerations. Current Pharmaceutical Biotechnology 2000;1(3):283-302.

[16]   Huang J, Garmise RJ, Crowder TM, Mar K, Hwang CR, Hickey AJ, et al. A novel dry powder influenza vaccine and intranasal delivery technology: induction of systemic and mucosal immune responses in rats. Vaccine 2004;23(6):794-801.

[17]   Garmise R, Mar K, Crowder T, Hwang CR, Ferriter M, Huang J, et al. Formulation of a dry powder influenza vaccine for nasal delivery. AAPS PharmSciTech 2006;7(1):E131-E7.

[18]   Maa Y-F, Nguyen P-A, Sweeney T, Shire SJ, Hsu CC. Protein Inhalation Powders: Spray Drying vs Spray Freeze Drying. Pharmaceutical Research 1999;16(2):249-54.

[19]   Costantino H, Firouzabadian L, Hogeland K, Wu C, Beganski C, Carrasquillo K, et al. Protein Spray-Freeze Drying. Effect of Atomization Conditions on Particle Size and Stability. Pharmaceutical Research 2000;17(11):1374-82.

[20]   Ziegler A, Simon S, Lee G. Comminution of carbohydrate and protein microparticles on firing in a ballistic powder injector. Journal of Pharmaceutical Sciences 2010;99(12):4917-27.

[21]   Ph. Eur. 2.06.01 Sterility. 8th ed. Strasbourgh, France: European Directorate for the Quality of Medicine, 2016.

[22]   Hochuli E. Interferon immunogenicity: technical evaluation of interferon-alpha 2a. Journal of Interferon and Cytokine Research: the official Journal of the International Society for Interferon and Cytokine Research 1997;17:S15-21.

[23]   Niven RW, Prestrelski SJ, Treuheit MJ, Ip AY, Arakawa T. Protein nebulization II. Stabilization of G-CSF to air-jet nebulization and the role of protectants. International Journal of Pharmaceutics 1996;127(2):191-201.

[24]   Serno T, Härtl E, Besheer A, Miller R, Winter G. The role of polysorbate 80 and HPβCD at the air-water interface of IgG solutions. Pharmaceutical Research 2013;30(1):117-30.

[25]   Treuheit M, Kosky A, Brems D. Inverse Relationship of Protein Concentration and Aggregation. Pharmaceutical Research 2002;19(4):511-6.

[26]   Sharma V, Kalonia D. Polyethylene glycol-induced precipitation of interferon alpha-2a followed by vacuum drying: Development of a novel process for obtaining a dry, stable powder. AAPS PharmSci 2004;6(1):31-44.

[27]   Krishnan S, Chi EY, Webb JN, Chang BS, Shan D, Goldenberg M, et al. Aggregation of Granulocyte Colony Stimulating Factor under Physiological Conditions: Characterization and Thermodynamic Inhibition. Biochemistry 2002;41(20):6422-31.

[28]   Thirumangalathu R, Krishnan S, Brems DN, Randolph TW, Carpenter JF. Effects of pH, temperature, and sucrose on benzyl alcohol-induced aggregation of recombinant human granulocyte colony stimulating factor. Journal of Pharmaceutical Sciences 2006;95(7):1480-97.

[29]   Dong A, Huang P, Caughey WS. Protein secondary structures in water from second-derivative amide I infrared spectra. Biochemistry 1990;29(13):3303-8.

[30]   Carpenter JF, Prestrelski SJ, Dong A. Application of infrared spectroscopy to development of stable lyophilized protein formulations. European Journal of Pharmaceutics and Biopharmaceutics 1998;45(3):231-8.

[31]   Tian F, Middaugh CR, Offerdahl T, Munson E, Sane S, Rytting JH. Spectroscopic evaluation of the stabilization of humanized monoclonal antibodies in amino acid formulations. International Journal of Pharmaceutics 2007;335(1–2):20-31.

[32]   Burkoth TL, Bellhouse BJ, Hewson G, Longridge DJ, Muddle AG, Sarphie DF. Transdermal and transmucosal powdered drug delivery. Critical Reviews in Therapeutic Drug Carier Systems 1999;16(4):331-84.

CHAPTER 5

FORMULATION SCREENING AND STORAGE STABILITY OF OVALBUMIN AT ELEVATED TEMPERATURES

1 INTRODUCTION

Vaccines are generally sensitive to environmental stress, especially to elevated temperatures and require a thorough formulation strategy to ensure stability of the vaccine during processing to a final drug as well as long term storage and distribution [1, 2]. In chapter 3 and 4 of this thesis it was shown that collapse freeze-drying and cryo-milling of the collapsed lyophilizates is a suitable method to generate highly dense and robust particles being appropriate for intradermal injection. Thereby, the formulation has not only to fulfill several criteria with regard to its suitability for intradermal injection, it has also to cope with the task to stabilize a vaccine antigen throughout the stress applied during processing and, moreover, during subsequent storage at different temperature conditions.

During collapse freeze-drying, cryo-milling and storage of the final drug several stress vectors are affecting the native conformation of the antigen. Denaturation of the antigen can occur e.g. during freezing due to cold denaturation [3-5], surface induced denaturation at the solid-liquid interface (ice and water) [6, 7] phase separation of the stabilizing amorphous excipient [8-10] or due to an increasing concentration of the solute [11, 12], which is often accompanied by pH-shifts [13-15]. Furthermore dehydration and denaturation of the antigen can take place during the drying step [16]. Subsequently the lyophilizate cakes are exposed to mechanical stress during cryo-milling in form of friction and shear forces [17], possibly leading to recrystallization of the excipients or aggregation of the antigen [18, 19]. Further chemical or physical

degradation of the antigen can also occur during storage and shipment, dependent on the ability of the formulation to preserve antigen quality, which also determines the shelf-life of the product [20].

It is well described in literature that cryoprotectants (sugars, polyols and polymers) can stabilize the antigen during freezing by preferential exclusion, an indirect interaction between the excipient and protein, allowing a thermodynamic favored, hydrated state of the protein [21, 22]. Lyoprotectants can build an amorphous glass in the freeze-dried cake and are responsible for the stabilization of the antigen against dehydration induced stress during freeze-drying and subsequent storage by a mechanism also known as "vitrification" [23-26].

Hence, a careful selection and combination of cryo- and lyoprotectants is needed with regard to the type of antigen which should be stabilized, the shelf life of the drug as well as to the route of drug administration.

The different formulation compositions of the following formulation screening and storage stability for the model antigen ovalbumin include the lyo- and cryo- protectants trehalose and mannitol, which showed a very good stabilizing effect on ovalbumin during collapse freeze-drying and cryo-milling, overcoming the aforementioned stress vectors and fulfilled satisfactory morphological characteristics [27]. In addition, polymers like dextran and hydroxyethylstarch were scrutinized regarding their behavior during storage at elevated temperatures as further components. It was stated in literature that these polymers would be essential to generate mechanical robust particles by spray-freeze-drying [28-30]. Again, for the intradermal route of administration using a ballistic device, mechanical robustness of the particles is crucial. However, the role of polymers in collapse freeze-dried and cryo-milled particles during storage is yet not well characterized and need further investigation. In addition, the amino acid phenylalanine was scrutinized as excipient in the formulation composition as it was shown in previous work of Bosch *et al.* that phenylalanine possess superior physico-chemical powder characteristics in aggressively freeze-dried formulations [31], which offers also promising properties for intradermal injection.

Though, the benefit of higher molecular weight polymers as stabilizers in freeze-dried formulations is controversy discussed. As described in chapter 3, formulations containing dextran with a molecular weight of 70 kDa showed a poor stabilizing effect on ovalbumin during storage at elevated temperatures [27]. This was also confirmed by Rochelle *et al.*, indicating a destabilizing effect of higher molecular weight polymers like dextran and hydroxyethylstarch on catalase in a spray freeze-dried formulation [32]. Similar results were obtained by Pikal *et al.* They could show that dextran 40 kDA in an amorphous conformation failed to stabilize human growth hormone [33].

However, the group of Maa *et al.* demonstrated superior stabilizing effect of a subunit influenza vaccine in a ternary formulation composition comprising trehalose, mannitol and dextran (10 kDa) [28]. This indicates that next to the type of protein also the length of the molecular chain of the polymer impact protein or antigen stability. Similar observations were made for freeze-dried ɣ-globulin, insulin, HBsAg, LDH and ß-galactosidase [28, 34, 35]. Moreover it was stated that the addition of these polymers in formulations (based on trehalose and mannitol) together with a high solid content of the liquid formulation were crucial to generate highly dense and mechanically robust particles by spray drying resulting in particles with appropriate properties for intradermal injection [28, 32, 36]. We could show in chapter 3 and chapter 4 that, next to the above mentioned formulation strategy, mechanically robust particles with a dense matrix structure and reduced surface area could be generated by a novel combination of firstly collapse-freeze drying of the liquid formulation and secondly cryo-milling of the freeze-dried cakes. However, a systematic screening of different formulation excipients and mixtures thereof as well as their ability to stabilize the model antigen ovalbumin throughout storage is still required. A more thorough understanding of the role of polymers and their molecular weight on antigen stability in collapse freeze-dried and cryo-milled powders during storage at elevated temperatures will be given in the following work. Furthermore, physico-chemical and morphological characteristics of the particles with focus on a dense matrix structure intended for intradermal injection will be investigated. Beyond this, a view is given on the possibility to increase the antigen load per powder dose and its impact on antigen stability and particle morphology.

2   INFLUENCE OF FORMULATION COMPOSITION ON ANTIGEN STABILITY

As already outlined in the introduction, formulation strategy for intradermal powders emphasizes ternary mixtures of polymers with mannitol and trehalose as they show superior physico-chemical characteristics in terms of powder density and mechanical robustness [28-30]. In order to gain a more detailed insight into the impact of different formulation compositions on the stability of the well characterized model antigen ovalbumin in collapse freeze-dried and cryo-milled formulations, ternary mixtures of trehalose, mannitol and polymers, including dextran with different molecular weight (6, 40 or 70 kDA) and hydroxyethylstarch (70 kDa), were investigated. Furthermore polymer-free formulations containing a binary combination of trehalose and mannitol or a binary combination of trehalose and the amino acid phenylalanine or solely the disaccharide trehalose were evaluated. Table 5.1 lists the different formulation compositions and abbreviations of the formulations which will be used in the following.

Table 5.1: Summary of all formulations used in the study

formulation composition	abbreviation	weight ratio
trehalose, mannitol, dextran (70 kDA)	TMD_70	(3:3:4)
trehalose, mannitol, dextran (40 kDA)	TMD_40	(3:3:4)
trehalose, mannitol, dextran (6 kDA)	TMD_6	(3:3:4)
trehalose, mannitol, hydroxyethylstarch (70 kDA)	TMHES_70	(3:3:4)
trehalose	T	-
trehalose, mannitol	TM	(1:1)
trehalose, phenylalanine	TP	(10:0.5)

All formulations contained 2.5% (w/w) ovalbumin, comprised a total solid content of 15% (w/w) and were collapse-freeze dried and subsequently cryo-milled as described in chapter 2. The cryo-milled powders were stored for a period of twelve weeks at 2-8°C, 25°C and 50°C. Stability of the model antigen ovalbumin was assed using different analytical methods. Primary protein structure was analyzed by HP-SEC, the standard analytical tool for the detection of soluble protein aggregates. The formation of insoluble protein aggregates and subvisible particles was analyzed by light obscuration and

turbidimetry measurement. The influence of the formulation composition on particle morphology and physico-chemical characteristics was scrutinized by the specific surface area of the particles, particle size distribution, residual moisture and X-ray powder diffraction measurement of the cryo-milled powders. With the intention to ascertain that the formulation process (collapse freeze-drying and subsequent cryo-milling of the lyophilizate cakes) did not harm the integrity of ovalbumin, the recovery of the different protein species of ovalbumin was analyzed by HP-SEC for both, the liquid formulations prior to collapse freeze-drying and directly after cryo-milling of the freeze-dried cakes (figure 5.1.).
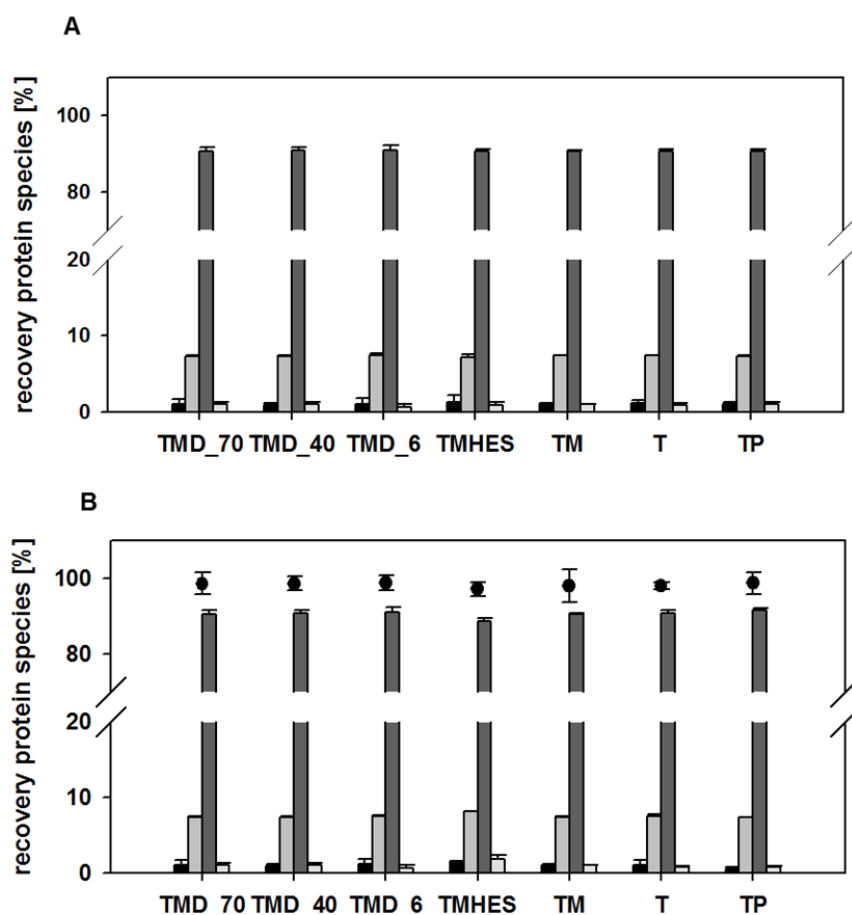
Figure 5.1: Recovery of ovalbumin protein species (%) of the liquid formulations prior to freeze-drying (A) and after collapse freeze-drying and subsequent cryo-milling (B) as determined by size exclusion chromatography. Black bars represent higher molecular weight aggregates, light grey bars represent dimers, dark grey bars represent monomers and white bars represents fragments. Filled circles represent the total protein recovery (average +/- SD, n=3).

The formulations had before and after collapse freeze-drying and cryo-milling same monomer, dimer, higher molecular weight aggregate and fragment pattern for all formulation compositions (figure 5.1.A). Collapse freeze-drying and subsequent cryo-milling had no impact on the formation of soluble for none of the formulations, as determined by the recovery of the protein species. Total protein recovery ranged from minimum 97.2% ± 1.9 (trehalose/mannitol/hydroxyethylstarch (70 kDa)) and maximum 98.9% ± 2.0 (trehalose/mannitol/dextran (6 kDa)) (figure 5.1.B), thus, indicating indirectly the absence of insoluble aggregates. This reaffirms the results described in chapter 3 and 4, and, in addition, shows that the process steps (collapse drying and cryo-milling) had no negative effect on antigen quality using formulation compositions including dextrans with different molecular weight chains, hydroxyethylstarch or phenylalanine.

In a next step storage stability of the cryo-milled powders was evaluated at 2-8°C, 25°C and 50°C for a time period of twelve weeks.

Figure 5.2 illustrates the results of size exclusion chromatography of trehalose/mannitol/dextran formulations containing 6, 40 and 70 kDa dextran prior to storage and after eight and twelve weeks of storage at 2-8°C or 50°C (samples stored at 25°C can be found in figure 9.1 and 9.2 in the appendix). Trehalose/mannitol/dextran 70 kDa formulations showed clearly an increase in higher molecular weight aggregates from 1.0% to 2.8% after eight and, respectively, twelve weeks of storage at 50°C. The increase of soluble higher molecular weight aggregates was accompanied by a decrease of the dimer species from 7.3% to 6.9%. This suggests that protein-protein interactions due to weak forces like van der Waals interactions, hydrogen bonding or hydrophobic and electrostatic interactions built up protein agglomerates of several dimer and monomer species of ovalbumin. These results further confirm the outcome of long term storage stability of trehalose/mannitol/dextran (70 kDa) formulations for twelve months at 50°C as outlined in chapter 3, showing a destabilizing effect of dextran (70 kDa) on ovalbumin.

Similar results were observed in trehalose/mannitol/dextran (40 kDa) formulations after eight and twelve weeks of storage at 50°C (figure 5.2. D).
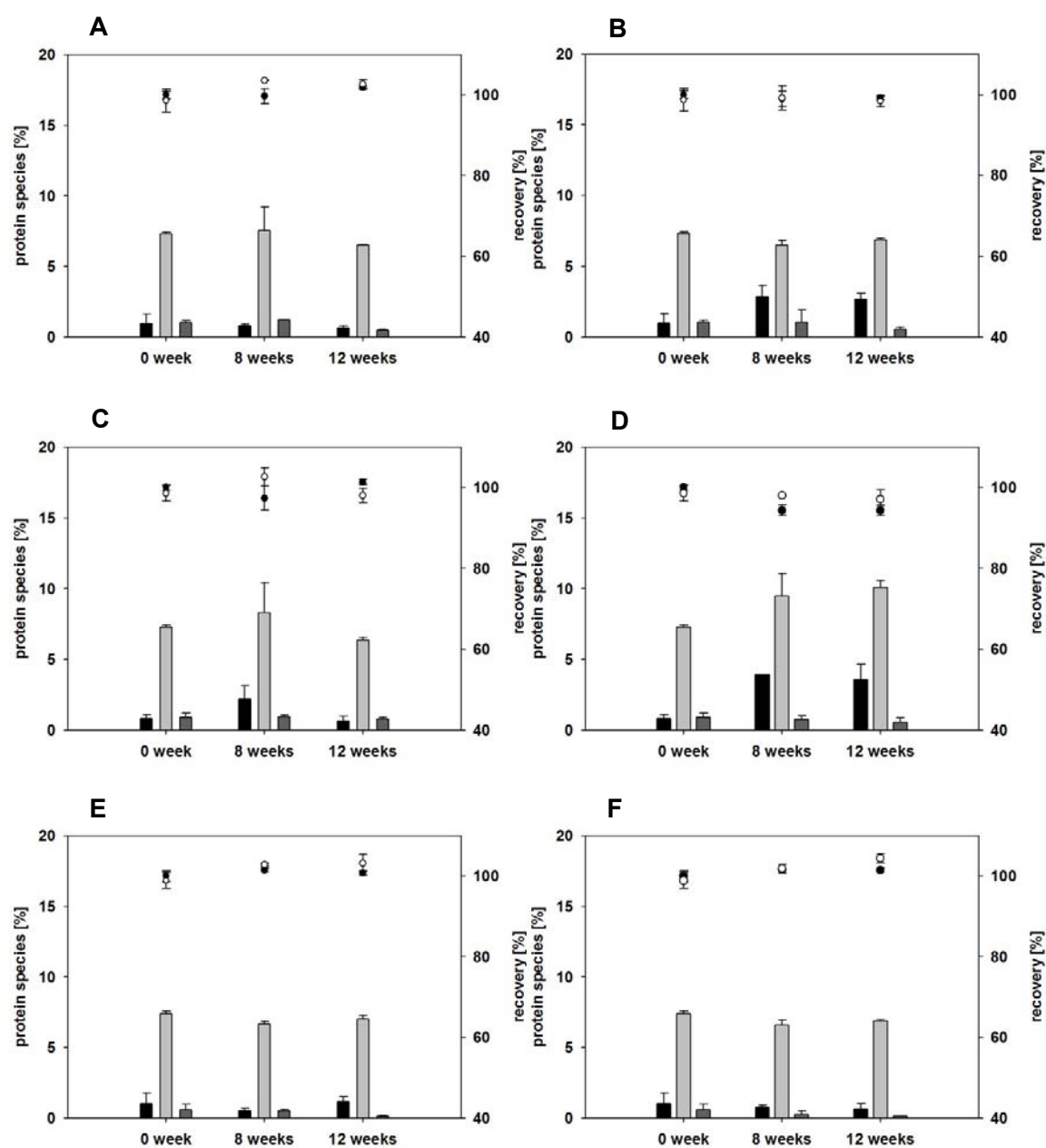
Figure 5.2: Recovery of ovalbumin protein species (%) as determined by size exclusion chromatography in cryo-milled powders after 0, 8 and 12 weeks of storage at 2-8°C (A, C, E) and 50°C (B, D, F). Trehalose/mannitol/dextran 70 kDa formulations are depicted in A and B. Trehalose/mannitol/dextran 40 kDa formulations are depicted in C and D. Trehalose/mannitol/dextran 6 kDa formulations are depicted in E and F. Black bars represent higher molecular weight aggregates, light grey bars represent dimers, dark grey bars represent fragments. Open circles represent the total protein recovery, filled circles represent monomer recovery (average +/- SD, n=3).

Next to the increase of higher molecular weight aggregates from 0.9% to 3.9%, an increase in soluble dimer from 7.3% to 10.9% was observed. At the same time a decrease in soluble monomer from 100.0% to 94.4% was detected.

However, both formulations (TMD_70 and TMD_40) did not fail to stabilize ovalbumin at lower temperature conditions of 2-8°C (figure 5.2 A, C) and 25°C (samples stored at 25°C can be found in figure 9.1 in the appendix) for a time period of twelve weeks.

In trehalose/mannitol/dextran (6 kDa) formulations no protein aggregation could be observed after twelve weeks of storage neither at 2-8°C (figure 5.2 E), 25°C (samples stored at 25°C can be found in figure 9.2 in the appendix) nor at 50°C (figure 5.2 F). No changes in the pattern of different protein species were observed. Recovery of soluble monomer and total protein recovery was constantly > 99% for the monitored time period.

Summing up the findings regarding the polymer dextran, a destabilizing effect on the native structure of ovalbumin could be observed in collapse freeze-dried and cryo-milled formulations containing dextran 40 kDA and dextran 70 kDA after eight and twelve weeks of storage at 50°C. Only formulations containing dextran 6 kDa exhibited a long term stabilizing effect on ovalbumin at elevated temperatures. Similar results were obtained, for instance, by Maa *et al.* [28]. They could show that low molecular weight dextran (10 kDa) was able to stabilize a subunit influenza vaccine in a spray freeze-dried ternary formulation composition comprising trehalose and mannitol. Pikal *et al.* observed a poor stabilizing effect of dextran 40 kDa on human growth hormone (hGh) in a freeze-dried formulation, leading to aggregation during storage at 40°C [33], thus pointing out that with rising molecular weight of dextran a destabilizing effect on proteins can be observed. Izutsu *et al.* [37] discussed as one possible option for the destabilizing effect on proteins of higher molecular weight dextran the hindrance of accessible hydroxyl groups to stabilize the protein by water-substitution mechanism. Interestingly, they observed perturbance of the secondary structure of the model protein BSA in freeze-dried formulations with low molecular weight dextrans (1.6 to 10.2 kDa) without exposing the formulations to elevated storage temperature. It was also anticipated that next to steric hindrance also phase separation in the freeze-concentrate could possibly

preclude higher molecular weight dextran or other large saccharide molecules to preserve the native conformation of the protein. More similar findings are reported in literature, supporting this theory that higher molecular weight polymers fail to inhibit conformational changes in proteins due to an increased steric hindrance of the molecules with rising molecular weight and hence a decreased H-bonding ability compared with smaller molecules [32, 38, 39].

Allison *et al.* could show that dextran with a molecular weight of 192 kDa was not able to stabilize actin during drying, however a combination of disaccharides and dextran showed superior storage stability of freeze-dried actin [40].

Contrary to this Yoshioka *et al.* showed that protein stability of freeze-dried γ-globulin formulations benefit from the excipient dextran with increasing molecular weight (10 kDa, 40 kDa, 70 kDa and 510 kDa). They explained that the stabilizing effect increases with increasing molecular chain of the polymer and is dependent on the molecular mobility of the formulation [34]. Supporting this theory, Tonnis *et al.* demonstrated that a number of proteins (insulin, HBsAG, LDH and β-galactosidase) were more stable at the presence of dextran 70 kDa than in the presence of dextrans with a lower molecular weight chain. Noteworthy, a substantially higher stabilizing effect was found in formulations containing dextran and trehalose in a 1:1 mixture in comparison to formulations containing dextran alone [35].

Based on the results of the formulation screening and the controversy discussed benefit of dextran with different molecular weight as stabilizing amorphous polymer in freeze-dried formulations, it can be concluded, that formulation composition (most notably the addition of disaccharides), the type of protein to be stabilized as well as the manufacturing process have to be considered in formulation development strategy. In this study only low molecular weight dextran (6 kDa) showed appropriate long term stabilizing effect on ovalbumin at elevated temperature in collapse freeze-dried and cryo-milled formulations.

Figure 5.3 A and B illustrates the results of size exclusion chromatography of trehalose/mannitol/hydroxyethylstarch 70 kDa after eight and twelve weeks storage at 2-8°C and 50°C (samples stored at 25°C can be found in figure 9.2 in the appendix). No

relevant changes in the protein species pattern of ovalbumin were visible in this formulation composition.

It is known that polymers like hydroxyethylstarch (and dextran) alone, without the addition of other excipients, mostly fail to stabilize a protein during freeze-drying [41]. However, in combination with a disaccharide like trehalose or mannitol they can increase the glass transition temperature of the final product and hence provide improved storage stability [42].
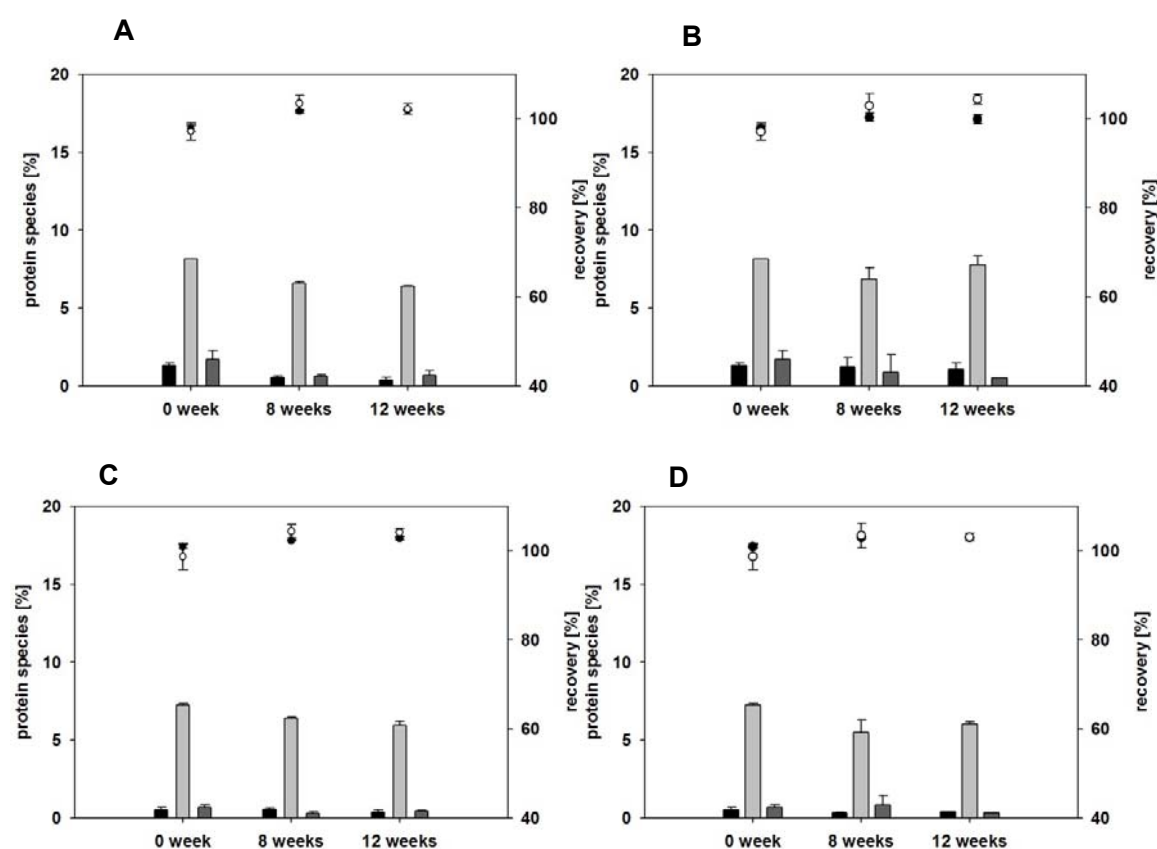
Figure 5.3: Recovery of ovalbumin protein species (%) as determined by size exclusion chromatography in cryo-milled powders after 0, 8 and 12 weeks of storage at 2-8°C (A, C) and 50°C (B, D). Trehalose/mannitol/hydroxyethylstarch formulations are depicted in A and B. Trehalose/phenylalanine formulations are depicted in C and D. Black bars represent higher molecular weight aggregates, light grey bars represent dimers, dark grey bars represent fragments. Open circles represent monomer recovery, filled circles represent the total protein recovery (average +/- SD, n=3).

Contrary to our findings, Rochelle *et al.* showed that hydroxyethylstarch 200 kDa in a ternary mixture with trehalose and mannitol had a detrimental effect on the remaining activity of catalase in a spray freeze-dried formulation [32].

However, Garzon-Rodriguez observed optimized storage stability of lyophilized recombinant human interleukin 11 using a formulation based on trehalose and hydroxyethylstarch with a mean molecular weight of hydroxyethylstarch of 200 kDa [43], hence supporting our findings. This emphasizes again, that apart from the formulation composition, the type of protein which has to be stabilized and also the manufacturing process have to be considered for each formulation individually in order to achieve optimal results regarding vaccine stability.

Similar results as for formulations containing hydroxyethylstrach were obtained for trehalose/phenylalanine formulations (figure 5.3 C and D). Monomer recovery as well as total protein recovery remained > 99 % after twelve weeks storage at 2-8°C, 25°C (samples stored at 25°C can be found in figure 9.3 in the appendix) and 50°C. This is also in line with the results obtained by Bosch *et al.*, who explored low amounts of phenylalanine as bulking agent in aggressively freeze-dried lyophilizates based on trehalose (ratio trehalose to phenylalanine (10:0.5)). The freeze-drying protocol used in the referred study was comparable to the collapse freeze-drying protocol used within this thesis. Excellent stabilization of an IgG1 monoclonal antibody (mab_T1) could be achieved after six months of storage at 50°C [31]. This points out that trehalose based formulations that contain low amounts of phenylalanine as bulking agent are well suited for the stabilization of sensitive proteins by applying aggressive freeze-drying protocols and are also able to preserve protein quality during cryo-milling and subsequent storage at elevated temperatures.

The binary combination of trehalose/mannitol and trehalose based formulations (figure 5.4) showed excellent stabilization of ovalbumin throughout storage at 2-8°C, 25°C (samples stored at 25°C can be found in figure 9.3 and 9.4 in the appendix) as well as at 50°C after twelve weeks. No significant changes in the pattern of the different protein species were observed. Recovery of soluble monomer and total protein recovery was constantly > 99% for the monitored time period.
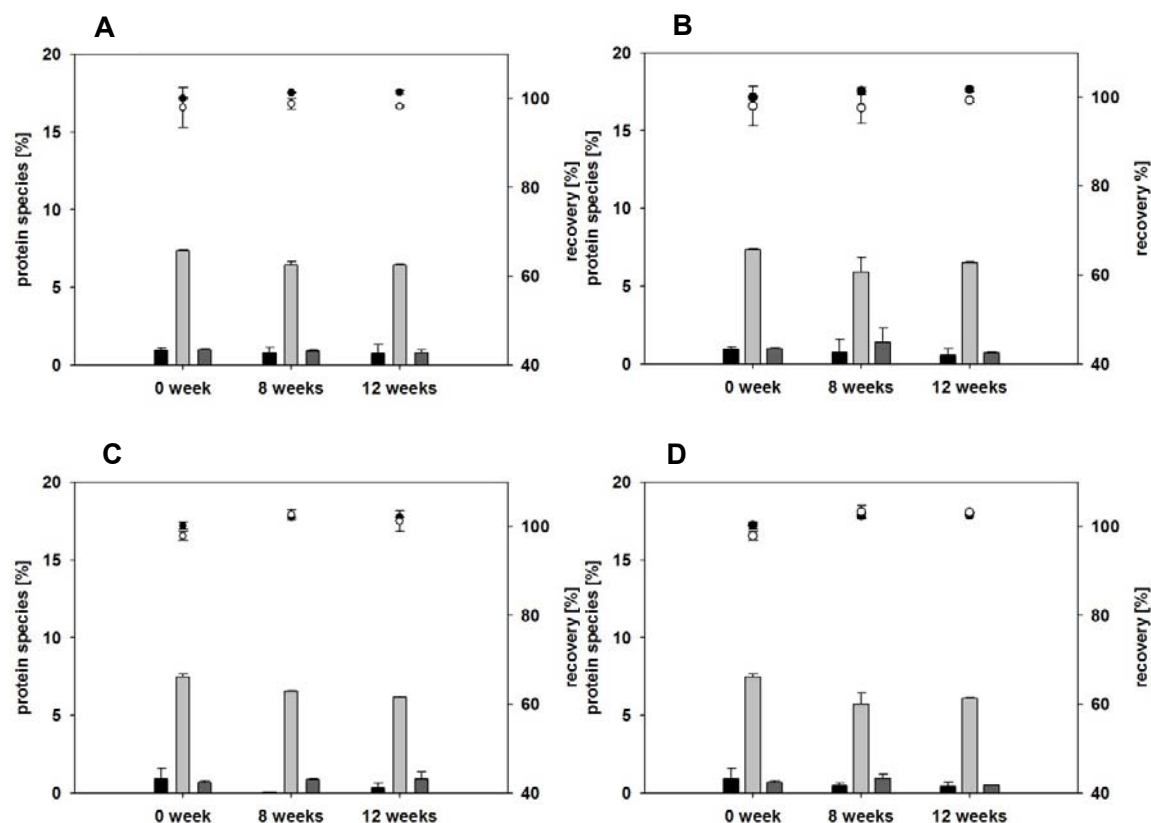
Figure 5.4: Storage stability of the cryo-milled powders after 8 and 12 weeks storage at 2-8°C and 50°C. Recovery of ovalbumin protein species (%) as determined by size exclusion chromatography in cryo-milled powders after 0, 8 and 12 weeks of storage at 2-8°C (A, C) and 50°C (B, D). Trehalose/mannitol formulations are depicted in A and B. Trehalose formulations are depicted in C and D. Black bars represent higher molecular weight aggregates, light grey bars represent dimers, dark grey bars represent fragments. Open circles represent monomer recovery, filled circles represent the total protein recovery (average +/- SD, n=3).

In order to assure the results given by size exclusion chromatography turbidity measurement and light obscuration analysis were used as orthogonal methods to assess the formation of large insoluble aggregates or subvisible particles.

Both methods provide valuable information about the product, however are not suitable to directly crosscheck the accuracy of size exclusion chromatography [44].
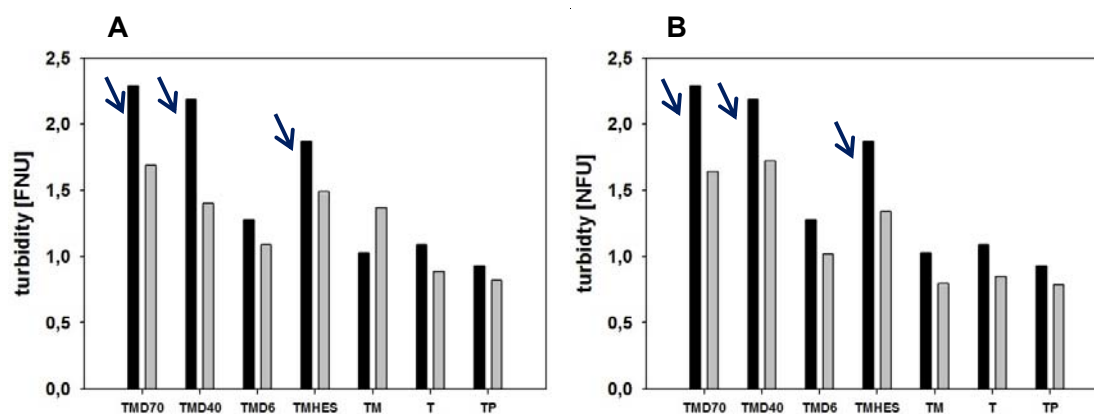
Figure 5.5: Turbidity of the cryo-milled powders after 0 (black bars) and 12 weeks (grey bars) of storage at 2-8°C (A) and 50°C (B).

According to the European Pharmacopoeia samples are regarded as clear if the turbidity level of the sample is below the degree of opalescence of the reference solution "I" [45]. The corresponding turbidity of this solution, determined using a NEPHLA turbidimeter (Dr. Lange, Düsseldorf, Germany), as described in chapter 2 was 3.2 FNU [45-47]. Turbidity measurements of the cryo-milled powders showed that formulations containing higher molecular weight polymers like dextran 70 or 40 kDa or hydroxyethylstarch 70 kDa exhibited higher turbidity levels than binary combinations of trehalose/mannitol, trehalose/phenylalanine or formulations based on trehalose/mannitol/dextran (6 kDa) or on trehalose alone (figure 5.5). However, the turbidity levels remained below 3.2 FNU, and are therefore, consistent with the European Pharmacopoeia, regarded as clear. Furthermore, turbidity levels did not change significantly after storage of the powders for twelve weeks either at 2-8°C or at 50°C. Yet, only a trend towards a destabilizing effect on ovalbumin of higher molecular weight polymers can be observed.

Figure 5.6 depicts the cumulative particle counts > 1 µm, > 10 µm and > 25 µm of the powders after cryo-milling and storage at 2-8°C and 50°C for twelve weeks.

Formulations containing dextran (70 kDa) showed after twelve weeks of storage at 2-8°C an increase in particle counts > 1 µm from 8304 ± 775 to 16963 ± 1339 (figure 5.6 A). Similarly an increase in particles > 1 µm to 16886 ± 23 could be observed after

twelve weeks of storage at 50°C. Formulations containing dextran (40 kDa) showed already initially particle counts > 1 µm in the range of 22783 ± 163. However, the number of particles did not further increase during storage at 2-8°C or 50°C. Formulations based on trehalose/mannitol/dextran (6 kDA) showed an increase in particle counts > 1µm after twelve weeks of storage at 2-8°C, though this was not the case at 50°C. The particle counts > 1 µm did not change significantly in trehalose/mannitol/hydroxyethylstarch (70 kDa), trehalose/mannitol or trehalose formulations after twelve weeks of storage at 2-8°C, but, interestingly, decreased after storage at 50°C. Trehalose/phenylalanine formulations showed an increase in particle counts > 1 µm after twelve weeks of storage at 2-8°C. However, this was not observed in samples stored at 50°C. Generally the numbers of particles > 1 µm were below 25000 counts for all formulations during the monitored time period, and can therefore only depict trends. The obtained results support the observations obtained by size exclusion chromatography, showing a trend towards a destabilizing effect of higher molecular weight dextran on ovalbumin.

The impact of the population of particles in the range of 1 µm to 10 µm in protein pharmaceutics, also known as subvisible particles, on drug safety is extensively discussed in literature [48-50]. Just recently an informational USP chapter, *"Subvisible Particulate Matter in Therapeutic Protein Injections <1787>"* [51, 52] was published, providing guidance on subvisible particles in the 2-µm to 10-µm range. The chapter does not provide count limits but highlights the determination of this inherent protein population and its character as an aid for the scientific development process for therapeutic protein products. Hence, the above-mentioned results in the subvisible particle range, obtained for formulations containing higher molecular weight polymers, should be assessed critically and in the overall context of stability assessment.

Formulations with higher molecular weight dextrans (70 and 40 kDa) and hydryoxyethylstarch (70 kDa) showed already initially higher total particle counts > 10 µm than the binary combinations of trehalose/mannitol, trehalose/phenylalanine formulations or trehalose formulations (figure 5.6. C, D). Trehalose/mannitol/dextran (70 kDa) formulations showed an increase in particles > 10 µm after storage at 2-8°C from

257 ± 9 to 312 ± 6 as well as after twelve weeks at 50°C to 377 ± 10. A decrease in particle counts > 10 µm after storage at 2-8°C and 50°C was observed in trehalose/mannitol/dextran (40 kDa) and trehalose/mannitol/hydroxyethylstarch (70 kDa) formulations. Trehalose/mannitol/dextran (6 kDa), trehalose/mannitol, trehalose/phenylalanine and trehalose formulations showed no relevant changes in particle counts > 10 µm after twelve weeks of storage at 2-8°C or 50°C.

In all samples particle counts > 10 µm were below 400 counts per containment, which is well in line with the specified limits of the European Pharmacopoeia (Ph. Eur.), requiring less than 6000 particles per containment in this size range.

Regarding particle counts > 25 µm, trehalose/mannitol/dextran (70 and 6 kDa) and trehalose/mannitol/hydroxyehtylstarch (70 kDa) showed higher levels in comparison to the other formulations (figure 5.6. E, F). However, particle counts decreased after storage at 2-8°C and 50°C. In all samples particle counts > 25 µm were below 35 counts per containment, which is well in line with the specified limits of the European Pharmacopoeia (Ph. Eur.), requiring less than 600 particles per containment in this size range.

It has to be emphasized that the results of light obscuration measurement were well within the limits of the European Pharmacopeia for all samples during storage at 2-8°C and 50°C for at least twelve weeks. The specified limits of the European Pharmacopeia are set for particulates in parenteral injectables in order to prevent clogging of blood vessels. Regarding subvisible particles in the 1 µm to 10 µm range, only little is known about the relevance of these inherent protein aggregates, and particularly in the above mentioned magnitude for other application routes, such as subcutaneous or intradermal injection. Though, in terms of early formulation development valuable information about the stability of the incorporated protein and trends towards protein aggregation can be obtained.
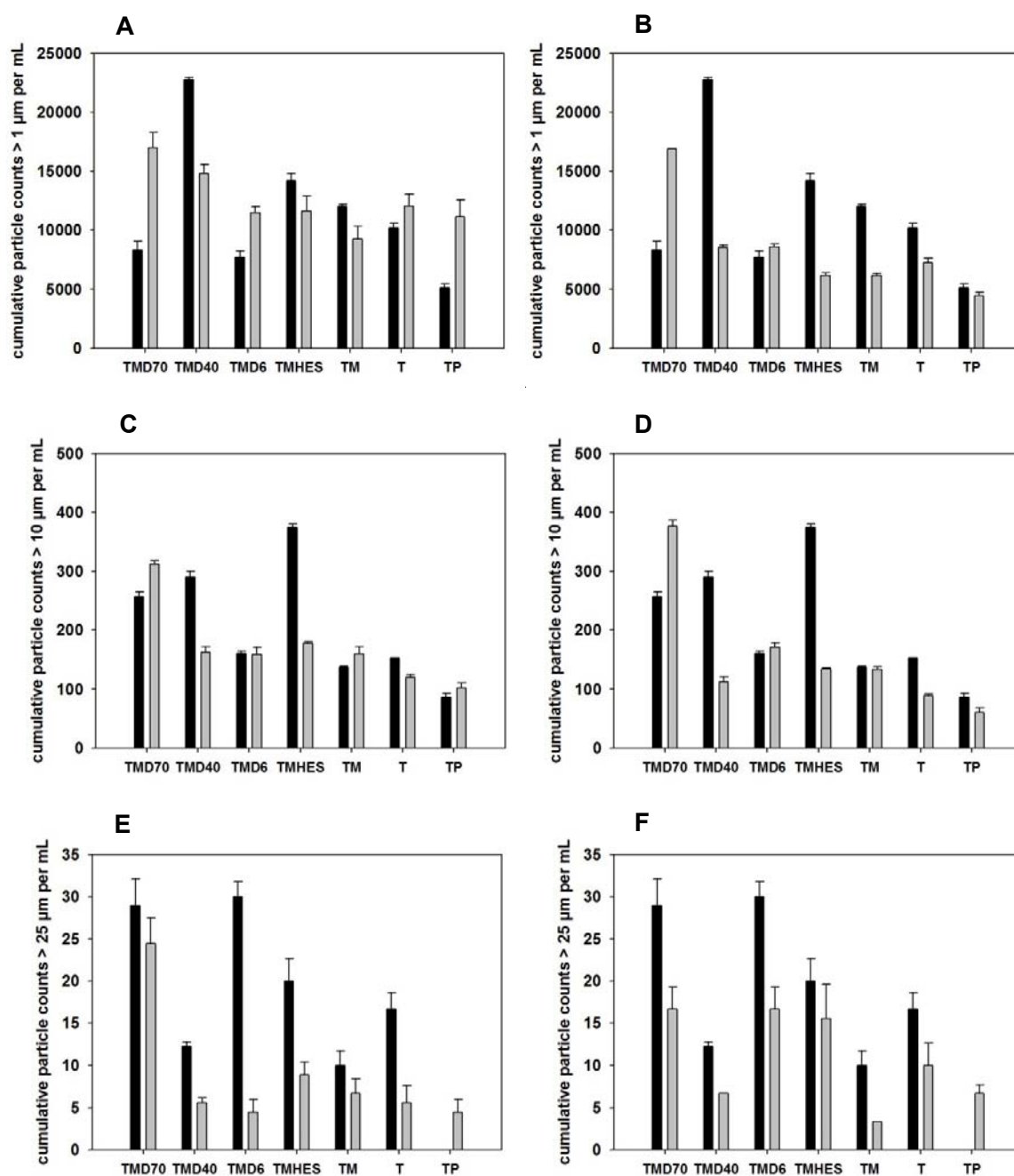
Figure 5.6: Cumulative particle counts > 1, 10 and 25 µm of cryo-milled powders as determined by light obscuration (average +/- SD, n=3) after 0 (black bars) and 12 weeks (grey bars) of storage at 2-8°C (A, C, E) and 50°C (B, D, F).

In summary, formulations with higher molecular weight polymers showed higher particle counts, which confirm the results obtained by turbidity measurements and size exclusion chromatography.

3   INFLUENCE OF FORMULATION COMPOSITION ON PHYSICO-CHEMICAL CHARACTERISTICS OF PARTICLES

Particle morphology of the cryo-milled powders was characterized by particle size measurement and determination of the specific surface area of the particles. Both characteristics are crucial for an intradermal ballistic application route as only dense and robust sugar particles with particle sizes between 20 µm and 70 µm can be accelerated to a certain velocity having a sufficient momentum to breach the outermost layers of the skin [28, 30, 53].

The cryo-milling process was selected according to the rigidity of the formulation composition and the established protocol as described in chapter 2 and 4. Thus, formulation compositions with higher molecular weight polymers were milled for 30 seconds at 25 Hz after a pre-cooling time of 10 min using a cryo-mill. All other formulations were milled for 15 seconds at 25 Hz after a pre-cooling time of 10 min, respectively. Consequently, a uniform particle size distribution in the targeted size range for intradermal injection could be achieved. The resulting particle size distribution of the powders was measured by laser light diffraction as described in chapter 2. Particle size distribution was calculated as an average of 6 measurements applying the Fraunhofer theory and was characterized with median diameter and span of the volume distribution. Each sample was measured at least in triplicates.

The median volume diameter of the cryo-milled particles varied between 21.3 ± 1.5 µm and 37.2 ± 0.5 µm (figure 5.7) for all formulations and the span of the volume distribution indicates a narrow particle size distribution with 3.3 to 5.5.

Table 5.2 illustrates the amount of particles > 100 µm and < 10 µm within the particle size distribution of each formulation. The separation of particle fractions > 100 µm and < 10 µm by sieving might be necessary, as particles > 100 µm can cause injuries on the skin surface [53-55]. Depending on the injection device used, particles < 10 µm fail to penetrate into the skin, as a low particle size in combination with a generally low true density of sugar particles result in a decreased impact momentum of the particles [28, 56-58]. Further relevant issues related to ballistic particle acceleration will be discussed in chapter 7.
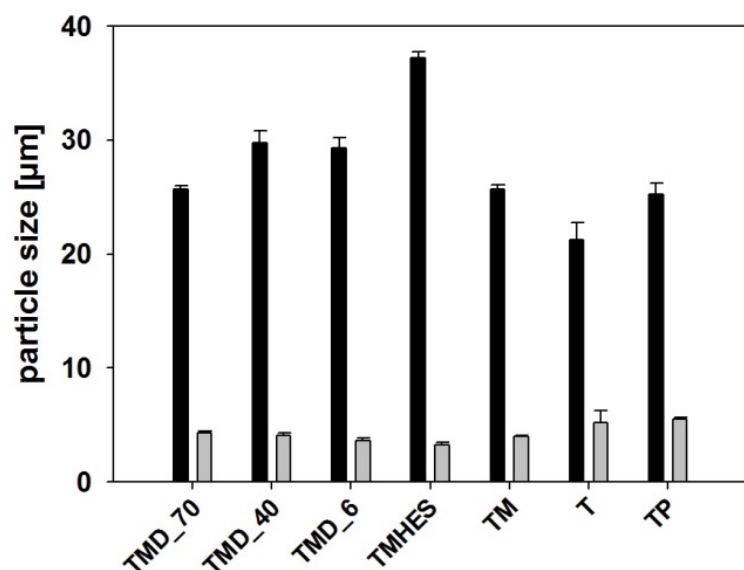
Figure 5.7: Particle size distribution of cryo-milled powders calculated as an average of three measurements and characterized with median diameter (black bars) and span (grey bars) of the volume distribution (average +/- SD, n=3).

Table 5.2: Particle size distributions after cryo-milling μm of the different cryo-milled powders and particle fractions > 100 μm and < 10 within each distribution.

formulation composition	particles > 100 μm [%] ± SD	particles < 10 μm [%] ± SD
TMD_70	12.0 ± 0.6	24.4 ± 0.3
TMD_40	13.4 ± 1.0	21.3 ± 0.7
TMD_6	12.0 ± 0.8	24.5 ± 0.6
TMHES_70	15.2 ± 1.2	17.8 ± 0.2
TM	10.9 ± 0.4	24.1 ± 0.3
T	11.9 ± 2.3	31.8 ± 1.5
TP	17.1 ± 0.9	30.1 ± 0.5

Formulations containing polymers or phenylalanine showed the highest proportion of particles > 100 μm. Trehalose and trehalose/phenylalanine formulations had the highest

amount of particles < 1µm. Trehalose/mannitol/hydroxyethylstarch (70 kDa), trehalose/mannitol/dextran (40 kDa) and trehalose/mannitol formulations had the highest proportion of particles in the desired size range with a yield of 65 to 67%.

As already discussed in chapter 3, not only collapse freeze-drying led to a strong reduction of the specific surface area of the sugar matrix and thereby to a dense matrix structure, but also the formulation composition itself has an impact on the specific surface area of the cryo-milled powder particles.

The specific surface area of the particles was determined by BET krypton gas adsorption as described in chapter 2. Figure 5.8 shows, that particles of formulations containing higher molecular weight polymers exhibited a lower specific surface (0.6 - 0.9 m^2/g) as particles of formulations containing lower molecular weight dextran, a binary combination of trehalose/mannitol, trehalose/phenylalanine or formulations based on trehalose (1.2 – 1.4 m²/g).
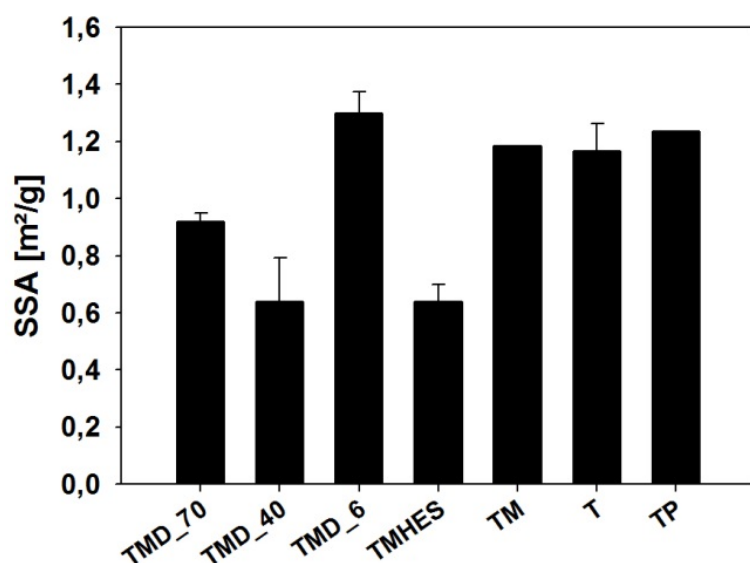
Figure 5.8: Specific surface are of the cryo-milled powders as determined by BET krypton gas adsorption (average +/- SD, n=3).

Generally, the two-stage process of collapse freeze-drying and cryo-milling resulted in a smaller specific surface area of the particles than known from other drying processes like spray-drying or spray-freeze-drying. For example, spray freeze-drying and spray freezing into liquid of the model protein lysozyme in a formulation based on trehalose resulted in a specific surface area of the particles in the range of 26.9 to 86.4 m²/g [59]. Webb *et al.* obtained a specific surface area of 12-14 m²/g for rh-IFNɣ in a spray freeze-dried formulation based on trehalose [60]. Commonly, spray freeze-dried particles exhibit low density, have a high internal porosity and hence, a high specific surface area [36]. A small surface area of the particles is related to low porosity and highly dense and robust particles. Therefore, a positive impact on the mechanical strength of the particles during ballistic acceleration and injection is expected [56].

Furthermore, it was reported by Abdul-Fattah *et al.* that a low specific surface area of the product enhanced storage stability of the incorporated protein in foam dried formulations such as trehalose/phenylalanine and trehalose/mannitol formulations [61].
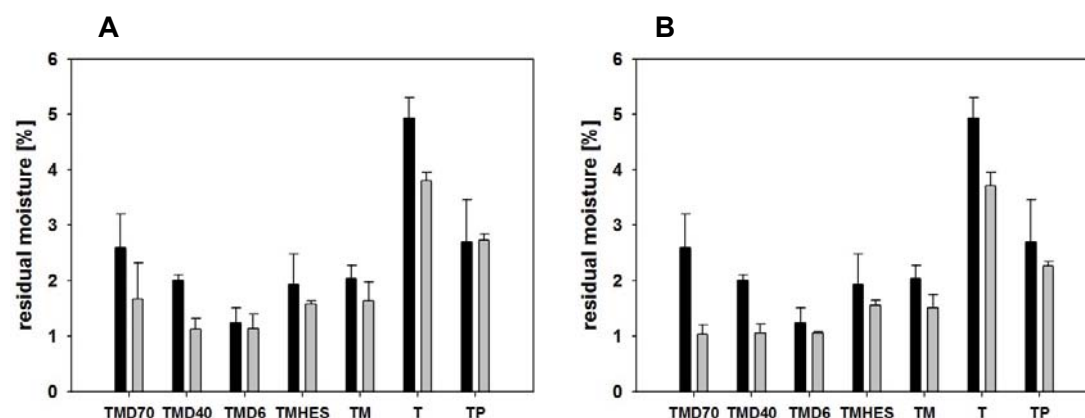
Figure 5.9: Residual moisture of the cryo-milled formulations after 0 (black bars) and 12 weeks (grey bars) of storage at 2-8°C (A) and 50°C (B), determined using the Karl-Fischer direct methanol extraction method.

Another characteristic of the powder formulation, which influences storage stability of the product, is the residual moisture of the powders.

Figure 5.9 shows the residual moisture of powders directly after cryo-milling and after twelve weeks of storage at 2-8°C and 50°C. Trehalose powders showed already at the beginning of the stability study the highest residual moisture levels with 4.9% ± 0.4 in

comparison to formulations based on the bulking agents mannitol (1.2% ± 0.3 to 2.6% ± 0.6) or phenylalanine (2.7% ± 0.8). This is in agreement with the common knowledge that the addition of bulking agents improves the drying behavior of lyophilizates [62]. No increase in residual moisture levels could be observed dependent on storage temperature. A slight decrease in residual moisture levels upon twelve weeks of storage was observed, which was caused most probably by water vapor permeability of the rubber stoppers.
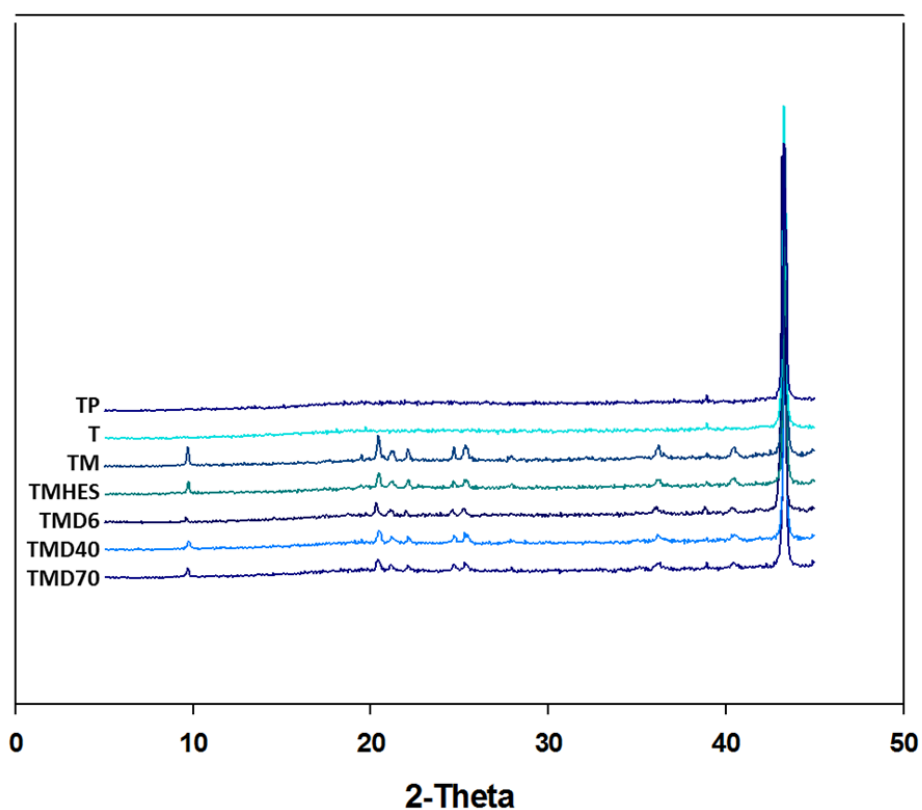
Figure 5.10: X-ray powder diffraction patterns of the cryo-milled powders after 12 weeks of storage at 50°C.

X-ray powder diffraction of the cryo-milled powders showed that trehalose and trehalose/phenylalanine powders were fully amorphous after freeze-drying and cryo-milling (figure 5.10). This is in good agreement with the characterization of aggressively freeze-dried trehalose-phenylalanine (ratio 10:0.5) formulations as demonstrated by

Bosch *et al.* [31]. This is particularly advantageous as it is known that amorphous components can act as water substitute in the dried state and hence provide an increased stability for the protein [63-65]. Trehalose/mannitol formulations and formulations containing polymers showed crystalline patterns. Mannitol crystallized into the δ-modification during freeze-drying, which is characterized by peaks at 9.7 °2-Theta, whilst no peaks were apparent at 17.9 °2-Theta. It is known that bulking agents like mannitol in the crystalline modification not only give mechanical strength to the lyophilized cake but also take influence on the drying behavior of the formulation and thus having impact on the residual moisture level of the freeze-dried cake. By doing so, mannitol in the crystalline modification acts indirectly as protein stabilizer as only mannitol in the amorphous state can prevent protein aggregation by molecular interactions [17, 66]. The different storage conditions did not influence the XRD-patterns after twelve weeks of storage at 50°C.

Table 5.3: Glass transition temperatures after collapse freeze-drying, cryo-milling and storage at 2-8°C, 25°C and 50°C as determined by DSC (average ± SD, n=3).

formulation composition	storage temperature [°C]	storage time [weeks]	T_g [°C] ± SD	Δc_p [J/gK] ± SD
T	-	0	69.83 ± 0.42	0.51 ± 0.02
	2-8°C	12	72.20 ± 4.12	0.41 ± 0.26
	25°C	12	51.20 ± 18.56	0.56 ± 0.06
	50°C	12	73.90 ± 0.90	0.54 ± 0.04
TP	-	0	87.30 ± 0.85	0.56 ± 0.15
	2-8°C	12	78.80 ± 16.83	0.53 ± 0.07
	25°C	12	48.00 ± 32.08	0.60 ± 0.05
	50°C	12	86.10	0.53
TM	-	0	73.75 ± 2.76	0.27 ± 0.05
	2-8°C	12	74.65 ± 0.35	0.27 ± 0.09
	25°C	12	70.17 ± 0.96	0.27 ± 0.02
	50°C	12	41.80 ± 15.32	0.33 ± 0.02

Physicochemical properties of the formulations like glass transitions and melting events were characterized by differential scanning calorimetry (DSC). Glass transition

temperatures could be determined in trehalose, trehalose/mannitol and trehalose/phenylalanine formulations by differential scanning calorimetry (table 5.3). As no melting peaks were detectable in trehalose and trehalose/phenylalanine formulations it can be concluded that both formulations were amorphous after collapse freeze-drying and cryo-milling as well as after twelve weeks storage at 2-8°C, 25°C and 50°C.

This is in good agreement with the results observed earlier by X-ray powder diffraction measurements. Trehalose/mannitol formulations showed a partly amorphous and partly crystalline structure, as glass transition events were detected next to melting peaks (figure 5.11). Tg was determined in trehalose/mannitol formulations in the range of 42 to 75°C and can be assigned to trehalose with regard to its residual moisture content [67, 68]. The glass transition temperature can be lowered by 10K for each percent of moisture in the product, as water acts as plasticizer [69]. The melting peak at 132-137°C with a shoulder at 139-151°C can be assigned to the melting point of mannitol. This is in good agreement with literature, as it was observed that δ-mannitol can be transformed at 130°C to ß-mannitol, showing a subsequent melting peak at 150 to 158 °C [70-72]. Furthermore, it has to be considered that all formulations are composed of mixtures and therefore the melting points can be shifted to lower temperatures as for pure materials.

No glass transition events could be determined in formulations containing either the polymer dextran or hydroxyethylstarch (figure 5.11). However, endothermic peaks were visible at 130°C - 138°C with a shoulder in the range of 140°C - 150°C, indicating the melting point of the crystalline components. Though, these formulations consist either of fully crystalline material, or, the glass transition temperature of these formulations is overlapped by the melting peak of the crystalline components. Contrary to our findings Rochelle *et al.* observed that spray-freeze-dried powders of catalase in a trehalose/mannitol formulation containing dextran or hydroxyethylstarch remained fully amorphous according to X-ray diffraction [32]. Hence, the different results can be attributed to the different manufacture processes.

117
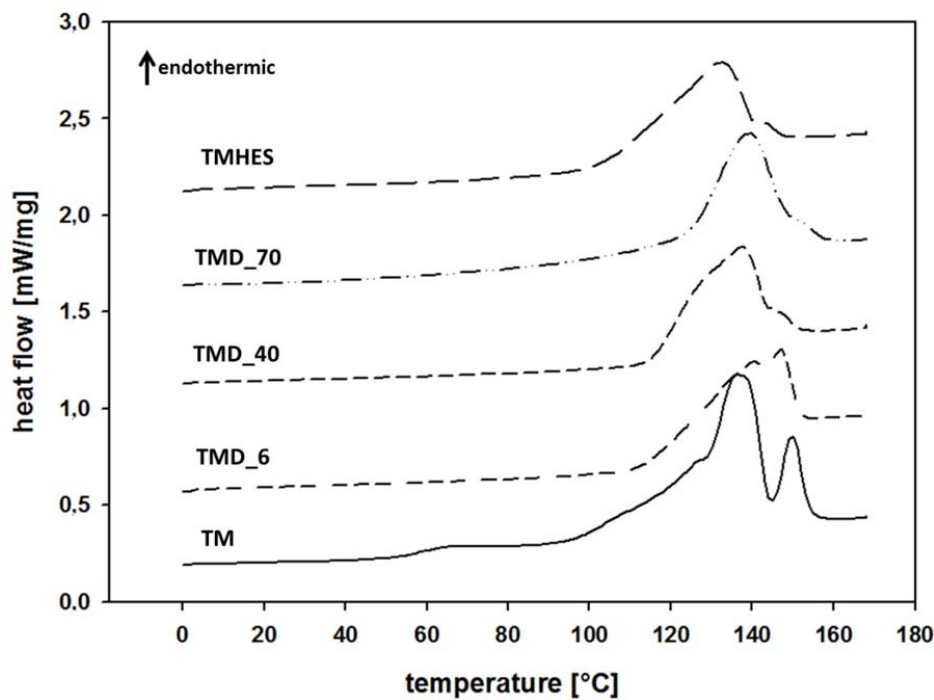
Figure 5.11: DSC heating scans (2nd scan) of collapse freeze-dried and cryo-milled formulations comprising the polymers dextran with different molecular weight or hydroxyethylstarch, showing melting endotherms of the crystalline components.

The glass transition of trehalose/mannitol formulations decreased during storage at 50°C, whereas it remained comparable prior to storage in trehalose and trehalose/phenylalanine formulations (table 5.3). High glass transition temperatures of the trehalose, trehalose/mannitol and trehalose/phenylalanine formulations (>70 °C) indicate superior storage stability.

4   SUMMARY AND CONCLUSION

To sum up the findings of the formulation screening and storage stability study, aggregate formation was observed in formulations containing higher molecular dextran (40 and 70 kDa) during storage at 50°C as determined by size exclusion chromatography. A destabilizing effect of higher molecular weight polymers on antigen conformation was further confirmed by turbidity and light obscuration measurements. No aggregate formation was detected in trehalose/mannitol/hydroxyethylstarch formulations, trehalose/mannitol formulations, trehalose/phenylalanine formulations and trehalose/mannitol/dextran 6 kDa and trehalose formulations after collapse freeze-drying and cryo-milling as well as during storage at accelerated temperatures. Trehalose/mannitol formulations show superior properties in terms of both, protein stability and particle morphology.

The median particle size of all formulations was within a narrow range between 21.3 ± 1.5 µm and 37.2 ± 0.5 µm and targeted hence our scope, however, trehalose/mannitol formulations, trehalose/hydroxyethylstarch and trehalose/mannitol/dextran 6 kDa formulations showed additionally the highest yield of particles in the range of 10 to 100 µm. Formulations containing higher molecular weight polymers exhibited the smallest specific surface area of particles within the formulation screening, which is associated with a high mechanical strength of the particles - a vital property for ballistic injection of the particles [56]. Notably, all formulations showed a low specific surface area of the particles in comparison to particles produced by other drying processes than collapse freeze-drying like spray-drying or spray-freeze-drying. The amorphous matrix structure of trehalose formulations, trehalose/phenylalanine formulations and the partly amorphous structure of trehalose/mannitol formulations together with the high glass transition temperatures of these formulations are associated with a superior protein stabilizing effect during storage. Among the last mentioned formulations, trehalose/mannitol formulations showed additionally low residual moisture levels throughout the time of storage.

In conclusion, trehalose/mannitol formulations exhibited excellent protein stability throughout storage at elevated temperatures and showed moreover superior physico-chemical and morphological characteristics.

5   EXCURSUS: HIGHLY CONCENTRATED OVALBUMIN FORMULATIONS

The skin, to be more precise, the epidermis, is an attractive target for needle-free vaccine injection as it possesses a network of immunocompetent cells. Intradermal vaccination can elicit mucosal immune responses as well as an enhanced cellular immunity in comparison to conventional vaccination via intramuscular injections [73]. Furthermore, the epidermis generally lacks blood vessels and sensory nerve endings, thus, a nearly pain free application comes into reach and hence, an increased acceptance among patients might be expected. However, due to the low thickness of this tissue layer of about 50 – 100 µm [74] it is not only challenging to reach this target in terms of accuracy. In addition, the epidermis has also only a limited capacity to take in a powdered vaccine dose [75]. Similarly, current devices for ballistic injection are restricted to retain a certain amount of powder. Dependent on the type of device the maximal payload of powder is limited to 1 to 2 mg [30] or 0.5 to 5 mg [76]. Although the effectiveness of low doses of intradermal vaccines is comparable to full doses of conventional intramuscular vaccines [77-85], so far, often more than one skin site had to be injected in order to apply an adequate vaccine dose [29].

A high load capacity of the powder with antigen is desirable and hence another objective in early formulation development.

Particularly for ballistic powder injections, an adequate ratio between the amount of excipients and the amount of antigen is crucial. The type and character of the excipient mixture as well as the manufacturing process influence the physical characteristic of the particles [28, 36]. A highly dense and mechanically robust structure of the particles is, as already mentioned previously, vital to breach the outermost layers of the skin by impacting at the skin surface [30, 56].

In this excursus, selected formulation compositions of the prior formulation screening were subjected to a study, investigating the influence of a higher antigen load of the powder particles on antigen stability and on physico-chemical characteristics of the powder particles. Challenges in the formulation strategy of highly concentrated protein formulations are analytical challenges, as for the most of the established analytical techniques dilution of the samples is required [86, 87]. Furthermore, the viscosity of

formulation composition, which is dependent on the excipient protein ratio, can be challenging for the sample preparation prior to analysis, too [87].

Even though the lyophilization step itself can be used to concentrate a liquid protein formulation, which can be reconstituted after lyophilization with a lower, desired solvent volume [87], little is known about the stability of high protein concentrations in solids.

Lyophilization with appropriate cryo- and lyoprotectants can act as stabilizing step also for high protein concentration solutions during formulation as the molecular mobility of the proteins is reduced in a rigid, amorphous matrix. It is postulated that the molar ratio of the lyoprotectant to the protein should be 360:1 or even greater to provide effective protection against protein aggregation [88]. Furthermore, it was shown in the previous section, that bulking agents like mannitol or phenylalanine, as well as polymers have a favorable influence on powder particles with regard to their residual moisture as well as on other physico-chemical characteristics like the specific surface area or particle size after cryo-milling.

An antigen load of powder particles with 25 µg of the model antigen ovalbumin per mg powder was well characterized previously. In this section the antigen load was increased from 25 µg/mg ovalbumin to 200 µg/mg. Four representative formulations (trehalose/mannitol/dextran 70 kDa, trehalose/mannitol/hydroxyethylstarch 70 kDa, trehalose/mannitol and trehalose/phenylalanine) were collapse freeze-dried and cryo-milled as described previously (see chapter 2). The influence of the higher antigen load of the formulation was scrutinized with regard to protein quality in terms of formation of aggregates and physico-chemical characteristics of the lyophilizates and powders.

5.1 INFLUENCE OF HIGH ANTIGEN LOAD ON PROTEIN STABILITY

The gold standard to analyze soluble protein aggregates is size exclusion chromatography. However, sample preparation required dilution of the samples to low concentrations. Therefore, it cannot be excluded, that the protein aggregates underwent self-dissociation [87].

Figure 5.12 shows the recovery of different ovalbumin protein species in trehalose/mannitol/dextran70 kDA and trehalose/mannitol/hydroxyethylstarch 70 kDa as determined by size exclusion chromatography.
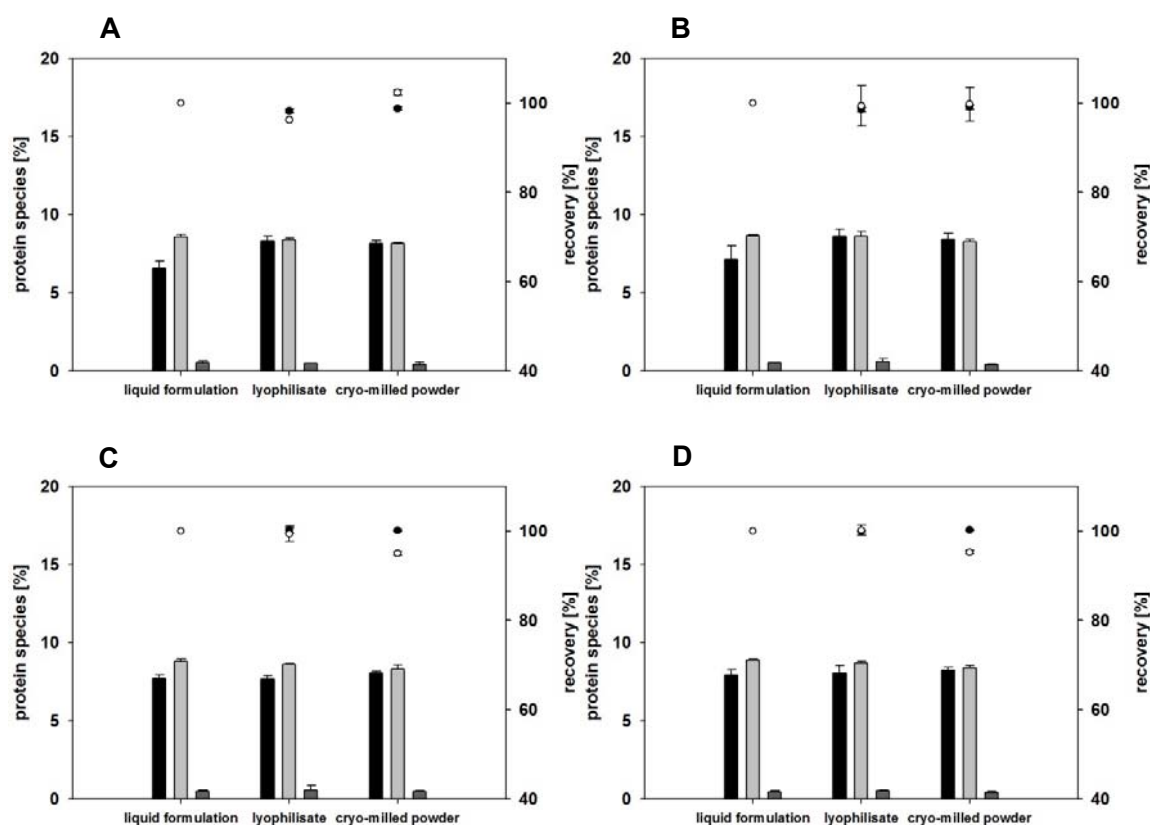
Figure 5.12: Recovery of ovalbumin protein species (%) as determined by size exclusion chromatography of highly concentrated ovalbumin formulations containing 200 µg/mg ovalbumin (A, C) in comparison to ovalbumin formulations containing 25 µg/mg ovalbumin (B, D). Trehalose/mannitol/dextran 70 kDa are depicted in A and B, trehalose/mannitol/hydroxyethylstarch formulations are depicted in C and D. Black bars represent higher molecular weight aggregates, light grey bars represent dimers, dark grey bars represent fragments. Open circles represent monomer recovery, filled circles represent the total protein recovery (average +/- SD, n=3).

Neither formulations with an antigen load of 25 µg/mg ovalbumin (figure 5.12 B, D) nor with an antigen load of 200 µg/mg (figure 5.12 A,C) showed additional formation of aggregates in comparison to the liquid formulation after freeze-drying or cryo-milling.
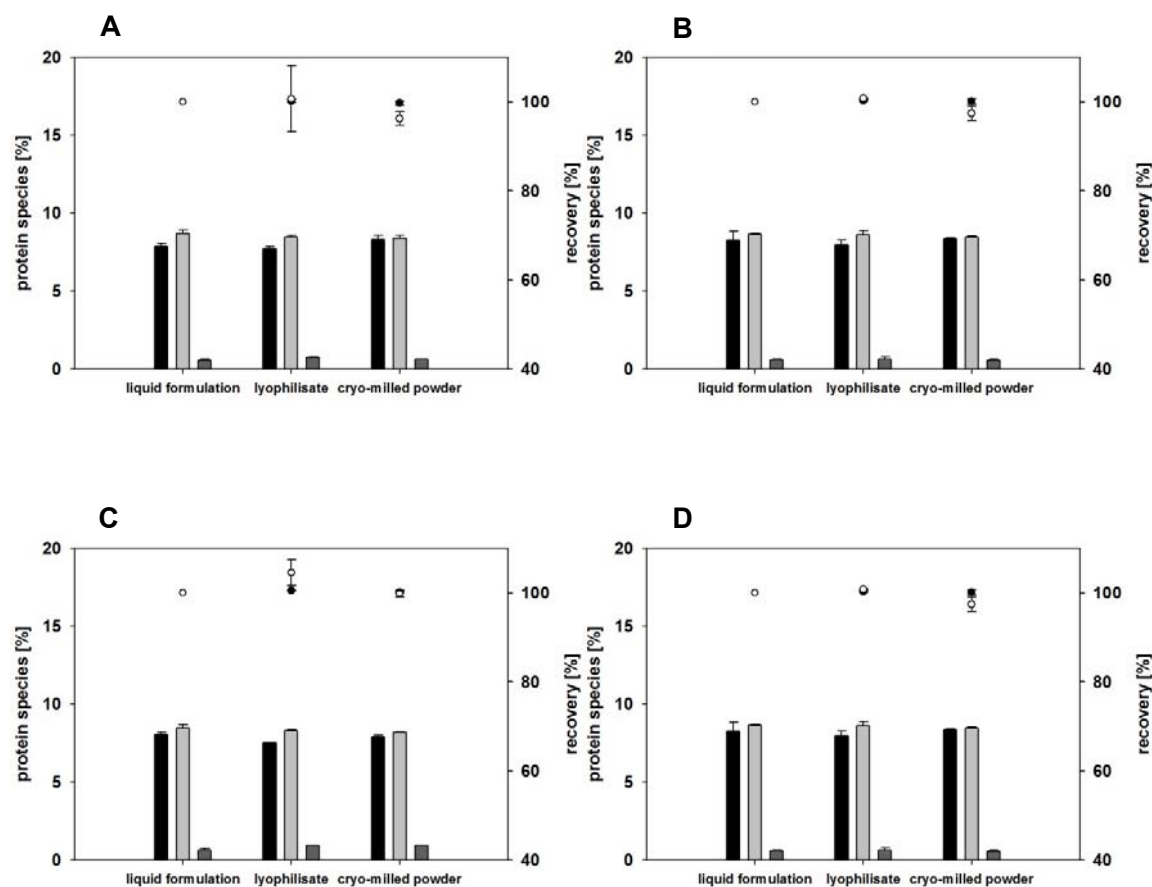
Figure 5.13: Recovery of ovalbumin protein species (%) as determined by size exclusion chromatography of highly concentrated ovalbumin formulations containing 200 µg/mg ovalbumin (A, C) in comparison to ovalbumin formulations containing 25 µg/mg ovalbumin (B, D). Trehalose/mannitol formulations are depicted in A and B, trehalose/phenylalanine formulations are depicted in C and D. Black bars represent higher molecular weight aggregates, light grey bars represent dimers, dark grey bars represent fragments. Open circles represent monomer recovery, filled circles represent the total protein recovery (average +/- SD, n=3).

It has to be mentioned, that the ovalbumin bulk used in this study showed a different protein species pattern as previously in the 3 months stability study, with higher molecular weight aggregate levels (HMWA) between 6.5 and 8% , dimer levels of 8.2 to 8.7% and monomer levels of 80% in the bulk solution. However, the amount of aggregates and the recovery of the soluble monomer did not change after freeze-drying and cryo-milling. Monomer recovery as well as total protein recovery of both polymer-

containing formulations was constantly > 98% and > 95%, respectively, independently of the antigen load.

Similarly, no relevant changes in the pattern of the different ovalbumin protein species pointing out the formation of soluble aggregates were detected in trehalose/mannitol formulations (figure 5.13 A, B) or trehalose/phenylalanine formulations (figure 5.13 C, D) due to the antigen load.
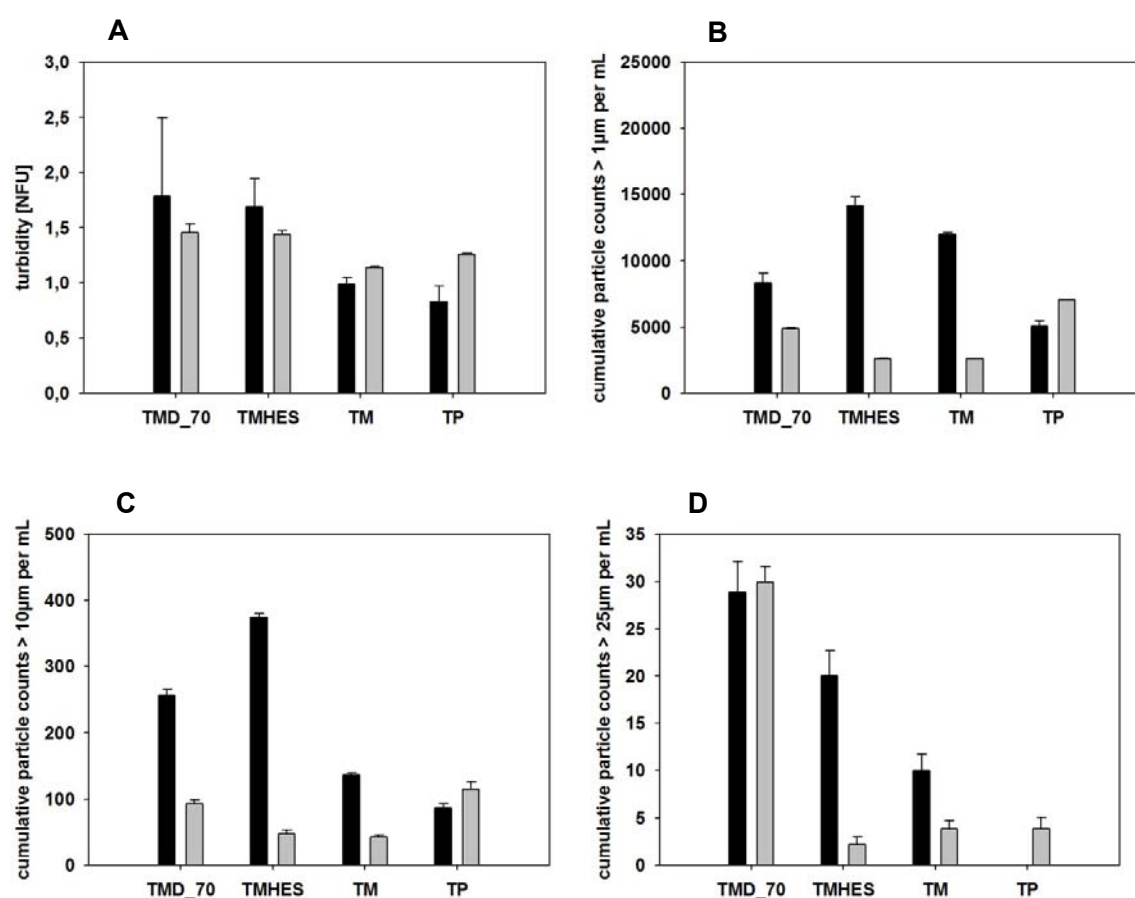
Figure 5.14: Turbidity of the cryo-milled powders as determined by nephelometric turbidity analysis (A). Cumulative particle counts > 1 µm (B), 10 µm (C) and 25 µm (D) of cryo-milled powders as determined by light obscuration (average +/- SD, n=3). Black bars: formulations containing 25 µg/mg ovalbumin. Grey bars: formulations containing 200 µg/mg ovalbumin.

Possible formation of insoluble aggregates or precipitated material due to the increase of protein concentration in the formulations was scrutinized by turbidity measurements and light obscuration. As the highly concentrated ovalbumin formulations exceeded the detection limit of these analytical methods, dilution of the samples prior to the measurement was necessary in order to compare equal protein concentrations to the low concentrated ovalbumin formulations. Further dilution of the samples and analysis was performed as described in chapter 2.

The different formulation compositions showed comparable turbidity levels in the range of 0.8 ± 0.1 to 1.8 ± 0.7 NFU, independently of the antigen load and in good agreement with the results obtained from the previous stability study (figure 5.14 A). Interestingly, light obscuration measurement showed that the number of particles > 1 µm was higher in trehalose/mannitol/dextran 70 kDa, trehalose/mannitol/hydroxyethystarch 70kDa and trehalose/mannitol formulations containing 25 µg/mg ovalbumin as in formulations with 200 µg/mg ovalbumin. Trehalose/phenylalanine formulations showed comparable particle counts independently of the antigen load (figure 5.14 B). Similarly, particle counts > 10 µm were higher in trehalose/mannitol/dextran 70 kDa, trehalose/mannitol/hydroxyethystarch 70kDa and trehalose/mannitol formulations containing 25 µg/mg ovalbumin as in formulations with 200 µg/mg ovalbumin. Particle counts > 25 µm were comparable in trehalose/mannitol/dextran 70 kDa formulations regarding both protein concentrations 25 µg/mg and 200 µg/mg. Trehalose/mannitol/hydroxyethylstarch 70kDa, trehalose/mannitol and trehalose/phenylalanine formulations with 200 µg/ml ovalbumin showed generally low particle counts > 25 µm with 2.2 ± 0.8, 3.9 ± 0.9 and 3.9 ± 1.2 particles. Again, the lower protein concentration (25 µg/mg) in trehalose/mannitol/hydroxyethylstarch 70k Da and trehalose/mannitol exhibited higher particle counts than formulations with an antigen load of 200 µg/mg.

It is known from literature that the protein concentration of a formulation itself can be an inducing factor for aggregation due to bimolecular interaction of molecules [89, 90]. However, this was not confirmed for ovalbumin formulations with an antigen load 200 µg/mg in various trehalose based formulations. Though it cannot be excluded, as

dilution of the formulations was necessary prior to analysis, that reversible association and dissociation of protein aggregates occurred.

5.2 INFLUENCE OF HIGH ANTIGEN LOAD ON PHYSICO-CHEMICAL CHARACTERISTICS OF THE LYOPHILIZATES AND POWDERS

The influence of an increase of the protein concentration on physico-chemical characteristics of the formulations was investigated by residual moisture measurement, particle size measurement and determination of the specific surface area of the cryo-milled powders.

Except in the case of trehalose/mannitol/dextran 70 kDa formulations, a slight decrease in the residual moisture of the formulations was observed due to the increase in the antigen load (figure 5.15).
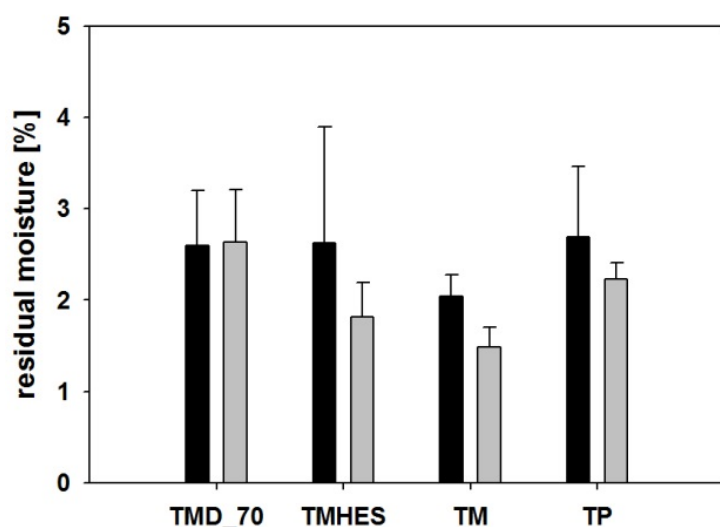
Figure 5.15: Residual moisture of the cryo-milled formulations determined using the Karl-Fischer direct methanol extraction method. Black bars: formulations containing 25 µg/mg ovalbumin. Grey bars: formulations containing 200 µg/mg ovalbumin.

Formulations with 25 µg/mg antigen load showed residual moisture levels in the range of 2.0% to 2.7% with a large standard deviation (SD 0.2 to 1.3), whereas formulations

with an antigen load of 200 µg/mg were in the range of 1.5% to 2.6% (SD 0.2 to 0.6). This can be attributed to the ability of proteins to act as bulking agents in freeze-dried formulations [91].
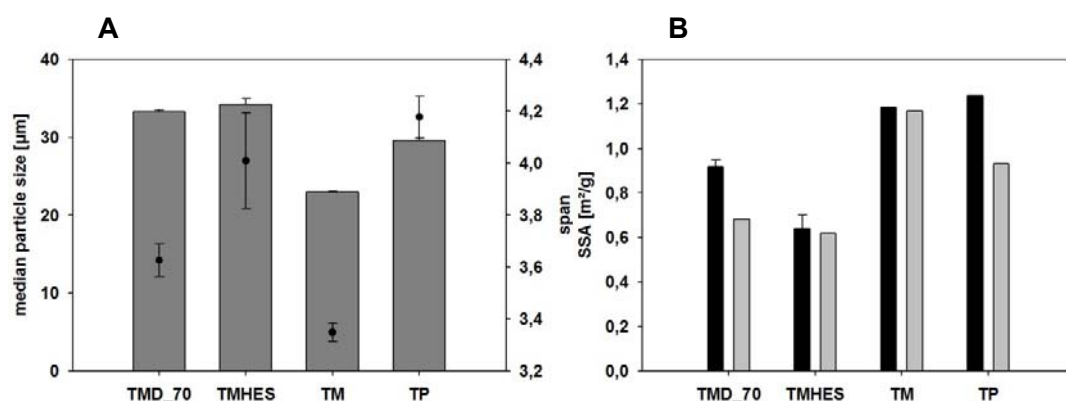
Figure 5.16: (A) Particle size distribution of cryo-milled powders containing 200 µg/mg ovalbumin calculated as an average of three measurements and characterized with median diameter (grey bars) and span (filled circles) of the volume distribution. (B) Specific surface are of the cryo-milled powders as determined by BET krypton gas adsorption (average +/- SD, n=3). Black bars: formulations containing 25 µg/mg ovalbumin. Grey bars: formulations containing 200 µg/mg ovalbumin.

The median particle size of cryo-milled formulations containing 200 µg/mg ovalbumin was 23 µm for formulations based on trehalose/mannitol and ranged between 30 to 35 µm for trehalose/mannitol/dextran 70 kDa, trehalose/mannitol/hydroxyethylstrach 70 kDa and trehalose/phenylalanine formulations (figure 5.16 A). As these results are comparable to the median particle size of cryo-milled formulations with the same excipient mixture containing 25 µg/mg ovalbumin, it can be concluded that the increase of the protein content of the formulation did not influence the particle size of the milled product.

The specific surface area (SSA) of the cryo-milled particles of highly concentrated ovalbumin formulations containing 200 µg/mg was also comparable to formulations with an antigen load of 25 µg/mg (figure 5.16 B). Abdul-Fattah $et\ al.$ determined the SSA of foam-dried carbohydrate formulations to range between 0.04 m^2/g and 0.17 m^2/g [61]. It

was pointed out that the SSA of the formulations increased with increasing mass ratio of protein to stabilizer. Though, in the referred example the protein ratio exceeded the stabilizer ratio. The increase of the concentration of ovalbumin from 25 µg/mg to 200 µg/mg did not affect the SSA of the particles as the stabilizer ratio still dominated particle characteristics.

5.3 SUMMARY AND CONCLUSION

The antigen load of four representative formulations using the model antigen ovalbumin was successfully increased from 25 µg to 200 µg per mg powder.

Complication during manufacturing associated with high protein concentrations, or perturbations of protein quality, were not observed. According to size exclusion chromatography comparable results were obtained for formulations containing 200 µg/mg ovalbumin as for formulations containing 25 µg/mg. Turbidity and light obscuration measurements showed even a superior performance of formulations containing 200 µg/mg ovalbumin.

Due to the route of application in form of dry powder particles, challenges like reconstitution, molar tonicity etc. were omitted. The physico-chemical attributes of the particles are met the requirements for ballistic injection. Particle size ranged with 23 µm to 35 µm in the desired scope [28, 29]. Also the SSA of the particles showed that a comparable dense matrix structure of the powder particles was achieved as for particles with an antigen load of 25 µg/mg.

In conclusion, it was possible to increase the ovalbumin load to 200 µg per mg powder in several formulation compositions without affecting protein quality and preserving the physico-chemical characteristics of the powder needed for ballistic injection.

6   REFERENCES

[1]   Kumru OS, Joshi SB, Smith DE, Middaugh CR, Prusik T, Volkin DB. Vaccine instability in the cold chain: Mechanisms, analysis and formulation strategies. Biologicals 2014;42(5):237-59.

[2]   Manning M, Chou D, Murphy B, Payne R, Katayama D. Stability of Protein Pharmaceuticals: An Update. Pharmaceutical Research 2010;27(4):544-75.

[3]   Graziano G, Catanzano F, Riccio A, Barone G. A reassessment of the molecular origin of cold denaturation. Journal of Biochemistry 1997;122(2):395-401.

[4]   Privalov PL. Cold Denaturation of Protein. Critical Reviews in Biochemistry and Molecular Biology 1990;25(4):281-306.

[5]   Dill KA, Alonso DOV, Hutchinson K. Thermal stabilities of globular proteins. Biochemistry 1989;28(13):5439-49.

[6]   Chang BS, Kendrick BS, Carpenter JF. Surface-induced denaturation of proteins during freezing and its inhibition by surfactants. Journal of Pharmaceutical Sciences 1996;85(12):1325-30.

[7]   Schwegman JJ, Carpenter JF, Nail SL. Evidence of partial unfolding of proteins at the ice/freeze-concentrate interface by infrared microscopy. Journal of Pharmaceutical Sciences 2009;98(9):3239-46.

[8]   Heller MC, Carpenter JF, Randolph TW. Protein formulation and lyophilization cycle design: Prevention of damage due to freeze-concentration induced phase separation. Biotechnology and Bioengineering 1999;63(2):166-74.

[9]   Randolph TW. Phase separation of excipients during lyophilization: effects on protein stability. Journal of Pharmaceutical Sciences 1997;86(11):1198-203.

[10]   Izutsu K-i, Kojima S. Freeze-concentration separates proteins and polymer excipients into different amorphous phases. Pharmaceutical Research 2000;17(10):1316-22.

[11]   Kasper JC, Friess W. The freezing step in lyophilization: Physico-chemical fundamentals, freezing methods and consequences on process performance and quality attributes of biopharmaceuticals. European Journal of Pharmaceutics and Biopharmaceutics 2011;78(2):248-63.

[12]   Franks F. Freeze-drying-from empiricism to predictability. Cryo-letters 1990;11(2):93-110.

[13]   Pikal MJ. Freeze drying. Encyclopedia of Pharmaceutical Technology, Marcel Dekker, New York 2002;1299:1326.

[14]   Tang X, Pikal M. Design of Freeze-Drying Processes for Pharmaceuticals: Practical Advice. Pharmaceutical Research 2004;21(2):191-200.

[15]   Sundaramurthi P, Shalaev E, Suryanarayanan R. Calorimetric and diffractometric evidence for the sequential crystallization of buffer components and the consequential pH swing in frozen solutions. The Journal of Physical Chemistry B 2010;114(14):4915-23.

[16]   Prestrelski SJ, Tedeschi N, Arakawa T, Carpenter JF. Dehydration-induced conformational transitions in proteins and their inhibition by stabilizers. Biophysical Journal 1993;65(2):661-71.

[17]   Izutsu K-i, Kojima S. Excipient crystallinity and its protein-structure-stabilizing effect during freeze-drying. Journal of Pharmacy and Pharmacology 2002;54(8):1033-9.

[18]   Maa Y-F, Prestrelski SJ. Biopharmaceutical powders: particle formation and formulation considerations. Current Pharmaceutical Biotechnology 2000;1(3):283-302.

[19]   Garmise R, Mar K, Crowder T, Hwang CR, Ferriter M, Huang J, et al. Formulation of a dry powder influenza vaccine for nasal delivery. AAPS PharmSciTech 2006;7(1):E131-E7.

[20]   Stotz C, Winslow S, Houchin M, D'Souza A, Ji J, Topp E. Degradation pathways for lyophilized peptides and proteins. Lyophilization of biopharmaceuticals Arlington: AAPS 2004:443-79.

[21]   Arakawa T, Prestrelski SJ, Kenney WC, Carpenter JF. Factors affecting short-term and long-term stabilities of proteins. Advanced Drug Delivery Reviews 2001;46(1-3):307-26.

[22]   Carpenter JF, Arakawa T, Crowe JH. Interactions of stabilizing additives with proteins during freeze-thawing and freeze-drying. Developments in Biological Standardization 1992;74:225-38; .

[23]   Franks F. Solid aqueous solutions. Pure and Applied Chemistry 1993;65(12):2527-37.

[24]   Fox KC. Biopreservation. Putting proteins under glass. Science 1995;267(5206):1922-3.

[25]   Crowe JH, Carpenter JF, Crowe LM. The role of vitrification in anhydrobiosis. Annual Review of Physiology 1998;60(1):73-103.

[26]   Chang LL, Shepherd D, Sun J, Ouellette D, Grant KL, Tang XC, et al. Mechanism of protein stabilization by sugars during freeze-drying and storage: Native structure preservation, specific interaction, and/or immobilization in a glassy matrix? Journal of Pharmaceutical Sciences 2005;94(7):1427-44.

[27]   Etzl EE, Winter G, Engert J. Toward intradermal vaccination: preparation of powder formulations by collapse freeze-drying. Pharmaceutical Development and Technology 2014;19(2):213-22.

[28]   Maa Y-F, Ameri M, Shu C, Payne LG, Chen D. Influenza vaccine powder formulation development: spray-freeze-drying and stability evaluation. Journal of Pharmaceutical Sciences 2004;93(7):1912-23.

[29]   Dean HJ, Chen D. Epidermal powder immunization against influenza. Vaccine 2004;23(5):681-6.

[30]   Schiffter H, Condliffe J, Vonhoff S. Spray-freeze-drying of nanosuspensions: the manufacture of insulin particles for needle-free ballistic powder delivery. Journal of the Royal Society Interface 2010;7(Suppl 4):S483-S500.

[31]   Bosch T. Aggressive Freeze-Drying: a fast and suitable method to stabilize biopharmaceuticals: München, Ludwig-Maximilians-Universität, Diss. ; 2014.

[32]   Rochelle C, Lee G. Dextran or hydroxyethyl starch in spray-freeze-dried trehalose/mannitol microparticles intended as ballistic particulate carriers for proteins. Journal of Pharmaceutical Sciences 2007;96(9):2296-309.

[33]   Pikal MJ, Dellerman KM, Roy ML, Riggin RM. The effects of formulation variables on the stability of freeze-dried human growth hormone. Pharmaceutical Research 1991;8(4):427-36.

[34]   Yoshioka S, Aso Y, Kojima S. Dependence of the molecular mobility and protein stability of freeze-dried γ-globulin formulations on the molecular weight of dextran. Pharmaceutical Research 1997;14(6):736-41.

[35]   Tonnis WF, Mensink MA, de Jager A, van der Voort Maarschalk K, Frijlink HW, Hinrichs WLJ. Size and Molecular Flexibility of Sugars Determine the Storage Stability of Freeze-Dried Proteins. Molecular Pharmaceutics 2015;12(3):684-94.

[36]   Sonner C, Maa Y-F, Lee G. Spray-freeze-drying for protein powder preparation: Particle characterization and a case study with trypsinogen stability. Journal of Pharmaceutical Sciences 2002;91(10):2122-39.

[37]   Izutsu K-i, Aoyagi N, Kojima S. Protection of protein secondary structure by saccharides of different molecular weights during freeze-drying. Chemical and Pharmaceutical Bulletin 2004;52(2):199-203.

[38]   Allison SD, Randolph TW, Manning MC, Middleton K, Davis A, Carpenter JF. Effects of Drying Methods and Additives on Structure and Function of Actin: Mechanisms of Dehydration-Induced Damage and Its Inhibition. Archives of Biochemistry and Biophysics 1998;358(1):171-81.

[39]   Gloger O, Witthohn K, Müller BW. Lyoprotection of aviscumine with low molecular weight dextrans. International Journal of Pharmaceutics 2003;260(1):59-68.

[40]   Allison SD, Manning MC, Randolph TW, Middleton K, Davis A, Carpenter JF. Optimization of storage stability of lyophilized actin using combinations of disaccharides and dextran. Journal of Pharmaceutical Sciences 2000;89(2):199-214.

[41]   Pikal M, Dellerman K, Roy M, Riggin R. The Effects of Formulation Variables on the Stability of Freeze-Dried Human Growth Hormone. Pharmaceutical Research 1991;8(4):427-36.

[42]   Carpenter J, Pikal M, Chang B, Randolph T. Rational Design of Stable Lyophilized Protein Formulations: Some Practical Advice. Pharmaceutical Research 1997;14(8):969-75.

[43]   Garzon-Rodriguez W, Koval RL, Chongprasert S, Krishnan S, Randolph TW, Warne NW, et al. Optimizing storage stability of lyophilized recombinant human interleukin-11 with disaccharide/hydroxyethyl starch mixtures. Journal of Pharmaceutical Sciences 2004;93(3):684-96.

[44]   Carpenter JF, Randolph TW, Jiskoot W, Crommelin DJA, Middaugh CR, Winter G. Potential inaccurate quantitation and sizing of protein aggregates by size exclusion chromatography: Essential need to use orthogonal methods to assure the quality of therapeutic protein products. Journal of Pharmaceutical Sciences 2010;99(5):2200-8.

[45]   Ph.Eur. 2.02.01. Clarity and degree of opalescence of liquids. 8th ed. Strasbourgh, France: European Directorate for the Quality of Medicine, 2016.

[46]   Hawe A, Friess W. Development of HSA-free formulations for a hydrophobic cytokine with improved stability. European Journal of Pharmaceutics and Biopharmaceutics 2008;68(2):169-82.

[47]   Schersch K, Betz O, Garidel P, Muehlau S, Bassarab S, Winter G. Systematic investigation of the effect of lyophilizate collapse on pharmaceutically relevant proteins I: Stability after freeze-drying. Journal of Pharmaceutical Sciences 2010;99(5):2256-78.

[48]   Singh SK, Afonina N, Awwad M, Bechtold-Peters K, Blue JT, Chou D, et al. An industry perspective on the monitoring of subvisible particles as a quality attribute for protein therapeutics. Journal of Pharmaceutical Sciences 2010;99(8):3302-21.

[49]   Carpenter JF, Randolph TW, Jiskoot W, Crommelin DJ, Middaugh CR, Winter G, et al. Overlooking subvisible particles in therapeutic protein products: gaps that may compromise product quality. Journal of Pharmaceutical Sciences 2009;98(4):1201-5.

[50]   Zölls S, Gregoritza M, Tantipolphan R, Wiggenhorn M, Winter G, Friess W, et al. How subvisible particles become invisible—relevance of the refractive index for protein particle analysis. Journal of Pharmaceutical Sciences 2013;102(5):1434-46.

[51]   Narhi L. AAPS update on USP expert committee for Sub visible particle analysis. Newsletter of the AAPS Aggregation and Biological Relevance Focus Group 2012;3(2).

[52]   USP U. General Information< 1787>,“. Measurement of Subvisible Particulate Matter in Therapeutic Protein Injections,” Pharmacopeia Forum; 2013; 2013.

[53]   Chen D, Endres RL, Erickson CA, Weis KF, McGregor MW, Kawaoka Y, et al. Epidermal immunization by a needle-free powder delivery technology: Immunogenicity of influenza vaccine and protection in mice. Nature Medicine 2000;6(10):1187-90.

[54]   Maa Y-F, Ameri M, Shu C, Zuleger CL, Che J, Osorio JE, et al. Hepatitis-B Surface Antigen (HBsAg) Powder Formulation: Process and Stability Assessment. Current Drug Delivery 2007;4:57-67.

[55]   Burkoth TL, Bellhouse BJ, Hewson G, Longridge DJ, Muddle AG, Sarphie DF. Transdermal and transmucosal powdered drug delivery. Critical Reviews in Therapeutic Drug Carier Systems 1999;16(4):331-84.

[56]   Ziegler A, Simon S, Lee G. Comminution of carbohydrate and protein microparticles on firing in a ballistic powder injector. Journal of Pharmaceutical Sciences 2010;99(12):4917-27.

[57]   Kendall M, Smith PW, Bellhouse B. Transdermal ballistic delivery of micro-particles: investigation into skin penetration. Engineering in Medicine and Biology Society Proceedings of the 22nd Annual International Conference of the IEEE, 2000. p. 1621-4.

[58]   Dean HJ, Fuller D, Osorio JE. Powder and particle-mediated approaches for delivery of DNA and protein vaccines into the epidermis. Comparative Immunology, Microbiology and Infectious Diseases 2003;26(5-6):373-88.

[59]   Yu Z, Johnston KP, Williams Iii RO. Spray freezing into liquid versus spray-freeze drying: Influence of atomization on protein aggregation and biological activity. European Journal of Pharmaceutical Sciences 2006;27(1):9-18.

[60]   Webb SD, Golledge SL, Cleland JL, Carpenter JF, Randolph TW. Surface adsorption of recombinant human interferon-γ in lyophilized and spray-lyophilized formulations. Journal of Pharmaceutical Sciences 2002;91(6):1474-87.

[61]   Abdul-Fattah AM, Truong-Le V, Yee L, Nguyen L, Kalonia DS, Cicerone MT, et al. Drying-induced variations in physico-chemical properties of amorphous pharmaceuticals and their impact on stability (I): Stability of a monoclonal antibody. Journal of Pharmaceutical Sciences 2007;96(8):1983-2008.

[62]   Wang W. Lyophilization and development of solid protein pharmaceuticals. International Journal of Pharmaceutics 2000;203(1-2):1-60.

[63]   Jain NK, Roy I. Effect of trehalose on protein structure. Protein Science 2009;18(1):24-36.

[64]   Liu Q, Brady JW. Anisotropic Solvent Structuring in Aqueous Sugar Solutions. Journal of the American Chemical Society 1996;118(49):12276-86.

[65]   Carpenter JF, Crowe JH. An infrared spectroscopic study of the interactions of carbohydrates with dried proteins. Biochemistry 1989;28(9):3916-22.

[66]   Izutsu K, Yoshioka S, Terao T. Effect of mannitol crystallinity on the stabilization of enzymes during freeze-drying. Chemical and Pharmaceutical Bulletin 1994;42(1):5.

[67]   Chen T, Fowler A, Toner M. Literature review: supplemented phase diagram of the trehalose–water binary mixture. Cryobiology 2000;40(3):277-82.

[68]   Kawai K, Suzuki T. Stabilizing effect of four types of disaccharide on the enzymatic activity of freeze-dried lactate dehydrogenase: step by step evaluation from freezing to storage. Pharmaceutical Research 2007;24(10):1883-90.

[69]   Angell CA. Formation of glasses from liquids and biopolymers. Science 1995;267(5206):1924-35.

[70]   Telang C, Suryanarayanan R, Yu L. Crystallization of D-Mannitol in Binary Mixtures with NaCl: Phase Diagram and Polymorphism. Pharmaceutical Research 2003;20(12):1939-45.

[71]   Burger A, Henck J-O, Hetz S, Rollinger JM, Weissnicht AA, Stöttner H. Energy/temperature diagram and compression behavior of the polymorphs of D-mannitol. Journal of Pharmaceutical Sciences 2000;89(4):457-68.

[72]   Hawe A, Frieß W. Physico-chemical lyophilization behavior of mannitol, human serum albumin formulations. European Journal of Pharmaceutical Sciences 2006;28(3):224-32.

[73]   Amorij J-P, Hinrichs WLJ, Frijlink HW, Wilschut JC, Huckriede A. Needle-free influenza vaccination. Lancet Infectious Diseases 2010;10(10):699-711.

[74]   Chen D, Maa Y-F, Haynes JR. Needle-free epidermal powder immunization. Expert Review of Vaccines 2002;1(3):265-76.

[75]   Widera G, Johnson J, Kim L, Libiran L, Nyam K, Daddona PE, et al. Effect of delivery parameters on immunization to ovalbumin following intracutaneous administration by a coated microneedle array patch system. Vaccine 2006;24(10):1653-64.

[76]   Kendall M, Mitchell T, Wrighton-Smith P. Intradermal ballistic delivery of micro-particles into excised human skin for pharmaceutical applications. Journal of Biomechanics 2004;37(11):1733-41.

[77]   Sugimura T, Ito Y, Tananari Y, Ozaki Y, Maeno Y, Yamaoka T, et al. Improved antibody responses in infants less than 1 year old using intradermal influenza vaccination. Vaccine 2008;26(22):2700-5.

[78]   Künzi V, Klap JM, Seiberling MK, Herzog C, Hartmann K, Kürsteiner O, et al. Immunogenicity and safety of low dose virosomal adjuvanted influenza vaccine administered intradermally compared to intramuscular full dose administration. Vaccine 2009;27(27):3561-7.

[79]   Chiu SS, Peiris JSM, Chan KH, Wong WHS, Lau YL. Immunogenicity and Safety of Intradermal Influenza Immunization at a Reduced Dose in Healthy Children. Pediatrics 2007;119(6):1076-82.

[80]   Belshe RB, Newman FK, Cannon J, Duane C, Treanor J, Van Hoecke C, et al. Serum Antibody Responses after Intradermal Vaccination against Influenza. The New England Journal of Medicine 2004;351(22):2286-94.

[81]   Kenney RT, Frech SA, Muenz LR, Villar CP, Glenn GM. Dose sparing with intradermal injection of influenza vaccine. The New England Journal of Medicine 2004;351(22):2295-301.

[82]   Auewarakul P, Kositanont U, Sornsathapornkul P, Tothong P, Kanyok R, Thongcharoen P. Antibody responses after dose-sparing intradermal influenza vaccination. Vaccine 2007;25(4):659-63.

[83]   Jo YM, Song JY, Hwang IS, Lee J, Oh SC, Kim JS, et al. Dose sparing strategy with intradermal influenza vaccination in patients with solid cancer. Journal of Medical Virology 2009;81(4):722-7.

[84]   Belshe RB, Newman FK, Wilkins K, Graham IL, Babusis E, Ewell M, et al. Comparative immunogenicity of trivalent influenza vaccine administered by intradermal or intramuscular route in healthy adults. Vaccine 2007;25(37-38):6755-63.

[85]   Van Damme P, Oosterhuis-Kafeja F, Van der Wielen M, Almagor Y, Sharon O, Levin Y. Safety and efficacy of a novel microneedle device for dose sparing intradermal influenza vaccination in healthy adults. Vaccine 2009;27(3):454-9.

[86]   Wang W. Protein aggregation and its inhibition in biopharmaceutics. International Journal of Pharmaceutics 2005;289(1):1-30.

[87]   Shire SJ, Shahrokh Z, Liu J. Challenges in the development of high protein concentration formulations. Journal of Pharmaceutical Sciences 2004;93(6):1390-402.

[88]   Cleland JL, Lam X, Kendrick B, Yang J, Yang Th, Overcashier D, et al. A specific molar ratio of stabilizer to protein is required for storage stability of a lyophilized monoclonal antibody. Journal of Pharmaceutical Sciences 2001;90(3):310-21.

[89]   Mahler H-C, Friess W, Grauschopf U, Kiese S. Protein aggregation: Pathways, induction factors and analysis. Journal of Pharmaceutical Sciences 2009;98(9):2909-34.

[90]   Treuheit M, Kosky A, Brems D. Inverse Relationship of Protein Concentration and Aggregation. Pharmaceutical Research 2002;19(4):511-6.

[91]   Colandene JD, Maldonado LM, Creagh AT, Vrettos JS, Goad KG, Spitznagel TM. Lyophilization cycle development for a high-concentration monoclonal antibody formulation lacking a crystalline bulking agent. Journal of Pharmaceutical Sciences 2007;96(6):1598-608.

CHAPTER 6

THE INTERFACE BETWEEN PARTICLES AND DEVICE SURFACE AND ITS CHALLENGES

1 INTRODUCTION

Chapter 3 and 4 summarized a) the implementation of a novel freeze-drying technology, collapse freeze-drying, for the generation of lyophilizates exhibiting a small specific surface area of the sugar matrix and b) the optimization of a subsequent cryo-milling step for the generation of powdered vaccine particles for ballistic intradermal application. Formulation screening and storage stability of powder particles containing ovalbumin, summarized in chapter 5, revealed a secondary mixture of trehalose and mannitol as a promising formulation with excellent protein stabilizing properties. In addition to the protein stabilizing properties, the particles showed satisfying morphological characteristics, especially in size and density, which are essential for intradermal application of the powdered particles.

This chapter addresses the interface between powder particles and the device surface, which plays an important role for the accurate delivery of the particles into the skin and thus has a decisive impact on the efficacy of the vaccination procedure.

As the adhesion of particles on the device surface is essential for the successful delivery of the particles into the skin, this interface has to fulfill several requirements. First, the adhesion of the particles on the device surface has to allow safe and stable storage as it has to retain the vaccine dose at the surface of the device part. The adhesion of the particles has to resist certain mechanical stress conditions such as

transport, storage and handling. However, at the same time, it has to allow the release of the solid vaccine dose from the device surface to a full or at least fully sufficient extent when actuated for injection into the skin. Second, a homogenous distribution of the particles on the device surface, ideally structured in a monolayer, is necessary to guarantee the later homogenous acceleration of the particles using the ballistic device and herein also a homogenous distribution of the particles in the targeted skin.

The following chapter first describes a method of attaching particles to a membrane surface by the use of oily substances, simulating the adhesion of the vaccine particles on the device surface. The oily substances selected for this approach should comprise all above listed properties. The assorted oily substances include also oily adjuvants or single components of oily adjuvants. The choice of oily adjuvants as adhesives was driven by the idea to combine the adhesive effect with a second function, i.e. the enhancement of the immunogenicity of the delivered vaccine. Many different adjuvants are known not only to activate the immune system sufficiently to induce long-lasting and protective immune responses but also to allow the use of lower antigen doses [1, 2]. It is also described in literature, that, especially using the approach of transcutaneous immunization, a robust immune response to antigens is dependent on the co-delivery of an adjuvant [3, 4]. Therefore, the suitability of different oily substances to adhere particles onto different membrane materials is challenged in different experimental set-ups in chapter 6.2.

In a second part the stability of the antigen loaded particles in combination with selected adjuvants was investigated in a short term stability study at elevated temperatures (chapter 6.3).

2   MECHANICAL ADHESION OF PARTICLES ON DIFFERENT SURFACES

The ability of oily substances and oily components of adjuvants to act as an adhesive between particles and different membrane surfaces for the use in a ballistic powder injection device was explored in different experimental setups.

2.1   EXPLORATION OF DIFFERENT SURFACE MATERIALS AND OILY SUBSTANCES FOR THE ADHESION OF PARTICLES ONTO THE DEVICE SURFACE

The oily components of MF59 (mixture of squalene, polysorbate 80 and Span® 85, as described in chapter 2), silicon oil and paraffin oil were explored as adhesives at the interface between aluminum membranes and glass particles. Glass particles were chosen as model particles for vaccine particles because of their well characterized and reproducible physical properties, allowing a high reproducibility of the conducted experiments. For the preparation of the oily components of the adjuvant MF59 squalene, polysorbate 80 and Span® 85 were mixed as described in chapter 2. The oily substances silicon oil and paraffin oil did not need any further preparation steps. Aluminum membranes, having a surface area of 6.28 cm², were covered with 10 µl adhesive (as described in chapter 2) and dipped subsequently in a bed of glass particles, so that the particles were fixed onto the membrane surface. The size of the glass particles ranged from 20 µm to 40 µm and particle density was 2.5 g/cm³. The excess particles were tapped off. The mass of adhesive and particles was determined gravimetrically. Only a thin film of adhesive was needed to attach the particles, as the ratio between the mass of adhesive and the mass of particles was approximately 1:10. The appearance of the membrane's surface covered with the adhesive and the particles is depicted in figure 6.1.

The mechanical force acting on the device during shipping, storage and handling was simulated using a jolting volumeter (figure 6.2). Therefore, the membranes were fixed on the inner surface of a petri dish and were attached headfirst to the jolting volumeter

with the particle covered side turned downwards. The border of the petri-dish served as a spacer to the surface of the jolting volumeter.

Figure 6.1: Aluminum membranes (d = 0.5 mm) covered with the oily components of MF59 and glass particles (size range 20-40 µm). (A): Magnification 100 x 50. (B): Magnification 100 x 500. The pictures were obtained using a Keyence VHX-500 F microscope.
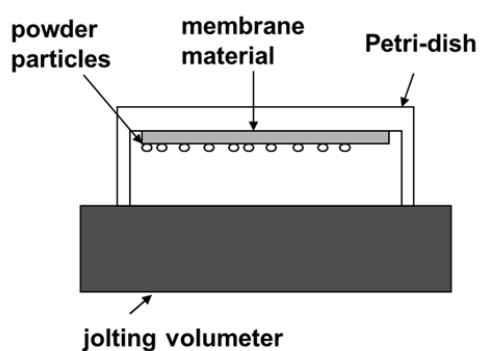
Figure 6.2: Schematic illustration of the experimental set-up using a jolting volumeter, simulating the mechanical force acting on the device during shipping, storage and handling.

The mass of particles and adhesive remaining on the membranes after 10, 20, 50, 100 and 500 beats performed by the jolting volumeter was determined gravimetrically.

After 500 beats 99.2% of the mass of glass particles remained adhered on the membrane using the oily components of MF59 and silicon oil as adhesive, and 98.6% of

the mass of glass particles remained adhered on the membrane using paraffin oil (figure 6.3). Thus the suitability of all three adhesives to attach the particles onto the surface of aluminum membranes was confirmed.
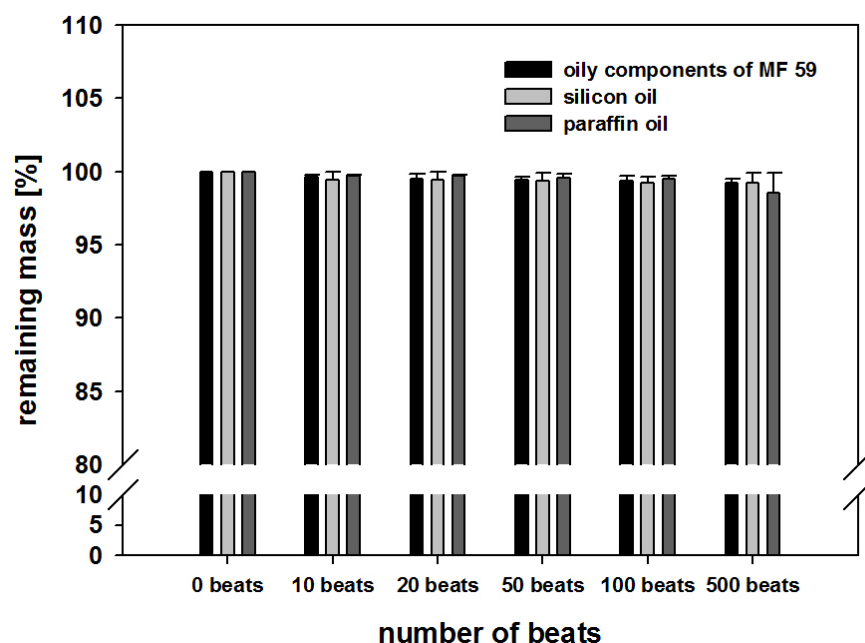
Figure 6.3: Remaining mass of particles (glass particles, 20 - 40 µm, particle density 2.5 g/cm³) and adhesive on aluminum membranes using the oily components of MF59, silicon oil and paraffin oil as adhesives after 10, 20, 50, 100 and 500 beats of the jolting volumeter. Number of replicates n=3.

In order to increase the stress simulated by the jolting volumeter a custom made drop apparatus was used (figure 6.4). A piece of membrane coated with adhesive and particles as described before was fixed in a metal clam and dropped from one meter height, using this experimental set-up. By the impact onto two distance pieces at the bottom of the drop apparatus, the metal clam was stopped abruptly from free-falling by a beat. The experiment was repeated 10 times with three replicates each. Thereby particles with a weak adherence were detached from the membrane surface. The mass of the particles and adhesive, which were not detached form the membrane, was determined gravimetrically.

141
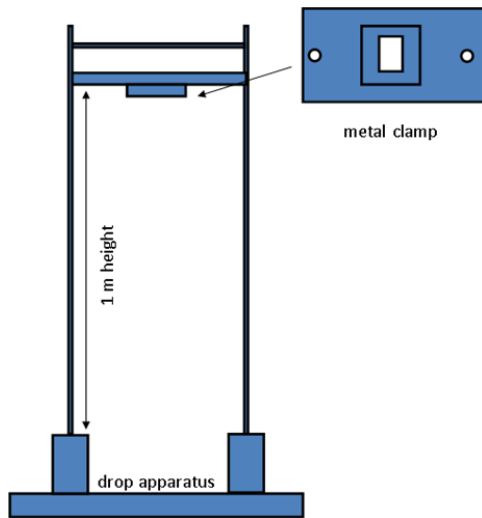
Figure 6.4: Schematic illustration of the custom made drop apparatus.

Using the principle of the custom made drop apparatus, different plastic materials suitable for the use as membrane surfaces in a ballistic powder injection device were explored. The membranes were covered with the mixture of the oily components of MF59 and coated with glass particles as described before.
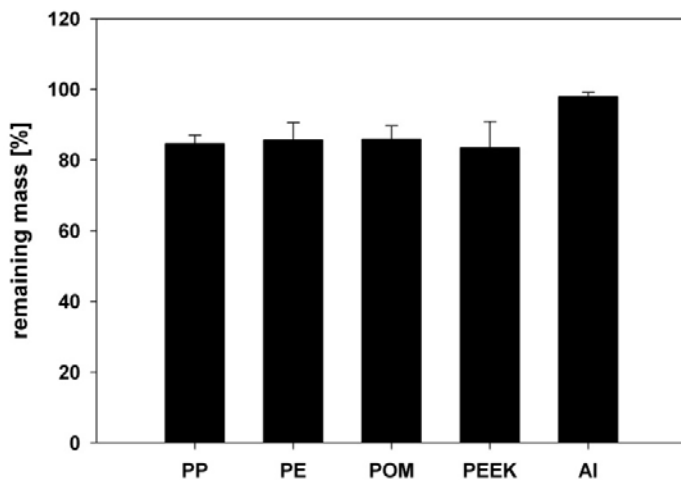
Figure 6.5: Adherence strength of glass particles on different membrane materials using the oily components of MF59 as adhesive. Polypropylene (PP), polyethylene (PE) polyoxymethylene (POM), polyether ether keton (PEEK), aluminum (AL). Number of replicates n=3.

After 10 drops from one meter height, 97.9% ± 1.2% of the mass of particles and adhesive were recovered using aluminum as membrane surface (figure 6.5). Also the use of other plastic materials like polypropylene (PP), polyethylene (PE) polyoxymethylene (POM), polyether ether keton (PEEK) confirmed the suitability of the oily components of MF59 as adhesive.

Once several membrane materials were found to be suitable to cover the device surface, further substances were explored to be used as adhesive. Therefore, the oily components of MF59, paraffin oil, silicon oil, miglyol, castor oil, squalene, polyethylene glycol 400, polyisobutylene and Freund's incomplete adjuvant, which is composed of 85% paraffin oil and 15% mannide monooleate, were investigated. Two different membrane surface materials, aluminum and polyethylene membranes, were covered with adhesive and glass particles, as described before. The mechanical force acting on the device during shipping, storage and handling was simulated by using the custom made drop apparatus, as described before.

After 10 drops from one meter height more than 78% of the mass of particles and adhesive remained on the surface of the aluminum membranes using the oily components of MF59, paraffin oil, silicon oil, castor oil, polyethylene glycol 400, polyisobutylene or Freund's incompletes adjuvant as adhesive (figure 6.6). Less adhesive strength could be observed by the use of miglyol with 46% ± 11% remaining mass of particles and adhesive. By the use of squalene 56% ± 12% remaining mass of particles and adhesive could be found. The adherence to PE surfaces was comparable to the adherence on aluminum surfaces, in some cases slightly higher or lower compared to aluminum surfaces.
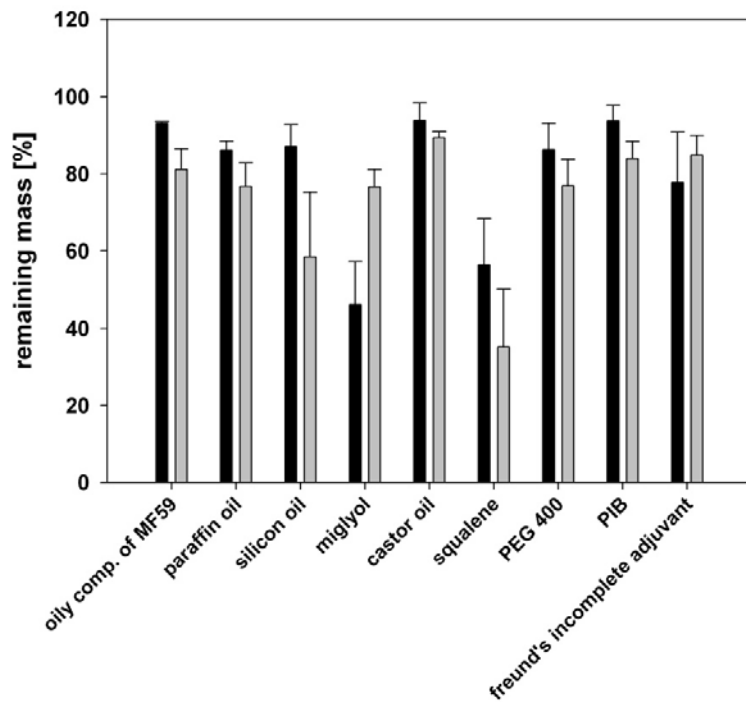
Figure 6.6: Adherence strength of glass particles on aluminum membranes (black bars) and PE-membranes (grey bars) using different adhesives. The custom made drop apparatus was used to investigate the adhesive force between the membrane surface and the particles. Number of replicates n=3.

Once several membrane materials and oily substances were investigated for their suitability to act as surface material and as adhesive at the interface between the device surface and particles, the role of the surface structure of the membrane material was explored. The adherence strength between glass particles and membranes is not only dependent on the type of adhesive and the membrane material itself, but also on the roughness of the surface membrane material. The adherence strength of glass particles on smooth surfaces was compared with the adherence strength on structured membrane surfaces (figure 6.7). The mixture of the oily components of MF59 was used exemplarily as adhesive in this experimental set-up. Aluminum and polyethylene membranes were prepared as described before and the adherence strength of the particles was challenged by dropping the membrane ten times from one meter height using the custom made drop apparatus.
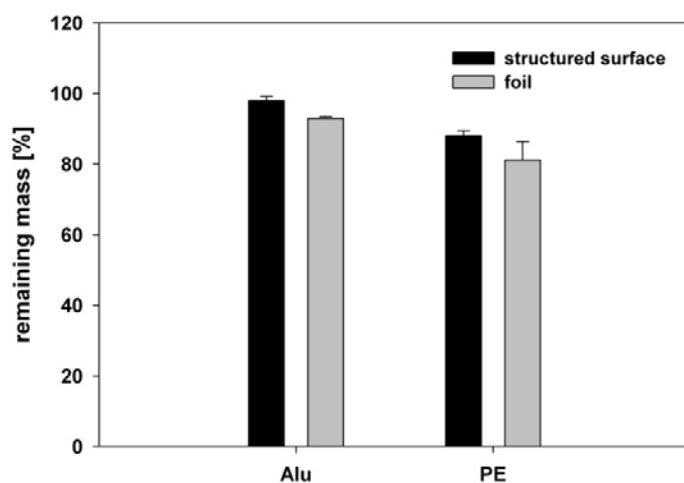
Figure 6.7: Adherence strength of glass particles on perfectly smooth foils (grey bars) or structured surfaces (black bars) using the oily components of MF59 as adhesive. Number of replicates n=3.

Regarding the adherence strength of the particles on aluminum and polyethylene membranes 98% and 88% of the glass particles, respectively, were retained on membranes having a structured surface. 93% and 81% of the particles were retained on perfectly smooth aluminum and PE foils. Thus, as expected, the surface structure of the membrane material has an influence on the adherence strength of the particles.

An additional option to adhere particles onto the surface of the membranes, the adherence by electrostatic interactions, was taken into consideration. Three different membrane materials (Teflon, aluminum and polyethylene) were dipped in a bed of glass particles having a particle size as described before in order to fix the glass particles onto the membrane surface without the use of an adhesive but only by electrostatic interactions. The mass of glass particles adherent on the membrane surface was determined gravimetrically. Likewise, the three different membrane materials were covered by the oily components of MF59. The amount of adhesive was determined gravimetrically. The membranes covered with adhesive were dipped in a bed of glass particles. The excess glass particles were tapped off. The mass of glass particles was determined gravimetrically.

145

Without the application of an adhesive only 5.73 mg glass particles were attached to Teflon membranes, 0.27 mg to aluminum membranes and 2.17 mg to polyethylene membranes due to electrostatic interactions. However, 18.23 mg, 12.53 mg and 15.00 mg glass particles were attached to Teflon membranes, aluminum membranes and polyethylene membranes, respectively, using the oily components of MF59 (table 6.1).

Table 6.1: Adhesion of glass particles on the surface of polyethylene membranes by the use of adhesives or electrostatic interactions

type of membrane	particle mass without the use of adhesive [mg]	particle mass using the oily components of MF59 as adhesive [mg]
Teflon	5.73 ± 1.42	18.23 ± 2.64
Aluminum	0.27 ± 0.06	12.53 ± 3.16
Polyethylene	2.17 ± 0.81	15.00 ± 6.10

This proves the ability of the oily components of MF59 to attach a substantial mass of glass particles on different membranes and demonstrate herein the rational for the use of adhesives.

2.2 RESISTANCE OF THE ADHERENT STRENGTH AT THE INTERFACE BETWEEN PARTICLES AND DEVICE SURFACE UNDER DIFFERENT TEMPERATURE CONDITIONS

The oily components of MF59 and Freund's incomplete adjuvant were investigated at different ambient temperature conditions for the use as adhesive agent between glass particles and membranes. Two different membrane surface materials, aluminum and PE membranes, were covered with adhesive as described before. The mechanical force acting on the device during shipping, storage and handling was simulated by dropping the membrane ten times from one meter height using the custom made drop apparatus, as described before. The samples as well as the custom made drop apparatus were tempered for two hours prior to the experiment to 2-8°C, 25°C or 40°C, respectively.
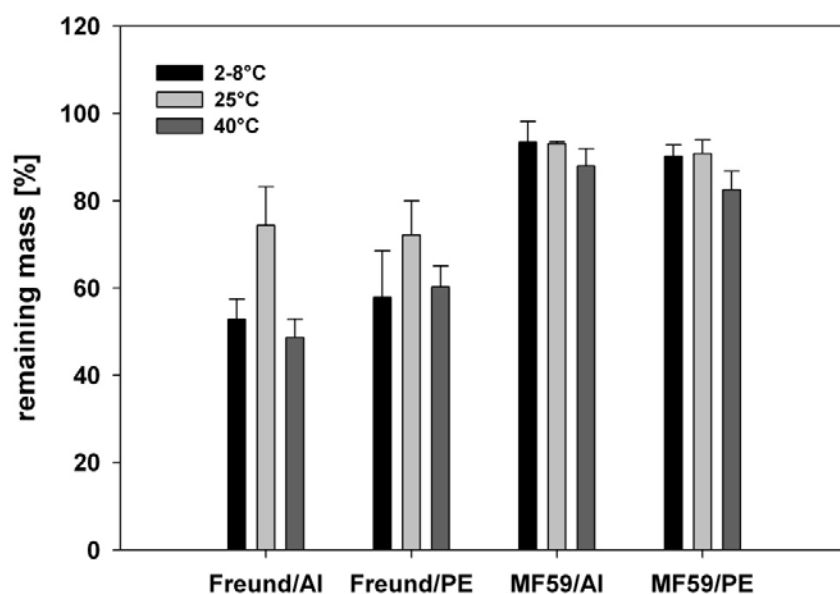
Figure 6.8: Adherence strength of glass particles on aluminum and polyethylene (PE) membranes using the oily components of MF59 or Freund's incomplete adjuvant as adhesive at 2-8°C (black bars), 25°C (grey bars) and 40°C (dark grey bars).

After ten drops from one meter height more than 82.5% of the mass of particles and adhesive remained on the surface of aluminum and polyethylene membranes using the oily components of MF59 as adhesive, independent of the present ambient temperature (figure 6.8). Optimal adherence was found at 25°C for samples using Freund's incomplete adjuvant as adhesive on both, aluminum and polyethylene membranes. Less adherence strength was observed at 2-8°C and 40°C with 49% to 60% remaining mass of particles and adhesive after ten drops from one meter height using the custom made drop apparatus.

The resistance of the adherence strength between the particles and the membranes after 12 weeks of storage at 2-8°C, 25°C and 40°C was investigated with regard to the storage stability of the composition.

The oily components of MF59 and Freund's incomplete adjuvant were used as adhesive agent between glass particles and PE and aluminum membranes. The samples were stored for 12 weeks at 2-8°C, 25°C and 40°C. After this storage period, the mechanical

strength of the adhesion was investigated using again the custom made drop apparatus as described before. The samples were re-tempered to room temperature prior to the experiment.
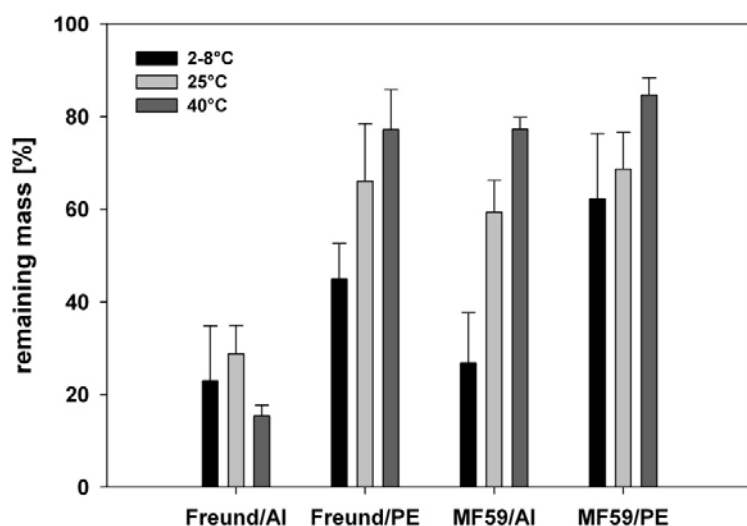
Figure 6.9: Adherence strength of glass particles on aluminum and polyethylene (PE) membranes using the oily components of MF59 or Freund's incomplete adjuvant as adhesive after 12 weeks of storage at 2-8°C (black bars), 25°C (grey bars) and 40°C (dark grey bars).

By using the oily components of MF59 as adhesive more than 60% of particles and adhesive were recovered after ten drops form one meter height after 12 weeks of storage at 25°C and 40°C using both membrane types (figure 6.9). Good adherence strength after 12 weeks of storage at 25°C and 40°C was shown for the use of PE membranes covered with Freund's incomplete adjuvant. Less adherence strength was found for aluminum membranes covered with Freund's incomplete adjuvant over the investigated period independently on the ambient temperature. The storage temperature of 2-8°C had also a negative influence on the adherence strength of the adhesives after 12 weeks of storage, except for the combination of PE membranes covered with the oily components of MF59.

Generally, the viscosity of the adhesives rises with decreasing temperature, hence having less capability to coat the particles. Therefore, the adherence strength seems to

decrease with a decreased contact area between adhesive and particles. In addition, the ability of the adhesive to spread on the membrane surface has also an impact on the mechanical strength of the adhesion. However, this interrelationship has to be evaluated for each adhesive and each surface material individually.

2.3 PROOF OF CONCEPT – RELEASE OF THE PARTICLES UPON ACTUATION OF THE DEVICE

The ability of the adhesive to assure the adherence of particles on the membrane surface during transport and storage is similar important as the ability to release the particles upon acceleration using a ballistic device.

A ballistic accelerator was used to simulate the ballistic injection process. The basic working principle of the ballistic accelerator is the generation of a repulsive force by a magnetic field which induces a turbulent electrical current in a metal carrier, e.g. an aluminum membrane, which is thereby accelerated to high velocities. The aluminum membrane acts as carrier surface for the particles and is stopped by a stopper plate, while the particles attached on the membrane are further accelerated (figure 6.10).
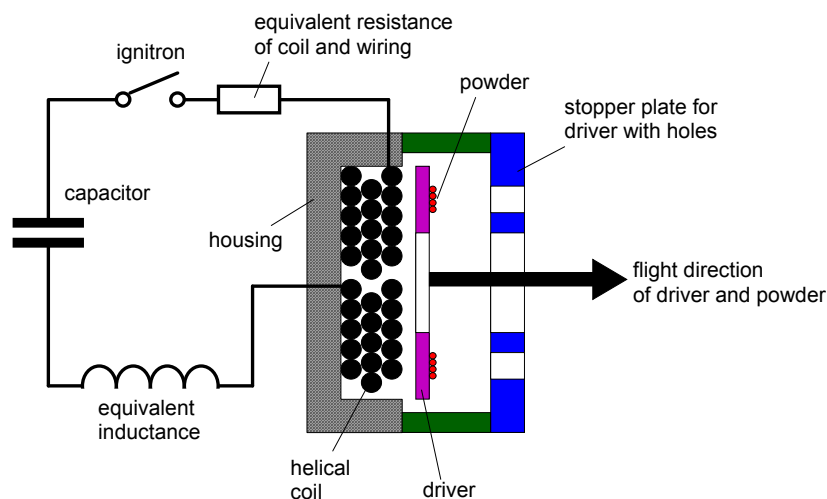
Figure 6.10 Schematic set-up of the ballistic accelerator (created by Dr. Lell, Pyroglobe GmbH).

Aluminum membranes were prepared as described before. Aluminum membranes were covered with the oily components of MF59 and glass particles of a size fraction of 20 µm to 40 µm were attached.

A

B
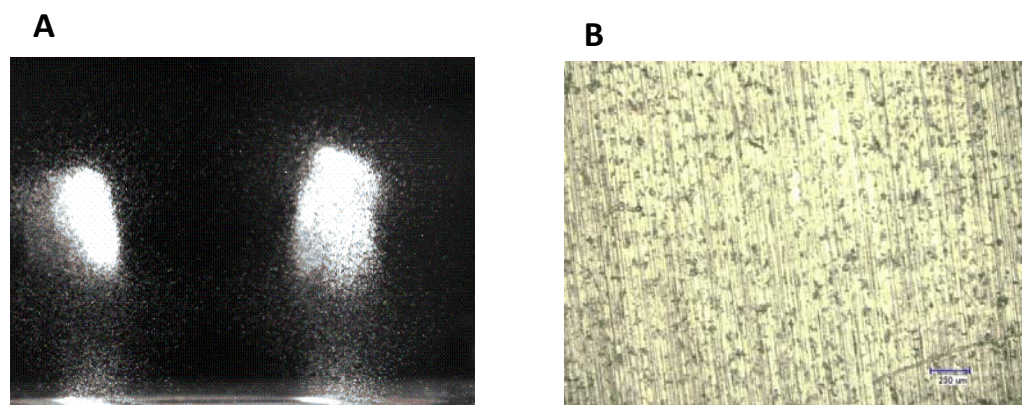
Figure 6.11: (A) Photograph taken by a Flash Cam PCO high speed camera (PCO, Kehlheim am Ufer, Germany), depicting two clouds of glass particles detached from the aluminum membrane and accelerated to high velocities. (B) Light micrograph of the surface of the aluminum membrane after the experiment, showing that the glass particles were completely detached from the membrane surface. The picture was obtained using a Keyence VHX-500 F microscope.

Upon acceleration using the ballistic accelerator glass particles attached with the oily components of MF59 were completely detached from the aluminum membranes gaining high velocity above 100 m/s (figure 6.11 A and B). This proves that the mechanical strength at the interface between glass particles and aluminum membranes using the oily components of MF59 as adhesive is on the one hand side strong enough to avoid powder loss during storage and shipping; but on the other hand side the particles can even so be detached upon acceleration using a ballistic accelerator.

The release of glass particles attached on aluminum membranes using the oily components of MF59 using a ballistic acceleration was compared to the use of polyisobutylene and superglue as adhesives. Glass particles attached with the oily components of MF59 on aluminum membranes were completely detached upon acceleration using the ballistic accelerator (figure 6.12 A). Particles attached with polyisobutylene on aluminum membranes were not detached upon acceleration and remained almost completely on the membrane surface (figure 6.12 B). Particles attached with superglue were partially detached in form of solid pieces which consisted of aggregates of glue and particles (figure 6.12 C).

Oily components of MF59   Polyisobutylene   Superglue
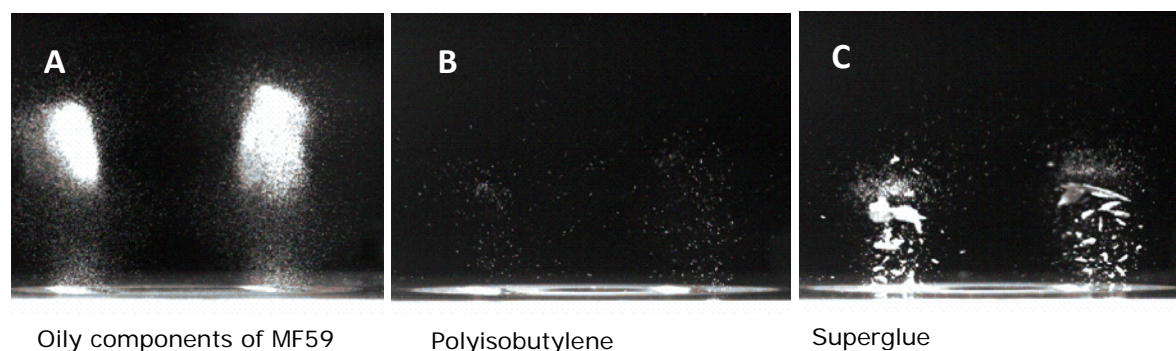
Figure 6.12: Photographs taken by a Flash Cam PCO high speed camera (PCO, Kehlheim am Ufer, Germany), depicting clouds of glass particles detached from the aluminum membrane attached with different adhesives.

A homogenous distribution of the particles and a disintegration of agglomerates into single particles are crucial for the penetration of the particles into the targeted layers of the skin. It is conceivable that large agglomerates will not be able to breach the outermost layer of the skin, the stratum corneum, and also might cause severe injuries on the skin when accelerated using a ballistic device. Hence, the texture of the adhesive plays an important role for its use at the interface between particles and the device surface of a ballistic injector. Conventional adhesives, as polyisobutylene or superglue, do not comprise these requirements, and furthermore, are not skin-compatible.

A further requirement on the adhesive is, besides the attachment of the particles during storage and handling and the release of the particles upon actuation of the injection device, that it can be entrained together with the particles during detachment from the membrane. An adjuvant effect of the adhesive can only be achieved, if a substantial amount of adjuvant is entrained together with the particles and herein injected into the skin.

In order to visualize if the adhesive is entrained together with the particles upon detachment from the interface to the device surface, a mixture of the oily components of MF59 was mixed with 1% Sudan red. Glass particles of a size fraction of 20 µm to 40 µm were attached onto aluminum membranes using the Sudan red dyed mixture of the oily components of MF59 as described before. Particles were detached upon

acceleration using the ballistic accelerator and caught on the surface of a second membrane. Figure 6.13 shows A) a light-micrograph of particles detached from the membrane surface upon acceleration and B) subsequently caught on a second membrane.

A   **B**
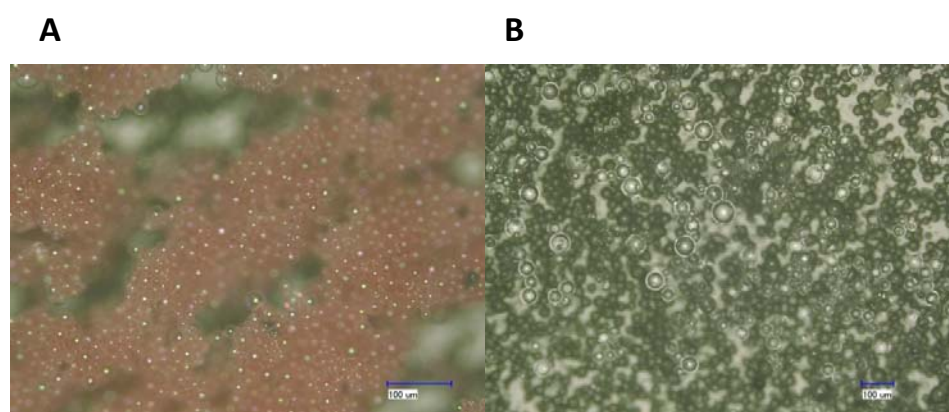
Figure 6.13: Light-micrographs of particles covered with adhesive (A) and without adhesive (B) after the impact on a second target membrane. The pictures were obtained using a Keyence VHX-500 F microscope. Scale bars 100 μm.

The glass particles were uniformly covered with the Sudan red dyed adhesive, showing that a substantial amount of adhesive was entrained together with the particles during detachment from the membrane and acceleration (figure 6.13 A). In comparison to that, figure 6.13 B shows the impact of the particles on the second membrane without the use of an adhesive, serving as blank test. Summarizing this tentative experiment, it is assumed that the adhesive can also be delivered together with the particles into the target using a ballistic injection device. However, this assumption has still to be verified in subsequent animal studies.

2.4   SUMMARY AND CONCLUSION

A simple method was developed to attach particles on different membrane surfaces by using of oily substances. After covering the membrane surface with the oily substances, the membrane was dipped into a tray filled with particles, attaching hereby approximately the tenfold higher mass of particles on the membrane surface in comparison to the mass of the adhesive. Particles were enclosed into a thin film of the oily substance, hence resulting in a partly or, if the amount of the oily substance was increased, full coverage of the surface of the particles. Using this approach, the particles can be potentially protected from air, humidity and other environmental factors. In order to challenge the adhesive strength in between the device surface and the particles, firstly a jolting volumeter was used to simulate the mechanical stress exerted during handling, shipping and storage of the device. As all tested oily substances showed excellent adhesive properties, the mechanical stress exerted by the jolting volumeter was further increased by the use of a custom made drop apparatus. Different membrane materials were investigated for their use to cover the device surface, whereby aluminum was found to show excellent properties. Several oily substances, including also oily adjuvants or single components of oily adjuvants, were explored as adhesives on aluminum and PE membranes. The adherence strength was despite of the tough mechanical challenge outstanding for several oily substances, including the oily components of MF59 and Freund's incomplete adjuvant. Furthermore it was found, that the surface structure of the membranes and the influence of electrostatic interactions as adhesive force between particles and the membranes plays a subordinate role. The adhesive strength of selected combinations of oily adjuvants and membrane materials, including Freund's incomplete adjuvant and the oily components of MF59 in combination with aluminum and PE-membranes, was investigated throughout a storage period of 12 weeks under different temperature conditions. Most notably the mixture of the oily components of MF59 was capable to attach particles on the different membrane surfaces for the monitored time period also at elevated temperature conditions.

Finally, the proof of concept was given by the release of the particles from the attachment situation upon actuation of the ballistic device. In doing so it was observed, that the adhesive was entrained together with the particles. Hence, the entrainment of the oily substances together with the particles offer the possibility to be co-injected into the skin and herein exert an adjuvant effect. Whether the amount of adhesive, which is entrained together with the particles, is sufficient to elicit an appropriate immune response, has to be proven in subsequent animal studies.

It has to be emphasized, that the experiments were made with model particles, since the use of glass particles enabled high reproducibility of the experiments. In future, the model has to be additionally challenged by the use of antigen loaded powder particles, in order to investigate the transferability of the model.

3   STORAGE STABILITY OF CRYO-MILLED PARTICLES ON OILY COVERED SURFACES

In section 2 of this chapter several oily substances were proven to be suitable to attach the powdered particles to the device surface, so that the dose could be fixed on place even under mechanical stress situations as this is the case during handling and storage. The oily substances were as well capable to release the particles upon actuation of the device. In a second step the storage stability and possible interaction between the oily substances and the antigen loaded powder particles was investigated.

Ovalbumin served as a model antigen in a formulation based on a secondary mixture of trehalose and mannitol (hereafter abbreviated as TM) at a weight ratio of 1:1 and a total solid content of 15% (w/w) herein with 2.5% (w/w) ovalbumin. The formulation was collapse freeze-dried and cryo-milled as described before. Five different kinds of adjuvants were assessed in a short term stability study at elevated temperatures: the oily components of MF59, squalane, squalene, Freund's incomplete adjuvant and paraffin oil. The mixture of the oily components of MF59 was selected for its use as oily adjuvant in this study as it comprises not only the ability to act as adhesive at the interface between the device surface and the particle load as described in chapter 6.2. but it is also known for its good safety and tolerability profile when used as whole water in oil emulsion in order to adjuvant vaccines [4-6]. MF59 is meanwhile licensed in more than 20 countries. Squalene is one component in this mixture and is also a natural component of cell membranes and part of the cholesterol biosynthesis. Consequently, squalene is both biodegradable and biocompatible. Its role as immunological adjuvant is controversy discussed in literature [7, 8]. Squalane is derived by hydrogenation of squalene and is, in contrast to squalene, not subjected to auto-oxidation [9-15]. Squalane was also included into this study due to its potential to be used as adhesive at the interface between vaccine particles and the device surface and its potential function as adjuvant. Freund's incomplete adjuvant has already been used in a number of veterinary vaccines and its adjuvant effect was also explored in combination with influenza and killed poliomyelitis vaccines in humans [16-18]. Its main components are

the mineral oil paraffin and mannide monooleate, also known as Arlacel-A. Arlacel-A is used as emulsifying agent. Prior to use, typically water is added to Freund's incomplete adjuvant in order to create a water-in-oil emulsion. For its application as adhesive at the interface between the device surface and vaccine particles, only the oily components were used without the addition of water. In consequence to its side-effects such as local reactions at the injection side, Arlacel-A induced carcinogenicity in mice and oil- induced neoplasmas in mice, it is currently not used in humans [2]. Paraffin oil is one of the components of Freund's incomplete adjuvant and was also included into this study. However, its potential to act as adjuvant as well as its efficacy and safety profile have still to be evaluated in further animal studies.

The samples were stored at 2-8°C, 25°C and 40°C for a time period of 12 weeks. In addition to the evaluation of the stability of the combination of vaccine powder and oily adjuvant, the stability of each component itself (either the powder containing ovalbumin or the oily substance) was investigated. Protein stability was assed using different analytical methods. Primary protein structure was assessed by HP-SEC and changes in the secondary structure by FTIR. The formation of protein aggregates was analyzed by light obscuration and turbidimetry. Changes in particle morphology were tracked by the measurement of the residual moisture of the powders and differential scanning calorimetry. The recovery and the degradation of the oily adjuvants after storage was assessed using gas chromatography in combination with mass spectroscopy.

3.1   REPROCESSING OF THE SAMPLES

In order to investigate protein stability of the samples, first a method had to be developed for the separation of the oily substances from the protein powder formulation as the oily adjuvants were shown to interfere with the established analytical methods. *Tert*-butyl-methyl ether (MTBE) was chosen as washing agent for the samples, as it was on the one hand side a suitable solvent for all oily substances selected for this study (as shown by the recovery of the oily substances determined by GC-MS, shown later in this chapter), and on the other hand side, the model antigen ovalbumin was not soluble in

MTBE (as shown by the recovery of the total protein content of ovalbumin after the reprocessing step using MTBE determined by HP-SEC, shown later in this chapter).

SAMPLE PREPARATION

For the preparation of the samples approximately 50 mg of protein powder formulation was bedded on a 10 µl thin film of the oily adjuvant on the surface of a 2R glass vial. The samples were washed three times in MTBE as described in chapter 2. The obtained powder pellet was subsequently vacuum dried in order to remove MTBE-solvent residues. The dried powder pellet was subsequently used for protein stability analysis.

INFLUENCE OF THE REPROCESSING OF THE SAMPLES ON PROTEIN STABILITY

The influence of the washing steps using MTBE on physical protein stability, the formation of soluble and insoluble aggregates, was assessed by light obscuration, turbidity measurements and size exclusion chromatography. The conformational stability of ovalbumin after the treatment with MTBE was assessed by FTIR transmission spectroscopy.

The extraction of the oils with MTBE was effective as the turbidity-levels of the samples were reduced to an appropriate level (between 3.23 and 4.36 FNU) which is within the detectable range of the analytical method (table 6.2). Generally, the reprocessing steps of the samples using MTBE caused an increase in turbidity (table 6.2) as well as an increase in cumulative particle counts greater than 1, 10 and 25 µm per mL (figure 6.14 and table 6.2) in both, trehalose-mannitol formulations containing ovalbumin (referred to TM) as well as in formulations without ovalbumin (referred to placebo).

The turbidity of trehalose-mannitol formulations containing ovalbumin increased from 0.94 FNU to 2.93 FNU after the reprocessing step with MTBE. Similarly cumulative particle counts increased from 17402 to 52423 for particles > 1 µm per mL, from 327 to 2422 for particles > 10 µm per mL and from 29 to 139 for particles > 25 µm per mL before and after the washing steps of the trehalose-mannitol formulations with MTBE (table 6.2 and figure 6.14).

Likewise the turbidity of the placebo formulations increased from 0.87 FNU to 3.88 FNU after the reprocessing step with MTBE. Cumulative particle counts increased from 5179 to 20361 for particles > 1 µm per mL, from 96 to 317 for particles > 10 µm per mL and from 9 to 28 for particles > 25 µm per mL, respectively, after the reprocessing step of the placebo samples with MTBE (table 6.2 and figure 6.14).

In conclusion, the comparison of placebo samples and samples containing ovalbumin revealed that the extraction procedure itself caused the formation of particles independently whether the samples contained protein or not (table 6.2 and figure 6.14). Hence, the nature of the particles could not be explained by the formation of insoluble aggregates.
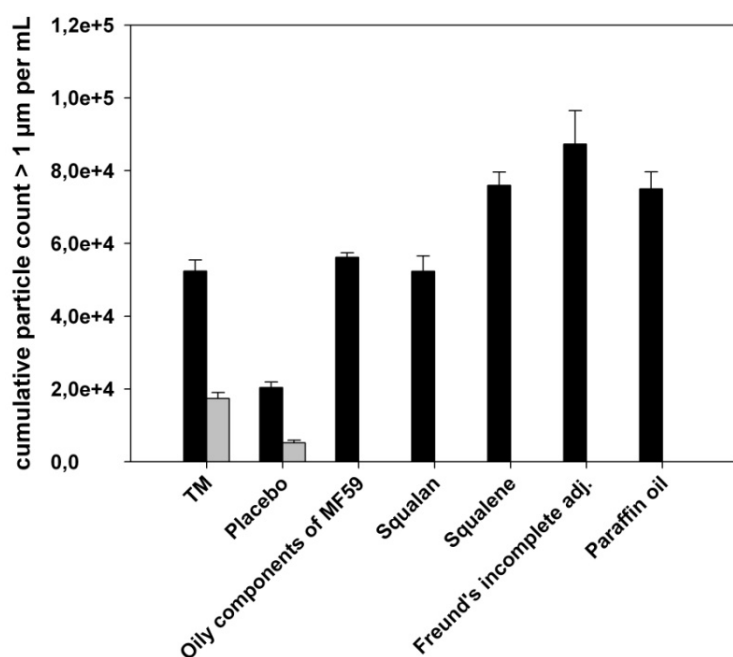
Figure 6.14: Cumulative particle counts > 1 µm per mL of reprocessed samples (three times washing with MTBE, black bars) or native samples (grey bars).

Samples consisted of ovalbumin powder based on trehalose/mannitol (TM), placebo powder based on trehalose/mannitol (placebo), or a mixed sample of ovalbumin powder based on trehalose/mannitol and an oily substance (e.g. squalan).
The mixed samples consisted of 50 mg ovalbumin powder based on trehalose/mannitol and 10 µl of the oily substance. Three of the mixed samples were pooled prior to analysis. The powder was reconstituted in 2 mL purified water prior to analysis.

Table 6.2: Cumulative particle counts > 10 μm per mL and > 25 μm per mL of reprocessed samples (three times washing with MTBE) or native samples. 150 mg of the powder was reconstituted in 2 mL purified water prior to analysis.

	Sample*	particles > 10 μm per mL ± SD	particles > 25 μm per mL ± SD	turbidity [FNU] ± SD
native samples	**TM**	327 ± 54	29 ± 14	0.94 ± 0.03
	Placebo	96 ± 11	9 ± 2	0.87 ± 0.02
reprocessed samples	**TM**	2422 ± 75	139 ± 17	2.93 ± 0.17
	Placebo	317 ± 23	28 ± 11	3.88 ± 0.01
	Oily comp. of MF59	1459 ± 107	101 ± 28	3.36 ± 0.12
	Squalane	1612 ± 115	93 ± 20	3.23 ± 0.18
	Squalene	2388 ± 84	106 ± 15	3.98 ± 0.14
	Freund's incomplete adj.	2803 ± 277	130 ± 31	4.36 ± 0.10
	Paraffin oil	1829 ± 79	104 ± 28	3.47 ± 0.13

*Samples consisted of ovalbumin powder based on trehalose/mannitol (TM), placebo powder based on trehalose/mannitol (placebo), or a mixed sample of ovalbumin powder based on trehalose/mannitol and an oily substance (e.g. squalan).
The mixed samples consisted of 50 mg ovalbumin powder based on trehalose/mannitol and 10 µl of the oily substance. Three of the mixed samples were pooled prior to analysis. The powder was reconstituted in 2 mL purified water prior to analysis.

It was not possible to quantitatively remove the oily substances from the powder formulations. Slightly higher turbidity levels were observed most notably in samples containing Freund's incomplete adjuvant. However, it was possible to remove the oily substances to an adequate level to assess protein stability within the detection range of the analytical method.

The stability of the reprocessed samples was investigated at elevated temperatures over a time period of 12 weeks, in order to reveal delayed effects of the reprocessing steps on protein integrity. After the reprocessing steps the turbidity level of the samples as well as the cumulative particle counts > 1, 10 and 25 μm (figure 6.15 and table 6.3) were increased in comparison to untreated samples. However, they did not further increase after 12 weeks of storage at 2-8°C, 25°C and 40°C (figure 6.15 A, B), similarly to unprocessed, native samples (figure 6.15 C, D).

Size exclusion chromatography showed 99.83% recovery of the soluble monomer of reprocessed trehalose-mannitol samples containing ovalbumin. The remaining soluble

monomer content of the liquid formulation was used as reference for the calculation of the soluble monomer recovery in the reprocessed samples. The recovery of the soluble monomer indicated that the reprocessing of the samples with MTBE did not affect protein stability in terms of the formation of soluble aggregates (figure 6.16).

The total protein recovery of the samples was 96.12% after the reprocessing procedure with MTBE. Hence, the reprocessing procedure was considered as suitable for the separation of the protein powder and the oily substances. Both, the soluble monomer recovery as well as the total protein recovery remained unchanged after storing at 2-8°C, 25°C and 40°C for 12 weeks, hence, the reprocessing step with MTBE did not influence protein integrity (figure 6.16).
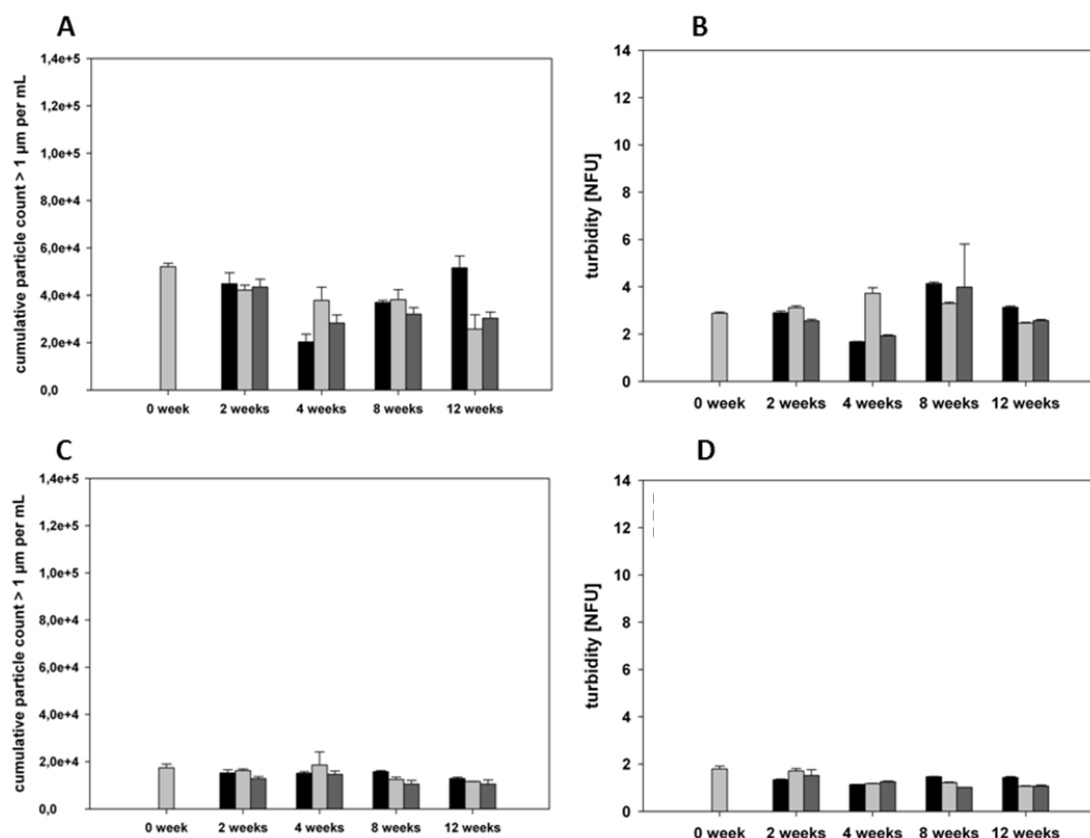
Figure 6.15: Cumulative particle counts > 1 μm per mL of reprocessed samples (three times washing with MTBE) (A) or native samples (C). Turbidity levels of reprocessed samples (B) and native samples (D). Samples were stored up to 12 weeks at 2-8°C (black bars), 25°C (light grey bars) or 40 °C (dark grey bars). 150 mg of the powder was reconstituted in 2 mL purified water prior to analysis.

To complete investigations on the effect of the reprocessing step with MTBE on protein stability, protein secondary structure and conformational stability of ovalbumin was assessed by FTIR transmission spectroscopy (figure 6.16 D). Figure 6.16 D shows the second derivative of FTIR transmission spectra of ovalbumin from trehalose-mannitol formulations after reprocessing with MTBE and reconstitution of the vacuum dried powder in purified water. Samples stored at 2-8°C, 25°C and 40°C for 12 weeks were compared to a standard sample that was not stored (t0). The amide I band is known to be sensitive to protein secondary structures and conformational changes. It arises from C=O stretching vibrations (1690-1620 cm^{-1}) of the peptide linkages, whereas the amide II band arises from C-N stretching vibrations and N-H in plane bendings [19-21]. It is known form literature, that ovalbumin exhibits the amide I band at two equal peaks at 1654 and 1640 cm^{-1} [22].

Table 6.3: Cumulative particle counts > 10 and > 25 µm per mL of reprocessed samples (three times washing with MTBE) or native samples. Samples were stored up to 12 weeks at 2-8°C, 25°C or 40 °C. 150 mg of the powder was reconstituted in 2 mL purified water prior to analysis.

	cumulative particle count	after 12 weeks of storage at 2-8°C	after 12 weeks of storage at 25°C	after 12 weeks of storage at 40°C
reprocessed samples	particles > 10 µm per mL ± SD	2436 ± 134	1032 ± 204	1328 ± 154
	particles > 25 µm per mL ± SD	152 ± 16	44 ± 10	89 ± 5
native samples	particles > 10 µm per mL ± SD	234 ± 29	230 ± 28	300 ± 31
	particles > 25 µm per mL ± SD	2 ± 2	10 ± 6	33 ± 20
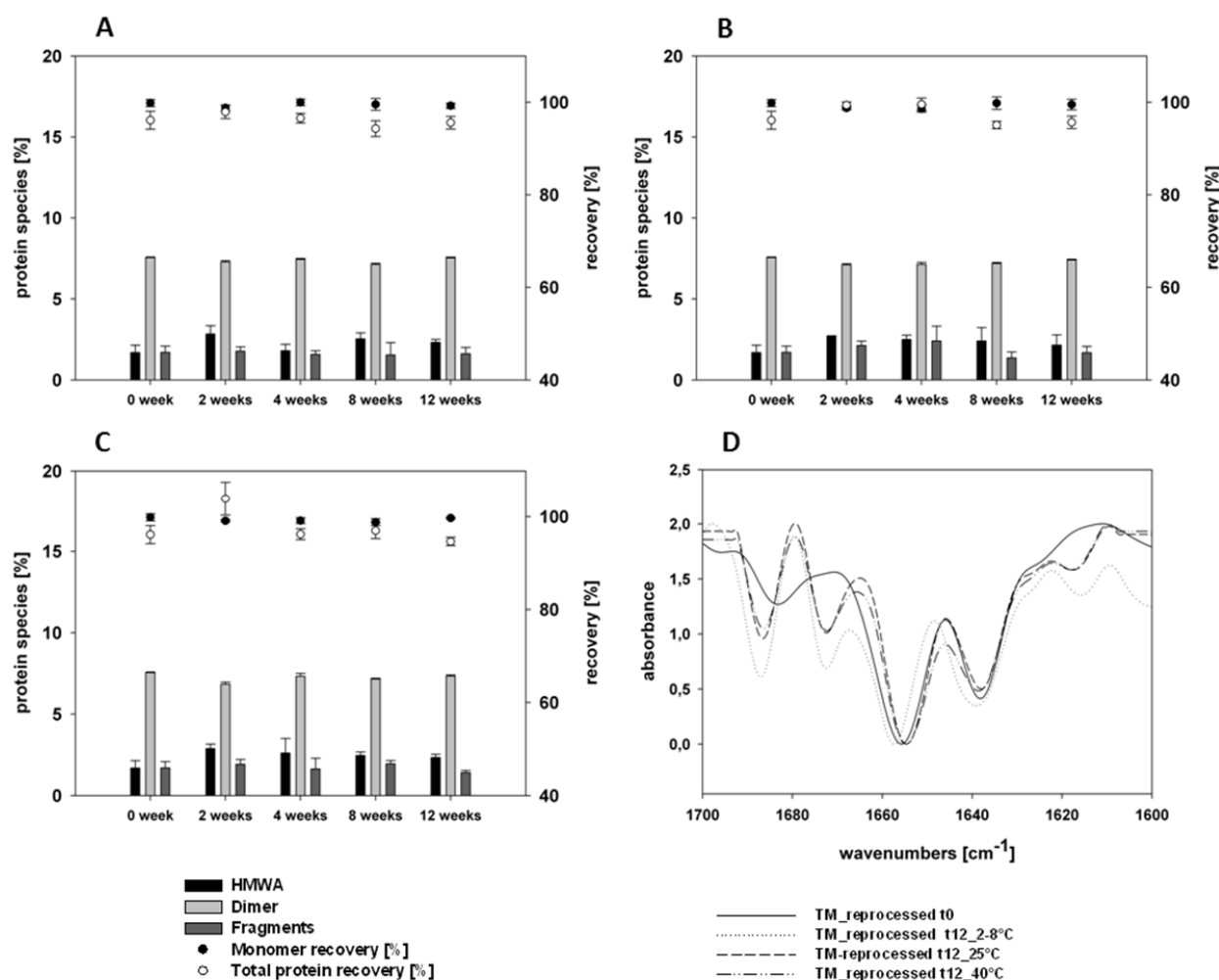
Figure 6.16: Higher molecular weight aggregates (black bars), dimers (light grey bars) and fragment (dark grey bars) protein species [%], total monomer recovery [%] (filled circles) and total protein recovery [%] (open circles) of reprocessed trehalose-mannitol samples containing ovalbumin (TM_reprocessed) as determined by size exclusion chromatography. Samples were incubated at 2-8°C (A), 25°C (B) and 40°C (C). Area-normalized 2nd derivative FTIR transmission spectra of samples after 12 weeks of storage at 2-8°C, 25°C and 40°C (D).

Figure 16.6 D shows the second derivative spectra of ovalbumin. The spectrum of the standard sample of ovalbumin, which was not stored (t0), exhibits two major bands at 1656 and 1638 cm^{-1} and a minor band at 1683 cm^{-1}. The band at 1638 cm^{-1} can be assigned to low-wavenumber ß-sheets, the bands at 1656 cm^{-1} to α-helix and the band at 1683 cm^{-1} to ß-turns [22]. After storage at 2-8°C, 25°C and 40°C for a duration of 12 weeks, two minor bands in the ß-turn region at 1687 cm^{-1} and 1672 cm^{-1} arose as well

as a band in the low wave-number ß-sheets at 1615 cm $^{-1}$. These alterations were indicative for only minor changes in the secondary structure of the protein, whereas changes in the intensities of the 1635/1638 cm $^{-1}$ and 1655/1657 cm $^{-1}$ bands are known to be indicative for thermally induced conformational changes in the ß-sheet and α-helix structures [22]. Background noise originated form the reprocessing step with MTBE was responsible for baseline slopes and distorted peak shapes. Only minor band shifts in these areas were observed, indicating conformational stability of ovalbumin. This was also in accordance with the findings of the size exclusion chromatography, showing that the reprocessing step with MTBE did not influence protein integrity.

In summary, the reprocessing step with MTBE of the samples and the subsequent vacuum drying step were a suitable method to remove the oily substances from the formulation without altering excessively protein integrity.

3.1.1 MORPHOLOGICAL STABILITY OF THE SAMPLES

Morphological changes in the formulation in terms of thermal events, glass transition temperature and residual moisture of the samples could be investigated without the need of the reprocessing step with MTBE as described previously (section 3.1.)

The physicochemical properties of ovalbumin formulations based on a binary mixture of trehalose and mannitol and changes thereof after storage at elevated temperatures was scrutinized.

Differential scanning calorimetry analysis showed that mannitol crystallized during collapse freeze-drying as two characteristic melting endotherms in the range of 135.5 to 138.2 °C and 147.9 to 151.5 °C were observed in the DSC thermograms (table 6.4). According to literature δ-mannitol is first transformed to β-mannitol at 130-140°C and shortly after the in-situ formed β-mannitol shows a second characteristic melting endotherm at 150-158°C. In the secondary mixture of trehalose and mannitol, the melting points of mannitol were lowered as compared to those of pure mannitol due to the presence of ovalbumin, trehalose and buffer salts. This was also in agreement with melting temperatures of mannitol observed by Hawe *et al* [23].

Table 6.4: Physicochemical properties of ovalbumin-containing trehalose-mannitol samples determined by differential scanning calorimetry after storage at 2-8°C, 25°C and 40°C for 12 weeks.

formulation	storage temperature	storage time [weeks]	Tg [°C] ± SD	Δ Cp [J/g*K] ± SD	characteristic melting endotherms [°C] ± SD	
TM lyophilizate	-	0	85.3 ± 2.0	0.327 ± 0.388	138.2 ± 0.6	151.5 ± 0.3
TM cryo-milled powder	-	0	62.0 ± 0.7	0.255 ± 0.052	138.2 ± 0.5	148.8 ± 0.2
	2-8°C	8	59.7 ± 1.8	0.394 ± 0.024	138.2 ± 0.9	148.4 ± 0.6
		12	64.4 ± 5.4	0.348 ± 0.027	138.2 ± 0.4	149.4 ± 0.5
	25°C	8	56.4 ± 1.5	0.345 ± 0.056	138.2 ± 0.9	147.9 ± 0.5
		12	59.7 ± 0.1	0.329 ± 0.034	138.2 ± 1.0	148.7 ± 0.3
	40°C	8	55.0 ± 4.6	0.379 ± 0.015	138.2 ± 0.1	148.0 ± 0.3
		12	54.7 ± 3.0	0.324 ± 0.015	138.2 ± 1.0	148.2 ± 0.7

Glass transition temperatures of the amorphous trehalose phase were 85.3± 2.0°C immediately after lyophilization. Glass transition values decreased during storage (table 6.4) due to the increase in residual moisture (figure 6.17). The glass transition temperature of lyophilized products can be lowered by 10K for each percent of moisture in the product, as water acts as plasticizer [24].

After cryo-milling the glass transition value decreased from 85.3 ± 2.0 °C to 62.0 ± 0.7°C and remained stable for a time period of 12 weeks at 2-8°C and 25°C. A further decrease of the glass transition temperature to 54.7 ± 3.0°C was only observed in samples stored for 12 weeks at 40°C. Similarly, the extent of change in heat capacity at the glass transition was just slightly decreased for cryo-milled samples after 12 weeks of storage. However, most importantly, glass transition temperatures of the samples were well above the highest storage temperature of 40°C, indicating good storage stability of the formulation.
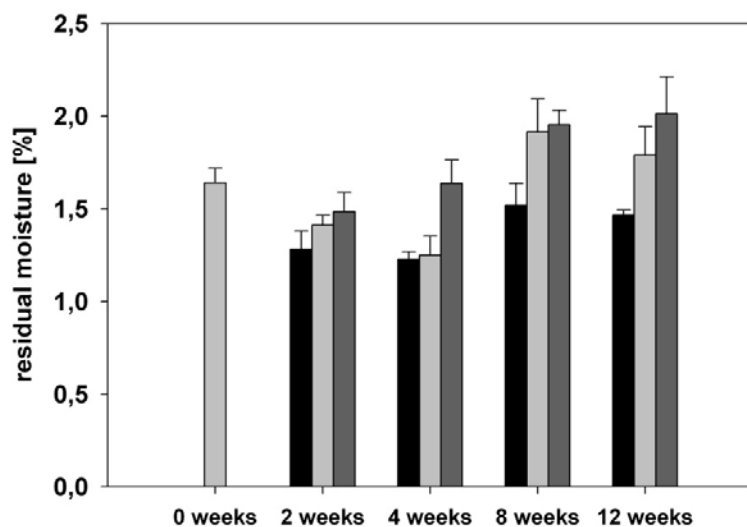
Figure 6.17: Residual moisture levels of trehalose-mannitol samples containing ovalbumin stored at 2-8°C (black bars), 25°C (light grey bars) and 40°C (dark grey bars) for 12 weeks.

3.2 STORAGE STABILITY OF THE OILY COMPONENTS OF MF59, SQUALENE AND SQUALANE

In order to find out if the oily substances degrade upon storage at elevated temperatures and if they interact with the protein powder particles, an accelerated stress test was initiated. Chemical stress was applied by incubation of the samples with 30% hydrogen peroxide and 1 N sodium hydroxide for 24 hours. Furthermore UV-light stress was applied for a time period of 7 days (as described in chapter 2). As UV-light stress caused also heat and thus resulted in increased sample temperatures of 35°C, samples were additionally exposed to heat stress at 35°C whilst being protected from light by an aluminum cover, respectively.

The mixture of the oily components of MF59 as well as its ingredient squalene were highly sensitive to UV-light and heat stress, resulting in a strong decrease in recovery as determined by GC/MS (figure 6.18).
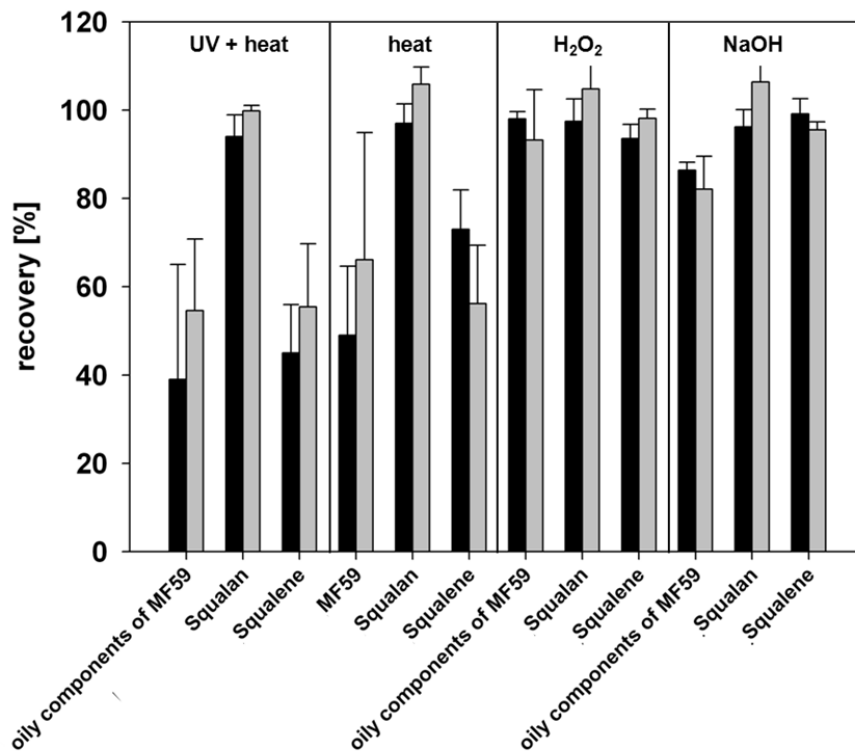
Figure 6.18: Recovery of the oily components of MF59, squalane and squalene as determined by GC/MS. GC/MS analysis was conducted by Dr. Christoph Müller (LMU, Munich). Oily substances incubated with protein powder formulation (black bars) and samples containing only oily substances (grey bars).

After UV-light exposure samples containing the mixture of the oily components of MF59 showed a recovery of 54.6 ± 16.3%. The decrease in recovery of the oily components of MF59 was even enhanced if the samples were incubated together with protein powder formulation, resulting in 39.0 ± 26.1% recovery. Samples exposed to heat stress showed similar results with 66.1 ± 28.8% recovery for samples containing the mixture of the oily components of MF59 and 49.0 ± 15.6% recovery for samples, where the mixture of the oily components of MF59 was incubated in the presence of the protein powder formulation. The surfactants polysorbate 80 and Span® 85 are both known to build peroxides and thus is highly promoted by light stress and temperature [25, 26].

Squalene samples showed a recovery of 55.5 ± 14.3% after UV-light exposure and 56.2 ± 13.2% recovery after heat stress. Samples incubated together with protein powder and squalene showed 45.0 ± 11.0% recovery after UV-light exposure and 73.0 ± 9.0% recovery after heat stress (figure 6.18).

The mixture of the oily components of MF59 as well as squalene samples responded less sensitive to chemical stress that was induced by hydroxide peroxide and sodium peroxide, independent of the presence of the protein powder. Squalane samples showed throughout less receptiveness for the applied stress conditions. Squalane was generally more chemically stable as it had no double bonds which were susceptible to oxidation [7]. The accelerated stress test showed that especially the oily components of MF59 and its ingredient squalene were sensitive to both, UV-light exposure and heat stress.

3.2.1 STABILITY OF OVALBUMIN IN A TREHALOSE-MANNITOL FORMULATION IN THE PRESENCE OF THE OILY COMPONENTS OF MF59 USED AS OILY ADJUVANT

A short term stability study was performed, in which the stability of ovalbumin and the stability of the oily components of MF59 was assessed for a time period of 12 weeks at elevated temperatures.

After 8 weeks of storage at 40°C a strong decrease up to 50% in the recovery of the mixture of the oily substances of MF59 stored together with the ovalbumin containing trehalose-mannitol powder particles was observed (figure 6.19).

The interaction of the oily adjuvant MF59 and ovalbumin containing trehalose-mannitol particles was already macroscopically visible (figure 6.20) in form of a yellow discoloration of the samples. A decrease in recovery of the oily substance in such an extent could not be observed in samples which were stored without the presence of the protein-sugar matrix. This indicated, that the instability was a matter of the interaction between the protein-sugar matrix and the oily adjuvant rather than due to the degradation of MF59 itself. As no degradation products in form of smaller chemical entities could be detected in the GC/MS spectra, the assumption was supported that

higher ordered agglomerates were reasonable for the decrease in the recovery of the oily substance.
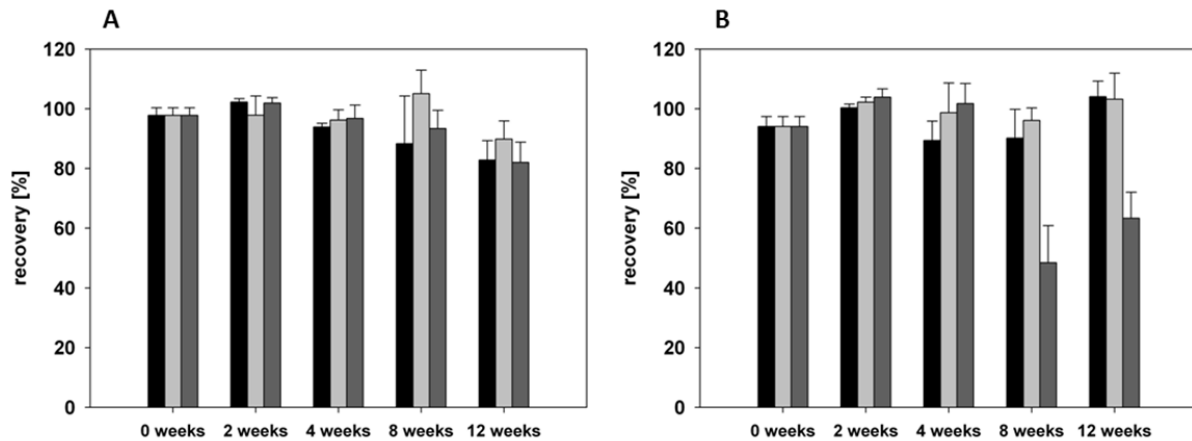
Figure 6.19: Recovery of the oily components of MF59, as determined by GC/MS. GC/MS analysis was conducted by Dr. Christoph Müller (LMU, Munich). Samples were incubated up to 12 weeks at 2-8°C (black bars), 25°C (light grey bars) and 40°C (dark grey bars). The oily components of MF59 were incubated either without the presence of the ovalbumin powder formulation (A) or in combination with the ovalbumin powder formulation (B).

Figure 6.20: Picture of trehalose-mannitol formulations stored at 40°C over a time period of 8 weeks together with the oily adjuvant MF59, showing a yellow discoloration of the powder.

In order to gain further insight into the effect of the oily substances of MF59 on ovalbumin, size exclusion chromatography was used to evaluate the formation of soluble and insoluble aggregates (using the recovery data), and FTIR transmission spectroscopy was applied to assess potential changes in the secondary structure of

ovalbumin. Figure 6.21 A-C displays the remaining monomer, total protein recovery as well as the recovery of the different protein species by size exclusion chromatography. A decrease in soluble monomer recovery as well as total protein recovery was observed after 8 weeks of storage at 2-8°C and 25°C (figure 6.21 A and B). Additionally, the formation of higher molecular weight aggregates was observed after 8 weeks of storage at 40°C, indicating the formation of soluble as well as insoluble aggregates (figure 6.21 C).
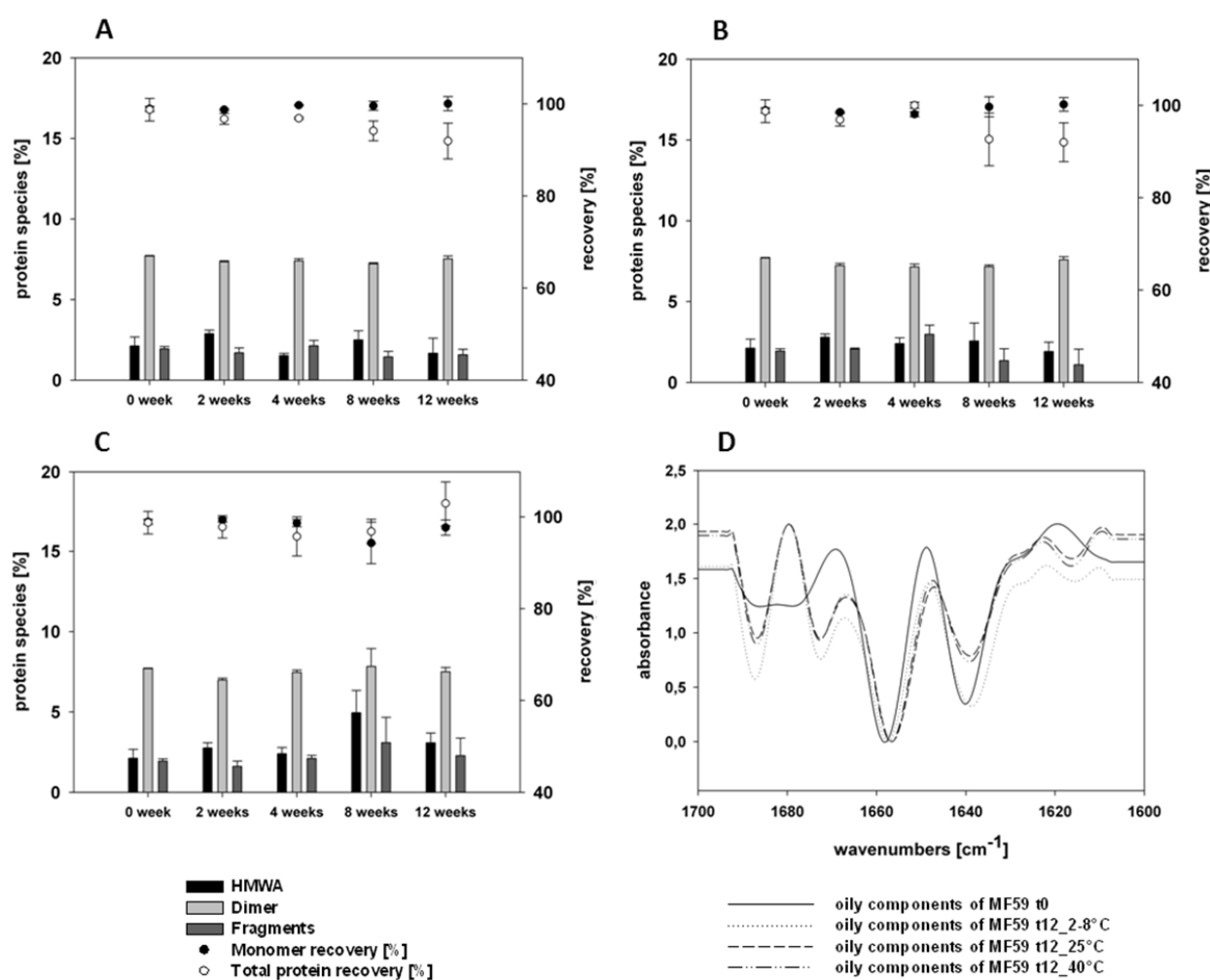
Figure 6.21: Higher molecular weight aggregates (black bars), dimers (light grey bars) and fragment (dark grey bars) protein species [%], total monomer recovery [%] (filled circles) and total protein recovery [%] (open circles) as determined by size exclusion chromatography. Samples were incubated with the oily components of MF59 at 2-8°C (A), 25°C (B) and 40°C (C). Area-normalized 2nd derivative FTIR transmission spectra of samples incubated with the oily components of MF59 (D).

The second derivate FTIR-transmission spectra of the samples are depicted in figure 6.21 D. After storage at 25°C and 40°C, respectively, the intensity of the 1638 cm^{-1} band of ovalbumin was decreased dramatically, indicating a thermally induced conformational change in the ß-sheet structures. Dong *et al.* showed, that the intensity change in the 1635/1638 cm^{-1} band of ovalbumin was highly sensitive to changes in temperature and was used to monitor the aggregation process of the protein [22]. The results of the FTIR measurements were confirmed by the results of size-exclusion chromatography, showing the onset of protein denaturation after 8 weeks of storage due to the interaction ovalbumin with the oily components of MF59.

Figure 6.22 shows turbidity levels and the formation particles determined by light obscuration of samples containing the oily components of MF59, supporting the results obtained by size exclusion chromatography and FTIR spectroscopy. A dramatic increase in turbidity up to > 8 NFU was observed in samples stored at 40°C after 8 and 12 weeks of storage. Likewise the cumulative particle counts > 1 µm per mL (figure 6.22 A) and > 10 µm per mL (table 6.5) increased after 8 and 12 weeks of storage at 40°C.
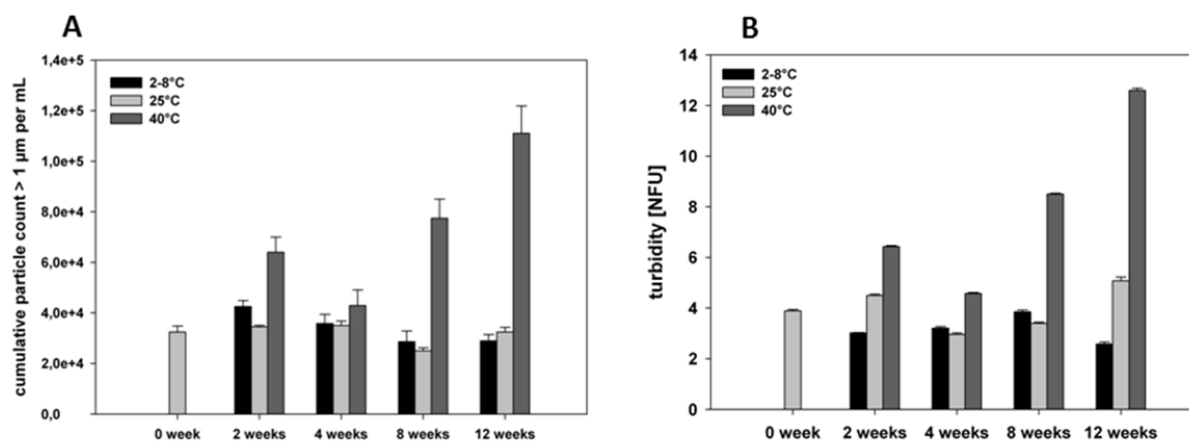
Figure 6.22: Cumulative particle counts > 1µm per mL of samples incubated with the oily components of MF59 (A) and turbidity levels (B) after 12 weeks of storage at 2-8°C (grey bars), 25°C (dark grey bars) and 40°C (black bars). Samples were reprocessed as described in chapter 3.1 in MTBE and were vacuum dried prior to analysis.

Table 6.5: Cumulative particle counts > 10 and 25 µm per mL of samples incubated with the oily components of MF59 after 12 weeks of storage at 2-8°C, 25°C and 40°C. Samples were reprocessed as described in chapter 3.1 in MTBE and were vacuum dried prior to analysis.

	after 12 weeks of storage at 2-8°C	after 12 weeks of storage at 25°C	after 12 weeks of storage at 40°C
particles > 10 µm per mL ± SD	1087 ± 12	896 ± 18	2831 ± 246
particles > 25 µm per mL ± SD	60 ± 15	99 ± 44	86 ± 13
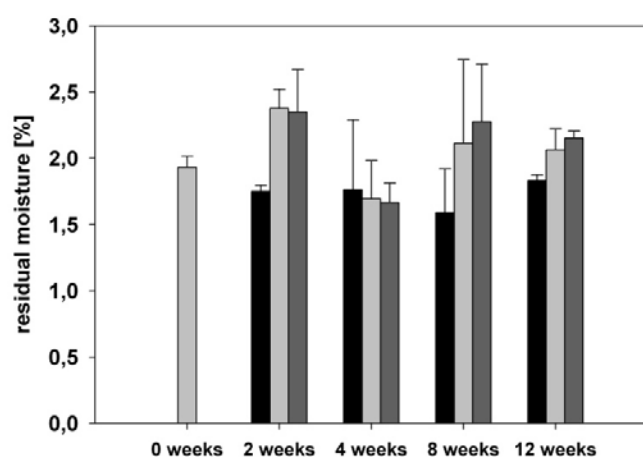
Figure 6.23: Residual moisture levels of trehalose-mannitol samples containing ovalbumin stored at 2-8°C (black bars), 25°C (light grey bars) and 40°C (dark grey bars) for 12 weeks in the presence of the oily components of MF59.

Figure 6.23 summarizes the residual moisture levels of trehalose-mannitol samples containing ovalbumin stored at 2-8°C, 25°C and 40°C in the presence of the oily components of MF59 for 12 weeks. A slight increase of residual moisture levels was observed for samples stored at 25°C and 40°C after 4 weeks of storage, which is also commonly reported in literature [27]. The residual moisture level of trehalose-mannitol formulations containing ovalbumin (figure. 6.17) was comparable to the samples stored in the presence of oily adjuvants.

Changes in particle morphology were also assessed by differential scanning calorimetry. Glass transition values decreased during storage at 25°C and 40°C after 12

weeks of storage, to 58.8 °C ± 1.1°C and 51.3°C ± 0.3°C, respectively, which was also in accordance with a slight increase in residual moisture (table 6.6). However, glass transition temperatures of the samples were still above the highest storage temperature at 40°C.

Table 6.6: Physicochemical properties of trehalose-mannitol samples stored in the presence of the oily components of MF59 as determined by differential scanning calorimetry after storage at 2-8°C, 25°C and 40°C for 12 weeks.

formulation	storage temperature	storage time [weeks]	Tg [°C] ± SD	Δ Cp [J/g*K] ± SD	characteristic melting endotherms [°C] ± SD	
oily components of MF59	-	0	59.1 ± 3.8	0.256 ± 0.082	137.3 ± 1.2	149.1 ± 1.1
	2-8°C	8	64.7 ± 0.6	0.292 ± 0.008	137.6 ± 1.0	149.6 ± 0.7
		12	60.1 ± 0.5	0.315 ± 0.013	137.0 ± 0.4	149.3 ± 0.3
	25°C	8	58.7 ± 1.1	0.301 ± 0.031	137.1 ± 1.2	149.2 ± 0.7
		12	58.8 ± 1.1	0.344 ± 0.020	135.5 ± 0.6	148.6 ± 0.3
	40°C	8	47.6 ± 2.6	0.283 ± 0.012	134.8 ± 0.8	146.8 ± 0.7
		12	51.3 ± 0.3	0.282 ± 0.030	135.2 ± 0.6	147.5 ± 0.5

The two characteristic melting endotherms of mannitol in the range of 134.8 to 137.6 °C and 146.6 to 149.6 °C (table 6.6) for samples stored in the presence of MF59 were unvaried in comparison to samples stored without the presence of any oily substance (table 6.4).

3.2.2 STABILITY OF OVALBUMIN IN A TREHALOSE-MANNITOL FORMULATION IN THE PRESENCE OF SQUALENE USED AS OILY ADJUVANT

GC/MS analysis of squalene samples stored for up to 12 weeks at 2-8°C, 25°C and 40°C showed only marginal alterations in the recovery of the oily substance (figure 6.24 A). Whereas the combination squalene together with powder particles containing ovalbumin showed a decrease in squalene recovery after 4 weeks of storage at 40°C (figure 6.24 B). This was also in accordance to the results obtained for the oily components of MF59. However, the decrease in squalene recovery was clearly lower with 88% recovery after 8 weeks of storage at 40°C in comparison to the recovery of the mixture of the oily components of MF59 with 48% recovery after 8 weeks of storage at

40°C. As no degradation products in form of smaller chemical entities were detected in the GC/MS spectra, again, the assumption was supported that higher ordered agglomerates were reasonable for the decrease in the recovery of the oily substance.
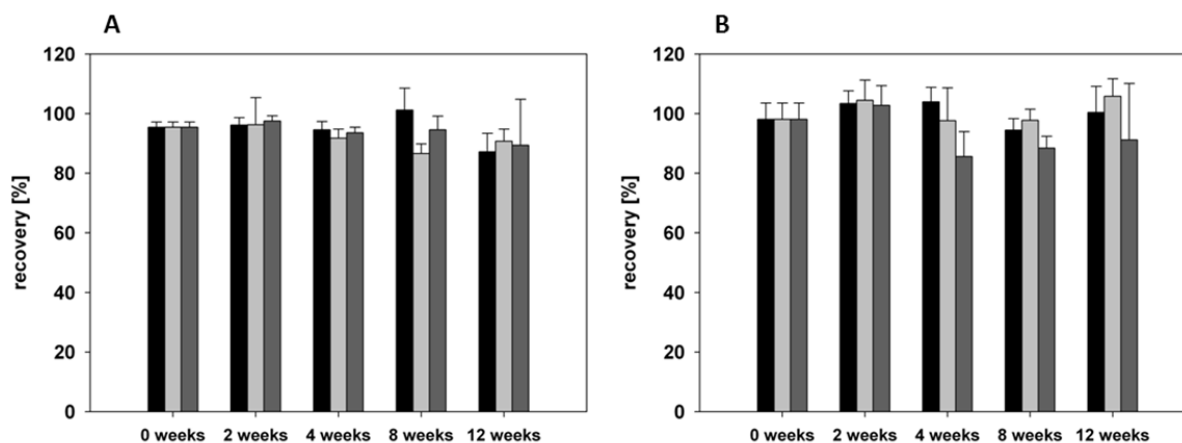
Figure 6.24: Recovery of squalene, as determined by GC/MS. GC/MS analysis was conducted by Dr. Christoph Müller (LMU, Munich). Samples were incubated up to 12 weeks at 2-8°C (black bars), 25°C (light grey bars) and 40°C (dark grey bars). Squalene was incubated either without the presence of the ovalbumin powder formulation (A) or in combination with the ovalbumin powder formulation (B).

Size exclusion chromatography was performed to investigate the protein stability of the samples stored in the presence of squalene (figure 6.25). Only marginal changes were observed after 12 weeks of storage at 40°C in form of a slight increase of higher molecular aggregates and a slight decrease in total protein recovery and recovery of soluble monomer (figure 6.25 C). Figure 16.25 D shows the second derivative spectra of ovalbumin after storage in the presence of squalene. Samples were reprocessed prior to analysis with MTBE as described before. The spectrum of the standard sample, which was not stored (t0), did just marginally alter from the spectrum of samples stored for 12 weeks at 2-8°C, 25°C or 40°C. This was attributed to the fact that the background noise, arising from the reprocessing step with MTBE, could not be completely eliminated and appeared in baseline slopes and distorted peak shapes. No changes in the intensities of the 1635/1638 cm^{-1} and 1655/1657 cm^{-1} bands were observed, which were known to be indicative for thermally induced conformational changes in the ß-

sheet and α-helix structures [22]. This suggested conformational stability of ovalbumin if stored together with squalene.
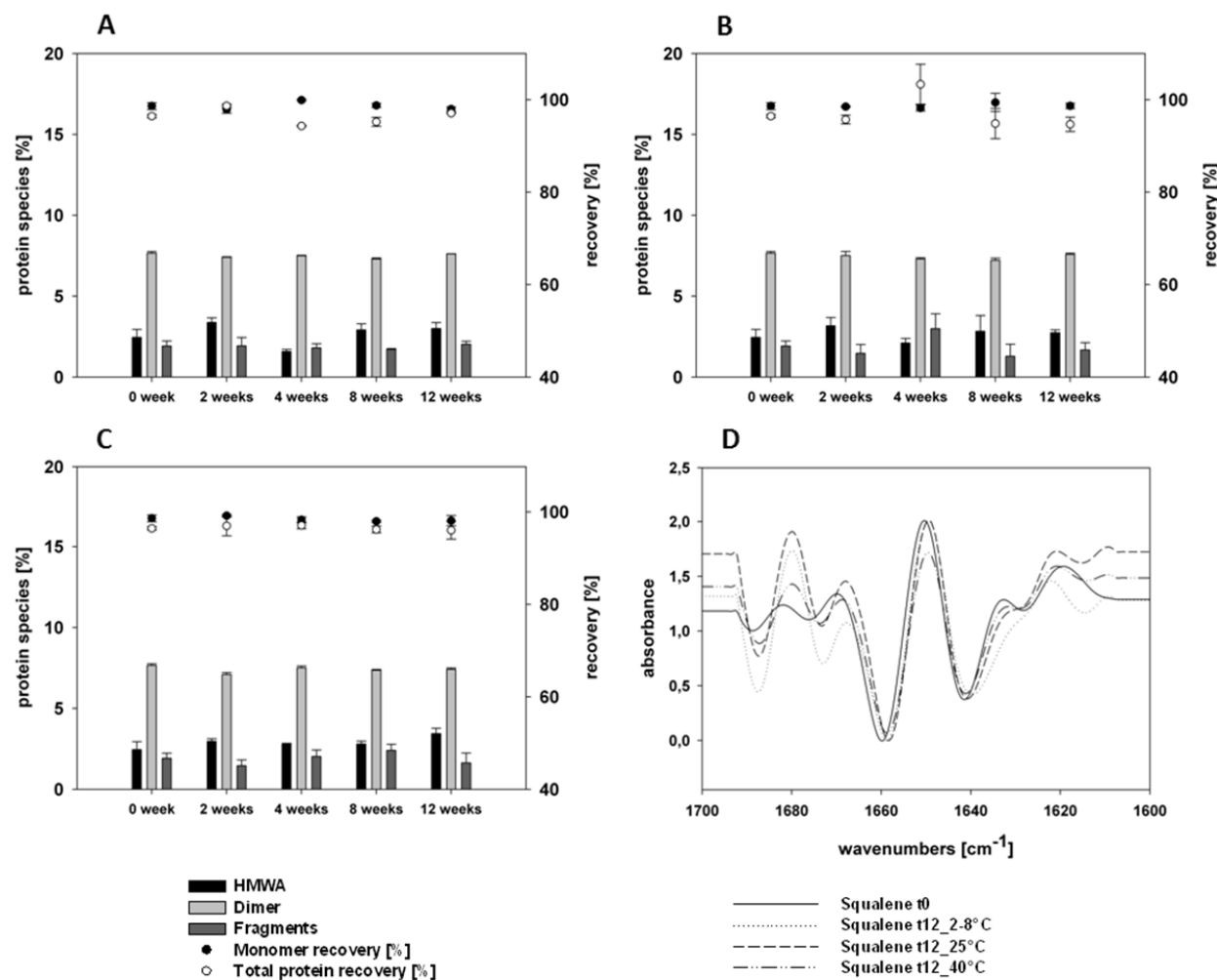
Figure 6.25: Higher molecular weight aggregates (black bars), dimers (light grey bars) and fragment (dark grey bars) protein species [%], total monomer recovery [%] (filled circles) and total protein recovery [%] (open circles) as determined by size exclusion chromatography. Samples were incubated with the oily components of MF59 at 2-8°C (A), 25°C (B) and 40°C (C). Area-normalized 2nd derivative FTIR transmission spectra of samples incubated with squalene (D).

The cumulative particle counts as well as turbidity levels of samples stored in the presence of squalene showed no remarkable changes (figure 6.26). Cumulative particle counts ranged between 79262 ± 8356 particles > 1 µm, 48330 ± 3185 particles > 1 µm

per mL and 58608 ± 2746 particles > 1 µm after storage for 12 weeks at 2-8°C, 25°C and 40°C, respectively, in comparison to an initial cumulative particle count of 56576 ± 3003 particles > 1 µm per mL.
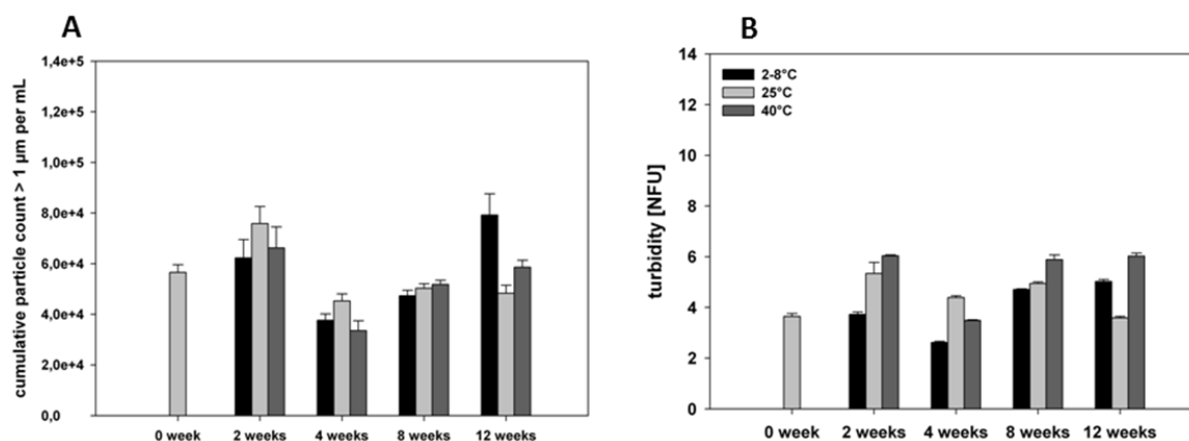
Figure 6.26: Cumulative particle counts > 1 µm per mL of samples incubated with squalene (A) and turbidity levels (B) after 12 weeks of storage at 2-8°C (grey bars), 25°C (dark grey bars) and 40°C (black bars). Samples were reprocessed as described in chapter 3.1 in MTBE and were vacuum dried prior to analysis.

Table 6.7: Cumulative particle counts > 10 and 25 µm per mL of samples incubated with squalene after 12 weeks of storage at 2-8°C, 25°C and 40°C. Samples were reprocessed as described in chapter 3.1 in MTBE and were vacuum dried prior to analysis.

	after 12 weeks of storage at 2-8°C	after 12 weeks of storage at 25°C	after 12 weeks of storage at 40°C
particles > 10 µm per mL ± SD	3548 ± 84	1856 ± 178	1940 ± 112
particles > 25 µm per mL ± SD	203 ± 9	81 ± 21	86 ± 10

Similarly no remarkable changes in particle morphology regarding the residual moisture or differential scanning thermograms were observed for samples stored together with squalene in comparison to samples which were stored without the presence of any oily substance (figure 6.27, table 6.8).
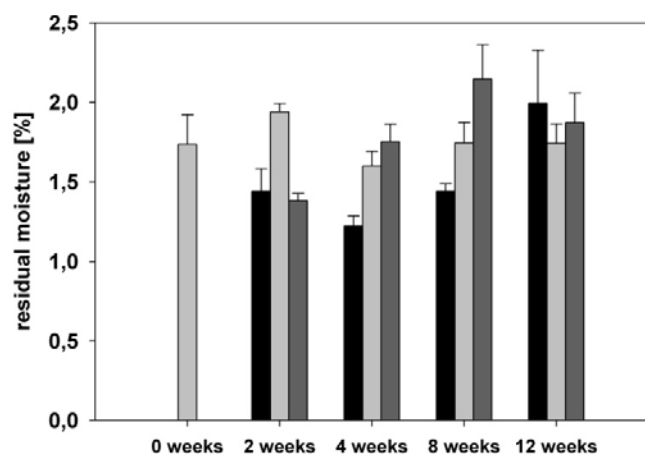
Figure 6.27: Residual moisture levels of trehalose-mannitol samples containing ovalbumin stored at 2-8°C (black bars), 25°C (light grey bars) and 40°C (dark grey bars) for 12 weeks in the presence of squalene.

Table 6.8: Physicochemical properties of trehalose-mannitol samples stored in the presence of squalene as determined by differential scanning calorimetry after storage at 2-8°C, 25°C and 40°C for 12 weeks.

formulation	storage temperature	storage time [weeks]	Tg [°C] ± SD	Δ Cp [J/g*K] ± SD	characteristic melting endotherms [°C] ± SD	
squalene	-	0	57.5 ± 9.1	0.278 ± 0.033	135.5 ± 3.0	149.1 ± 1.1
	2-8°C	8	65.9 ± 0.7	0.294 ± 0.035	138.9 ± 0.7	149.6 ± 0.7
		12	61.1 ± 0.3	0.313 ± 0.029	136.7 ± 0.4	149.3 ± 0.3
	25°C	8	61.9 ± 6.8	0.269 ± 0.036	136.8 ± 0.5	149.2 ± 0.7
		12	61.3 ± 1.5	0.308 ± 0.030	136.0 ± 1.1	148.6 ± 0.3
	40°C	8	55.8 ± 2.5	0.316 ± 0.014	136.2 ± 0.6	146.8 ± 0.7
		12	56.7 ± 1.6	0.282 ± 0.041	135.2 ± 0.4	147.5 ± 0.5

3.2.3 STABILITY OF OVALBUMIN IN A TREHALOSE-MANNITOL FORMULATION IN THE PRESENCE OF SQUALANE USED AS OILY ADJUVANT

The stability of ovalbumin in a trehalose-mannitol formulation that was incubated together with squalane over a time period of 12 weeks at 2-8°C, 25°C and 40°C was investigated. GC/MS results showed that the recovery of squalane was not altered if the samples were stored as single components (figure 6.28 A). Only a slight decrease in the

recovery of squalane could be observed after 12 weeks of storage at 25°C (83.6% ± 16%) and 40°C (88.8% ± 13%), if the samples were stored together with powder particles containing ovalbumin (figure 6.28 B). This is in accordance with the previously performed stress test (figure 6.18), confirming the negligible sensitivity of squalane to heat stress.
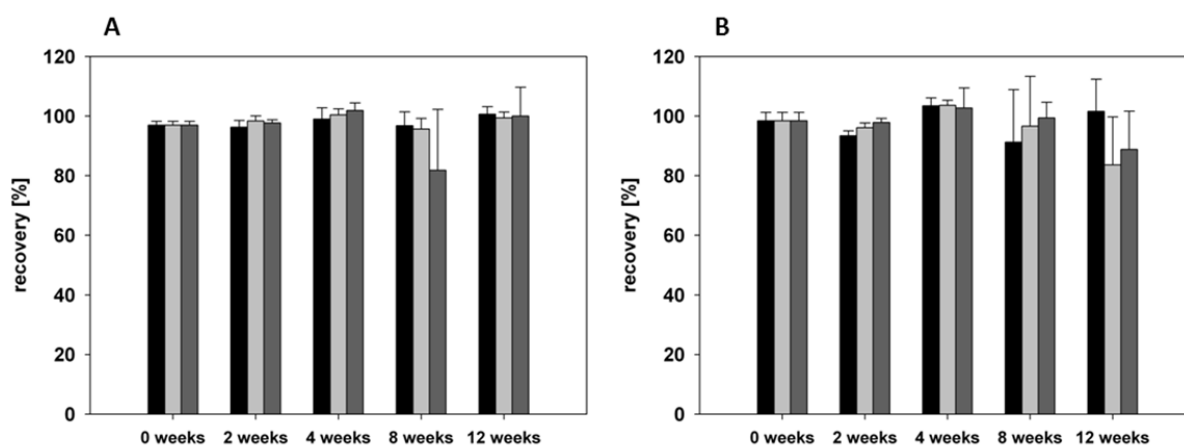
Figure 6.28: Recovery of squalane, as determined by GC/MS. GC/MS analysis was conducted by Dr. Christoph Müller (LMU, Munich). Samples were incubated up to 12 weeks at 2-8°C (black bars), 25°C (light grey bars) and 40°C (dark grey bars). Squalane was incubated either without the presence of the ovalbumin powder formulation (A) or in combination with the ovalbumin powder formulation (B).

Regarding the protein stability of ovalbumin samples stored in presence of squalane size exclusion chromatography (figure 6.29 A, B, C), FTIR (figure 6.29 D), light obscuration (figure 6.30 and table 6.9) as well as turbidity measurements (figure 6.30) confirmed that the oily substance squalane had no negative influence on protein integrity.
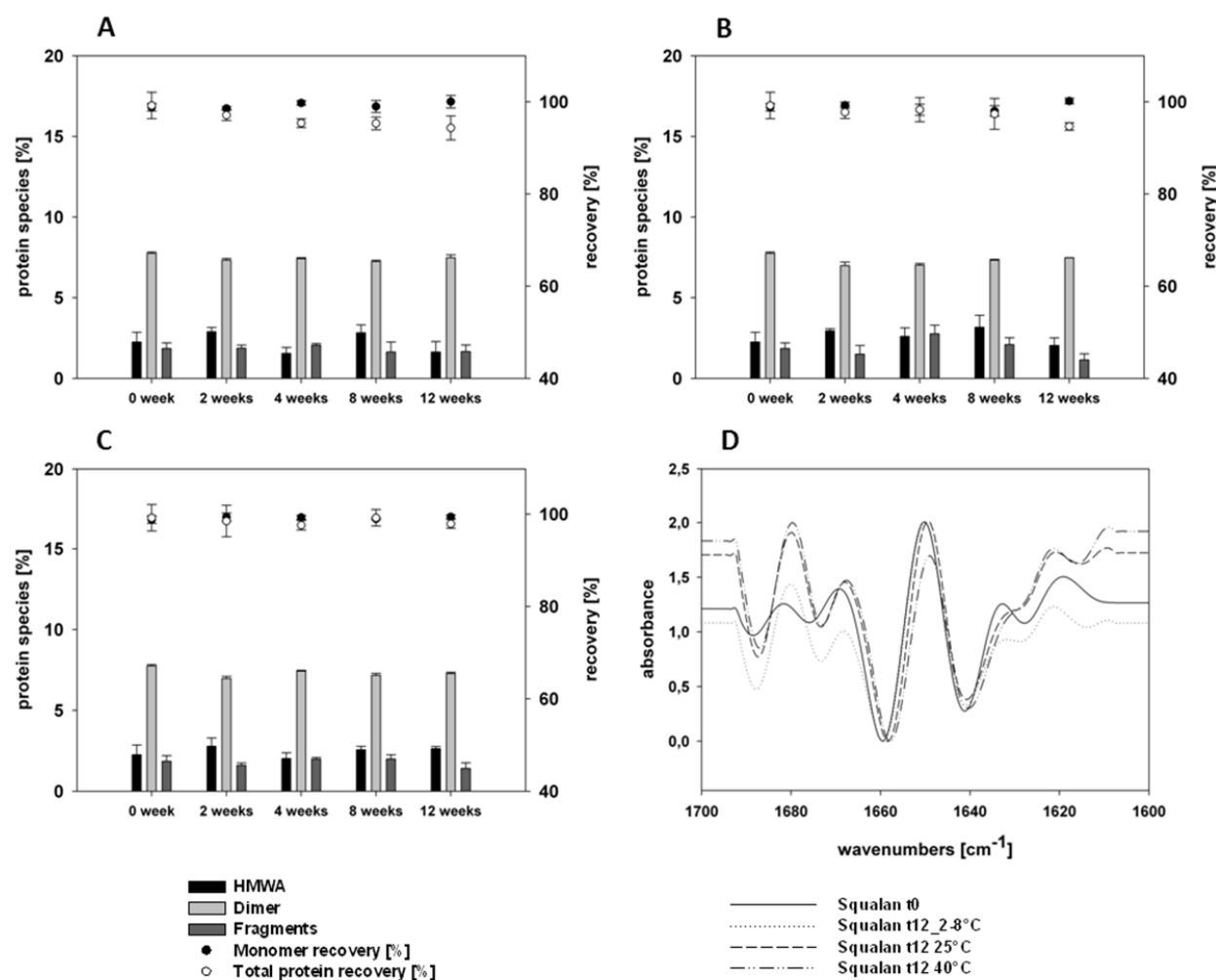
Figure 6.29: Higher molecular weight aggregates (black bars), dimers (light grey bars) and fragment (dark grey bars) protein species [%], total monomer recovery [%] (filled circles) and total protein recovery [%] (open circles) as determined by size exclusion chromatography. Samples were incubated with squalane at 2-8°C (A), 25°C (B) and 40°C (C). Area-normalized 2nd derivative FTIR transmission spectra of samples incubated with squalane(D).

Similarly to the results of the protein stability, no additional changes in particle morphology were observed in the presence of squalane, regarding residual moisture (figure 6.31) or differential scanning calorimetry (table 6.10) of samples stored in the presence of squalane in comparison to samples without the presence of any oily substance (table 6.4 and figure 6.17).
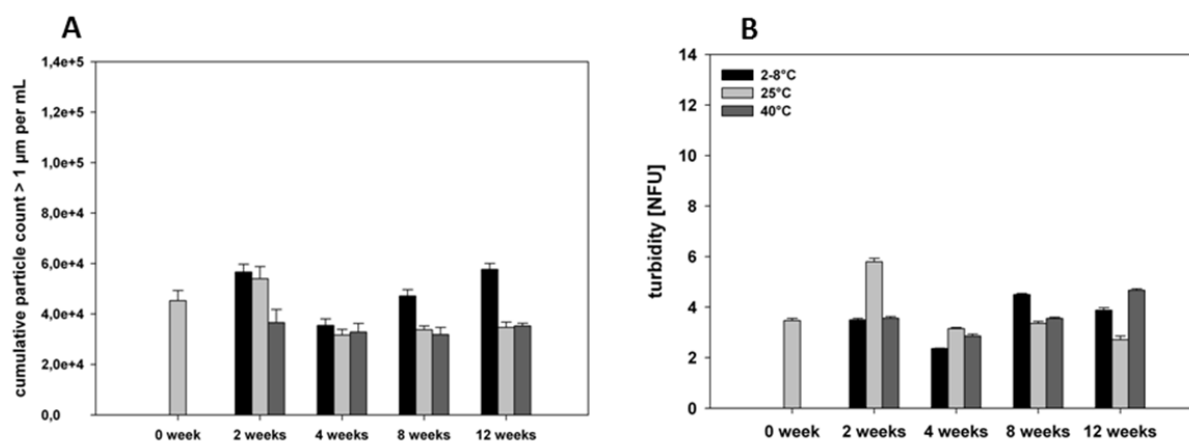
Figure 6.30: Cumulative particle counts > 1 µm per mL of samples incubated with squalane (A) and turbidity levels (B) after 12 weeks of storage at 2-8°C (grey bars), 25°C (dark grey bars) and 40°C (black bars). Samples were reprocessed as described in chapter 3.1 in MTBE and were vacuum dried prior to analysis.

Table 6.9: Cumulative particle counts > 10 and >25 µm per mL of samples incubated with squalane after 12 weeks of storage at 2-8°C, 25°C and 40°C. Samples were reprocessed as described in chapter 3.1 in MTBE and were vacuum dried prior to analysis.

	after 12 weeks of storage at 2-8°C	after 12 weeks of storage at 25°C	after 12 weeks of storage at 40°C
particles > 10 µm per mL ± SD	2322 ± 42	1531 ± 97	1510 ± 43
particles > 25 µm per mL ± SD	156 ± 3	76 ± 13	86 ± 14
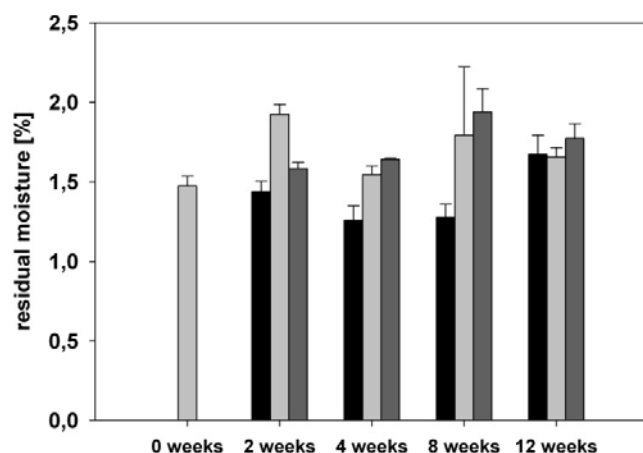
Figure 6.31: Residual moisture levels of trehalose-mannitol samples containing ovalbumin stored at 2-8°C (black bars), 25°C (light grey bars) and 40°C (dark grey bars) for 12 weeks in the presence of squalane.

Table 6.10: Physicochemical properties of trehalose-mannitol samples stored in the presence of squalane as determined by differential scanning calorimetry after storage at 2-8°C, 25°C and 40°C for 12 weeks.

formulation	storage temperature	storage time [weeks]	Tg [°C] ± SD	Δ Cp [J/g*K] ± SD	characteristic melting endotherms [°C] ± SD	
	-	0	64.7 ± 1.4	0.236 ± 0.032	138.4 ± 0.4	150.1 ± 0.3
	2-8°C	8	67.0 ± 0.6	0.268 ± 0.013	138.3 ± 0.1	150.0 ± 0.2
		12	63.6 ± 0.4	0.288 ± 0.012	136.9 ± 0.3	149.2 ± 0.2
squalane	25°C	8	57.0 ± 7.3	0.282 ± 0.051	135.8 ± 0.8	148.3 ± 0.7
		12	62.0 ± 2.1	0.330 ± 0.042	137.1 ± 0.3	149.2 ± 0.6
	40°C	8	59.0 ± 0.6	0.327 ± 0.019	137.0 ± 0.8	146.2 ± 0.6
		12	53.8 ± 3.2	0.377 ± 0.144	132.9 ± 1.2	147.9 ± 0.6

Only a slight decrease of the glass transition temperature was observed, which was in accordance to the increase of residual moisture at elevated storage temperature (figure 6.31 and table 6.10). The glass transition temperature of lyophilized products can be lowered by 10K for each percent of moisture in the product, as water acts as plasticizer [24].

3.3 STORAGE STABILITY OF THE OILY COMPONENTS OF FREUND'S INCOMPLETE ADJUVANT AND PARAFFIN OIL USED AS OILY ADJUVANT

An accelerated stress test, inducing chemical stress by the incubation of the samples with 30% hydrogen peroxide or 1 N sodium hydroxide for 24 hours was performed. Chemical stress was applied to samples containing either Freund's incomplete adjuvant, paraffin oil or either of them in combination with powder particles containing ovalbumin in a trehalose-mannitol formulation. The stress test served to estimate if the oily substances interact with protein powder particles and if they degrade upon the applied stress conditions.
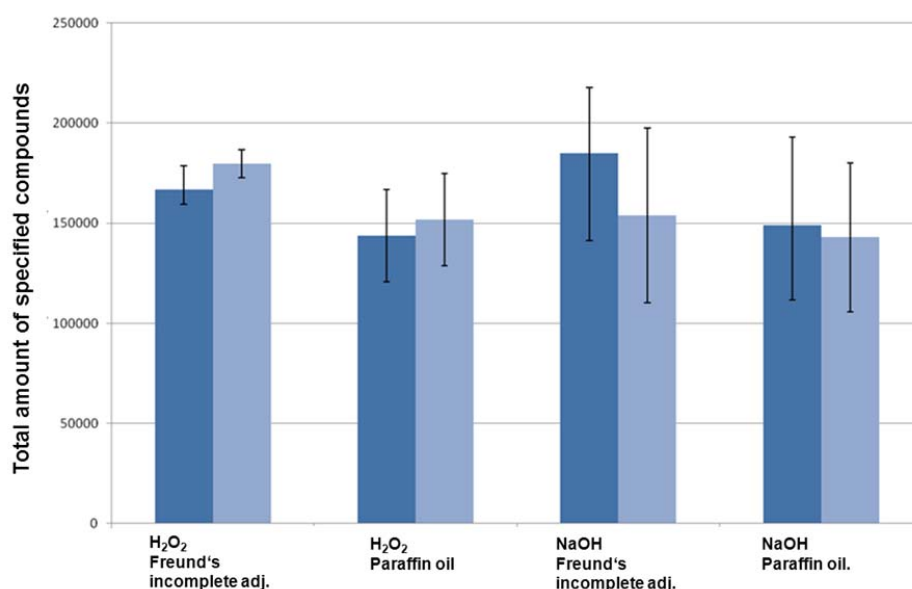
Figure 6.32: Recovery of Freund's incomplete adjuvant and paraffin oil as determined by GC-FID. GC-FID analysis was conducted by Dr. Florian Plößl (ZInstSanBW, Munich). Oily substances incubated with protein powder formulation (dark blue bars) and samples containing only oily substances (light blue bars).

No significant differences between Freund's incomplete adjuvant or paraffin oil incubated in combination with protein powder formulation or the oily substance by itself was observed, regardless whether the samples were stressed with H_2O_2 or NaOH (figure 6.32).

Due to the chemical structure of both, Freund's incomplete adjuvant and paraffin oil, degradation due to UV-light stress or heat stress was not expected.

3.3.1 STABILITY OF OVALBUMIN IN A TREHALOSE/MANNITOL FORMULATION IN THE PRESENCE OF FREUND'S INCOMPLETE ADJUVANT

Size exclusion chromatography was applied to evaluate the formation of soluble and insoluble aggregates (using the recovery data), and FTIR transmission spectroscopy was applied to assess potential changes in the secondary structure of ovalbumin after incubation with Freund's incomplete adjuvant for 12 weeks at elevated temperatures.

Figure 6.33 A-C displays the remaining monomer, total protein recovery as well as the recovery of the different protein species by size exclusion chromatography.No significant changes in soluble monomer recovery as well as total protein recovery were observed after 12 weeks of storage at 2-8°C and 25°C (figure 6.33 A and B). However, the formation of higher molecular weight aggregates was observed after 8 and 12 weeks of storage at 40°C (4.0% after 8 weeks and 4.5% after 12 weeks in comparison to initially 2.9%) (figure 6.33 C).

The second derivate FTIR-transmission spectra of the samples incubated with Freund's incomplete adjuvant are depicted in figure 6.33 D. After storage at 25°C and 40°C, respectively, the intensity of the 1638 cm^{-1} band of ovalbumin was decreased and the bands were shifted to lower wavenumbers. This indicated a thermally induced conformational change in the ß-sheet structures of ovalbumin [22]. The onset of protein conformational changes in samples containing Freund's incomplete adjuvant after 8 weeks of storage due to heat exposure supports also the findings of the size exclusion chromatography.
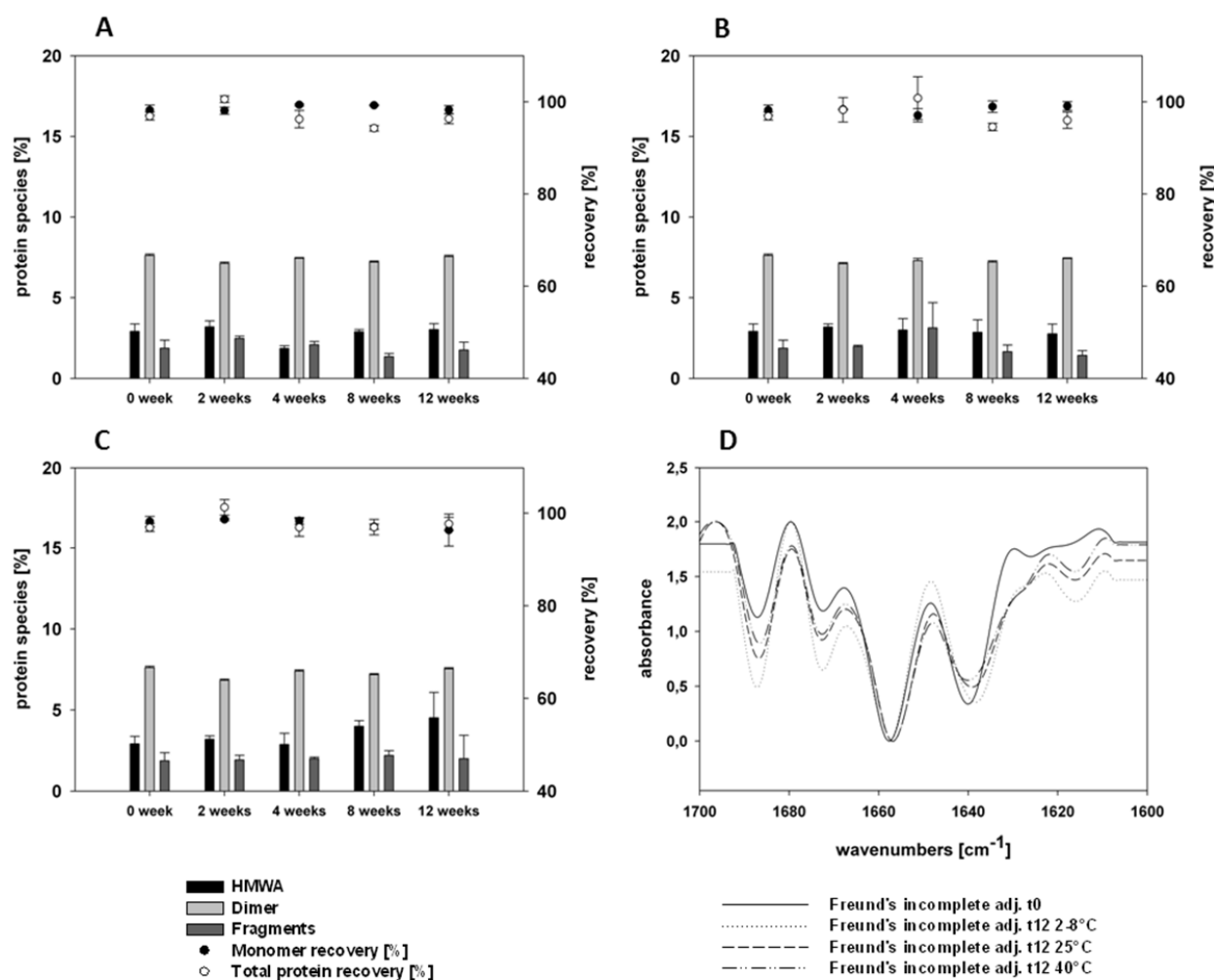
Figure 6.33: Higher molecular weight aggregates (black bars), dimers (light grey bars) and fragment (dark grey bars) protein species [%], total monomer recovery [%] (filled circles) and total protein recovery [%] (open circles) as determined by size exclusion chromatography. Samples were incubated with Freund's incomplete adjuvant at 2-8°C (A), 25°C (B) and 40°C (C). Area-normalized 2nd derivative FTIR transmission spectra of samples incubated with Freund's incomplete adjuvant (D).

Table 6.11: Cumulative particle counts > 10 and 25 μm per mL of samples incubated with Freund's incomplete adjuvant after 12 weeks of storage at 2-8°C, 25°C and 40°. Samples were reprocessed as described in chapter 3.1 in MTBE and were vacuum dried prior to analysis.

	after 12 weeks of storage at 2-8°C	after 12 weeks of storage at 25°C	after 12 weeks of storage at 40°C
particles > 10 μm per mL ± SD	2407 ± 184	1746 ± 198	1460 ± 79
particles > 25 μm per mL ± SD	149 ± 32	109 ± 45	81 ± 8
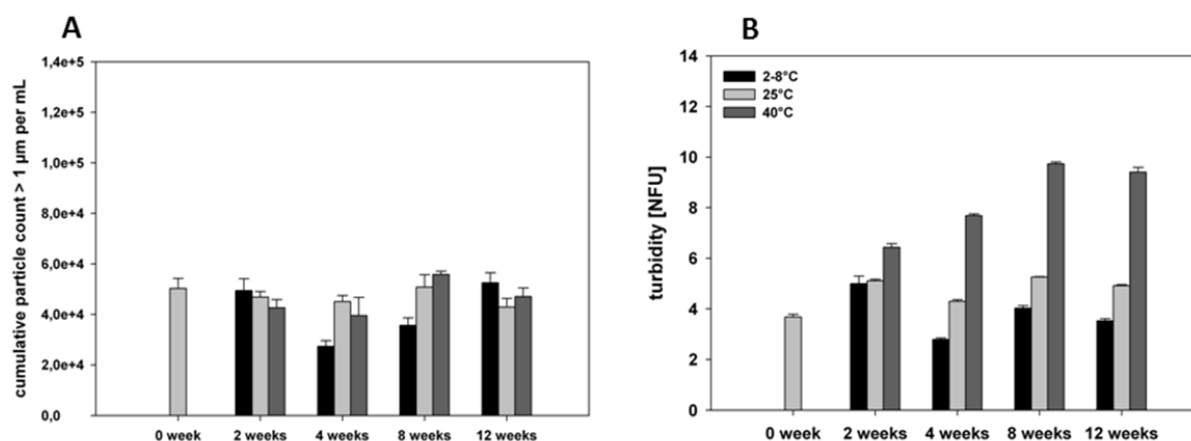
Figure 6.34: Cumulative particle counts > 1 μm per mL of samples incubated with Freund's incomplete adjuvant (A) and turbidity levels (B) after 12 weeks of storage at 2-8°C (grey bars), 25°C (dark grey bars) and 40°C (black bars). Samples were reprocessed as described in chapter 3.1 in MTBE and were vacuum dried prior to analysis.

Figure 6.34 A and table 6.11 show cumulative particle counts of samples incubated with Freund's incomplete adjuvant as determined by light obscuration. The formation of particles could not be observed in samples incubated with Freund's incomplete adjuvant. However, an increase in turbidity levels was visible after storage at 40°C, with an onset after 2 weeks (figure 6.34 B). This was consistent with the results obtained by size exclusion chromatography.

Table 6.12: Physicochemical properties of trehalose-mannitol samples stored in the presence of Freund's incomplete adjuvant as determined by differential scanning calorimetry after storage at 2-8°C, 25°C and 40°C for 12 weeks.

formulation	storage temperature	storage time [weeks]	Tg [°C] ± SD	Δ Cp [J/g*K] ± SD	characteristic melting endotherms [°C] ± SD	
	-	0	76.4 ± 0.6	0.556 ± 0.041	133.9 ± 6.1	146.4 ± 4.9
	2-8°C	8	63.3 ± 0.5	0.317 ± 0.029	137.1 ± 0.2	149.4 ± 0.2
Freund's		12	59.3 ± 2.4	0.320 ± 0.015	136.8 ± 0.3	149.1 ± 0.3
incomplete	25°C	8	52.4 ± 3.6	0.283 ± 0.039	135.1 ± 1.1	148.2 ± 1.1
adjuvant		12	58.7 ± 0.5	0.339 ± 0.021	135.2 ± 0.5	149.0 ± 0.5
	40°C	8	50.1 ± 6.2	0.279 ± 0.009	134.9 ± 1.9	147.0 ± 1.8
		12	54.8 ± 1.0	0.334 ± 0.064	135.9 ± 0.4	148.4 ± 0.4
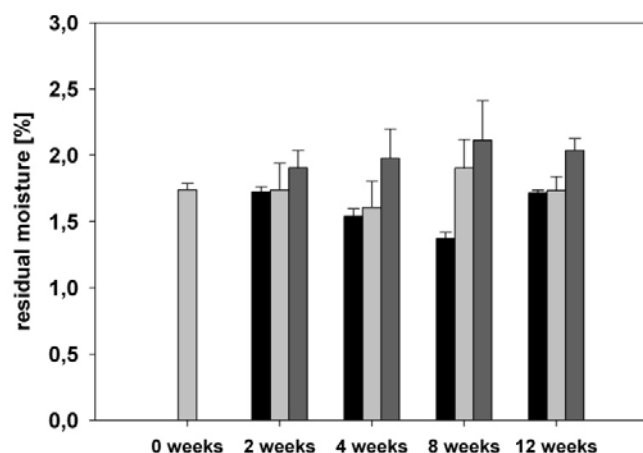
Figure 6.35: Residual moisture levels of trehalose-mannitol samples containing ovalbumin stored at 2-8°C (black bars), 25°C (light grey bars) and 40°C (dark grey bars) for 12 weeks in the presence of Freund's incomplete adjuvant.

Residual moisture levels of the samples incubated with Freund's incomplete adjuvant did just slightly increase after 4 weeks of storage at 40°C (figure 6.35), similarly to the residual moisture levels of samples stored without the presence of any oily substances.

Changes in particle morphology were monitored by differential scanning calorimetry. Glass transition values decreased during storage with increasing temperature (table 6.12), which was in accordance with a slight increase in residual moisture (figure 6.35). The glass transition temperature of lyophilized products can be lowered by 10K for each percent of moisture in the product, as water acts as plasticizer [24].

The two characteristic melting endotherms of mannitol in the range of 133.9 to 137.1 °C and 146.6 to 149.4 °C in the DSC thermograms (table 6.12) for samples stored in the presence of Freund's incomplete adjuvant did not vary in comparison to samples stored without the presence of any oily substance (table 6.4).

3.3.2 STABILITY OF OVALBUMIN IN A TREHALOSE-MANNITOL FORMULATION IN THE PRESENCE OF PARAFFIN OIL

Size exclusion chromatography was performed to investigate the protein stability of trehalose-mannitol samples containing ovalbumin stored in the presence of paraffin oil (figure 6.36). Samples were reprocessed prior to analysis with MTBE as described before. Only a slight decrease in total protein recovery could be observed after 12 weeks of storage at 40°C (figure 6.36 C).
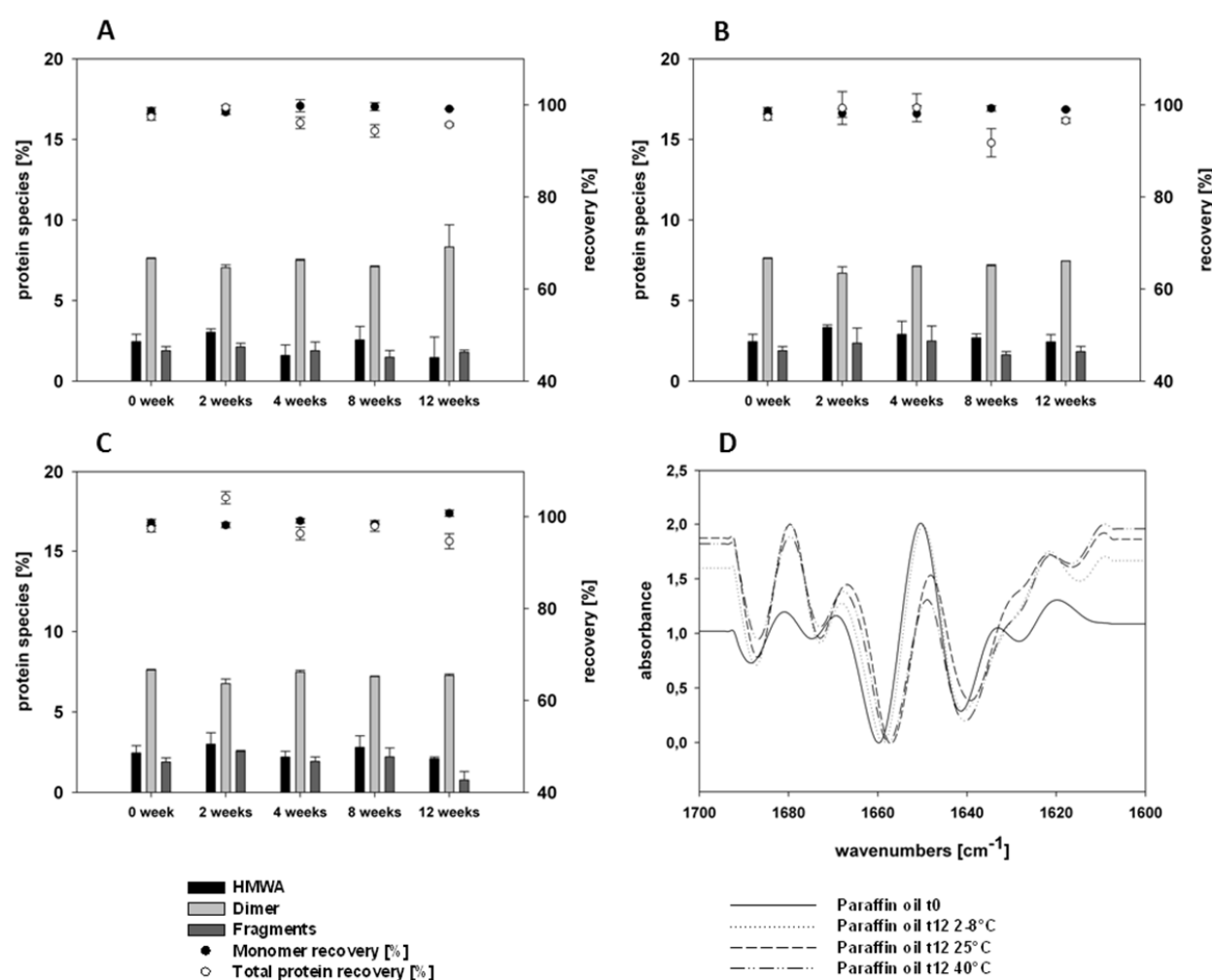
Figure 6.36: Higher molecular weight aggregates (black bars), dimers (light grey bars) and fragment (dark grey bars) protein species [%], total monomer recovery [%] (filled circles) and total protein recovery [%] (open circles) as determined by size exclusion chromatography. Samples were incubated with the oily components of MF59 at 2-8°C (A), 25°C (B) and 40°C (C). Area-normalized 2nd derivative FTIR transmission spectra of samples incubated with paraffin oil (D).

Figure 6.36 D shows the second derivative spectra of ovalbumin after storage in the presence of paraffin oil. Shifts to lower wavenumbers were observed for the bands at 1635/1638 cm^{-1} and 1655/1657 cm^{-1} bands, indicating a decrease in conformational stability of ovalbumin if stored together with paraffin oil.

Figure 6.37 shows the turbidity levels and the formation of particles determined by light obscuration of samples incubated in the presence of paraffin oil. No remarkable changes were observed in the turbidity levels as well as in the cumulative particle counts > 1 µm (figure 6.37) per mL, > 10 µm per mL and > 25 µm per mL (table 6.13) after storage at 2-8°C, 25°C or 40°C for 12 weeks. An increase in turbidity as well as in the cumulative particle counts was observed after 2 weeks of storage at 25°C and 40°C, however, these results could not be confirmed after 4, 8 and 12 weeks of storage.
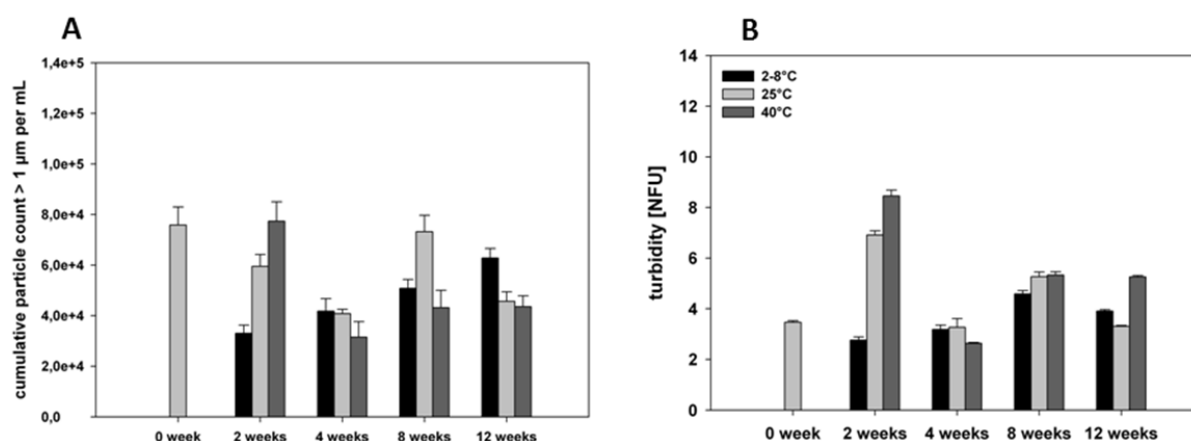
Figure 6.37: Cumulative particle counts > 1µm per mL of samples incubated with paraffin oil (A) and turbidity levels (B) after 12 weeks of storage at 2-8°C (grey bars), 25°C (dark grey bars) and 40°C (black bars). Samples were reprocessed as described in chapter 3.1 in MTBE and were vacuum dried prior to analysis.

A slight increase in the residual moister levels in samples incubated with paraffin oil was observed during storage (figure 6.38), though being consistent with the residual moisture levels of trehalose-mannitol formulations containing ovalbumin, which were stored without the presence of an oily substance in reference (figure 6.17).

187

Table 6.13: Cumulative particle counts > 10 and 25 μm per mL of samples incubated with paraffin oil after 12 weeks of storage at 2-8°C, 25°C and 40°C. Samples were reprocessed as described in chapter 3.1 in MTBE and were vacuum dried prior to analysis.

	after 12 weeks of storage at 2-8°C	after 12 weeks of storage at 25°C	after 12 weeks of storage at 40°C
particles > 10 μm per mL ± SD	2556 ± 274	2119 ± 37	1953 ± 62
particles > 25 μm per mL ± SD	154 ± 21	138 ± 20	124 ± 15
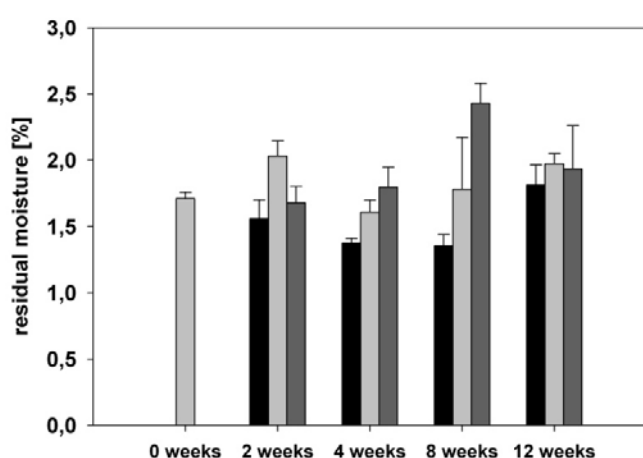
Figure 6.38: Residual moisture levels of trehalose-mannitol samples containing ovalbumin stored at 2-8°C (black bars), 25°C (light grey bars) and 40°C (dark grey bars) for 12 weeks in the presence of paraffin oil.

Table 6.14: Physicochemical properties of trehalose-mannitol samples stored in the presence of paraffin oil as determined by differential scanning calorimetry after storage at 2-8°C, 25°C and 40°C for 12 weeks.

formulation	storage temperature	storage time [weeks]	Tg [°C] ± SD	Δ Cp [J/g*K] ± SD	characteristic melting endotherms [°C] ± SD	
paraffin oil	-	0	63.1 ± 0.8	0.305 ± 0.015	137.0 ± 0.3	149.4 ± 0.2
	2-8°C	8	59.6 ± 6.0	0.237 ± 0.030	137.6 ± 1.0	150.1 ± 1.4
		12	60.6 ± 1.1	0.308 ± 0.016	136.8 ± 0.7	149.2 ± 0.7
	25°C	8	57.5 ± 0.0	0.320 ± 0.002	137.4 ± 1.6	149.9 ± 1.3
		12	61.0 ± 2.5	0.322 ± 0.027	136.4 ± 0.6	147.8 ± 1.7
	40°C	8	55.7 ± 0.6	0.267 ± 0.038	135.3 ± 2.1	147.8 ± 1.7
		12	58.0 ± 2.7	0.301 ± 0.018	135.6 ± 0.5	148.6 ± 0.3

Changes in particle morphology of trehalose-mannitol samples containing ovalbumin incubated together with paraffin oil were also investigated by differential scanning calorimetry. Glass transition values decreased only marginally during storage at 25°C and 40°C after 12 weeks of storage, which is in accordance with a slight increase in residual moisture (table 6.14). However, glass transition temperatures of the samples were still above the highest storage temperature at 40°C, indicating good storage stability of the formulation.

3.4   SUMMARY AND CONCLUSION

The storage stability and possible interaction between oily adjuvants and ovalbumin loaded powder particles was investigated in a short term stability study at elevated temperatures. Prior to analysis a reprocessing step of the samples was necessary. The samples were washed three times with MTBE and the powder pellet was subsequently vacuum dried. This was effective to separate the oily substances from the protein powder and a mandatory step prior to the assessment of protein stability using established analytical methods, as the oily substances did interfere with the analytical methods. Size exclusion chromatography of the reprocessed samples showed, that MTBE did not affect protein integrity. Turbidity measurements and the assessment of the cumulative particle counts of the reprocessed samples revealed, that it was not possible to remove the oily substances quantitatively, however, to an adequate level in order to assess protein stability.

An accelerated stress test, inducing UV-light stress, heat stress and chemical stress showed that the oily components of MF59 and squalene were both highly sensitive to UV-light exposure and heat stress. Squalane was not sensitive to the applied stress conditions, contrary to squalene and MF59, which are both subjected to auto-oxidation [11, 12]. The surfactants polysorbate 80 and Span® 85, which are both ingredients in the mixture of the oily components of MF59, are known to be sensitive to oxidative stress, which is further promoted by heat stress [25, 26]. The recovery of the mixture of the oily components of MF59 decreased dramatically, up to 50%, after incubation with ovalbumin containing trehalose-mannitol particles at 40°C for eight weeks. As only a slight decrease in the recovery of the oily components of MF59 was observed when incubated without the presence of the powder particles, the loss in recovery could be addressed to an interaction between the oily components of MF59 and the powder particles. This was also supported by size exclusion chromatography, FTIR measurements as well as by light obscuration and turbidity measurements of the samples. Only marginal alterations in the recovery of squalene were observed after storage of the samples at 40°C for 12 weeks. However, squalene in combination with ovalbumin containing trehalose-mannitol particles showed a slight decrease in squalene

recovery after four weeks of storage at 40°C. This trend was further reflected by size exclusion chromatography, light obscuration and turbidity measurements. The secondary structure of ovalbumin was not altered when incubated with squalene. Particle morphology regarding residual moisture and physicochemical properties of the powder were comparable to samples stored without the presence of squalene.

Freund's incomplete adjuvant was not sensitive towards chemical stress. However, size exclusion chromatography showed a slight increase in higher molecular weight aggregates after eight weeks of incubation at 40°C. This was also confirmed by FTIR and turbidity measurements, however not by light obscuration measurements. Samples stored in the presence of paraffin oil showed only a slight decrease in total protein recovery after 12 weeks of storage at 40°C. A slight decrease in conformational stability was observed by FTIR measurements after 12 weeks of storage at 40°C, thus confirming the results obtained by size exclusion chromatography. Only marginal changes were found in turbidity levels and cumulative particle counts as well as in particle morphology. As the composition of Freund's incomplete adjuvant is mainly based on paraffin oil, the increase in turbidity and the formation of higher molecular weight aggregates in samples incubated with Freund's incomplete adjuvant could be attributed to its second compound, the surfactant mannide monooleat.

Generally, glass transition values of samples incubated with oily substances were slightly decreased with increasing residual moisture levels, however, to a comparable extent as in ovalbumin containing trehalose-mannitol samples, which were not stored in combination with oily substances.

4   FINAL SUMMARY AND CONCLUSION

Several oily adjuvants were explored as adhesives at the interface between vaccine loaded particles and the surface of a ballistic device for intradermal injection. The oily adjuvants were intended to fulfill several requirements: first, to attach the particles safely during storage and handling onto the device surface and second, to release the particles upon actuation of the device. The oily components of MF59 and Freund's incomplete adjuvant, as well as their components squalene and paraffin oil, respectively, showed good adherence strength when challenged by applying mechanical stress. Different membrane materials were explored for their use to cover the surface of the ballistic device, beneath aluminum showed excellent properties. The adherence strength of the oily components of MF59 and Freund's incomplete adjuvant was also assessed after storage for 12 weeks under different temperature conditions. The mixture of the oily components of MF59 showed good adherence strength, particularly at elevated temperatures. As the particles were enclosed into a thin film of the oily substance, the oily substance was entrained together with the particles upon actuation of the device. Thus, offering the possibility to co-inject the oily substance together with the particles into the skin and herein to exert an adjuvant effect.

O'Hagan *et al.* stated that the mechanism of action of MF59 is based on the cellular recruitment to the injection site, creating hereby a local immunocompetent environment [5, 28]. Calabro *et al.* found out that only the fully formulated MF59 (squalene oil, the surfactants Span® 85 and polysorbate 80 in citrate buffer) were able to induce innate and adaptive immune activation. They came to this conclusion by co-injection an influenza vaccine with MF59 in mice or in combination with one of the individual components. It is still controversy discussed, if the formation of small emulsion droplet is necessary for the adjuvant efficacy [5, 29-31]. The feasibility that vaccine particles, which are covered with oily adjuvants are presented as a microparticulate system in the superficial layers of the skin has to be explored in subsequent animal studies. Also the efficacy of the co-injection of the oily substance as well as its adjuvant effect when applied into the skin has still to be proven.

In addition to the experiments investigating the adherence strength of particles at the interface to the device surface, the storage stability and possible interaction between selected oily substances and ovalbumin loaded powder particles was explored in a short term stability study at elevated temperatures.

In summary, HP-SEC and FTIR-spectroscopy demonstrated that protein integrity was kept during storage at 40°C for 12 weeks if samples were incubated with squalane, squalene, or paraffin oil. Only a slight decrease in protein stability was found for samples incubated with Freund's incomplete adjuvant. In contrast, the occurrence of higher-ordered aggregates and significant perturbations of the secondary protein structure was observed after a minimum incubation time of 8 weeks at 40°C in samples incubated with the oily components of MF59. Therefore, the application of its component squalene should be given preference, when incubated at accelerated temperatures.

5   REFERENCES

[1]   Glenn GM, O'Hagan DT. Adjuvants: progress, regress and pandemic preparedness. Expert Review of Vaccines 2007;6(5):651-2.

[2]   Gupta RK, Siber GR. Adjuvants for human vaccines - current status, problems and future prospects. Vaccine 1995;13(14):1263-76.

[3]   Giudice EL, Campbell JD. Needle-free vaccine delivery. Advanced Drug Delivery Reviews 2006;58(1):68-89.

[4]   Glenn GM, Kenney RT, Ellingsworth LR, Frech SA, Hammond SA, Zoeteweij JP. Transcutaneous immunization and immunostimulant strategies: capitalizing on the immunocompetence of the skin. Expert Review of Vaccines 2003;2(2):253-67.

[5]   O'Hagan DT. MF59 is a safe and potent vaccine adjuvant that enhances protection against influenza virus infection. Expert Review of Vaccines 2007;6(5):699-710.

[6]   Mannino S, Villa M, Apolone G, Weiss NS, Groth N, Aquino I, et al. Effectiveness of adjuvanted influenza vaccination in elderly subjects in northern Italy. American Journal of Epidemiology 2012;176(6):527-33.

[7]   Fox CB. Squalene emulsions for parenteral vaccine and drug delivery. Molecules 2009;14(9):3286-312.

[8]   Allison AC, Byars NE. An adjuvant formulation that selectively elicits the formation of antibodies of protective isotypes and of cell-mediated immunity. Journal of Immunological Methods 1986;95(2):157-68.

[9]   Yang Y-W, Wei A-C, Shen S-S. The immunogenicity-enhancing effect of emulsion vaccine adjuvants is independent of the dispersion type and antigen release rate—a revisit of the role of the hydrophile–lipophile balance (HLB) value. Vaccine 2005;23(20):2665-75.

[10]   Yang Y-W, Shen S-S. Enhanced antigen delivery via cell death induced by the vaccine adjuvants. Vaccine 2007;25(45):7763-72.

[11]   Allison AC. Squalene and squalane emulsions as adjuvants. Methods 1999;19(1):87-93.

[12]   Reddy LH, Couvreur P. Squalene: A natural triterpene for use in disease management and therapy. Advanced Drug Delivery Reviews 2009;61(15):1412-26.

[13]   Stone HD, Xie Z. Efficacy of experimental Newcastle disease water-in-oil oil-emulsion vaccines formulated from squalane and squalene. Avian Diseases 1990:979-83.

[14]   Yang Y-W, Wu C-A, Morrow W. Cell death induced by vaccine adjuvants containing surfactants. Vaccine 2004;22(11):1524-36.

[15]   Carelli C, Audibert F, Chedid L. Persistent enhancement of cell-mediated and antibody immune responses after administration of muramyl dipeptide derivatives with antigen in metabolizable oil. Infection and Immunity 1981;33(1):312-4.

[16]   Edelman R. Vaccine adjuvants. Review of Infectious Diseases 1980;2(3):370-83.

[17]   Gupta RK, Relyveld EH, Lindblad EB, Bizzini B, Ben-Efraim S, Gupta CK. Adjuvants—a balance between toxicity and adjuvanticity. Vaccine 1993;11(3):293-306.

[18]   Salk J, Salk D. Control of influenza and poliomyelitis with killed virus vaccines. Science 1977;195(4281):834-47.

[19]   Ngarize S, Herman H, Adams A, Howell N. Comparison of changes in the secondary structure of unheated, heated, and high-pressure-treated β-lactoglobulin and ovalbumin proteins using Fourier transform Raman spectroscopy and self-deconvolution. Journal of Agricultural and Food Chemistry 2004;52(21):6470-7.

[20]   Byler DM, Susi H. Examination of the secondary structure of proteins by deconvolved FTIR spectra. Biopolymers 1986;25(3):469-87.

[21]   Smith D, Galazka VB, Wellner N, Sumner IG. High pressure unfolding of ovalbumin. International Journal of Food Science & Technology 2000;35(4):361-70.

[22]   Dong A, Meyer JD, Brown JL, Manning MC, Carpenter JF. Comparative fourier transform infrared and circular dichroism spectroscopic analysis of α 1-proteinase inhibitor and ovalbumin in aqueous solution. Archives of Biochemistry and Biophysics 2000;383(1):148-55.

[23]   Hawe A, Frieß W. Physico-chemical lyophilization behavior of mannitol, human serum albumin formulations. European Journal of Pharmaceutical Sciences 2006;28(3):224-32.

[24]   Angell CA. Formation of glasses from liquids and biopolymers. Science 1995;267(5206):1924-35.

[25]   Ha E, Wang W, Wang YJ. Peroxide formation in polysorbate 80 and protein stability. Journal of Pharmaceutical Sciences 2002;91(10):2252-64.

[26]   Wang W, Wang YJ, Wang D. Dual effects of Tween 80 on protein stability. International Journal of Pharmaceutics 2008;347(1):31-8.

[27]   House J, Mariner J. Stabilization of rinderpest vaccine by modification of the lyophilization process. Developments in Biological Standardization 1995;87:235-44.

[28]   O'Hagan DT, Ott GS, De Gregorio E, Seubert A. The mechanism of action of MF59 – An innately attractive adjuvant formulation. Vaccine 2012;30(29):4341-8.

[29]   Calabro S, Tritto E, Pezzotti A, Taccone M, Muzzi A, Bertholet S, et al. The adjuvant effect of MF59 is due to the oil-in-water emulsion formulation, none of the individual components induce a comparable adjuvant effect. Vaccine 2013;31(33):3363-9.

[30]   Brito LA, Malyala P, O'Hagan DT. Vaccine adjuvant formulations: a pharmaceutical perspective. Seminars in Immunology; 2013: Elsevier; 2013. p. 130-45.

[31]   O'Hagan DT, Fox CB. New generation adjuvants–From empiricism to rational design. Vaccine 2015;33:B14-B20.

CHAPTER 7

DEVICE DEVELOPMENT

1   INTRODUCTION

Vaccines are commonly delivered by injection through conventional needles. Whilst this method is widely practised, the use of hypodermic needles holds the risk of transmission of blood borne diseases like HIV and hepatitis by needle-stick injuries or reuse of needles [1]. Therefore, novel needle-free technologies offer a safe and effective method for vaccination.

The skin is an attractive target for vaccine delivery, as the epidermal layer of the skin comprises a dense population of immunocompetent cells, which are able to trigger an appropriate immune reaction [2-4]. The lack of vasculature and the low density of sensory nerve endings in the epidermal layer of the skin provide the opportunity for save and painless vaccine administration [5]. One major challenge for targeting this skin site is its accessibility The low thickness of this tissue layer of about 50–100 µm makes the deposition of an accurate vaccine dose difficult [2]. Ballistic particle injection is a needle-free injection method accelerating dry particles, so that they penetrate the stratum corneum and are deposited in the epidermis or the superficial layers of the dermis [2]. The use of dry vaccine formulation provides enhanced stability and thus avoids the need of a cold chain for drug supply [6-8]. Hence, dry vaccine formulations offer an economic alternative which can cover the supply of a broad population. Delivery of powder particles into superficial skin layers by entrapping the particles into a helium gas flow [9-12] was reported in literature and showed promising results in preclinical and clinical trials [12-15]. Hereby DNA or protein based vaccine antigens were precipitated onto gold particles or formulated with sugar excipients into powder particles and were injected into the skin [5, 12, 16-18]. The use of medical grade helium gas or

gold particles, however, makes the competitiveness of these devices with single use syringes questionable.

The effectiveness of ballistic particle injection depends on different parameters. These include the performance of the delivery device, the device-target interaction and diverse particle parameters, such as the shape of the particles, their density and size, velocity, impact on the skin surface, penetration of the particles as well as their distribution in the epidermal layer of the skin.

In this study a novel principle of particle acceleration to deliver vaccine loaded powder particles by a needle-free approach was investigated. In this approach particles were not entrapped in a gas stream but accelerated by momentum transfer. Therefore a surrogate apparatus, the Lell's Foucault accelerator (LWB), was evaluated in preliminary experiments to determine different parameters mandatory for the development of new devices for epidermal ballistic powder injection. The effective application of a pharmaceutical by ballistic injection requires a thorough understanding of the delivery device, the physical properties of the formulation as well as the functional interaction of both. A method to determine the velocity of particles, the dependency of particle velocity on major particle parameters like size and density as well as a method to load the device with particles were established.

The penetration of particles into model gelatine gels imitating the mechanical properties of skin [19] was explored in order to determine the threshold velocity to breach the outermost layers of the skin. The collected information of the preliminary experiments was transferred on the development of a pyrotechnically driven delivery device. After optimization of the pyrotechnically driven device, proof of concept was showed in *ex-vivo* excised pig skin.

2 EVALUATION OF A SURROGATE APPARATUS FOR THE BALLISTIC ACCELERATION OF PARTICLES

The surrogate apparatus used in the following study, Lell's Foucault accelerator (LWB 3/20 kV, Pyroglobe, Hettenshausen, Germany), was invented and built by Dr. Lell. All experiments were carried out cooperatively with Dr. Lell and his team.

The technical know-how was contributed by Dr. Lell.

2.1 THE FUNCTIONAL PRINCIPLE OF LELL'S FOUCAULT ACCELERATOR

Lell's Foucault accelerator is a custom made apparatus that can be used i.a. for the evaluation of parameters necessary for the development of needle-free ballistic injection devices. A schematic setup of the Lell's Foucault accelerator is depicted in figure 7.1.
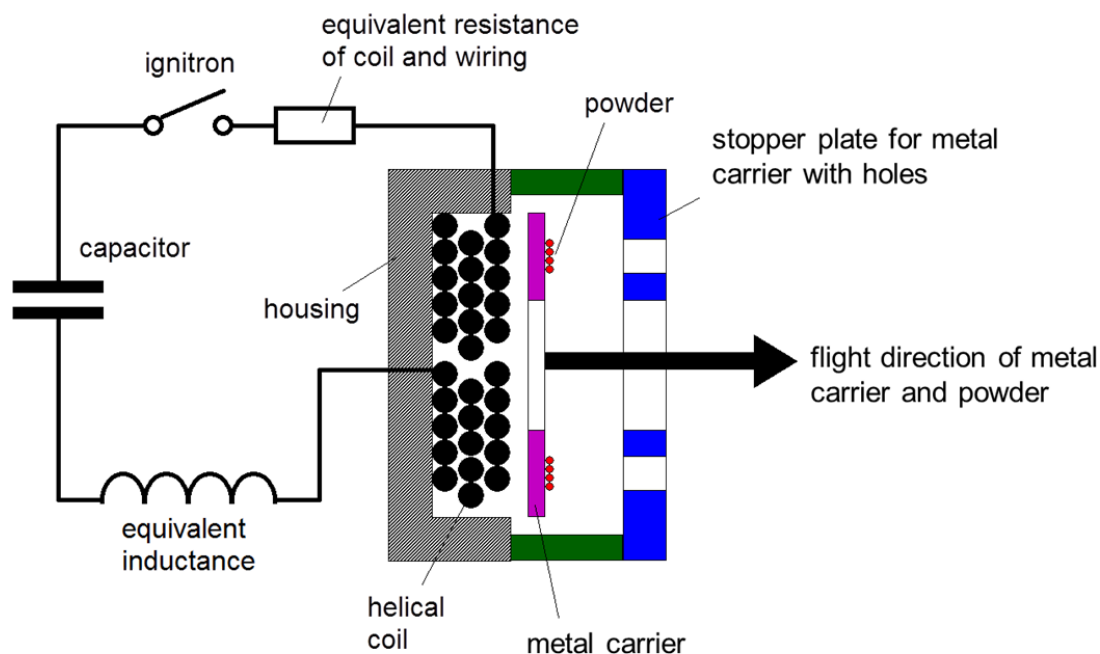
Figure 7.1: Schematic illustration of the experimental set-up of the acceleration of the particles using an electromagnetic coil actuated with Lell's foucault-current accelerator (LWB).

The functional principle of the Lell's Foucault accelerator can be described as follows. A capacitor bank serves as electrical current source for the system. The repulsive force to accelerate particles is generated by a magnetic field in an electromagnetic helical coil, which induces a turbulent electrical current in a metal carrier. Aluminum disks (Al-disk) with a diameter of 30 mm, a punched hole in the middle of the disk with 10 mm diameter and disk thickness of 0.5 mm or 1.0 mm are used as metal carriers. The surface of the metal carriers was loaded with particles. Upon acceleration, the aluminum disk was abruptly stopped by a stopper plate, while the particles on the disk surface continued their flight course through holes in the stopper plate and flew towards a target (figure 7.1 and 7.2).

A

B

10 mm

30 mm

25 mm
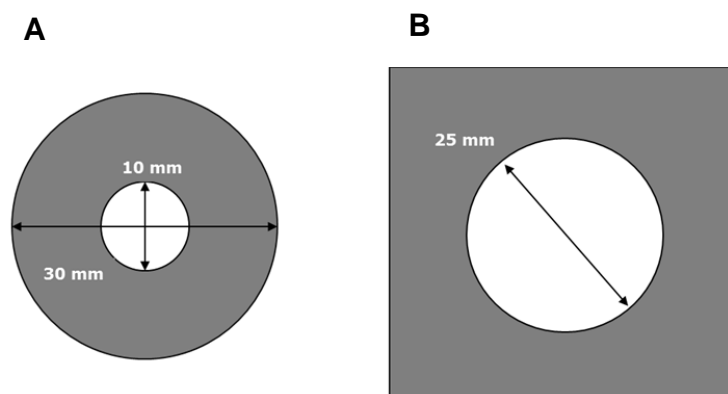
Figure 7.2: Schematic illustration of an Al-disk (A) and (B) of a stopper plate.

2.2 VELOCITY MEASUREMENT OF AL-DISKS

In order to determine the velocity of the carrier plates/Al-disks a Flash Cam PCO high speed camera was attached to the LWB. The triggering points of the LWB and the high speed cameras were controlled by a programmable 20 MHz function generator and initiated by a photo flash (Metz, Zirndorf, Germany). After receiving the trigger signal of the LWB upon actuation, the camera took several pictures in series in a certain timeframe. The timeframe was given by the interval of shots (in μs) of the high speed camera. The velocity of the Al-disks was calculated from the distance between two disks in the serial pictures divided by the timeframe between these two pictures. The distance between the disks was calibrated using a scale (figure 7.3).
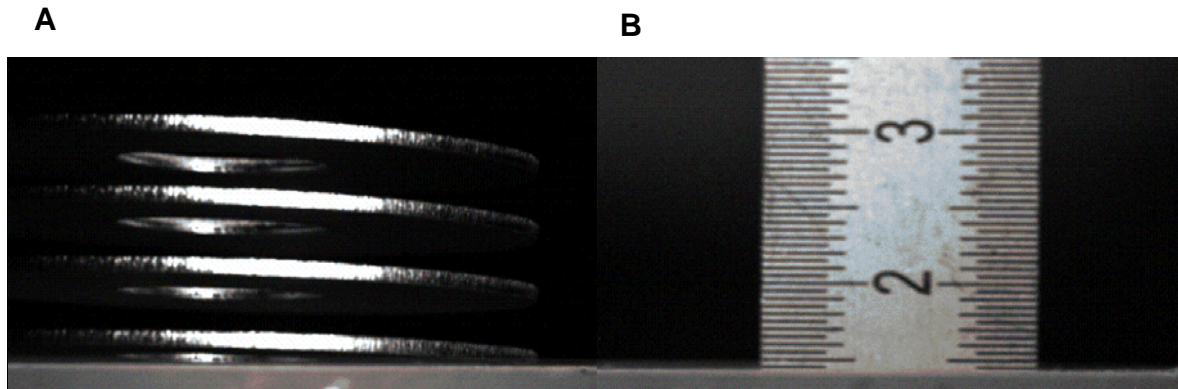
Figure 7.3: Determination of the velocity of Al–disks using a Flash Cam PCO high speed camera. The distance between the disks was measured by aligning the distance to a scale. A serial picture of an Al-disk during flight is depicted in (A). The scale for the calibration of the distance is depicted in (B).
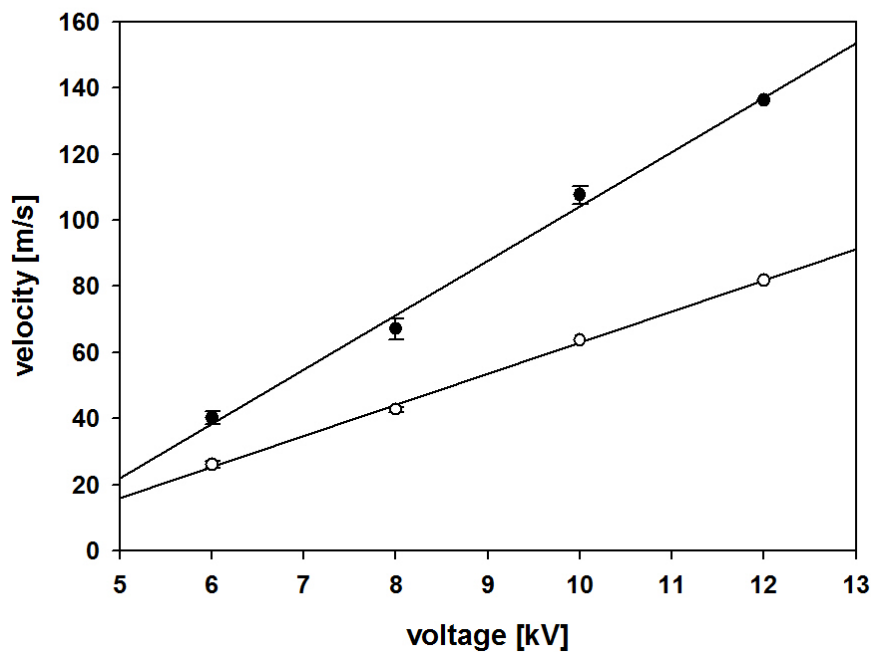
Figure 7.4: Velocity measurement of 0.5 mm (black dots) and 1.0 mm (white dots) Al-disks as a function of the voltage of the capacitor bank determined using a Flash Cam PCO high speed camera (average +/- SD, n=3).

The velocity of aluminum disks, accelerated at a pre-selected voltage of 6 kV up to 12 kV on the LWB, was determined (figure 7.4). Aluminum disks with 0.5 mm and 1.0 mm thickness were used.

It was observed that the velocity of the Al-disk was dependent on the mass of the disk. Al-disks with a thickness of 1.0 mm had a higher mass and hence, a different velocity profile than Al-disk with a thickness of 0.5 mm. Aluminum disks with 0.5 mm were accelerated up to 136 m/s at 12 kV. Aluminum disks with 1.0 mm were accelerated up to 82 m/s at 12 kV. A linear regression was observed between the velocity of the AL-disks and the voltage of the capacitor bank.

The method to determine of the disk velocity using the high speed camera was appropriate, as the standard deviations of the triplicate measurement varied between 0 and 3 m/s.

2.3   FIXATION OF PARTICLES ON AL-DISKS PRIOR TO ACCELERATION

Particles were fixed on Al-disks by covering the disks with a thin layer of adhesive as outlined in chapter 6. The amount of adhesive as well as the weight of the particles was determined gravimetrically. Figure 7.5 depicts exemplarily glass particles of 40 – 63 μm size on an Al-disk adhered with a thin layer of paraffin. In the following velocity measurements of particles were carried out using paraffin as type of adhesive if not stated otherwise.

A   **B**
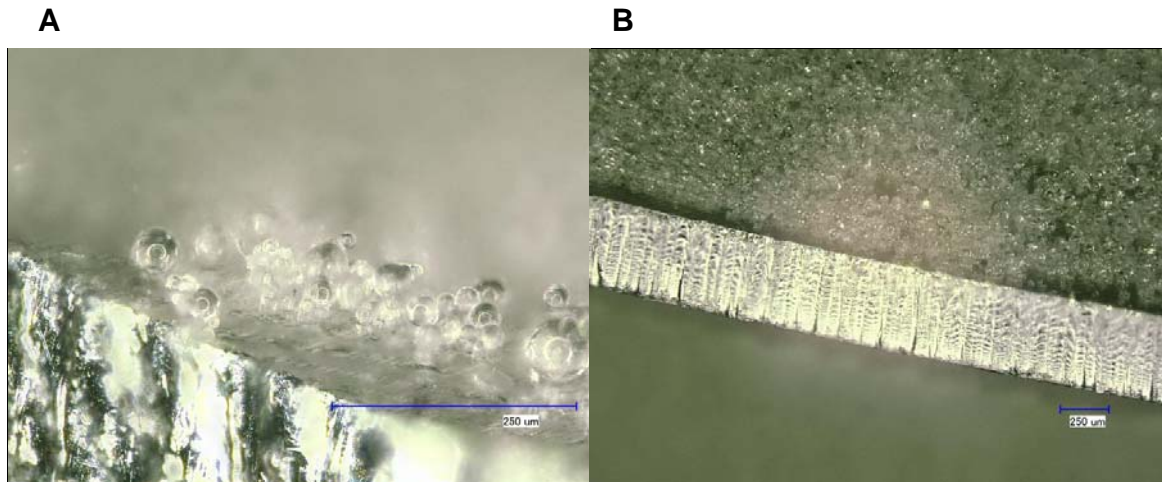
Figure 7.5: Microscopic photograph of glass particles (fraction 40 - 63 µm) on an Al-disk (d = 0.5 mm) using a Keyence VHX-500 F microscope. A: Magnification 100 x 50. B: Magnification 100 x 500.

2.4   VELOCITY MEASUREMENT OF PARTICLES

The velocity of particles and powders in the µm-range respectively, was measured using a set of two synchronised Flash Cam PCO high speed cameras (PCO, Kehlheim am Ufer, Germany). As powders in the µm-range cannot be singularized in individual particles macroscopically, the powder cloud was examined. The cameras were positioned in a 90° angel to each other. The setup of the LWB and the high speed cameras was actuated with a photo flash (Metz, Zirndorf, Germany). The distance of the particle cloud starting from the electromagnetic coil to the front line of the powder cloud, was calibrated using a scale, analogue to the velocity measurement of the Al-disks. The velocity of the powder cloud was calculated by the distance travelled of the powder cloud (determined from two pictures taken by the synchronised high speed cameras and aligned with the scale) divided by the timeframe between the first and the second camera (figure 7.6).

The velocity of the particle cloud was calculated according to equation (7.1):

$$\text{velocity [m/s]} = \frac{\text{flight distance particle cloud \#1 [m] - flight distance particle cloud \#2 [m]}}{\text{time of actuation camera \#1 [s] - time of actuation camera \#2 [s]}} \qquad (7.1)$$
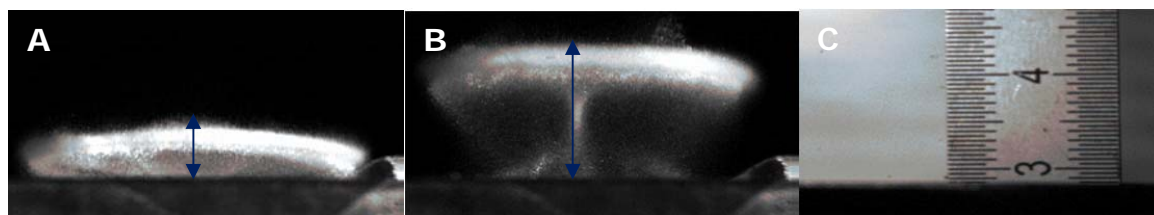
Figure 7.6: Determination of the velocity of particles using two synchronised Flash Cam PCO high speed cameras. (A) and (B) depict two pictures of a particle cloud taken by camera #1 (A) 25 µs and camera #2 (B) 100 µs after actuation of the LWB. The distance from the stopper plate to the particle cloud (indicated by the arrows) was measured for each picture using a calibrated scale (C). The flight distance of the particle cloud was calculated as the deviation of both. Velocity of the particle cloud was calculated by the quotient of the flight distance and the therefore required time.

2.5 PRELIMINARY EXPERIMENTS: DEPENDENCY OF PARTICLE VELOCITY ON PARTICLE PARAMETERS

One major aim of the study using the LWB was to experimentally evaluate the dependency of particle velocity on major particle parameters like size and density.

Firstly, regularly shaped round polystyrene and glass particles were used as model particles to investigate the influence of particle size and density on particle velocity as they are known for their well- characterized and reproducible physical properties (figure 7.7). Secondly, the behaviour of irregularly shaped sugar particles upon acceleration was investigated. Table 7.1 summarize the different particle parameters.
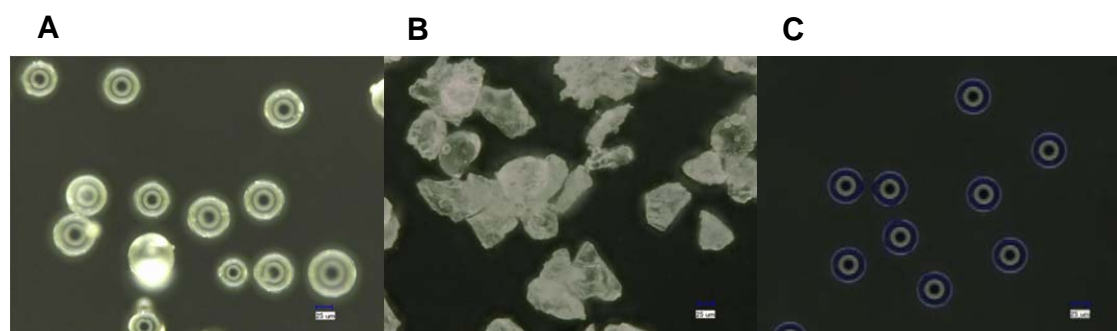
Figure 7.7: Digital micrographs of glass particles (density 2.5 g/cm³, 20-40 µm) (A), freeze-dried and subsequently cryo-milled sugar particles (density 1.45 g/cm³, 20-40 µm)(B) and (C) blue polystyrene particles (density 1.1 g/cm³, 40 µm. Scale bar 25 µm.

Table 7.1: Size and density of different types of particles

Particles	size [µm]	density [g/cm³]
glass	20-40	2.5
glass	40-63	2.5
glass	63-70	2.5
hollow glass	11	1.1
hollow glass	18	0.6
sugar	20-40	1.45
sugar	40-63	1.45
polystyrene	20	1.1
polystyrene	40	1.1
polystyrene	60	1.1

Figure 7.8 depicts the velocity of polystyrene particles upon acceleration at 12 kV using the LWB equipped with an electromagnetic coil made of a 1.12 mm copper wire and 6*11 windings. Particle velocity was measured using a set of two synchronised Flash Cam PCO high speed cameras as described before. Clearly, the velocity of polystyrene particles increased with increasing size of the particles. Contrary to our findings Kendall *et al*. observed that smaller particles were accelerated to higher velocity using a needle-free device where particles were entrained in a high-speed gas flow [3]. As expected, particle kinetics is subjected to the kind of acceleration and hence differs basically from delivery device to delivery device.
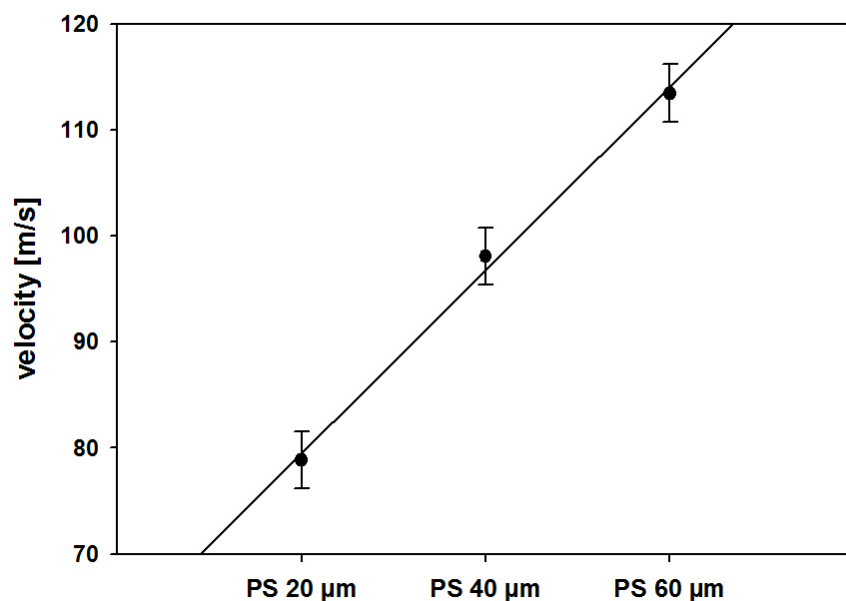
Figure 7.8: Velocity measurements of polystyrene particles (density 1.1 g/cm³). Particles were accelerated at 12 kV using the LWB and an electromagnetic coil made of a 1.12 mm copper wire and 6*11 windings (average +/- SD, n=2).

Hollow glass particles with different density and size were used to evaluate their influence on particle velocity. A pre-selected voltage of 12 kV was adjusted at the LWB. The velocity of glass particles depends on both, size and density of the particles (figure 7.9). An increase of particle velocity was observed with increasing density and size of the particles. However, overlapping effects of size and density have to be taken into consideration. Glass particles of 18 µm diameter sizes had a density of 0.6 g/cm³ and were therefore accelerated to lower velocity than particles of 11 µm diameter size and 1.1 g/cm³ density. No linear correlation was found between density of the particles and particle velocity.
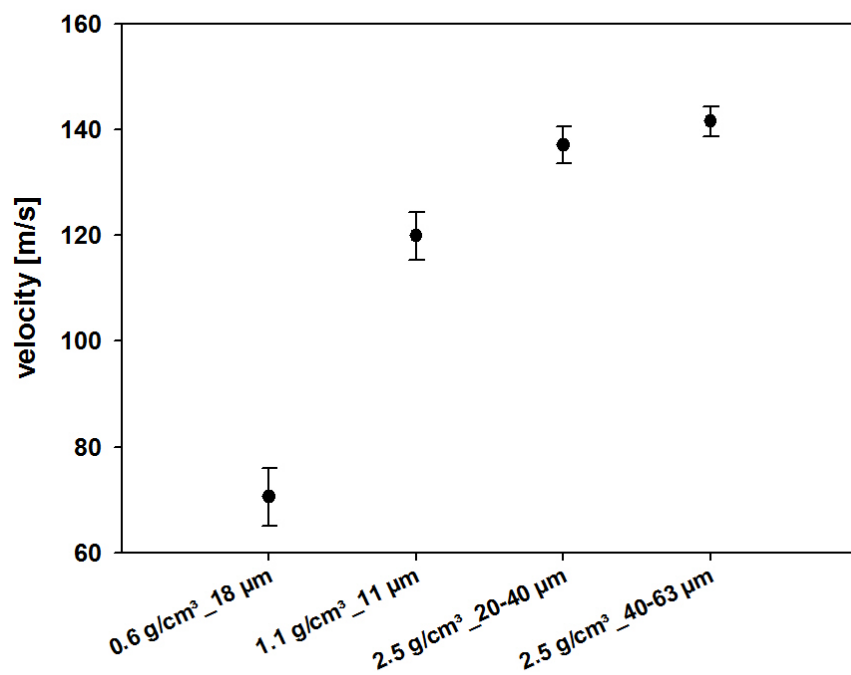
Figure 7.9: Influence of particle size and density on the velocity of glass particles. Particles were accelerated at 12 kV using the LWB and an electromagnetic coil made of a 1.12 mm copper wire and 6*12 windings (average +/- SD, n=3).

The kinetics of irregularly shaped sugar particles upon acceleration was compared to spherical glass particles. Sugar particles were obtained by collapse-freeze drying and subsequent cryo-milling of trehalose-mannitol lyophilizates as described in chapter 4. Due to kind of the manufacturing process of the sugar particles, it was not possible to separate single particles of defined size for the experiments. Therefore, defined particle fractions of the sugar particles in the range of 20-40 µm and 40-63 µm were generated by sieving of the cryo-milled particles using custom made stainless steel sieves. Likewise, comparable size fractions of spherical glass spheres were generated. Figure 7.10 depicts the velocity of non-spherical sugar particles next to spherical glass particles after acceleration of the particles at 12 kV using the LWB.
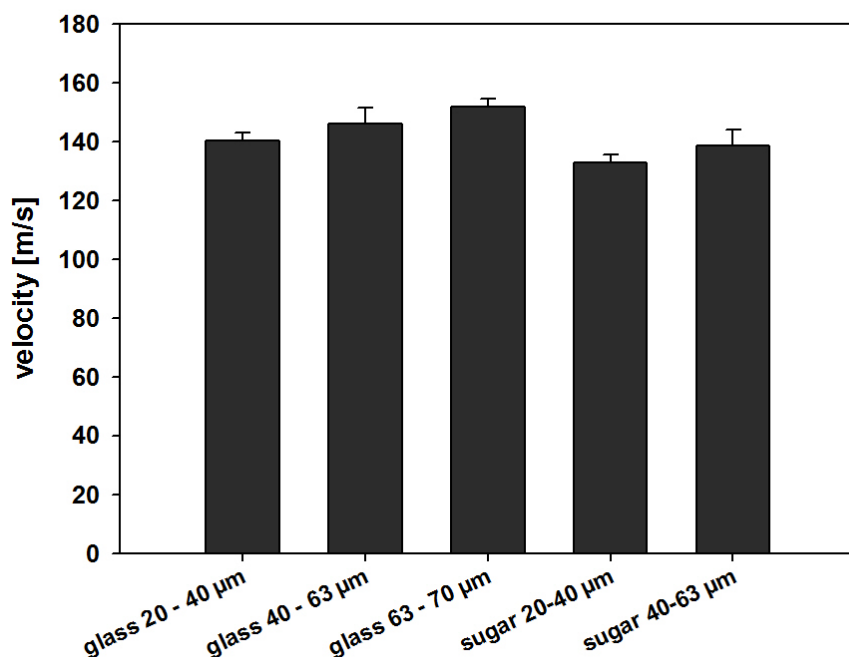
Figure 7.10: Velocity measurements of glass and sugar particles, accelerated at 12 kV using the LWB and an electromagnetic coil made of a 1.12 mm copper wire and 6*12 windings (average +/- SD, n=3).

Velocity of both particle populations showed an increase with increasing size of the particles. Glass particles could be accelerated to slightly higher velocity due to their higher density with 2.50 g/cm³ in comparison to 1.45 g/cm³ of the sugar particles. The difference in the velocity of regularly round shaped glass particles and angular shaped sugar particles was too small to draw conclusion regarding the influence of the shape of particles on particle velocity.

Generally, at least two forces act on the particle during acceleration. The kinetic energy which drives the particle towards the target and the ambient resistance force acting against it. The kinetic energy of the particle is proportional to the volume of the particle (equation 7.2) whereas resistance force of the particle is proportional to the cross-sectional area of the particle (equation 7.3).

Hence, larger particles of a population with equal density can store more kinetic energy and fly faster.

$$E_{kinetic} \sim V_{sphere} \sim r^3 \qquad\qquad (7.2)$$

$$F_{resistance} \sim A_{sphere} \sim r^2 \qquad\qquad (7.3)$$

Figure 7.11 shows the velocity profiles of glass and sugar particles accelerated at pre-selected voltages of 6 to 12 kV. Sugar particles show similar velocity profiles to glass particles ranging from 42.5 to 123.0 m/s and 51.5 to 147.4 m/s, respectively, depending on the pre-selected voltage of the capacitor bank. Sugar particles reach in general lower absolute velocities due to their lower density. Interestingly, the difference in the absolute velocity between glass and sugar particles was higher the higher the pre-selected voltage of the capacitor bank was. Though a linear correlation can be drawn between the velocity of particles and the pre-selected voltage of the LWB, comparison of the velocity of different particles can only be made at pre-defined acceleration conditions.
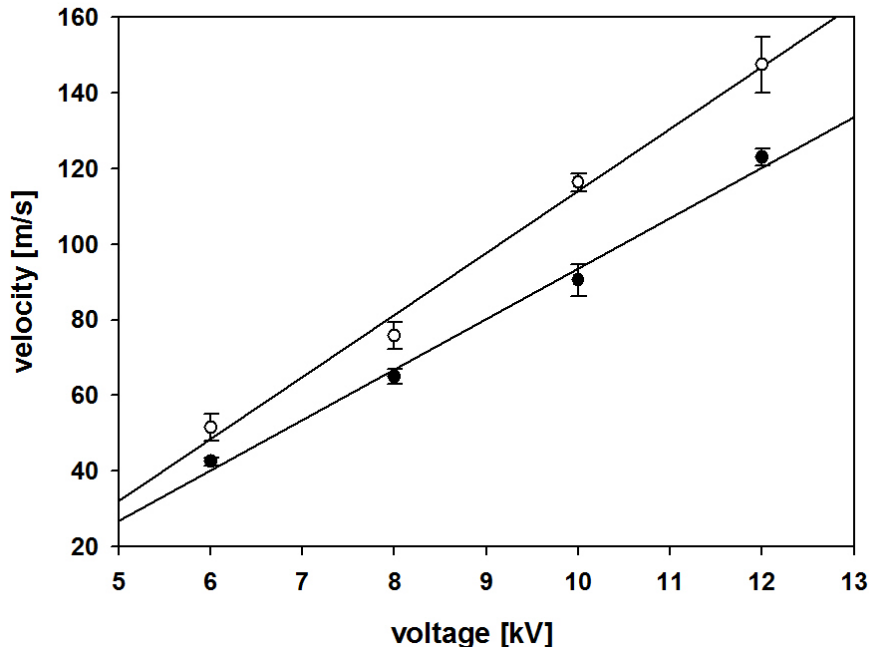
Figure 7.11: Velocity measurement of sugar particles (black dots) and glass particles (white dots) as a function of the voltage of the capacitor bank of the LWB determined using a Flash Cam PCO high speed camera (average +/- SD, n=3).

209

The influence of the type of adhesive on the velocity of glass particles was determined in the same manner. Approximately 5 µl of the oily components of MF59, silicon oil or paraffin oil were used to cover the Al-disks. Glass particles with a diameter range of 20 to 40 µm and 2.5 g/cm³ density were fixed with the different adhesives onto 0.5 mm thick aluminum disks and accelerated using the LWB at pre-selected voltages of 6 to 12 kV.
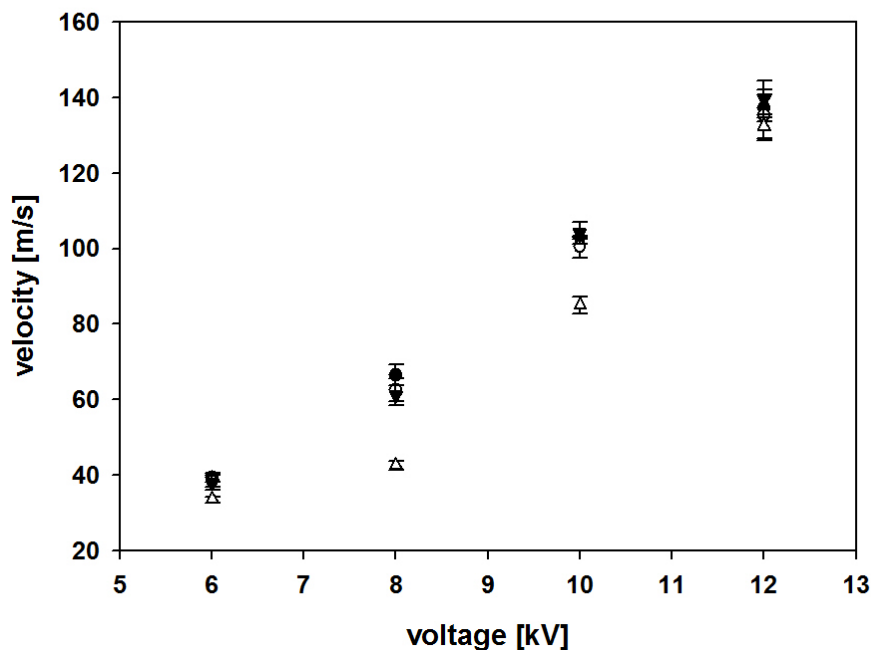
Figure 7.12: Velocity of glass beads (fraction 20-40 µm) fixed with different adhesives onto 0.5 mm thick aluminum disks. Filled circles represent samples fixed with the oily components of MF59. Open circles represent samples fixed with paraffin oil. Filled triangles represent samples fixed with silicon oil. Open triangles represent samples fixed without the use of an adhesive. Particles were accelerated at 12 kV using the LWB and an electromagnetic coil made of a 1.12 mm copper wire and 6*12 windings (average +/- SD, n=3).

No differences in the velocity of glass particles were observed using either the oily components of MF59, paraffin oil or silicon oil as adhesive (figure 7.12). Deviations in the velocity of samples attached on Al-disks without the use of an adhesive were observed at 8 and 10 kV. These differences are most probably attributed to uneven distribution of the glass particles on the Al-disks.

2.6 FURTHER OPTIMIZATION STEPS OF THE SET-UP OF THE LWB

Several development steps were made on the geometry of the electromagnetic coils connected with the LWB as described in section 2.3 in order to increase the velocity of particles. Hereby, particle velocity could be increased to a maximum of 275 to 300 m/s at 18 kV.

Due to the escalation of particle and Al-disk velocity and Al-disks were pushed through the holes of the stopper plate at 300 m/s. Therefore the geometry of the stopper plate had to be adjusted once more. The new geometry of the stopper plate featured three holes of each 3 mm diameter, thus providing a larger contact face for the Al-disks but at the same time offering equal loading area for the particles.

Dependent on the shape of the stopper plate the resolution of the particle clouds varied. Using the stopper plate with two rectangular holes, two separate particle clouds appeared on the images of the high speed cameras (figure 7.13 A). If the velocity of the particles exceeded 250 m/s, velocity calculation was performed using a single 600 µm glass sphere in favour of a better resolution of the high speed camera images. Particle velocity > 250 m/s was determined analogue to the velocity measurement of the Al-disks as described before. Hence, high speed camera shots of velocity measurements using a stopper plate with 3 holes display an overlapped serial picture of a single glass sphere as depicted in figure 7.13 B.

A   **B**
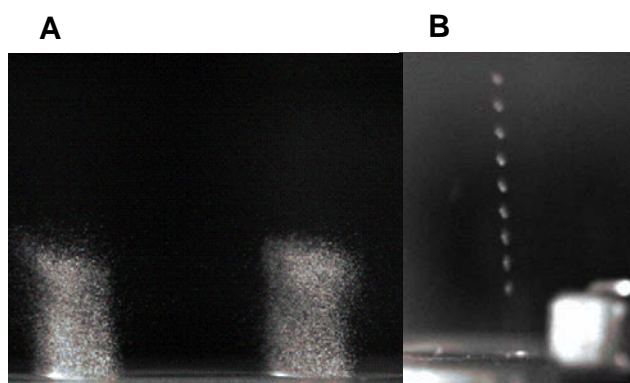
Figure 7.13: Determination of the velocity of glass particles using a Flash Cam PCO high speed camera. (A) depicts two clouds of glass beads corresponding to the geometry of the stopper plate. (B) depicts a serial picture of a 800 µm glass sphere during flight.

A further attempt to increase the performance of the LWB was the reduction of the mass of the Al-disks by broadening the inner diameter of the Al-disk, as the magnetic repulsive force generated act mainly on the outer border of the Al-disk. An increase in particle velocity to 400 m/s was achieved, however also the Al-disk was destroyed and felt apart into pieces. Hence, the use of Al-disks with reduced inner diameter was not feasible.

In summary the experimental setup of the LWB provided a reliable method to evaluate the relationship between the velocity of particles and different particle parameters. Hence, it is a unique tool for the evaluation of new delivery devices as well as for the evaluation of the physical properties of new vaccine formulations intended for ballistic powder injection However, the LWB was limited to a maximal achievable particle velocity of 300 m/s.

3   IN-VITRO PENETRATION OF PARTICLES INTO GEL MODELS AND PIG SKIN AFTER BALLISTIC ACCELERATION USING THE LWB

For a thorough understanding of device and target interaction penetration depth of particles accelerated by the LWB towards different model gelatine gels was scrutinized. A series of gelatine gels with different mechanical properties were used in order to investigate the dependency of particle velocity on their penetration depth. The gels were developed and validated by a member of our group, Dr. Deng, in order to simulate the mechanical properties of the skin [19, 20].

3.1   PRELIMINARY EXPERIMENTS

Glass particles of 20-40 µm size and a density of 2.5 g/cm³ were accelerated to 137 m/s with the LWB as described before. Gelatine gels were placed into 1 cm distance from the stopper plate. Penetration depth into different types of gelatine gels (marked as gel A-D) with varying mechanical rigidity was measured by light microscopy. Cross sections of the gels after particle bombardment are depicted in Figure 7.14.

Prior to cross-sectioning the surface of the gels were wiped in order to remove particles at the surface of the gels which failed to penetrate into the gels upon impact. Approximately 1/3 of the particles remained on the gel surface. As expected, deepest penetration of glass particles, with a mean penetration depth of 290 µm, was found in gelatine gels composed of a gelatine/glycerol mix (w/w) ratio of (3.5/6.5) with lowest mechanical rigidity (gel A) (figure 7.15). A mean penetration depth of 112 µm was found in gels composed of a gelatine/glycerol mix (w/w) ratio of (5/5). The higher the mechanical rigidity of the gels, the lower was the penetration depth and number of glass particles found in the gels.
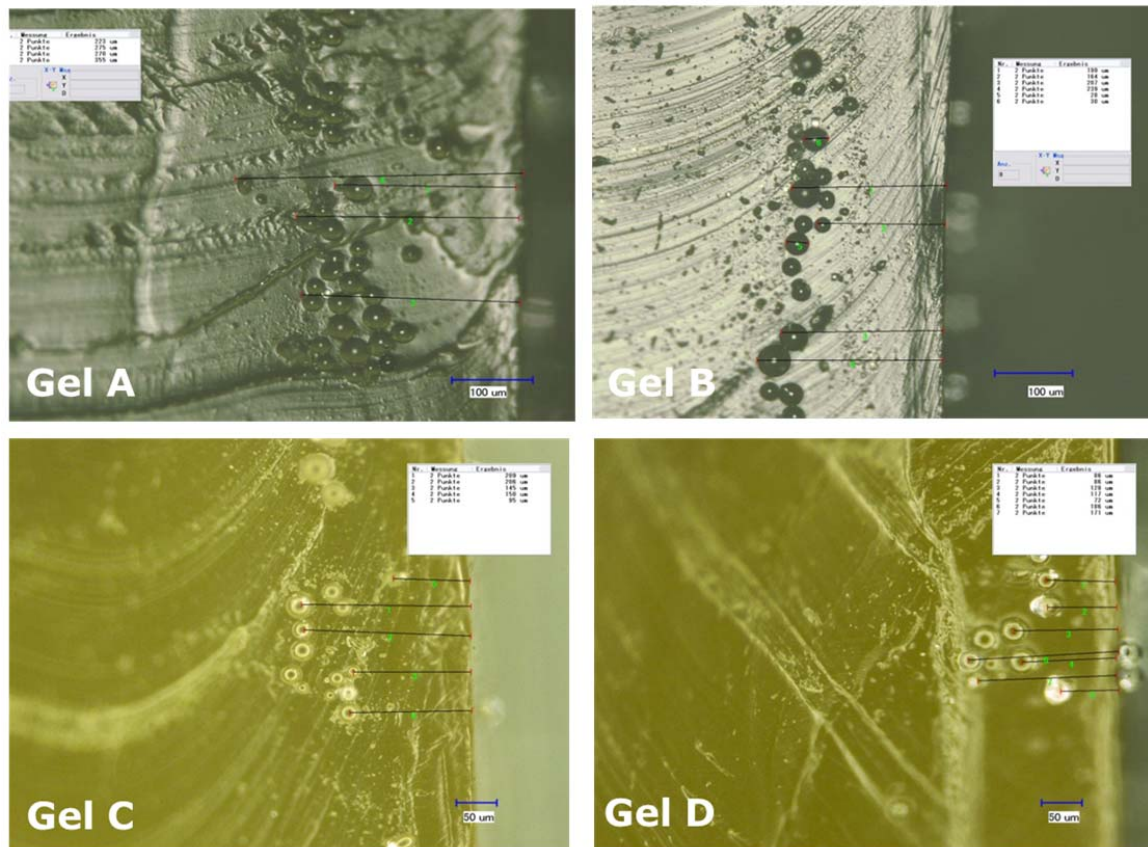
Figure 7.14: Gelatine gels composed of different mix-ratios of gelatine and glycerol, with different mechanical rigidity rising from A to D: Gel A: gelatine/glycerol (w/w) ratio (3.5/6.5), Gel B: gelatine/glycerol (w/w) ratio (4/6), Gel C: gelatine/glycerol (w/w) ratio (4.5/5.5), Gel D: gelatine/glycerol (w/w) ratio (5/5). The light micrographs show cross sections of the gelatine gels A-D after glass particle bombardment (20-40 µm) with a mean velocity of 137 m/s. Penetrations depth of model particles in gel models was determined by digital light microscopy. Scale bars Gel A and Gel B 100 µm. Scale bars Gel C and Gel D 50 µm.

The impact momentum of the particles necessary to penetrate into the gels depends, next to the size and density of the particles, on particle velocity [3]. Polystyrene particles, reaching 80-100 m/s, with 40 µm diameter and 1.1 g/cm³ density failed to penetrate into gelatine gels. Hence, the threshold of the impact monument was not reaches for these particles.
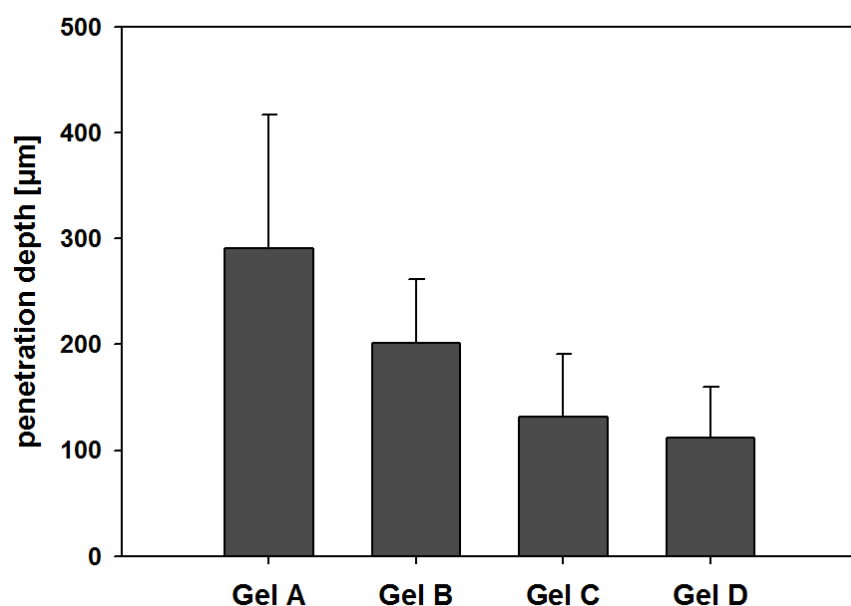
Figure 7.15: Mean penetration depth of glass particles (20-40 µm) with a mean velocity of 137 m/s in different gelatine gels. Gelatine gels were composed of different mix-ratios of gelatine and glycerol, with rising mechanical rigidity from A to D: Gel A: gelatine/glycerol (w/w) ratio (3.5/6.5), Gel B: gelatine/glycerol (w/w) ratio (4/6), Gel C: gelatine/glycerol (w/w) ratio (4.5/5.5), Gel D: gelatine/glycerol (w/w) ratio (5/5).

3.2 PENETRATION STUDIES IN GELATINE GELS USING THE OPTIMIZED SET-UP OF THE LWB

Penetration studies of glass particles into gelatine gels were accomplished using the optimized set-up of the LWB, reaching a maximum particle velocity of 254 m/s. Gelatine gels were placed into 1 cm distance from the stopper plate. The penetration of 20-40 µm glass particles into the gels was analyzed by histological sectioning and light microscopy. Glass particles remaining on the gel surface were removed prior to sectioning. Again, approximately 1/3 of the particles remained on the gel surface. Despite the higher particle velocity using the optimized set-up of the LWB, glass particles did not penetrate deeper into more rigid gels (Gel C and Gel D). Only in gels with a mix ratio of gelatine/glycerol (w/w) (3.5/6.5), Gel A, an enhancement of the mean penetration depth was visible from 291 µm to 378 µm (figure 7.16).
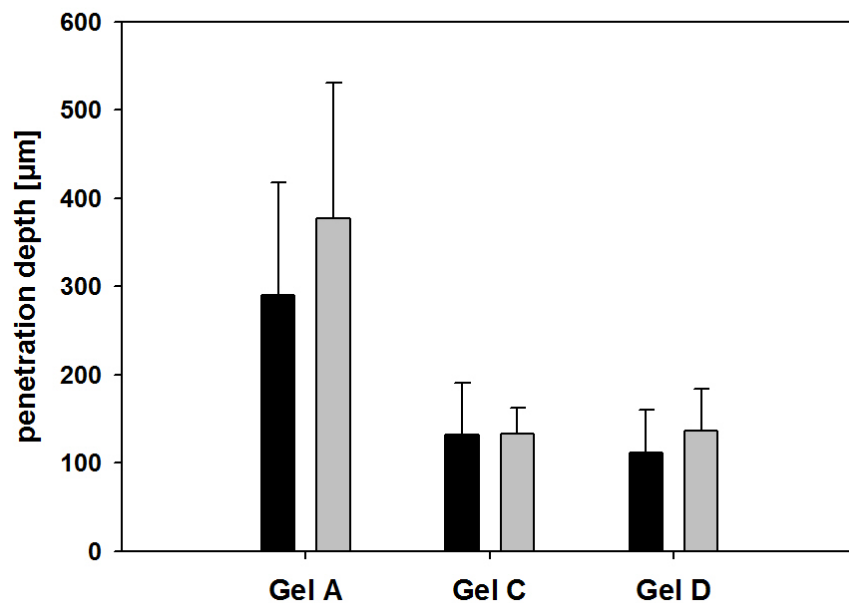
Figure 7.16: Mean penetration depth of 20-40 µm glass particles into gelatine gels, with a mean velocity of 137 m/s (black bars) and 254 m/s (grey bars) in gelatine gels A, C and D. Gelatine gels were composed of different mix-ratios of gelatine and glycerol, with rising mechanical rigidity from A to D: Gel A: gelatine/glycerol (w/w) ratio (3.5/6.5), Gel C: gelatine/glycerol (w/w) ratio (4.5/5.5), Gel D: gelatine/glycerol (w/w) ratio (5/5).

Again, polystyrene particles (40 µm) failed to penetrate into the gels.

The results obtained from the penetration studies in gelatine gels show that there are at least three processes regarding particle injection to be considered. First, the acceleration of the particles, second the impact of the particles at the gel surface and their momentum needed to breach the gel surface and third, the kinetics of the deceleration of the particles in the gel matrix, thus determining the penetration depth of the particles as a function of gel rigidity. This theory is also supported by the bilayer approximation of the epidermis posed by Kendall *et al.*in a theoretical penetration model [21].

3.3 **PROOF OF CONCEPT: PENETRATION STUDIES INTO EXCISED PIG SKIN**

Polystyrene particles (40 µm, ≤ 275 m/s) failed to penetrate into the gel models, mimicking the mechanical properties of the skin. This indicates that the impact momentum of the particles was not sufficient to breach the gel surface. Proof of concept was performed in excised pig skin. Pig skin was chosen for the penetration studies as it is known from literature that abdominal and ear pig skin respectively, have similar mechanical properties to human skin [19].

FITC-labeled polystyrene particles were chosen as model particles for the penetration studies in excised pig skin as they were firstly, easily detectable by confocal laser microscopy, a non-invasive detection method, and secondly, they had similar particle density as sugar particles. 40 µm FITC-labeled polystyrene particles were accelerated using the improved set-up of the LWB at 18 KV and shot into excised pig skin. The excised pig skin was placed into 1 cm distance from the stopper plate. Particle velocity of approximately 275-300 m/s was measured using a 600 µm glass sphere (density 2.5 g/cm³). Hence, polystyrene particles may exhibited lower velocity than 275 m/s, as particle velocity decreases with decreased particle density and size.

The penetration depth of the particles into excised pig skin was analyzed by confocal laser scanning microscopy (LSM 510 META, Carl ZEISS, Germany). The method to determine the depth of particles in a skin sample using CLSM analysis was validated and performed by Dr. Deng [20]. CLSM offers the chance to visualize thin optical sections through the skin without the need for physical sectioning.

Prior to analysis, the skin was rinsed with water and wiped with paper tissue in order to remove not penetrated particles from the skin surface. CLSM micrographs of FITC-labeled polystyrene particles in excised pig skin are depicted in figure 7.17.

The majority of the particles remained on the outermost barrier of the skin, the stratum corneum, and failed to penetrate in the epidermal and dermal layers of the skin. This is line with the results obtained from the penetration studies into gelatin gels.
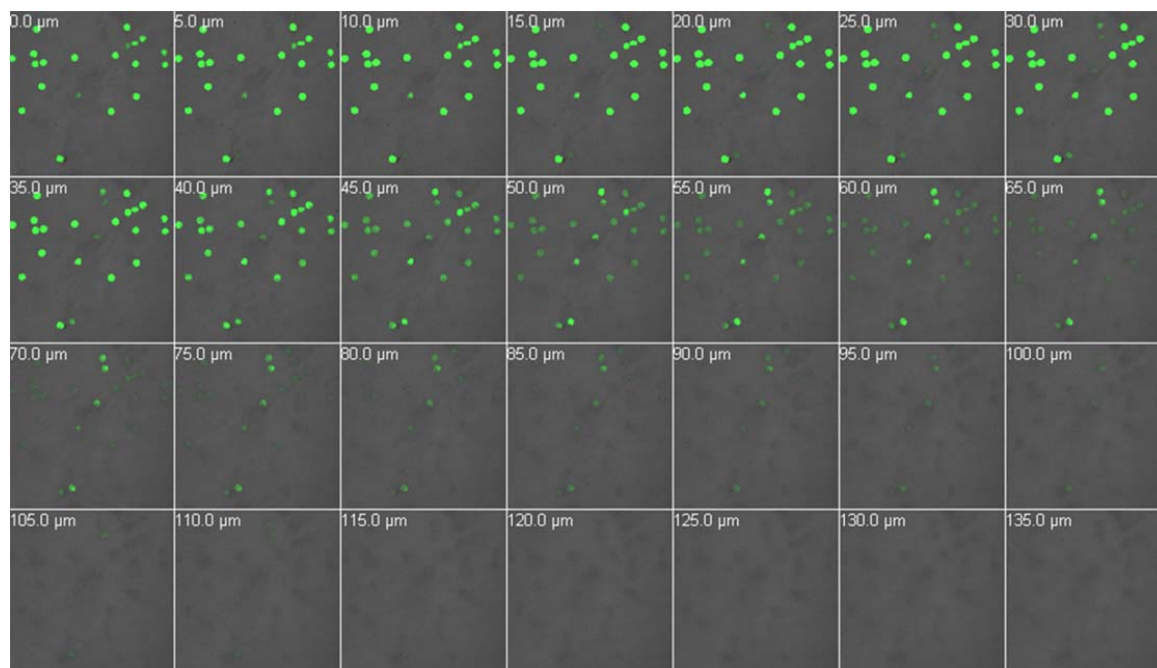
Figure 7.17: CLSM images of FITC-labeled polystyrene particles in pig skin. Visualization of multiple depths in 5.0 µm-steps per recording. Particles penetrated in average 20-30 µm deep into excised pig skin. Deeper slices show a decrease in fluorescence intensity.
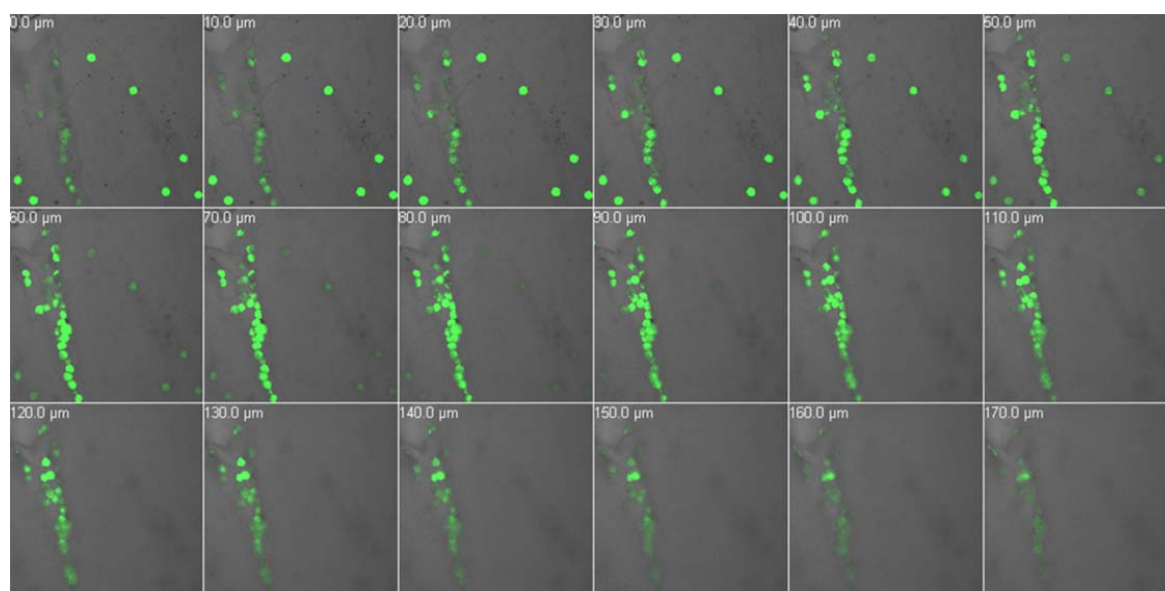
Figure 7.18: CLSM images of FITC-labeled polystyrene particles in pig skin. Visualization of multiple depths in 5.0 µm-steps per recording. FITC-polystyrene particles are located string in line in an average penetration depth of 50 to 70 µm.

Figure 7.18 shows polystyrene particles string in line in an average penetration depth of 50 to 70 μm. Due to the special formation of the particles this observation can be attributed to abnormalities in the skin tissue, wrinkles in the skin or due to specific characteristics resulting of the acceleration of the particles. Hence, a penetration of the particles was precluded.

In conclusion, polystyrene particles with 40 μm size and < 254 m/s were not able to penetrate into gelatin gels or breach the stratum corneum of excised pig skin.

Kendall *et al.* postulated that the penetration depth of particles into skin is a function of density (tap density), velocity and radius of particles [3]. They recommended a threshold value of 7 kg m^{-1} s^{-1} to ascertain the penetration of particles into the skin. According to this recommendation the threshold was undercut by the polystyrene particles with a value (calculated with the true density of the particles) of 5.6 kg m^{-1} s^{-1}. However, the above mentioned theory was build up on experimental data using a needle-free injection device, which accelerated particles by entrapping them into a high speed helium gas flow [3, 22, 23]. As the device and target interaction is a determining factor for effective drug targeting a thorough investigation of this relationship and proof of concept is vital for the development of new devices for powder injection.

4   PYROTECHNICAL DEVICE DEVELOPMENT

All device prototypes described in the following were invented and built by our cooperation partner Dr. Lell. The experiments were carried out cooperatively with Dr. Lell and his team.

4.1   REQUIREMENTS ON THE PYROTECHNICAL DEVICE

The effective application of a dry powder vaccine into the skin using a needle-free method depends decisively on the performance of the application device. A detailed literature screening and conclusions drawn out of the experiments using the surrogate accelerator LWB identified several requirements on the device:

- The particle payload of the device has to be accelerated to high velocity, achieving a sufficient impact momentum to breach the stratum corneum of the skin [3, 24, 25]. Investigations with the surrogate accelerator LWB proved particle velocity > 300 m/s necessary for particles with low density and 20-63 µm size (like sugar particles).

- The device has to hold a vaccine dose of at least 1-5 mg, which should be homogeneously distributed on the device surface (this aspect was already discussed in chapter 6 of this thesis).

- A precise control of the location and depth of the injected particles is desirable. As already outlined in the introduction, the epidermal and upper dermal layers of the skin are low on sensory nerve endings and blood vessels and have a high density of immunocompetent cells. If this region is precisely targeted, an enhanced immune reaction can be expected [2-4]. Furthermore, by avoiding pain sensation and bleeding the acceptance of vaccination can be promoted among patients.

- The device has to be economic and ideally be competitive with single use needle and syringes. Hence, a low cost production of the device is required.

- High controllability of the escapement of the device is needed.

These requirements can be addressed using pyrotechnical modules in the core principle of the device. Pyrotechnical modules are fast, reliable, self-sustaining and independent of an external energy source, enabling storage, transport and distribution of the device at least over the shelf life of the vaccine without the need for maintenance. At the same time they offer maximum security as they can be designed in a manner to not explode, not even upon exposure to fire. The following work is based on a patent [26] of our cooperation partner and outlines the development of a device targeting the above mentioned requirements.

4.2 PROTOTYPE DEVICES

4.2.1 DEVELOPMENT OF THE GAS-CHAMBER DEVICE

The core principle of the prototype device was based on the expansion of gas, which expanded in an airtight burning chamber (figure 7.19). The gas was produced by a gas producing pyrotechnical powder. Thereby, a shock pressure was transferred onto a membrane. Prior, glass particles were attached to the membrane. Upon actuation of the system particles were detached from the membrane surface and accelerated towards a target.

However, the velocity of the glass particles reached only approximately 30 m/s as the pressure increase of the gas producing pyrotechnical powder was not fast enough to transfer a shock pressure onto the membrane.
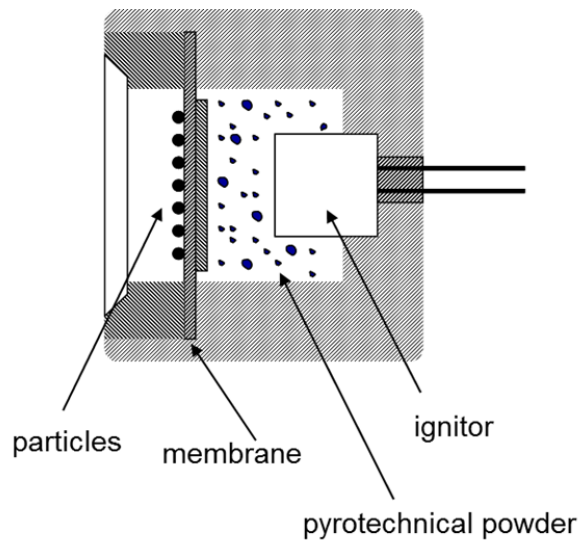
Figure 7.19: Schematic illustration the gas chamber device.

4.2.2 DEVELOPMENT OF THE LAVAL-NOZZLE DEVICE

In another prototype device a Laval-nozzle was implemented on the exit of the burning chamber in order to accelerate the gas produced in the burning chamber towards the membrane with the particle payload.

Membrane integrity could be maintained with several materials; however, none of the set-ups with the tested materials and material compositions were able to accelerate the particles to the desired velocity (> 300 m/s).

4.2.3 DEVELOPMENT OF THE PROTOTYPE PYROTECHNICAL DEVICE

The challenge to transfer a shock wave to the membrane without destroying the membrane of the device but accelerating the particles to high velocity was resolved in the prototype pyrotechnical device by (i) the implementation of a high energy gas generator in the device and (ii) by filling the burning chamber with an oleogel (based on castor oil and silicon dioxid) and (iii) by the choice of the membrane material.

The most important requirements on the membrane were that the material had to be as light as possible (low mass) and had to provide a high resistance against the pressure of the shock wave, which was generated in the burning chamber. Furthermore it had to be flexible enough to transfer the shock wave and hence the kinetic energy on the particles on the membrane surface. Another vital requirement of the membrane material was its compatibility with the pharmaceutical drug-payload. Therefore several membrane materials in several thicknesses and combinations of layered structures were investigated. Velocity measurements of different model particles using the prototype pyrotechnical device are exemplified in section 4.3.

4.3 VELOCITY MEASUREMENTS OF MODEL PARTICLES USING THE PROTOTYPE PYROTECHNICAL DEVICE

The prototype pyrotechnical device was able to generate particle velocities > 300 m/s. In order to reassess the accuracy of the velocity measurements of the particles, as described in section 1 of this chapter, a third high speed camera was implemented perpendicular to the other two high-speed cameras in the set-up.
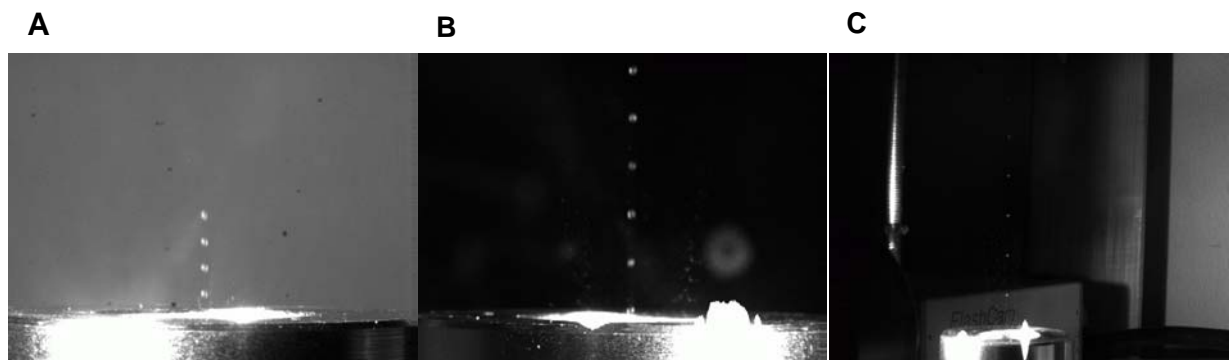
Figure 7.20: Pictures taken by a set of three Flash Cam PCO high speed cameras of a 600 μm glass particle (2.5 g/cm³) accelerated by the pyrotechnical device. A: Camera #1 with a time interval of 5 μs. B: Camera #2 with a time interval of 10 μs. C: Camera #3 with a time interval of 30 μs.

Glass particles (600 μm, 2.5 g/cm³) served as model particles for the velocity measurements. Figure 7.20 shows a single glass particle in a serial recording after

acceleration by the prototype pyrotechnical device. Depending on the time interval between each picture (figure 7.20 A, B and C) a different median velocity of the particle was calculated (figure 7.21). Velocity measurement using high speed camera #1 resulted in an average velocity of 508 ± 28 m/s. Using high speed camera #2 a velocity of 453 ± 35 m/s was obtained having a time interval of 10 µs between each serial picture. High speed camera #3 showed a mean velocity of 422 ± 41 m/s, recorded using a time interval of 30µs. This phenomenon correlated with the accuracy of the measurement.
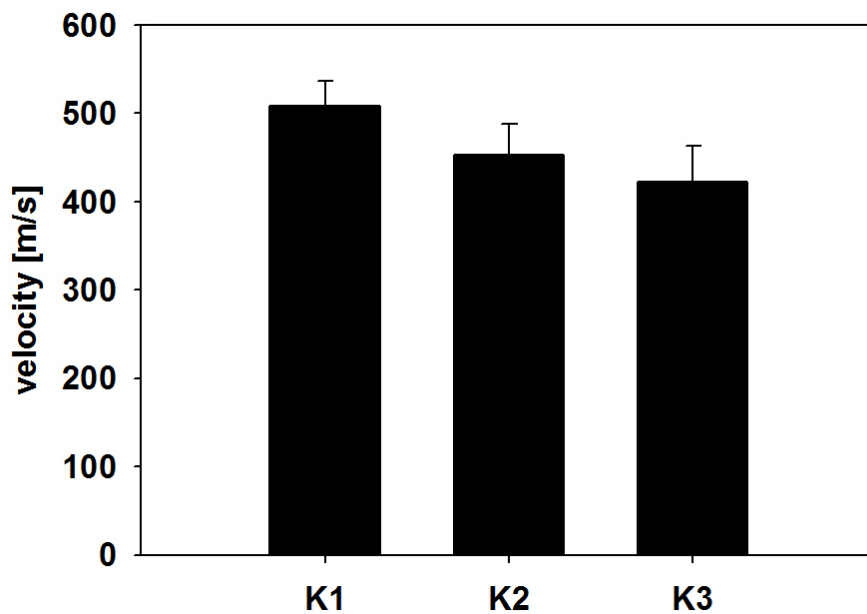
Figure 7.21: Median velocity of a 600 µm glass particle (2.5 g/cm³) after acceleration using the pyrotechnical device as calculated using the high-speed pictures of camera #K1, #K2 and #K3.

A   B
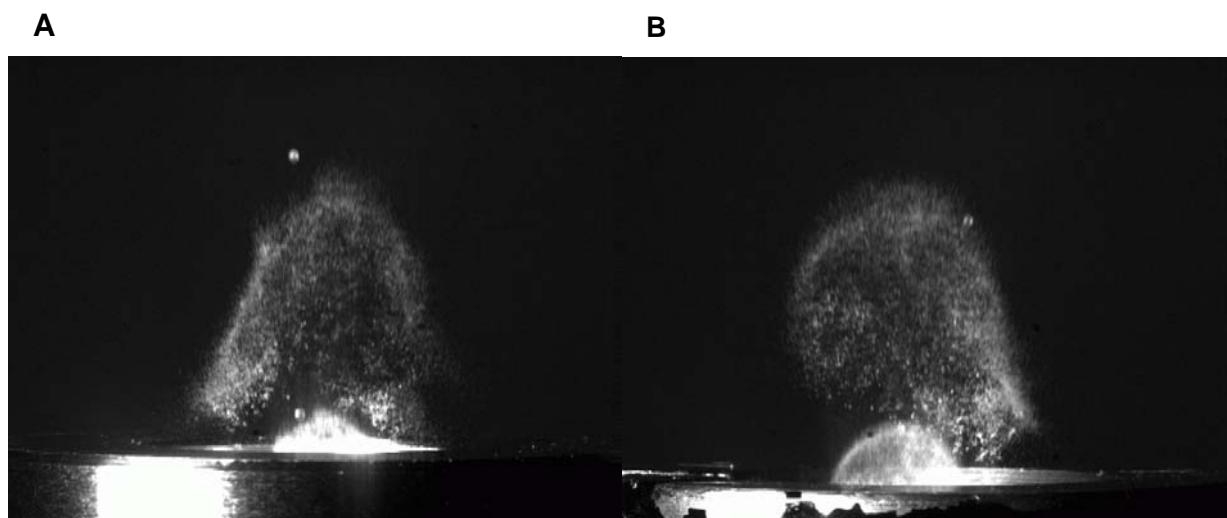
Figure 7.22: FITC-labelled polystyrene particles (40 µm, 1.1 g/cm³) and a 600 µm glass particle after acceleration with the pyrotechnical device. The glass particle is flying slightly ahead of the polystyrene powder cloud. A: camera #1. B: camera #2.

The velocity of FITC labelled polystyrene particles and sugar particles based on a binary mixture of trehalose and mannitol had to be calculated using the distance between two powder clouds divided by the time interval between the two pictures. Using this method, only an average velocity distribution of the particles could be calculated

In comparison to a 600 µm glass particle, the powder cloud of particles in the lower µm-size < 60 µm had a lower speed as the glass particle. The glass particle was flying ahead of the powder cloud, confirming the observations using the LWB (figure 7.22).

Figure 7.23 shows the median velocity of glass, polystyrene and trehalose-mannitol-particles. Glass particles had a mean velocity of 461 ± 41 m/s as calculated as the mean value of the three high speed camera measurements. FITC-labelled polystyrene particles had a velocity of 404 ± 16 m/s and trehalose-mannitol particles of 380 ± 28 m/s.
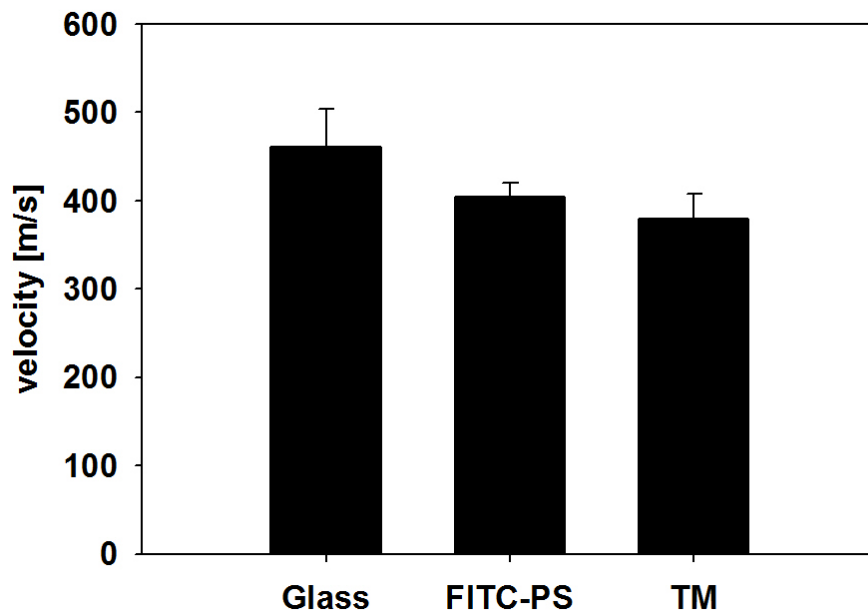
Figure 7.23: Median velocity of a 600 µm glass sphere, 40 µm FITC-labelled polystyrene particles and trehalose-mannitol particles (20-40 µm).

Though all particles were accelerated using the same conditions, particle velocity of polystyrene and trehalose-mannitol particles was lower as of glass particles.

Thus, the results obtained in the preliminary investigations using the LWB were confirmed. As already observed at a lower velocity range, particle velocity depends on size and density of the particles, being still valid for high velocity ranges, breaching the supersonic speed barrier of 343 m/s.

5 IN-VITRO PENETRATION OF PARTICLES INTO EXCISED PIG SKIN AFTER BALLISTIC ACCELERATION USING THE PROTOTYPE PYROTECHNICAL DEVICE

The penetration pattern and depth of FITC-labelled-polystyrene-particles into excised pig skin using the prototype pyrotechnical device was investigated by confocal laser scanning microscopy (LSM 510 META, Carl ZEISS, Germany) and verified by cryo-sectioning. The skin was rinsed with water and wiped with paper tissue in order to remove not penetrated particles from the skin surface, prior to CLSM and histological analysis. The method to determine the depth of particles in a skin sample using CLSM analysis was validated and performed by Dr. Deng [20] as described before.

Prior to bombardment of the skin section particle velocity was determined using three synchronized Flash Cam PCO high speed cameras. FITC-labelled polystyrene particles had a velocity of 404 ± 16 m/s.

5.1 CONFOCAL LASER SCANNING MICROSCOPY (CLSM)

The CLSM pictures showed a dense impact of a large number of particles in the upper layer of the skin (figure 7.24). A red fluorescent dye (TRITC) was used to indicate the rough skin surface [20]. Yellow spots appeared upon overlapping areas of the red (TRITC) and green (FITC) fluorescent dyes. Optical sectioning in 10 μm steps showed a penetration of particles up to 30 to 40 μm depth. Hence, particles breached the stratum corneum of the skin (figure 7.25). Deeper located particles were not observed.

In conclusion, FITC-labelled polystyrene particles (40 μm diameter and 1.1g/cm³ density) accelerated to a mean velocity of 404 ±16 m/s overstepped the threshold to breach the stratum corneum of the skin. Thus, these results confirm the theory that a threshold value of at least 7 kg m^{-1} s^{-1}, calculated from the density, velocity and radius of the particles, is needed to penetrate into the skin [3]. According to this function a value of 9 kg m^{-1} s^{-1} was achieved (calculated using the true density of the particles).
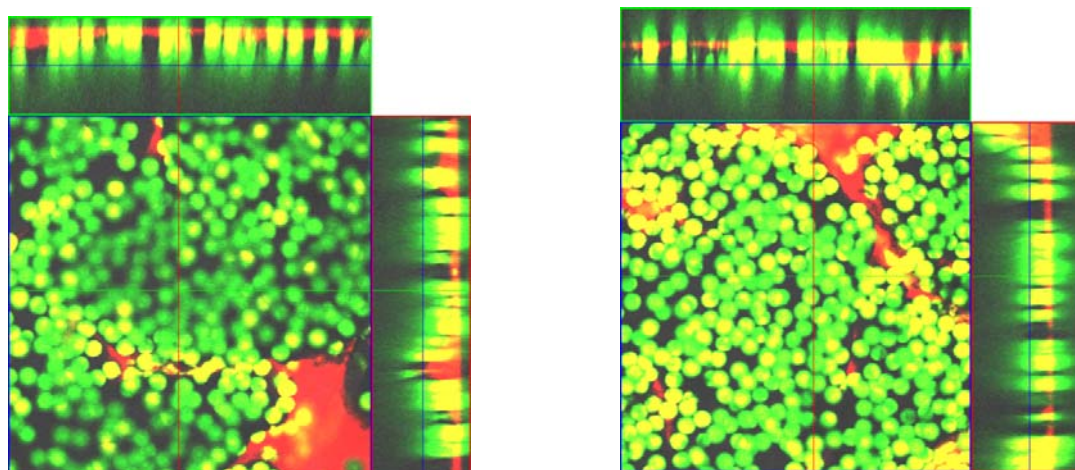
Figure 7.24: CLSM pictures of excised pig skin after bombardment with FITC-labeled polystyrene particles (40 µm). Skin surface was marked with red fluorescent dye (TRITC). Top view of the skin surface and orthogonal sections are shown.
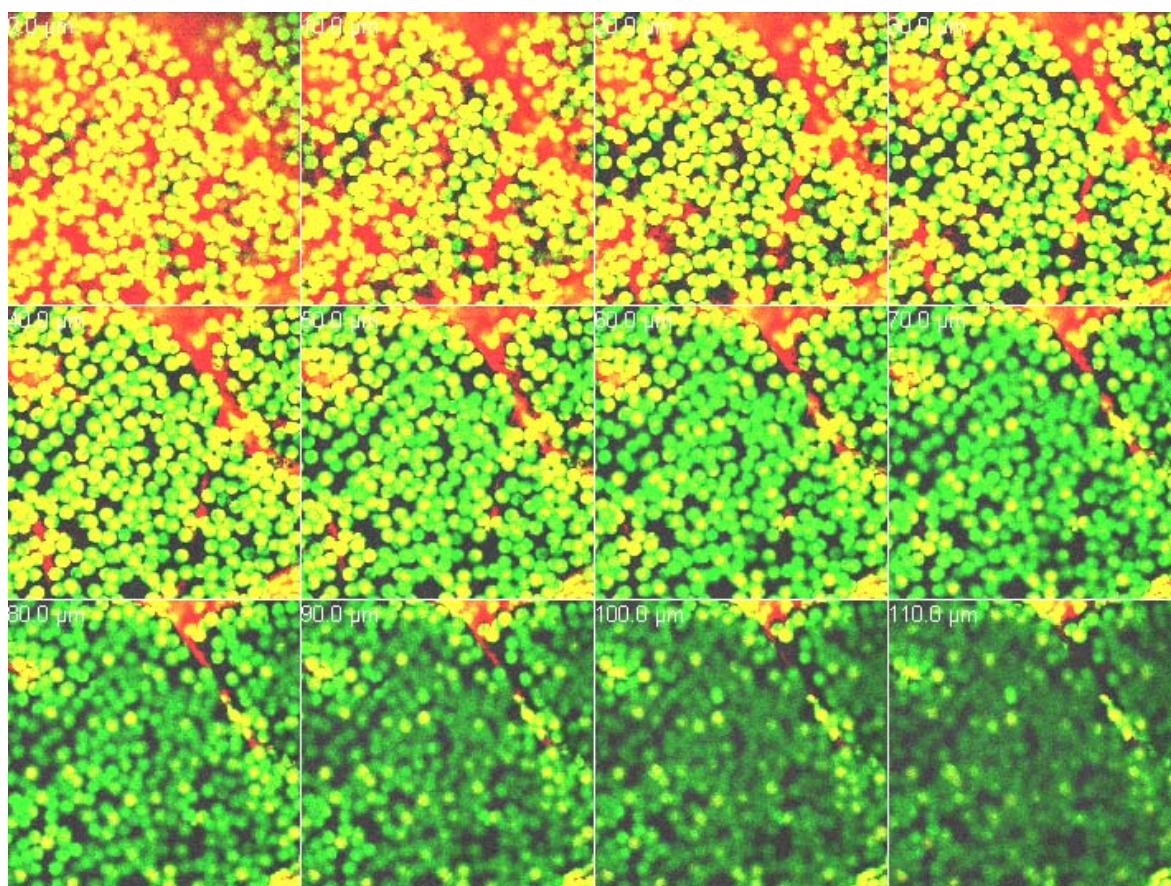
Figure 7.25: Penetration of 40 µm FITC-labelled polystyrene particles into excised pig skin as determined by CLSM measurement. Skin surface was marked with red fluorescent dye (TRITC). Visualization of multiple depths in 10.0 µm-steps per recording. Mean penetration depth 30-40 µm.

Though the above mentioned thesis was drawn out of experimental data using a needle-free injection device accelerating particles by entrapping them into a high speed helium gas flow [3, 22, 23], the obtained data indicate that this function is also valid using the prototype pyrotechnical device, accelerating particles by momentum transfer in a static environment. As polystyrene particles exhibit similar particle density and size as the final vaccine payload based on sugar particles, similar penetration of sugar particles is expected.

5.2 CRYO-SECTIONING

Cryo-cross sections of the pig skin samples confirmed the results obtained by CLSM (figure 7.26). Polystyrene particles (40 µm) breached the stratum corneum and were found 30 to 40 µm deep in the skin tissue.
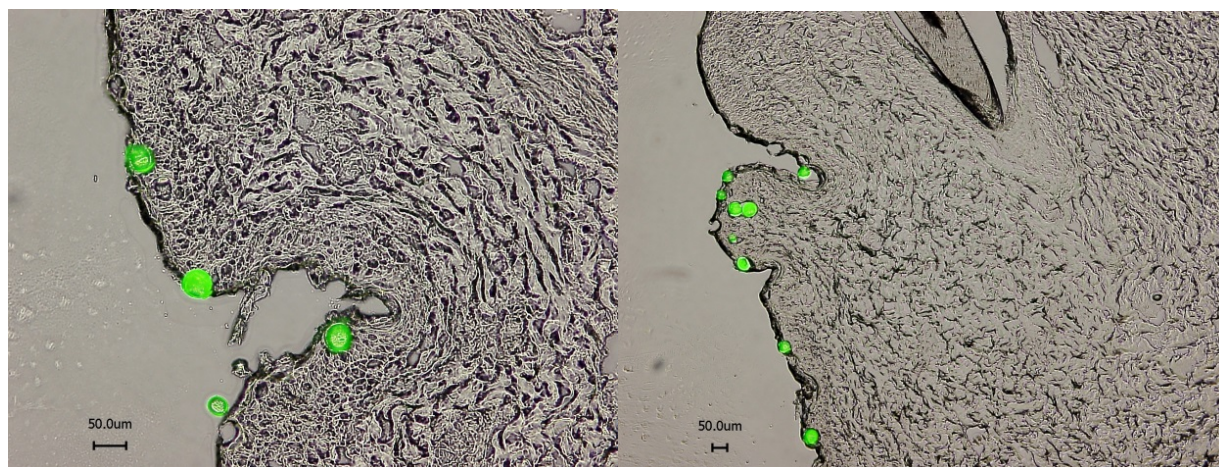
Figure 7.26: Slices of excised pig skin prepared by cryo-sectioning after particle bombardment using 40 µm FITC-labelled polystyrene particles. Particles were accelerated to 404 ±16 m/s using the prototype pyrotechnical device. Scale bars 50 µm.

6   SUMMARY AND CONCLUSION

The surrogate accelerator LWB enabled the evaluation of basic principles for the acceleration of particles by momentum transfer in a static environment. A method for the measurement of the velocity of particles using high speed cameras was developed and the dependency of particle velocity on particle parameters like size, density and shape was evaluated. It was shown that particle velocity increases with increasing size and density of the particles. The shape of particles had no significant influence on particle velocity in the range of 80-180 m/s. However, limitations were given using this system in terms of the maximal achievable particle velocity, dependent on the type of particle, at approximately 300 m/s.

Gel models, simulating the mechanical properties of skin, were used to analyze particle penetration after acceleration using the LWB. The maximum achieved velocity of ≤ 275 m/s of 40 µm polystyrene particles, using an optimized set-up of the LWB for the acceleration of the particles, was not sufficient to penetrate into the gel models. Proof of concept in excised skin confirmed the results obtained after particle bombardment in different gelatin gels. The treshold of particle velocity to breach the stratum corneum and penetrate into excised skin samples was not exceeded using the LWB.

In a number of development steps a prototype pyrotechnical device was built which enabled the acceleration of particles to supersonic velocity. The functional principle of the device based on a pyrotechnical core which generated a shock wave in a burning chamber and transferred kinetic energy on a membrane. Several optimization steps involved the filling of the burning chamber with an oleogel in order to regulate the transfer of the shock wave to the particle coated membrane. Furthermore a highly robust and flexible pre-formed membrane material was identified which was compatible with the pharmaceutical payload. Velocity measurements of different model particles revealed that particles breached the supersonic speed barrier with a median velocity of 380-461 m/s, dependent on the type of particle. The accuracy of velocity measurement in this high speed range was re-evaluated.

The penetration of 40 µm FITC-labelled polystyrene particles in excised pig skin accelerated to supersonic speed using the prototype pyrotechnical device was

experimentally demonstrated. Particles reached a medium velocity of 404 ±16 m/s. CLSM measurements as well as cryo-sectioning of the skin samples showed that particles breached the stratum corneum and were deposit in an average penetration depth of 30-40 μm. Hence, the prototype pyrotechnical device fulfilled the scope of the project to inject low density particles successfully into the skin.

Penetration of vaccine loaded particles into skin, quantification of the injected vaccine dose as well as evaluation of the immunization efficacy of this innovative needle-free injection device in an animal model was beyond the scope of this thesis and will be discussed in further work.

7 REFERENCES

[1]   WHO. Saftey of Injections:Global Facts and Figures. World Health Organization, Geneva: World Health Organization, 2004.

[2]   Chen D, Maa Y-F, Haynes JR. Needle-free epidermal powder immunization. Expert Review of Vaccines 2002;1(3):265-76.

[3]   Kendall M, Mitchell T, Wrighton-Smith P. Intradermal ballistic delivery of micro-particles into excised human skin for pharmaceutical applications. Journal of Biomechanics 2004;37(11):1733-41.

[4]   Chen D, Payne LG. Targeting epidermal Langerhans cells by epidermal powder immunization. Cell Research 2002;12(2):97-104.

[5]   Dean HJ, Fuller D, Osorio JE. Powder and particle-mediated approaches for delivery of DNA and protein vaccines into the epidermis. Comparative Immunology, Microbiology and Infectious Diseases 2003;26(5-6):373-88.

[6]   Amorij JP, Huckriede A, Wilschut J, Frijlink H, Hinrichs W. Development of Stable Influenza Vaccine Powder Formulations: Challenges and Possibilities. Pharmaceutical Research 2008;25(6):1256-73.

[7]   Amorij J-P, Hinrichs WLJ, Frijlink HW, Wilschut JC, Huckriede A. Needle-free influenza vaccination. Lancet Infectious Diseases 2010;10(10):699-711.

[8]   Abdul-Fattah A, Truong-Le V, Yee L, Pan E, Ao Y, Kalonia D, et al. Drying-Induced Variations in Physico-Chemical Properties of Amorphous Pharmaceuticals and Their Impact on Stability II: Stability of a Vaccine. Pharmaceutical Research 2007;24(4):715-27.

[9]   Burkoth TL, Bellhouse BJ, Hewson G, Longridge DJ, Muddle AG, Sarphie DF. Transdermal and transmucosal powdered drug delivery. Critical Reviews in Therapeutic Drug Carier Systems 1999;16(4):331-84.

[10]   Liu Y, Costigan G, Bellhouse BJ. Performance studies of a conical nozzle designed for the macromolecular skin delivery. Journal of Drug Targeting 2008;16(3):206-12.

[11]   Liu Y, Costigan G, Bellhouse BJ. Swirling effects on the performance of the micro-particle acceleration and penetration: parametric studies. Powder Technology 2008;183(2):189-95.

[12]   Dean HJ, Chen D. Epidermal powder immunization against influenza. Vaccine 2004;23(5):681-6.

[13]   Chen D, Endres RL, Erickson CA, Weis KF, McGregor MW, Kawaoka Y, et al. Epidermal immunization by a needle-free powder delivery technology: Immunogenicity of influenza vaccine and protection in mice. Nature Medicine 2000;6(10):1187-90.

[14]   Chen D, Zuleger C, Chu Q, Maa YF, Osorio J, Payne LG. Epidermal Powder Immunization with a Recombinant HIV gp120 Targets Langerhans Cells and Induces Enhanced Immune Responses. AIDS Research and Human Retroviruses 2002;18(10):715-22.

[15]   Osorio JE, Zuleger CL, Burger M, Chu Q, Payne LG, Chen D. Immune responses to hepatitis B surface antigen following epidermal powder immunization. Immunology and Cell Biology 2003;81(1):52-8.

[16]   Chen D, Burger M, Chu Q, Endres R, Zuleger C, Dean H, et al. Epidermal powder immunization: cellular and molecular mechanisms for enhancing vaccine immunogenicity. Virus Research 2004;103(1-2):147-53.

[17]   Dean HJ. Epidermal delivery of protein and DNA vaccines. Expert Opinion on Drug Delivery 2005;2(2):227-36.

[18]   Drape RJ, Macklin MD, Barr LJ, Jones S, Haynes JR, Dean HJ. Epidermal DNA vaccine for influenza is immunogenic in humans. Vaccine 2006;24(21):4475-81.

[19]   Deng Y, Winter G, Myschik J. Preparation and validation of a skin model for the evaluation of intradermal powder injection devices. European Journal of Pharmaceutics and Biopharmaceutics 2012;81(2):360-8.

[20]   Deng Y. Investigations on the administration of dry vaccines for epidermal powder injection: München, Ludwig-Maximilians-Universität, Diss. ; 2013.

[21]   Kendall M, Rishworth S, Carter F, Mitchell T. Effects of Relative Humidity and Ambient Temperature on the Ballistic Delivery of Micro-Particles to Excised Porcine Skin. Journal of Investigative Dermatology 2004;122(3):739-46.

[22]   Quinlan NJ, Kendall MAF, Bellhouse BJ, Ainsworth RW. Investigations of gas and particle dynamics in first generation needle-free drug delivery devices. Shock Waves 2001;10(6):395-404.

[23]   Liu Y, Mark AFK. Optimization of a jet-propelled particle injection system for the uniform transdermal delivery of drug/vaccine. Biotechnology and Bioengineering 2007;97(5):1300-8.

[24]   Liu Y, Truong N, Kendall M, Bellhouse B. Characteristics of a micro-biolistic system for murine immunological studies. Biomedical Microdevices 2007;9(4):465-74.

[25]   Kendall MAF. The delivery of particulate vaccines and drugs to human skin with a practical, hand-held shock tube-based system. Shock Waves 2002;12(1):23-30.

[26]   Lell P. Needleless injection device with pyrotechnic drive. U.S. Patent No. 7,160,265. 2007.

CHAPTER 8

FINAL SUMMARY, CONCLUSION AND OUTLOOK

The increasing knowledge of immune responses induced by targeting the intradermal layers of the skin has driven the engineering of devices for intradermal vaccination. Needle-free delivery devices injecting dry vaccine particles into the skin combine considerable advantages as (i) it eliminates the possibility of needle-stick injuries und re-use of needles, (ii) ease of handling, so that vaccine administration may be carried out after minimal operator training [1], (iii) dry powder vaccine formulations can offer improved stability, opening up the possibility for independence from cold-chain transport and storage [2-4] and (iiii) offer the potential for vaccine dose reduction [5-10].

The objective of the present thesis was to develop a dry powder formulation with appropriate characteristics for intradermal injection and superior stabilizing effect on antigens during storage at elevated temperatures. Furthermore a ballistic device system was developed to accelerate powder particles to high velocities in order to deliver the particles to the target site of vaccination, the epidermal layers of the skin.

In **Chapter 1** a general introduction to needle-free vaccination targeting the skin and an overview of formulations strategies and drying techniques for the generation of dry powder vaccine formulations is given. A second focus is set on delivery devices targeting for the intradermal application of vaccines, evaluating the pros and cons of each system. Closing Chapter 1 the objectives of the thesis are summarized and the materials and methods used throughout this thesis are described in **Chapter 2**.

In **Chapter 3** it was shown that a two-step approach combining collapse freeze-drying and cryo-milling was successful to generate particles with appropriate characteristics for

ballistic injection, including a narrow particle size distribution in the desired range of 20-70 μm and a highly dense matrix structure exhibiting a low specific surface area. Remarkably, these particle characteristics could be achieved by this approach independent of the formulation composition (in particular polymers like dextran) or the solid content of formulation, which was stated to be crucial for these features. Furthermore it could be shown, that the stability of the model antigen ovalbumin was preserved in formulations based on trehalose during collapse freeze-drying and cryo-milling as well as after 12 months of storage at 2-8°C and after 12 weeks of storage at 50°C.

In **Chapter 4** the cryo-milling process for the production of vaccine loaded powder particles was optimized. Cooling of the samples prior to milling was shown to be necessary to prevent local melting of the particles during milling.

A fast, efficient and gentle process tailored according to the respective rigidity of the formulation was established, resulting in a high yield in the targeted particle size range and a narrow particle size distribution. Furthermore it was possible to set up a sterile production process. This is very promising and it will be interesting to evaluate it the cryo-milling process can be scaled-up to industrial standards and if this at least two-step process will be competitive with other particle manufacturing process like spray-drying or spray-freeze-drying. The applicability of the cryo-milling process on the model protein rh-GCSF could be demonstrated, however not for IFN-α-2a. The formation of insoluble aggregates was observed in IFN-α-2a formulations after collapse freeze-drying as well as after cryo-milling. As the formulation composition determines decisively protein stability, stability after cryo-milling has to be evaluated for each antigen individually. Future studies will certainly lead to a better understanding of applicability of this two-step process on other vaccines and antigens.

Formulation screening and an accelerated storage stability study of the model antigen ovalbumin formulations at 2-8°C, 25°C and 50°C was scrutinized in **Chapter 5.** In the course of these studies, the effect of collapse freeze-drying and subsequent cryo-milling on antigen stability and powder characteristics was thoroughly investigated by

comparing different formulations. Formulations containing higher molecular weight dextran (40 and 70 kDa) showed aggregation of ovalbumin at 50°C with an onset after 8 weeks. Formulations based on a binary combination of trehalose and mannitol exhibited excellent protein stability throughout storage at elevated temperatures and showed superior physico-chemical and morphological characteristics of the powder regarding the requirements for ballistic injection. Furthermore, it could be demonstrated that an increase of the antigen load of the powder formulation from 25 µg/mg to 200 µg/mg ovalbumin in several formulation compositions was possible without affecting physical characteristics of the particles or having a negative influence on antigen stability.

In **Chapter 6** several oily adjuvants were explored as adhesives at the interface between particles and the surface of a ballistic device for intradermal injection. In order to simulate the mechanical stress exerted during handling, shipping and storage of the device, the adhesive strength in between the device surface and the particles (model glass particles) was investigated and was outstanding for several oily substances, including the oily components of MF59 and Freund's incomplete adjuvant, also after storage at elevated temperature. It could be shown that approximately the tenfold higher mass of particles in comparison to the mass of the adhesive (10 µl) could be attached onto the membrane surface, enclosing the particles into a thin film of the oily substance. Proof of concept was given by the release of the particles from the membrane surface upon actuation of the ballistic device. Thereby the adhesive was entrained together with the particles, offering the possibility to be co-injected into the skin and herein to exert an adjuvant effect.

In addition to the experiments investigating the adherence strength of particles at the interface to the device surface, the storage stability and possible interaction between selected oily substances and ovalbumin loaded powder particles was explored in a short term stability study at elevated temperatures.

A comprehensive investigation of the stability of ovalbumin demonstrated that antigen stability was maintained during storage at 40°C for 12 weeks in samples incubated with squalane, squalene, or paraffin oil. Only a slight decrease in protein stability was found for samples incubated with Freund's incomplete adjuvant. In contrast, the occurrence of

higher-ordered aggregates and significant perturbations of the secondary protein structure were observed in samples incubated with the oily components of MF59 with an onset after 8 weeks of storage at 40°C. Therefore, preference should be given to its component squalene in the selection as oily adjuvant.

In **Chapter 7** a highly versatile and controllable surrogate apparatus, the Lell's Foucault accelerator (LWB), was used to evaluate basic principles for the acceleration of particles by momentum transfer in a static environment. A method was developed for the measurement of particle velocity using high speed cameras and the dependency of particle velocity on particle parameters like size, density and shape was evaluated.

It was shown that particle velocity increases with increasing size and density of the particles. The threshold of particle velocity (model particles polystyrene, 40 µm, 1.1 g/cm³) to breach the stratum corneum and penetrate into gel models, simulating the mechanical properties of skin, or excised skin samples was not achieved with the maximum achieved velocity of ≤ 275 m/s using the LWB.

In a number of development steps a prototype device based on a pyrotechnical principle was built (by our cooperation partner Dr. Lell, Pyroglobe, Hettenshausen, Germany), which enabled the acceleration of particles to 380-461 m/s, breaching the supersonic speed barrier. The penetration of FITC-labelled polystyrene particles (40 µm, 1.1 g/cm³) into excised pig skin in an average penetration depth of 30-40 µm was demonstrated by CLSM measurements and cryo-sectioning. Hence, the prototype pyrotechnical device fulfilled the scope of the project to inject low density particles successfully into the skin.

In conclusion, following major achievements were reached within this thesis:

- A dry powder antigen formulation based on a binary combination of trehalose and mannitol with appropriate characteristics for intradermal injection was developed by applying a two-step approach combining collapse freeze-drying and cryo-milling. The powder formulation showed excellent antigen stability throughout storage at elevated temperatures. A cryo-milling process for the production of vaccine loaded powder particles was established which is fast, efficient and opens up the possibility to up-scale the process to industrial

standards, resulting in a high yield of particles in the targeted size range and a narrow particle size distribution.

- The use of oily adjuvants as adhesives at the interface between particles and the surface of a ballistic device for intradermal injection was shown to successfully attach particles onto the device surface by enclosing them into a thin film of the oily substance. The adherence strength between particles and device surface was sufficient to fix the particles on the device surface during handling, shipping and storage of the device, but likewise the particles could also be released from the membrane surface upon actuation of the ballistic device. The entrainment of adhesive together with particles offers the possibility to be co-injected into the skin and herein to exert an adjuvant effect. Furthermore, it was proven that antigen stability could be preserved in the combination of ovalbumin loaded powders with selected oily adjuvants like Freund's incomplete adjuvant or squalene during storage at elevated temperatures.

- A prototype device based on a pyrotechnical principle was built which enabled the acceleration of particles to supersonic speed. Proof of concept was given by the penetration of the particles into excised pig skin.

In summary, the conducted studies provided the basis for needle-free ballistic delivery of a powdered vaccine. Further studies demonstrating the ability of the delivery device to inject vaccine powder particles together with oily adjuvants into the skin are necessary and it would be still of interest to investigate the ability of this application method to provoke an adequate immune response in an animal model. In this context, the transferability of the presented results to other vaccines, which are in the focus of mass vaccination programs (e.g. influenza), is of great interest, as mass vaccination programs would capitalize the most from a needle-free and cold chain independent vaccination method.

REFERENCES

[1]   Kim Y-C, Jarrahian C, Zehrung D, Mitragotri S, Prausnitz MR. Delivery systems for intradermal vaccination. Current Topics in Microbiology and Immunology 2012(351):77-112.

[2]   Amorij J-P, Hinrichs WLJ, Frijlink HW, Wilschut JC, Huckriede A. Needle-free influenza vaccination. Lancet Infectious Diseases 2010;10(10):699-711.

[3]   Abdul-Fattah A, Truong-Le V, Yee L, Pan E, Ao Y, Kalonia D, et al. Drying-Induced Variations in Physico-Chemical Properties of Amorphous Pharmaceuticals and Their Impact on Stability II: Stability of a Vaccine. Pharmaceutical Research 2007;24(4):715-27.

[4]   Amorij JP, Huckriede A, Wilschut J, Frijlink H, Hinrichs W. Development of Stable Influenza Vaccine Powder Formulations: Challenges and Possibilities. Pharmaceutical Research 2008;25(6):1256-73.

[5]   Auewarakul P, Kositanont U, Sornsathapornkul P, Tothong P, Kanyok R, Thongcharoen P. Antibody responses after dose-sparing intradermal influenza vaccination. Vaccine 2007;25(4):659-63.

[6]   Bryan JP, Sjogren MH, Macarthy P, Cox E, Legters LJ, Perine PL. Persistence of antibody to hepatitis B surface antigen after low-dose, intradermal hepatitis B immunization and response to a booster dose. Vaccine 1992;10(1):33-8.

[7]   Herbert FA, Larke RPB, Markstad EL. Comparison of Responses to Influenza A/New Jersey /76-A/Victoria/75 Virus Vaccine Administered Intradermally or Subcutaneously to Adults with Chronic Respiratory Disease. Journal of Infectious Diseases 1979 August 1, 1979;140(2):234-8.

[8]   Kenney RT, Frech SA, Muenz LR, Villar CP, Glenn GM. Dose sparing with intradermal injection of influenza vaccine. The New England Journal of Medicine 2004;351(22):2295-301.

[9]   Egemen A, Aksit S, Kurugöl Z, Erensoy S, Bilgiç A, Akilli M. Low-dose intradermal versus intramuscular administration of recombinant hepatitis B vaccine: a comparison of immunogenicity in infants and preschool children. Vaccine 1998;16(16):1511-5.

[10]   Pancharoen C, Mekmullica J, Thisyakorn U, Kasempimolporn S, Wilde H, Herzog C. Reduced-Dose Intradermal Vaccination against Hepatitis A with an Aluminum-Free Vaccine Is Immunogenic and Can Lower Costs. Clinical Infectious Diseases 2005;41(10):1537-40.

CHAPTER 9

APPENDIX

1   ADDITIONAL FIGURES
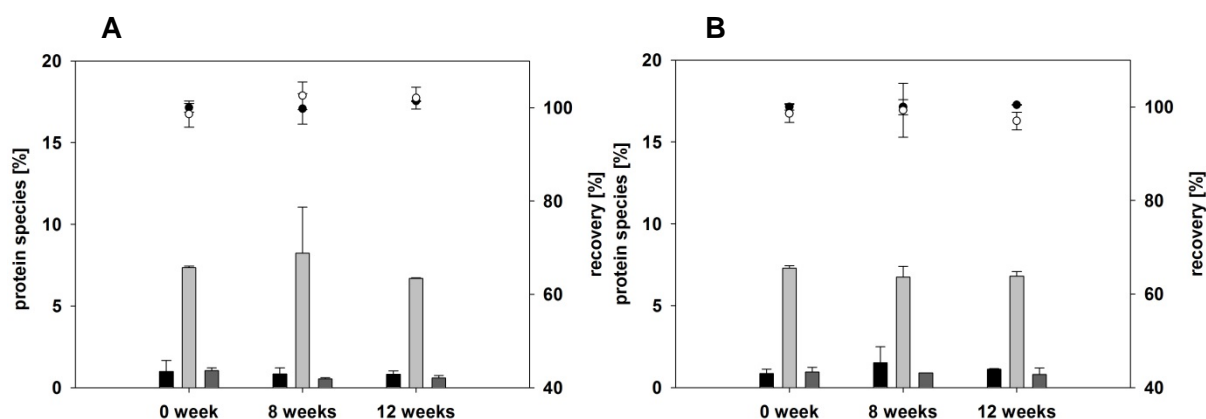
Figure 9.1: Recovery of ovalbumin protein species (%) as determined by size exclusion chromatography in cryo-milled powders after 0, 8 and 12 weeks of storage at 25°C. Trehalose/mannitol/dextran 70 kDa formulations are depicted in A, trehalose/mannitol/dextran 40 kDa formulations are depicted in B. Black bars represent higher molecular weight aggregates, light grey bars represent dimers, dark grey bars represent fragments. Open circles represent the total protein recovery, filled circles represent monomer recovery (average +/- SD, n=3).
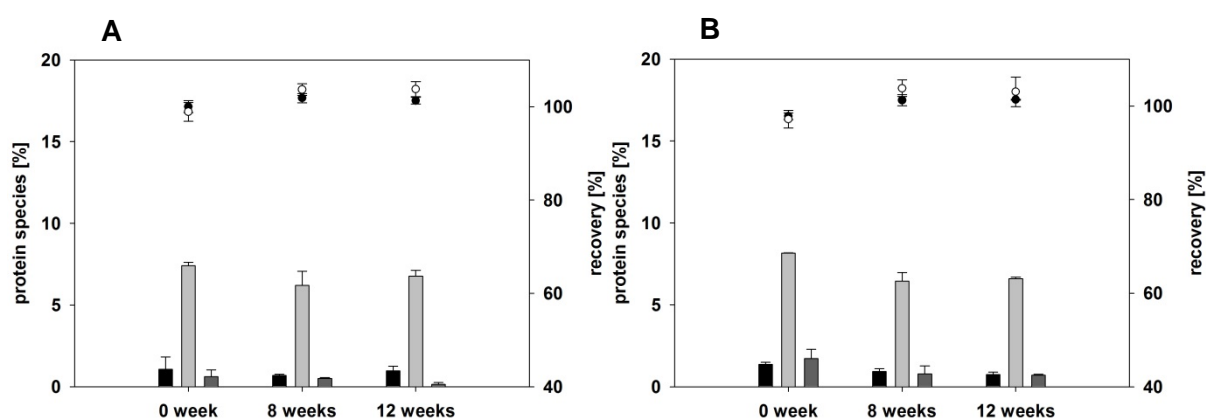
Figure 9.2: Recovery of ovalbumin protein species (%) as determined by size exclusion chromatography in cryo-milled powders after 0, 8 and 12 weeks of storage at 25°C. Trehalose/mannitol/dextran 6 kDa formulations are depicted in A, trehalose/mannitol/hydroxyethylstarch formulations are depicted in B. Black bars represent higher molecular weight aggregates, light grey bars represent dimers, dark grey bars represent fragments. Open circles represent the total protein recovery, filled circles represent monomer recovery (average +/- SD, n=3).
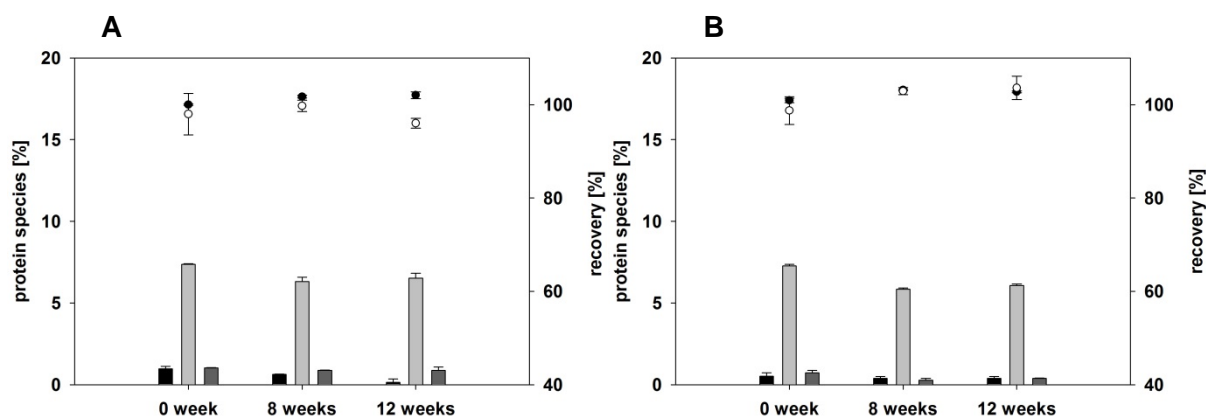
Figure 9.3: Recovery of ovalbumin protein species (%) as determined by size exclusion chromatography in cryo-milled powders after 0, 8 and 12 weeks of storage at 25°C. Trehalose/mannitol formulations are depicted in A, trehalose/phenylalanine formulations are depicted in B. Black bars represent higher molecular weight aggregates, light grey bars represent dimers, dark grey bars represent fragments. Open circles represent the total protein recovery, filled circles represent monomer recovery (average +/- SD, n=3).
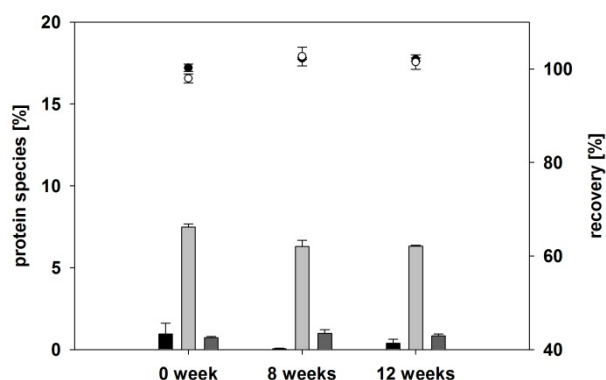
Figure 9.4: Recovery of ovalbumin protein species (%) in trehalose formulations as determined by size exclusion chromatography in cryo-milled powders after 0, 8 and 12 weeks of storage at 25°C. Black bars represent higher molecular weight aggregates, light grey bars represent dimers, dark grey bars represent fragments. Open circles represent the total protein recovery, filled circles represent monomer recovery (average +/- SD, n=3).

2 REVIEW ARTICLE: DEVICES FOR INTRADERMAL VACCINATION

The review was published in *Vaccine:*

Kis EE, Winter G, Myschik J*. Devices for intradermal vaccination. Vaccine 2012; 30(3):523-38.

* Corresponding author

The review presented here was written together with Julia Engert (nee Myschik). The section 2.3 and the correspondig tables 9.1 and 9.2 were written by Julia Engert. The other sections were written by Elsa Etzl (nee Kis). The following review would not have been possible without the guidance for the preparation of the manuscript of my supervisor Gerhard Winter and the remarkable support by Julia Engert (nee Myschik). Sarah C. Gordon has to be thank for proof-reading of the manuskript. Julia Engert submitted the manuscript to the Journal.

ABSTRACT

New insights in vaccine development, the need for safe, economic and efficient vaccine administration and the increasing mechanistic knowledge of immune responses induced by targeting the intradermal layers of the skin have all driven the engineering of devices for intradermal vaccination. In this review we highlight different delivery devices that make the epidermal and dermal layers of the skin accessible for vaccine administration. Depending on the device the desired vaccine can be applied either as a liquid formulation or as solid, powdered vaccine particles. The process of intradermal injection employs micron-sized needles that are inserted 1.5 mm perpendicularly into the skin, and which inject approximately 100-200 µl of a liquid vaccine formulation into the dermal skin layers. Tattoo devices, on the other hand, can be used to deliver liquid vaccine formulations into the dermal layer of the skin by the use of oscillating needles. Microneedle arrays are made of vaccine-coated solid microneedles or biodegradable microneedles. These are inserted into the dermal layers of the skin where either the vaccine coating is dissolved, or the microneedle itself dissolves in place. Jet-injectors operate by generating a high pressured stream, which flushes the liquid vaccine formulation into the deeper skin layers. Delivery devices using liquid vaccine formulations are advantageous, as established vaccine formulations can be used as provided without the need for reformulation. However, approaches that deliver vaccines in a solid form may also prove to be promising. One such method is the ballistic approach, in which solid vaccine particles or vaccine-coated gold particles are accelerated towards the skin by needle-free devices, so that the particles are deposited in the epidermal and dermal layers of the skin. These various delivery devices are explored in this review with regard to their delivery mechanism and ease of handling, their efficacy in clinical trials and their suitability for practical use.

245

2.1 INTRODUCTION

Vaccination is the core principle for the prevention of life-threatening infectious diseases, and can be dated back to the first vaccination carried out by Edward Jenner in 1796 [1-3]. Despite the availability of a wide range of vaccines for many and varied applications, infectious diseases remain a major global problem, especially in developing countries [4-6].

One reason for this fact is that many vaccines still require the use of needles and syringes for administration. Particular in developing countries, the application of vaccines via needles and syringes carries significant risk. Professional healthcare workers are needed for the administration of vaccines to patients, and these persons are potentially exposed to needle-stick injuries. Furthermore, sharps waste management and the reuse of needles are both considerable problems.

Novel vaccination strategies should ideally allow for safer injection practices, while still being cost-effective and capable of evoking sufficient immune responses in patients [4, 7]. As a safe injection practice is the primary priority postulated by the World Health Organization (WHO) [8], the development of needle-free technologies has experienced a significant upturn in the past years [9]. Needle-free injection devices avoid unsafe injection practices and can enhance patient compliance by evoking less pain and stress.

The skin is an attractive target for vaccination as it constitutes the major barrier for the entry of environmental pathogens, while at the same time being easily accessible for vaccine administration [10-15]. Immunocompetent antigen presenting cells (APCs) such as the Langerhans cells (LCs) in the epidermis and dendritic cells in the underling dermis are able to capture and process foreign antigens. APCs are able to migrate to lymph nodes and here present processed antigens on their surface to other cells of the immune system [15, 16]. In addition, the lack of sensory nerve endings and blood vessels in the epidermal layer of the skin provides the possibility of application of the vaccine without causing any pain or bleeding. In terms of efficiency, the intradermal route of vaccine application has been stated to induce protective immune responses superior to those induced after intramuscular injection and in the case of some vaccines, allow for the use of smaller quantities of antigen [17-33].

A broad review of clinical trials comparing the intradermal and subcutaneous (s.c.) or intramuscular (i.m.) route of administration of several licensed vaccines is given in a

publication by the Program for Appropriate Technology in Health (PATH) [34]. Several clinical trials have been conducted to evaluate whether equivalent or superior immune responses could be elicited by administering vaccines via the intradermal route in comparison to intramuscular or subcutaneous injection. Clinical trials with influenza [25, 35, 36] and rabies [37] vaccines verified that intradermal vaccination was able to elicit equivalent immune responses to the vaccine given intramuscularly or subcutaneously, while utilizing only 10-20% of the antigen dose. Similar results were obtained for hepatitis B vaccines [38, 39], while only limited clinical trials have been carried out for other commercially available vaccines such as the polio, measles, tetanus toxoid and hepatitis A vaccines [34, 40-43].

However, most of these studies were not designed to compare identical vaccine doses given by the intradermal and the s.c. or i.m. route. Therefore, it is unclear whether the antigen dose contained within the s.c. and i.m. injection could also have been reduced, with continued vaccine efficacy. A further point of concern is that many of the conducted trials used conventional needles and syringes for injection via all three routes of administration. It can therefore be brought into question if the LCs in the epidermal and dermal layer of the skin were effectively targeted.

The traditional administration of vaccines via needle and syringe cannot effectively target the LCs in the epidermis of the skin, as deeper subcutaneous regions or muscle tissue will be reached due to the length of the needle and the applied standard technique [13, 44]. Intradermal injection methods using needles and syringes, such as the Mantoux technique, require considerable expertise and are seldom used for intradermal vaccinations and only for bacilli calmette guérin (BCG vaccination), for tuberculosis and for post-exposure rabies vaccination [45]. Therefore, there is an urgent need for devices to facilitate correct and accurate intradermal administration. This need is attempted to be met by the development of a variety of delivery systems intended specifically for the intradermal administration of vaccines [46].

Vaccines may pass through the skin passively via diffusion (transcutaneously) or by penetration through the stratum corneum (SC) into the deeper skin layers (intradermally) [9, 47-49]. The terminology used to describe vaccination via these mechanisms has not always been used consistently, with the process of introducing vaccines into the skin sometimes referred to as transdermal, epidermal or

percutaneous delivery interchangeably. Only molecules smaller than 500 Dalton [50] can pass the SC by diffusion or permeation. Glenn *et al.* proposed the use of diffusion patches to enhance the permeability of the SC and thereby enable the delivery of large recombinant antigens greater than 1 Mega Dalton (MDa), leading to the introduction of systemic immune responses [51]. Other methods used to breach the SC such as tape stripping, brushing with sandpaper, application of depilatory agents, ultrasound, electroporation, microporation or ablation by laser or heat are widely described in literature, however only a few of these methods have been tested in clinical trials [52-57]. Most of these approaches are furthermore associated with disadvantages such as difficulties in handling, the need for expensive tools and the induction of considerable pain in the vaccination subject. Some such approaches may even combine these disadvantages.

Ballistic approaches however have already reached the stage of clinical trials in humans [58], and recently a microinjection system delivering a seasonal influenza vaccine has gained approval [59].

As mentioned, a major requirement for such delivery devices is ease of handling, so that vaccine administration may be carried out after minimal operator training, already. The cost of the device should prove to be competitive with that of conventional needle and syringe systems, and a superior long term stability of the vaccine would also be desirable, allowing for avoidance of a cold chain and so increasing the ease with which vaccines may be distributed.

In this review we highlight delivery systems that facilitate the intradermal application of vaccines (see table 9.1) and thereby target the LCs (figure 9.5). We focus on methods that apply the vaccine directly into the skin; methods involving application of the vaccine onto the skin surface or enabling vaccine penetration by other means (e.g. penetration enhancers, or SC ablation methods such as tape stripping or abrasion) have been well described elsewhere [60] and are therefore not discussed in the current review.

Table 9.1: An overview of different devices for liquid and solid formulation administration

	Type of device	Reference examples
Devices for liquid formulation administration	Needle and syringe Mantoux technique	[45, 61-64]
	Intradermal microinjection BD Soluvia™	[35, 36, 65-71]
	Tattoo devices for vaccination	[72-77]
	Hollow microneedle arrays	[78-81]
	Liquid jet injectors Biojector™ 2000 PharmJet® device Vitajet 3® device (polymer particles in liquid) Iject® device	[33, 82-84]
Devices for solid formulation administration	Solid microneedle arrays	[78, 81, 85-89] (see also table 2)
	Ballistic injectors Gene gun Powderject XR device Convergent-divergent supersonic nozzle (CDSN) device Contoured shock tube (CST) device Venturi device	[90-99]
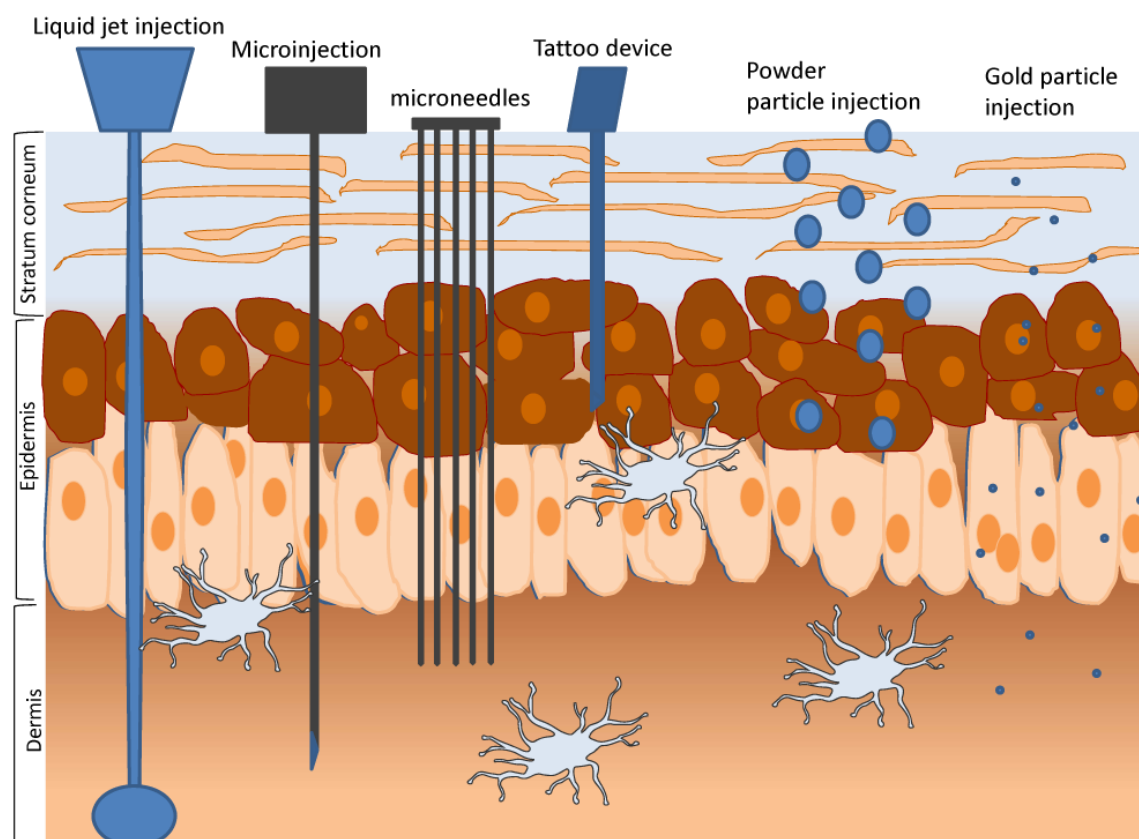
Figure 9.5: Delivery systems enabling the intradermal application of vaccines: Liquid jet injection, microinjection, microneedles, tattoo vaccination, powder particle injection, gold particle injection. Adopted after Mitragotri S. [9].

2.2 DEVICES

2.2.1 NEEDLE AND SYRINGES

The intradermal injection of vaccines using the Mantoux technique dates back to Charles Mantoux, a French physician, who first used this technique for tuberculosis diagnostics [100]. Using the Mantoux technique, the skin must be stretched and the needle is inserted parallel to the skin surface (figure 9.6).

Figure 9.6: The Mantoux technique. The skin has to be stretched and the needle has to be inserted parallel to the skin surface, a technique which can only be carried out by trained personnel. Figure originates from the Centers for Disease Control and Prevention's Public Health Image Library (PHIL), identification number 6806.

The experience of the person carrying out the injection is crucial for successful targeting of the dermal tissue. Today this technique is still used for the intradermal administration of BCG vaccines and rabies [45], however, due to difficult handling and inconsistency of the delivered vaccine dose, the Mantoux technique has not been established for routine use [61-64]. The use of bifurcated or pronged needles, first introduced by Benjamin A. Rubin [101, 102], or the application of multiple puncture injections [103] are considered to lead to inaccurate dosing and loss of vaccine [7, 104].

2.2.2 INTRADERMAL MICROINJECTION

The BD Soluvia™ (Becton Dickinson, Franklin Lakes, NJ, USA) is an intradermal microneedle injection system that consists of a 30 gauge needle of 1.5 mm in length,

and a syringe which has the capacity to hold 100 to 200 µl of a liquid formulation. This system enables intradermal vaccination [65]. The needle must be inserted perpendicular to the skin surface. A specially designed needle-penetration depth limiter ensures an appropriate insertion depth. An additional mechanism integrated into the syringe serves for the prevention of reuse or injury. After vaccine administration, the microneedle is covered with a plastic shield by pressing the plunger further [66]. The advantage of such a system is the ease of handling, allowing the vaccine to be administered also by untrained staff. The intradermal microinjection system ensures consistent vaccine dosing and is compatible with conventional liquid vaccine formulations. Due to the low penetration depth of the needle almost no sensation of pain can be perceived.

Laurent *et al.* investigated various performance criteria of the BD microinjection system, including the fluid distribution and histological changes at the injection site, as well as the accuracy of the volume of the injected fluid in comparison to the Mantoux technique. Such investigations were performed by the use of different techniques like X-ray and 3D-ultrasound echography [61]. The authors observed a larger fluid distribution at the injection site using the BD microinjection technique as the liquid infiltrated the papillary and reticular dermis, indicated by the visible formation of a skin wheal at the injection site. In comparison to considerable pain often resulting from employment of the Mantoux technique, the procedure of needle insertion with the BD microinjection system was observed to be almost pain free. The Mantoux technique caused in general more pain and tissue damage because of the right angle and upward position of the needle during injection. Furthermore, the intuitive handling of the BD microinjection system may mean that operation solely by highly trained healthcare personnel is unnecessary. However, while significant advantages were associated with the operation and needle insertion phase of the system, pain was perceived during fluid injection. Local adverse events such as blood at the injection site, redness and itching were also reported. A mean fluid leakage volume of 2-3 µl was observed due to back-flow from the injection site. The group of Gupta *et al.* investigated parameters affecting infusion pressure and associated pain perceived during microneedle injection, using glass microneedles [105]. Whilst the insertion depth had no bearing on the infusion pressure, an increase in pressure was observed by increasing the volume of the liquid delivered into the skin. However, a typical intradermal injection volume of 100 µl required a pressure of

less than 100 mmHg, similar to s.c. injection. This can be explained by compression of the dense fibers in the dermis, caused by perpendicular microneedle insertion. It could be also observed, that microneedle-based intradermal insertions were less painful than hypodermic needle insertion, which led to the formation of skin wheals at the injection site. The group of Laurent *et al.* studied the appropriate microneedle length for intradermal injection by echographic measurements [65]. They evaluated skin thickness at different body sites, such as the deltoid, suprascapular, waist and thigh area in different ethnic groups (Caucasian, Asian, and Black) as a function of gender, age and body mass index. Gender and body mass index were found to have an impact on impact on skin thickness, whereas average thickness of the skin was seen to remain constant in the age range of 18 to 70 years, independent of ethnic origin. No differences in skin thickness among ethnic groups were measured at the deltoid and suprascapular region, having a mean thickness of 2.02 mm and 2.54 mm respectively; both areas are therefore considered as being appropriate sites for intradermal injection [65, 106]. Furthermore it was found that a needle length of 1.5 mm was suitable to target the dermal skin layer, with this length being independent of the patient's gender, age, ethnicity or body mass index.

Several preclinical and clinical trials applying rabies, anthrax recombinant protective antigen vaccine and influenza vaccine have been conducted using the BD Soluvia™ microinjection system [35, 36, 66-68, 70, 107]. Laurent *et al.* observed that intradermal delivery of a reduced dose (25% of the standard i.m. dose) of a rabies vaccine in humans, using the BD microneedle, resulted in similar humoral immune responses as immunization with the full dose via the i.m. route [108]. This underlines the potential for dose sparing if vaccination is carried out intradermally. The group of Mikszta *et al.* investigated the intradermal delivery of an adjuvanted anthrax vaccine at several dose levels in rabbits, using the BD microneedle in comparison to i.m. vaccination [68]. A superior immune response after intradermal injection over i.m. injection was found during the first two weeks following primary and booster vaccination, though the immune response equalized at the later stages. Higher protection levels were found after aerosol challenge in the groups immunized intradermally than in the groups immunized using the i.m. route.

Immunogenicity of a trivalent inactivated seasonal influenza vaccine, delivered by i.m. or intradermal injection using the same quantity of antigen was investigated in a

three year, randomized phase 3 trial in 3707 elderly persons [66]. The intradermal vaccine contained 15 µg HA/strain per 0.1 ml whereas the i.m. vaccine contained 15 µg HA/strain per 0.5 ml dose. Neither of the vaccines contained adjuvants. A superior seroprotection rate was observed using the intradermal injected vaccine. Visible, local injection site reactions like pruritus, erythema, swelling, indurations and pain were more frequent after intradermal vaccine delivery, whereas systemic reactions induced by intradermal and i.m. injections were comparable [66, 108]. Whether the greater incidence of local inflammation resulting from intradermal injection may potentially lead to an enhanced efficiency of immunization is a point for discussion. As the elderly are in general poorly immunoresponsive, different immunization strategies have to be chosen to optimize responses to vaccination. Potential strategies include the use of adjuvanted formulations, or other application routes such as intradermal administration. The group of Van Damme *et al.* compared the immunogenicity of an adjuvanted seasonal influenza vaccine administered by i.m. injection and a non-adjuvanted influenza vaccine administered by intradermal microinjection, using a pre-filled microneedle injection system (Becton Dickinson; Franklin Lakes, NJ, USA). The intradermal influenza vaccine compared favorably with the i.m. vaccine in this study – both routes were well tolerated and fulfilled the European Medicines Agency (EMA) immunogenicity criteria for influenza vaccines in the elderly [107]. Similar results were obtained using a MicronJet device (NanoPass Technologies Ltd., Nes Ziona, Israel), which is mounted on a commercial syringe, having an array of 0.45 mm long microneedles [69]. The MicronJet device from NanoPass Technologies gained FDA clearance in 2010, intended for the use of commercially available vaccines [109].

Figure 9.7: Intanza® (Sanofi Aventis, Germany), a microinjection device, was approved and released on the market for a seasonal influenza vaccine for elderly patients by Sanofi Pasteur, Lyon, France in 2009. Figure reprinted courtesy of Sanofi Pasteur MSD GmbH, Leimen, Germany.

In 2009, Intanza® (figure 9.7), also known as both ID flu® and Fluzone®, was approved and released on the market as a seasonal influenza vaccine for elderly patients administered using the BD Soluvia™ microinjection system [59, 71]. A full dose of 15 µg hemagglutinin per strain is approved for the prevention of seasonal influenza in the elderly population (aged ≥60 years), whereas a reduced dose of 9 µg hemagglutinin per strain is approved for adults up to the age of 60 years [59].

2.2.3 MICRONEEDLE ARRAYS

Microneedle arrays are small, minimally invasive devices consisting of an arrangement of micron-sized needles. In contrast to microneedles used for intradermal injection of fluids (see section 2.2.), microneedle arrays are usually solid needles coated with drug or biodegradable solid needle arrays that dissolve upon insertion.

The development of microneedle arrays for transdermal drug delivery dates back to the early 1970s, but not until the advancement of microelectronics technology in the 1990s was the preparation of microneedle arrays of defined needle sizes and lengths made possible. From the late 1990s onwards there has been rapid progress in the evaluation of different materials and approaches that can be used for microneedle array fabrication. An overview is given in table 2, showing some examples of the variety of different materials and preparation techniques that may be employed for

fabrication of microneedle arrays, as well as needle shapes and lengths, additional features, and loading procedures for drugs, antigens, or vaccines.

Microneedle arrays can be broadly divided into the following different groups: solid microneedles made from non-degradable, solid material such as titanium [110], silicon [78, 111, 112], stainless steel [113, 114] or glass [85]; and, or solid, hollow microneedles made from similar materials but being equipped with a hole in the needle center [78-80] (figure 9.8). Both types can be attached to an adhesive patch [81, 115-118]. In addition, microneedles can be made from polymers that are either degradable (such as PLG, PLGA) [86] or non-degradable (e.g. polystyrene) [85]. Lastly, self-dissolving microneedles can be prepared from sugars [87, 88, 119] or other rapidly dissolving materials [120].

The first microneedle arrays were prepared from non-degradable, solid materials. Research groups have successfully shown that microneedles of different shapes, geometries and lengths [78, 113, 121, 122] can be prepared using techniques such as chemical etching, alone or laser etching [123] followed by a cleaning technique such as electro-polishing. The importance of needle geometry for penetration efficiency and mechanical stability of the needles has also been reported. Drug loading of liquid formulations has been carried out by dip coating [113, 114], surface coating after chemical treatment of the microneedles [113], or layer coating. As dip coating is strongly influenced by factors such as the wetting behavior of the liquid on the needle surface, the viscosity of the formulation, and the surface tension, these factors have also been investigated. In order to circumvent some of the above mentioned influencing factors, needles have been pre-coated with silicon oxide or PLGA, to increase the surface energy [113]. A variety of drugs, peptides, protein, antigens and even vaccines have been coated onto solid microneedles and have been successfully tested *in vivo* [114, 124-126]. In addition to coating the drug on the microneedle surface, the simple induction of microchannels by the microneedles has also been explored and shown to result in enhanced penetration of drugs or nanoparticles.

Table 9.2: An overview of different microneedle arrays

	Solid microneedles	Hollow microneedles	Polymers	Self-dissolving microneedles
Material	Titanium [85] Silicon [78, 111, 112] Stainless steel [113, 114] Stainless steel or titanium sheets [122, 126] Glass [78, 85] Nickel [85] Copper [85]	Silicon [78] Metal [78] Glass [78, 79] Radel R (PPSU) [80]	PLGA [78, 86] Polycarbonate [85, 127] PLA [78, 128] PGA [78] PLA microneedle roller (2D array) + CMC [129] Polystyrene [85]	Maltose [87, 88, 130] Carboxymethylcellulose [128, 131] Amylopectin [128] Methylvinylether maleic anhydride (PVEIMA) [132] Sodium hyaluronate + dextran [120] Chondroitin sulphate + dextran [120, 133]
Preparation technique	Chemical etching [78] Electropolishing [113] Laser cutting [113]	Electrodeposition on polymer mold [78] Micropipette puller for glass needles [78] Plasma etching (of silicon) [134]	Micromolding [78, 129]	Molding process (e.g. for maltose), heat (140°C), followed by curing step Simultaneous formation and curing [130] Preparation of concentrated hydrogel, filling in molds followed by centrifugation [128]
Shape / Geometry	Conical Pyramidal Octagonal-pyramidal [135]	Tapered, beveled [78] Beveled [80]	Conical shape [128] Pyramidal shape [136] Beveled tip [86] Tapered cone [86]	Conical cone shape [128, 130] Tetrahedron shape [88]
Length	~ 150 µm, radius at tip ~ 1 µm [78] 430 µm 1000 µm, sharp tip [121] 700 µm [113, 126] 700 µm, 160 µm width at base [85, 114] 480-1450 µm; width 160-245 µm [122] 225, 400, 600 µm [62]	500 – 800 µm, tip 60 µm [78] 150 – 1000 µm [78] 1200 µm long, 250 µm at base [80]	600 µm height, 10 µm diameter tip [137] 200 – 500 µm [127]	1200 µm, 60 µm flat tip diameter [130] 600 µm, tip radius 100 µm [130] ~ 500 µm [88, 120, 138] 500 µm needles with a pitch of 350 µm [87] ~ 115 µm [131]
Special feature	Microneedle induced microchannels can be used for enhanced penetration of drugs or nanoparticles. Adhesive patch backing [115, 124]can be added	Enables active fluid flow Vibration of microneedle arrays used to increase microinjection, partial retraction increases flow rate [79, 80]	Biodegradable polymers are slowly degrading Microparticles incorporated into polymer microneedle [139]	Fast dissolving within 20 min [119] Tips of needles dissolved in 10 s, after 1 h microneedles fully dissolved [128] No sharp waste [130] Low cost of material [132]
Loading	Coating with liquid formulation (1) dip coating (factors: wetting behavior, viscosity, surface tension) [113, 114] (2) surface coating of stainless steel needles with silicon oxide [113] (3) surface coating with PLGA [113] (4) layer coating [113] (5) Coating with adjuvant[140]		(1) Coating with liquid formulation 2) Incorporation of drug into matrix 3) Microneedle completely made of drug (4) Casting of drug into mold followed by drying and subsequent addition of polymer [136]	(1) Incorporation of drug into matrix (2) Microneedle completely made of drug

256

Table 9.2 *(Continued)*

	Solid microneedles	Hollow microneedles	Polymers	Self-dissolving microneedles
Drug/fluorescent marker/antigen/vaccine	OVA [124] OVA, OVA + TMC [125] Oligonucleotides [81] Insulin [78, 81, 113] Protein and DNA vaccines [81] BSA [78, 113] Latex nanoparticles Plasmid DNA [111] Riboflavin [113] Virus-like particles [85, 114, 126] Influenza [141] Hepatitis B [111] Hepatitis C [142] HPV BCG [118] Desmopressin [116] Parathyroid hormone [143]	Insulin [78, 79, 81] OVA [80] Luciferase [80] DNA [80] Influenza Anthrax [144] Rabies vaccine	Calcein [127] BSA [86] Phenylephrine [137]	BSA [128] Lysozyme [128] Low molecular weight heparin [145] EPO [133, 138] Ascorbic-acid-2-glucoside [119] Ascorbate-2-glicoside [87] Sodium salicylate [87] Calcein [87, 88] Niacinamide [128] Insulin [89, 132] Sumatriptan [120] Interferon Human growth hormone (HGH) Fluvax2008 [131] OVA [131]
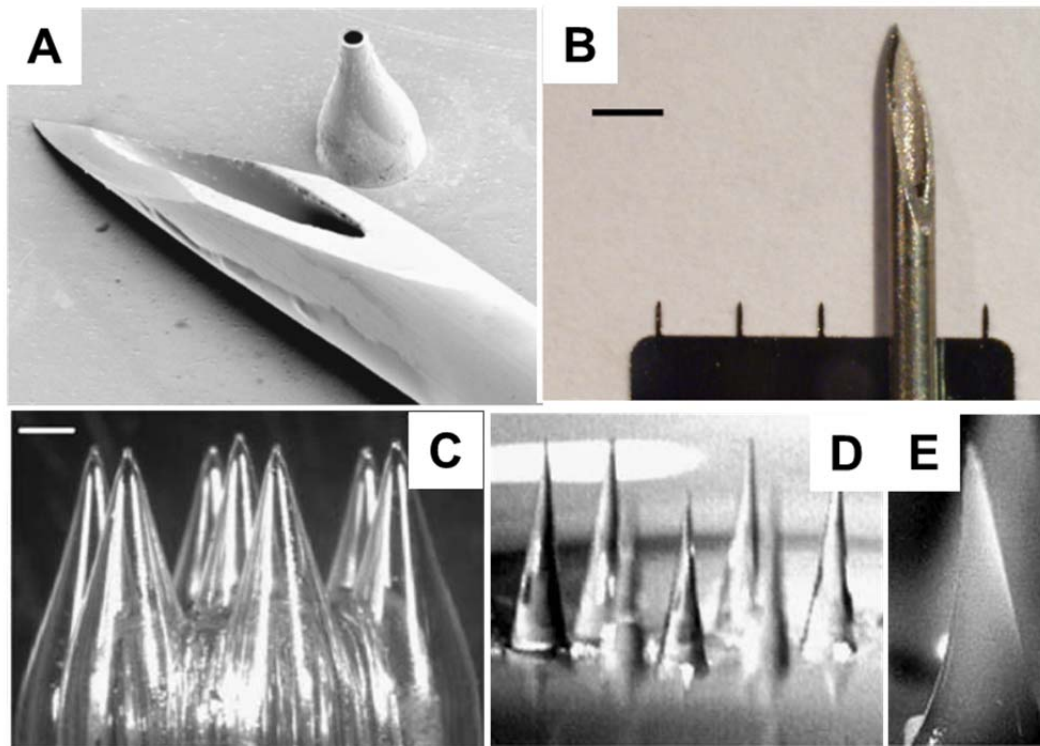
Figure 9.8: (A) Hollow microneedle (500 µm tall) formed by electrodeposition of metal onto a polymer mold next to the tip of a 27 gauge hypodermic needle. Image was adapted and reproduced with permission from Davis *et al.* [146]. **(B)** Stainless steel microneedle array fabricated using laser cutting and electropolishing next to a 20 gauge hypodermic needle (scale bar = 150 µm). Image was adapted and reproduced with permission from Kim *et al.* [147]. **(C)** Image of glass microneedles assembled into an array using epoxy resin. **(D)** Poly-lactide-co-glycolide polymer microneedle array and **(E)** poly-glycolide polymer microneedle molded from glass microneedle masters (scale bars = 100 µm).Image (C), (D) and (E) was adapted and reproduced with permission from Wang et al.[79].

Hollow microneedles have been prepared from silicon, metal, glass [78, 79, 148] or polymers [80] using either electrodeposition of a metal on a polymer by the use of a mold [78], using a micropipette puller in the case of glass needles, or etching of silicon [134]. Again, different lengths and shapes (tapered, beveled tip) [78, 80] have been prepared. The special feature of hollow microneedles is the possibility to allow for active fluid flow through the needle hole [81]. This can be even further enhanced if the needle array is partially retracted after insertion [79]. In addition, vibration of the arrays has been explored and used to increase microinjection [80]. The group of Zahn *et al.* investigated the use of polysilicon micromolding for the fabrication of hollow microneedles, allowing for the implementation of complicated geometries in the needle as well smaller, sharper and smoother microneedles [149]. Additional functionalities such as continuous micropumping are also facilitated by this

fabrication process [150]. The ability of hollow microneedle injection to penetrate the SC and deliver small molecule drugs was tested by Sivamani *et al.* [151, 152]. It was proven, that hollow glass microneedles were able to effectively penetrate the SC and deliver drugs directly into the epidermis, despite the hindrance of skin elasticity.

More detailed reviews of hollow microneedles are provided by Sivamani *et al.* [153] and Kim *et al.* [154].

Another intradermal injection system, the 3M's hollow Microstructured Transdermal System (hMTS), is a device containing 18 polymeric, hollow microneedles/cm² which is connected to a conventional glass cartridge, containing the drug reservoir. The liquid formulation is forced through the hollow microneedles by the power of a spring. The patch requires a wear time of 3 to 40 min, depending on the formulation injected. Burton *et al.* used this system to perform intradermal injections delivering small molecule salts and proteins from 0.5 ml up to 1.5 ml in domestic pigs [155]. The pharmacokinetic profiles and relative bioavailability achieved using the hMTS were comparable to profiles obtained after s.c. injection. The 3M's hollow Microstructured Transdermal System has yet not gained FDA approval.

The Macroflux® microneedle array patch is one example where solid microneedles are combined with an adhesive patch [115, 116]. Here, the drug can be coated onto the needles, and with the patch allowing for a longer residence time during which the drug can diffuse into the skin [124]. In addition, an occlusive effect of the patch on the skin can be observed. The effect of microneedle pore closure with and without occlusion has been investigated, with pore closure being found to occur more quickly under non-occlusive conditions [156, 157]. A variety of polymers have been used for the preparation of microneedle arrays, including the biodegradable polylactic acid (PLA) [78, 119], polylactic-co-glycolic-acid (PLGA) [86], polyglycolic acid (PGA) [78] as well as non-biodegradable polymers such as polystyrene [85]. These microneedles can be prepared by micromolding, which allows for the preparation of different needle lengths and shapes [86, 136]. In contrast to solid microneedles prepared from titanium, stainless steel, or silicon, the drug can not only be dip-coated onto the needle, but also directly incorporated into the needle matrix. In addition, needles can be prepared from drug, or microparticles can be incorporated into the polymer microneedle [86].

The largest and fastest growing group of microneedle arrays investigated in the last years is the group of self-dissolving needles. These can be prepared from sugar or sugar derivatives such as maltose [87, 88, 119], carboxymethylcellulose [131], or amylopectin. These needles have the obvious advantage that they dissolve rapidly within minutes after insertion into the skin, leaving no sharp waste to be disposed of [130]. The material for preparation of self-dissolving needles can be obtained at low cost [132], and many excipients employed in the preparation process are already used in pharmaceutical products without any safety concerns. Additionally, if the self-dissolving needles break upon insertion, no residuals will remain in the skin due to the fast dissolution of the material. The drug to be administered can be incorporated directly into the matrix, or microneedles can be prepared consisting theoretically solely of drug. Again, factors such as mechanical stability must be kept in mind when preparing needles using such readily degradable substances. Some preparation procedures require a curing step to achieve sufficient mechanical stability, which may result in volume loss of the needle and may complicate the production process.

The group of Bal *et al.* investigated the immunization efficiency of N-Trimethyl chitosan (TMC) adjuvanted diphtheria toxoid (DT) vaccines in mice before and after microneedle treatment of the skin [158]. The vaccine was formulated either as solution or DT was loaded onto TMC nanoparticles. Alum adjuvanted DT served as a positive control and was applied s.c. Two different types of microneedles were used, either microneedles that were manufactured from commercially available 30G needles or stainless steel microneedles prepared by electrical discharge machining. Both, TMC/DT nanoparticles as well as the solution induced equally strong immune responses as the positive control, independent of the microneedle array used or the sequence of the microneedle treatment. However, 8-fold higher IgG titers were obtained after immunization with the TMC/DT solution in comparison to the TMC/DT nanoparticles. It was discussed that the distribution of the TMC/DT solution was broader compared to the TMC/DT nanoparticles due to electrostatic interactions between the positively charged nanoparticles and the negatively charged skin, leading to a blockage of the conduits which were formed by the microneedles. Similar results were obtained by Ding *et al* after immunization of mice against diphtheria toxoid combined with several adjuvants after microneedle array pre-treatment [159]. A 1000-fold increase of diphtheria toxoid specific serum IgG levels were obtained after microneedle array pre-treatment compared to administration of the vaccine onto

intact skin. A further enhancement of the immune-response could be obtained by co-administration of adjuvants such as lipopolysaccharides, Quil A, CpG oligodeoxynucleotide or cholera toxin. Contrary to the use of DT, the application of influenza vaccine onto intact skin as well as on skin pre-treated with microneedles failed to evoke appropriate immune responses [141]. The group of Hiraishi *et al.* demonstrated that vaccination of guinea pigs using a BCG vaccine coated microneedle array patch resulted in robust antigen-specific cellular immune responses, comparable to those induced by traditional intradermal BCG vaccination using a 26G needle [118]. Immunogenicity of microneedle patches coated with 4 µg of an influenza virus like particle (VLP) vaccine in mice was investigated by the group of Kim *et al* [85]. Virus specific IgG was significantly increased after immunization using the microneedle patch in comparison to naïve mice and was further enhanced in the case of vaccine formulation coatings, which were stabilized with trehalose. After challenge with a lethal dose of the influenza virus only those mice survived, which were immunized with trehalose-stabilized influenza VLP coated microneedles. These results point out that the stabilization of the coated vaccine is crucial in order to preserve the protective efficacy of the vaccine.

In summary, a large number of drugs, proteins, model antigens and vaccines have been tested with regards to the physical/chemical stability of the microneedle array and/or the bioactive, together with the effect *in vivo* [67, 108, 114, 125, 126, 142, 147, 158-164]. Microneedle arrays are a promising novel device, targeting the intradermal layer of the skin.

2.2.4 TATTOO DEVICES FOR VACCINATION

The use of tattoo devices to introduce DNA and peptide vaccines into the dermal layer of the skin has been investigated as a new approach for puncture-mediated gene transfer [72-77].

For this purpose a short needle or a bundle of needles oscillate at high frequency, thereby puncturing the skin and introducing the vaccine formulation. The major advantage of this technique would be that the vaccine is distributed over a large surface area, which is thought to facilitate the transfection of a broad cell population.

The group of van den Berg *et al.* determined the influence of several tattoo setting parameters on antigen expression and transfection efficiency in an *ex-vivo* human

skin model, in order to optimize this technique for clinical application. An increase in needle depth, tattoo duration time, and DNA concentration were seen to lead to an increase in antigen expression, although the transfection efficiency was very low [72]. Pokorná *et al.* delivered human papillomavirus type 16-derived peptides adjuvanted with CpG motifs by the use of a tattoo device, and compared the immune responses to s.c. delivered peptides or gene gun mediated transfection. Vaccine delivery by tattooing elicited higher specific cellular and humoral immune responses than s.c. needle injection. DNA tattoo vaccination stimulated immunity comparable to immunizations delivered by the gene gun, however a 10-fold higher dose was used for tattoo vaccination in comparison to gene gun delivery [75]. Quaak *et al.* investigated the potential for damage to a DNA vaccine as a result of the tattoo procedure. The authors observed a reduction of only 3% of the supercoiled pDNA content and formation of open circular pDNA; the impact on the induction of immune responses was marginal [77].

With regard to patient compliance, it is very questionable if tattooing will be widely accepted given that it causes local tissue damage and involves a painful and complex vaccination procedure.

2.2.5 LIQUID JET INJECTORS

Jet injectors were developed in the 1930s and have been used in human mass vaccination programs for measles, polio and smallpox for over 50 years [33, 82]. The first generation of liquid jet injectors was developed for multiple uses. Major drawbacks of the multi-use-nozzle were safety hazards like the transmission of blood borne diseases, e.g. hepatitis B [165]. Therefore, new generations of jet injectors have disposable cartridges in order to avoid cross-contamination.

The mechanism of liquid jet injectors relies on the principle of forcing fluids through a small orifice, generating a high pressured stream that penetrates into the skin with high velocity of approximately 100 m/s. The impact of the fluid on the skin generates a hole through which the liquid is forced into the tissue [166]. The actuation of the jet injector can either be spring-powered, harnessing the relaxation of a spring, gas-powered using pressurized carbon-dioxide or helium gas, or pyrotechnically driven [167, 168]. The delivery of a liquid vaccine formulation by a liquid jet injector can be divided into three general stages. At first a peak pressure phase is observed,

followed by the delivery or dispersion phase, and concluding with the drop-off phase [169]. During the first stage, when the first stream of liquid pierces the skin, small amounts of the liquid can splash back and leave some product residues on the skin surface. While any resulting loss of vaccine is negligible, such an occurrence may serve to alert the operator to an incorrectly performed administration. The second stage provides a wide dispersion of the liquid into the tissue as it forces a path through low resistance regions [170]. The depth and shape as well as the completeness of the injection is dependent on several technical parameters such as the stand-off distance of the device from the skin, the nozzle diameter, the velocity of the liquid stream, the mechanical properties of the skin, and the properties of the liquid formulation including volume, viscosity and surface tension [82, 166, 171]. It has been found, that for the velocity of the liquid stream, a threshold value of at least 60 to 80 m/s must be reached in order to achieve penetration into the skin. For a complete optimal penetration the velocity of the liquid stream has to be approximately 150 m/s [166].

Conflicting opinions exist as to whether the equal or even enhanced immune response evoked by the use of liquid jet injectors in comparison to i.m. injections can be attributed to the large dispersion pattern of the vaccine and the targeting of more APCs located in the superficial layers of the skin [9, 33, 172-175]. Also the possibility of a slight inflammation at the injection site might be the reason for enhanced immune responses [7, 173, 176]. However, liquid administered by a liquid jet injector is flushed through the epidermal and dermal layer of the skin down to the subcutaneous fatty tissue, and even to the muscular tissue. Hence, depending on the site of the delivery, an effective targeting of LC might not be reached, as such cells are generally resident in the epidermal layer of the skin [44].

Immunogenicity of a malaria DNA vaccine in rabbits after intramuscular injection using a needle and syringe or intramuscular and intradermal jet injection using a Biojector™ 2000 (Bioject Inc., Portland, OR, USA) device was investigated by the group of Aguiar *et al.* [177]. Enhanced immune responses were observed using the jet injection device in comparison to i.m. needle-injection. Similar antibody responses were observed comparing i.m. or a combination of i.m. and intradermal jet injection, suggesting that both application methods are equivalent.

Fractional doses of an inactivated poliovirus vaccine were given to children in Oman using either the Biojector™ 2000 (Bioject Inc., Portland, OR, USA) device, which was additionally equipped with a spacer for intradermal administration, or the full dose of the vaccine using a conventional needle and syringe system for i.m. administration [40]. Similar levels of seroconversion were achieved after the intradermal vaccination with fractional doses as after i.m. vaccination with the full dose. However, significantly lower median titers were found in the fractional dose group in comparison to the full dose group. In contrast to this study significantly lower seroconversion rates were found after immunization with fractional doses of an inactivated poliovirus given intradermally with the Biojector™ 2000 -device, equipped with an intradermal spacer, in comparison to the full dose given i.m. [41].

The Biojector™ 2000 has FDA clearance for i.m. and s.c. injection of liquid medicines, including vaccines; however intradermal injections are at the moment just performed in clinical trials.

The possibility to deliver polystyrene and PLGA polymer particles into the skin by liquid jet injection using a Vitajet 3® device (Bioject Medical Technologies Inc., Tualatin, OR, USA) was explored by Michinaka *et al.* [83]. It was found that the effectiveness of particle penetration into the skin was proportional to the injection volume. The dispersion area of the polystyrene particles was also observed to decrease with increasing particle size.

Needle-free jet-injection devices have some drawbacks in comparison to the use of a needle-syringe system. These include higher costs per unit, the need for maintenance of multi-use devices, and a greater complexity of the device in comparison to needle and syringe systems. Drawbacks of spring-powered devices are the limited range of force and versatility, which do not take into account the broad differences in skin thickness occurring as a function of gender and age; gas-powered devices also have a distinct disadvantage as they are dependent on an exhaustible energy source [169].

A further disadvantage of liquid jet injection is that pain is caused, both by penetration of the liquid into deeper skin layers and by disturbance of sensory nerve endings. Blood vessels may also be disrupted as a result of liquid jet administration, meaning that bleeding can occur. Local reactions like swelling, erythema, hematoma and pain have been reported after vaccination with liquid jet injectors, however the

occurrence of these adverse effects might also be dependent on the type of vaccine administered and the presence of adjuvants in the formulation [61, 172, 174, 178].

It has also been discussed, whether shear forces, generated as a result of forcing liquid through a small orifice, could damage the administered product. The group of Benedek *et al.* investigated the effects of liquid jet injection using the Iject® system (Bioject Inc., Portland, OR, USA) on different model proteins, with a particular focus on degradation and aggregation. No damaging effects were observed for the selected proteins using the Iject® device. However, these results cannot be generalized to all vaccine formulations or to all jet injector devices – each device and vaccine formulation must be evaluated individually [84]. The Iject® device as well as the Vitajet 3® device from Bioject Medical Technologies Inc. are not readily available and proposed only for investigational use.

The spring powered PharmaJet® device (PharmaJet Inc., Golden, CO) has been used for s.c./ i.m. vaccination of pigs, administering a DNA vaccine against swine influenza [179]. In comparison to the i.m. vaccination applying a conventional needle and syringe injection, the needle-free delivery method using PharmaJet® elicited improved immune responses and comparable post-challenge results.

In 2011 PharmaJet® Inc. (Golden, CO) gained FDA marketing clearance for their 0.1 ml intradermal needle-free injection system [180]. This device can be used with standard off-the-shelf licensed vaccines.

Major advantages of the liquid jet injection technique are the eradication of hazards associated with needle-stick injuries, as all devices provide a needle-free injection technique; the potential of liquid jet injections for mass vaccination campaigns using existing, approved liquid vaccines is also a considerable positive factor [169].

2.2.6 BALLISTIC INJECTORS

In comparison to liquid jet injectors, ballistic injectors do not accelerate a liquid stream towards the skin, but dry, solid particles.

GENE GUN

The first "gene gun" for particle mediated gene transfer was developed in 1987 by Sanford and colleagues [90]. Initially, the gene gun was used to deliver DNA coated metal particles of 1 µm diameter into plants in order to modify these genetically. In the early 1990s, conventional vaccines and DNA vaccines were delivered to humans using the gene gun [91, 92]. A commercially available bench top device, the so called Helios device (Bio-Rad, Hercules, CA, USA), is mainly used for genetic immunization research and is restricted to research purposes. An adjustable helium pulse of 100 to 600 psi propels DNA-coated gold microparticles from the inner wall of a Tefzel™ tubing system and accelerates them towards a target. Several parameters of the target bombardment process have to be optimized in order to enhance transfection efficacy and avoid tissue damage.

Amongst other parameters, the helium pulse and several particle preparation conditions must be adjusted experimentally depending on the target. In addition, cells containing gold particles may undergo cell death, thereby limiting the effectiveness of gene gun-mediated immunization. The costs and complexity of the gene gun prohibits its use as a vaccination device for clinical human use or in mass vaccination programs.

DEVICES AND VACCINE CARRIER PARTICLES FOR PARTICLE-MEDIATED EPIDERMAL DELIVERY (PMED) AND EPIDERMAL POWDER IMMUNIZATION (EPI)

The following section gives an overview of different devices utilized for PMED, i.e. injecting gold particles into the skin or for EPI, where vaccine/sugar particles are injected into the skin. A brief summary of preclinical and clinical studies applying these techniques is also given.

On the basis of the gene gun principle, PowderMed Vaccines Inc. (former PowderJect, acquired by Pfizer in 2006) and the Bellhouse group at Oxford University have developed the PowderJect XR device. This is a multi-use research

device that has been used in several preclinical trials, suitable for PMED. The device is dependent on an external power and gas source [91]. The device is actuated by pressing a trigger, thus opening an electric solenoid valve that controls the release of pressurized helium from an external tank. A disposable plastic nozzle containing the vaccine cartridge is attached with a snap lock on the device. The vaccine is precipitated onto gold particles, which are resuspended in ethanol and filled into the tubing of the vaccine cartridge. After drying, the gold particles cover the inner walls of the tubing [93]. Upon release of the pressurized helium gas, vaccine coated gold particles are entrained in the gas flow, removed from the tubing of the vaccine cartridge and accelerated to high velocities.

Convergent-divergent supersonic nozzle (CDSN) devices

The same Oxford University group has also developed a hand-held, single use, disposable device which is suitable for clinical research and the delivery of vaccine powders for EPI, the PowderJect ND device. The design of the nozzle is convergent – divergent (Laval nozzle), which allows for acceleration of the vaccine particles to supersonic speed. [94]. This device comprises a cartridge with pressurized helium or nitrogen of 2-6 MPa and a vaccine cassette made up of two rupture polyurethane or polycarbonate membranes of approximately 20 µm thickness. The vaccine cassette can hold a powdered payload of approximately 0.5- 5 mg [94]. Upon actuation of the delivery device, the compressed helium rapidly expands, rupturing the diaphragms of the vaccine cassette and drawing the particles into the helium gas flow. The particles are propelled down the convergent-divergent nozzle towards the skin with high velocity. A silencer, attached around the nozzle, dampens the noise level by laterally venting the gas. The forward momentum of the particles allows them to penetrate into the superficial layers of the target skin site [58, 181-183].

Investigations of the gas and particle dynamics of this device revealed that after the starting process the emergent gas flow undergoes flow separation before converting to a quasi-steady supersonic flow. Large variations in gas density and velocity induce non-uniformities in the resulting particle velocity, which ranges from 200 m/s to 800 m/s. Inconsistent spatial particle distributions are a further result of gas density and velocity variations [95, 184, 185].

Contoured shock tube (CST) - devices

The convergent-divergent nozzle design of the first prototype devices was replaced by a CST design (figure 9.9) enabling the acceleration of vaccine particles to more uniform velocity (> 700 m/s [96]) and spatial particle distribution. Employing this approach led to drastic reduction in variations in the free-jet particle velocity at the device exit [95].
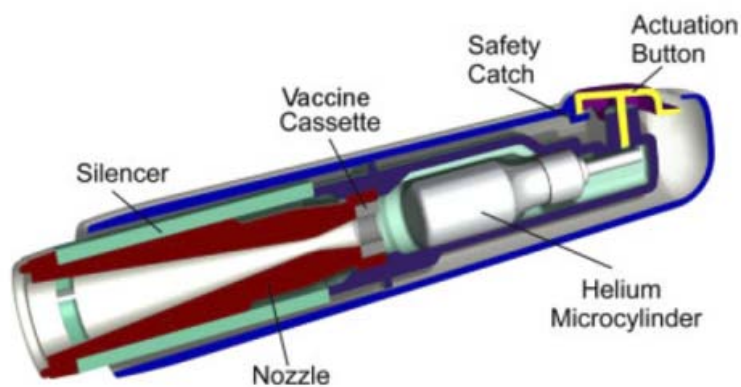
Figure 9.9: Hand-held PowderJect device with a convergent-divergent supersonic nozzle design. Figure reprinted from Liu Y *et al.* [186].

One of the drawbacks of a vaccine cartridge comprising rupture membranes is the potential risk that fragments of the sealing membranes are incorporated together with the particles in the gas flow and are also accelerated towards the target. However, no damage to the target was found as a result of membrane fragments in *in vitro* and *in vivo* experiments [187].

Another initial disadvantage of the CST device was the noise level of the device. A silencer was therefore attached around the nozzle [95]. The addition of a silencer and the creation of a standing-off shock wave in the impingement region reduced the particle impact velocity from 699 ± 4.7 m/s as simulated in a free jet to 504.5 ± 64.46 m/s [186, 188].

Additionally drawbacks, such as unsatisfactory spatial particle distributions with particle overload in the central target area, and the entrapment of considerable volumes of vaccine powder on the rupture membranes and on the inner walls of the device, led to further optimization of the device and vaccine cartridge design [98, 99, 185].

Venturi devices

The development of devices called Venturi devices has been described by Liu and co-workers [97-99]. In this setup, the vaccine particles are not enclosed in polycarbonate membranes but are loosely packed in the cavity of the device. Upon actuation a high speed gas flow is generated that carries the particles down a conical nozzle. The authors state that the Venturi device provides more uniform velocity distributions compared to earlier developed devices. The computed particle velocities in a free jet covered a range from 400 – 800 m/s, with a mean velocity of 654.4 m/s ± 11.96 m/s [98].

Gold particles for PMED

Different physical particle characteristics such as size, density, shape and morphology determine whether particles are able to breach the SC of the skin and have an influence on the penetration depth of the particles. A tight mono-modal particle distribution as well as a high rigidity of the particles is necessary for efficient and targeted particle delivery.

Gold particles of 1-3 µm in size have a high density and can be introduced into the skin by ballistic injection. These particles are mainly deposited intracellularly [189]. For the delivery of DNA vaccines, gold particles are generally used for direct targeting of immunocompetent cells in the epidermal layers of the skin [91, 190, 191]. Deceleration of the particles within the tissue leads to stress and shock waves within the tissue. Direct impact of the gold particles can result in cell death [187, 192].

Proponents of PMED vaccination emphasize that PMED is a quick and easy procedure, applicable for all types of cell targeting and requiring only small amounts of DNA. However, the amount of DNA that can be precipitated onto the gold particles is limited by the surface capacity of the particles. Gold particles tend to agglomerate if higher amounts of vaccines are used. Furthermore, dependent on the type of DNA vaccine, the amount of DNA delivered within one payload might not be sufficient to evoke an appropriate immune response and therefore multiple shots at multiple

delivery sites may be necessary [183, 190, 193]. Advantages of the PMED method using gold particles are that with one vaccine particle payload a large number of cells are directly targeted. This offers higher transfection efficiency, unlike other approaches that perfuse the extracellular space with liquid vaccine formulation [91, 194, 195]. The use of gold particles as carrier particles may also prove too costly for mass vaccination campaigns.

Preclinical and clinical studies applying PMED

Tacket *et al.* investigated the safety and immunogenicity of a DNA vaccine encoding for hepatitis B surface antigen delivered by a PowderJect XR1 device in a phase I study to seven healthy volunteers [193]. Two administrations of vaccine were given onto two skin sites on the posterior upper arm, choosing one of three different helium pressure levels of the PowderJect XR1 device. The schedule was repeated after 56 days. Local site reactions appeared within minutes following vaccine delivery, their severity correlated to the used helium pressure level. Local site reactions generally lasted for minutes, with a faint area of erythema persisting for 56 days in some volunteers. No primary immune responses were observed.

The dose-response relationship of hepatitis B virus DNA vaccine coated on gold microparticles and administered using the PowderJect device was investigated by the group of Roy *et al.* All three dose levels (1, 2 or 4 µg) administered at two to four delivery sites induced protective antibody responses and proliferation of antigen specific CD8$^+$ and CD4$^+$ T cells after three immunization intervals [183]. Rottinghaus *et al.* found similar results when comparing a Hepatitis B DNA vaccine to a conventional vaccination in non-responders [196]. Chen *et al.* demonstrated that skin bombardment with antigen coated gold particles using the PowderJect XR1 device was able to induce both augmented antibody and CTL responses against several viral protein antigens in mice. Histological examinations of the skin vaccination sites revealed intracellular localization of the gold particles in keratinocytes and also in LCs in the draining lymph nodes. In a skin target area of approximately 113 mm² approximately 50% of the LCs were directly targeted [189].

A prophylactic nucleic acid vaccine against Hepatitis B virus was coated on gold particles and delivered using either a PowderJect XR-1 device or the commercial prototype device ND 5.5. The vaccine was administered as a single boost in previously immunized healthy adults. A 2 µg amount of DNA was precipitated onto 1 mg gold particles and was administered to two or four skin sites, resulting in a total

dose of 4 µg or 8 µg DNA respectively. Both devices demonstrated similar performance and were able to boost both antibody and cell-mediated immune responses [93].

A dose escalation trial was conducted by the group of Drape *et al.* evaluating a monovalent influenza DNA vaccine delivered by PMED. All three dose levels studied led to serum haemagglutination inhibition (HAI) antibody responses. However, only the highest dose level, administered four times, met the requirements of the Committee for Proprietary Medical Products (CPMP) [197].

Powdered sugar particles for EPI

In addition to gold particles, vaccine antigen can also be delivered in the form of powdered sugar particles. In this case vaccine antigen is mixed with excipients like trehalose, mannitol or dextran and formulated into dry particles by applying different processes such as spray drying, spray freeze-drying, freeze-drying, spray coating or simple desiccation [198-203]. Applying freeze-drying or desiccation requires a subsequent pulverizing step where particle sizes are reduced to diameters of 20 to 70 µm [182, 199]. As in the case of gold particles, the powdered sugar particles are accelerated to high velocities by the use of appropriate ballistic devices in order to penetrate the superficial layers of the skin. Sugar particles are generally larger in size, approximately 20-70 µm or 25-100 µm, as compared to gold particles. Larger sizes are used to achieve the necessary impact to penetrate skin due to their lower density (~700-1,200 kg/m³) compared to gold [204, 205].

Due to their size and high water solubility, sugar particles are predominantly deposited in the extracellular region, and dissolve rapidly [190]. Antigen entrapped within these particles can therefore be endocytosed by immunocompetent APCs in targeted tissue.

Advantages of powdered sugar particles include a cheap and easy manufacturing process, a high loading capacity of the sugar matrix with vaccine antigen, and the ability to store the formulation at room temperature without cooling [15]. However, as mentioned above sugar particles have a markedly lower density (~1,000 kg/m³) in comparison to gold particles [206], which may hinder ballistic delivery. Furthermore, the hygroscopicity of the sugar particles requires gas-tight packaging of the vaccine cartridge.

Preclinical and clinical studies applying EPI

Chen *et al.* investigated the immunogenicity of an influenza vaccine and protection responses induced following challenge in a mouse model [182]. The vaccine was formulated with trehalose and prepared by desiccation, grinding and sieving in order produce powder particles of 20 to 53 µm in size. The powdered vaccine particles were administered using a PowderJect ND device, and the results were compared to conventional i.m. or s.c. injection. Prime immunization using powder injection elicited higher serum immunoglobulin titers to influenza virus than i.m. or s.c. injection. After boosting, the powder immunization elicited antibody titers 300% and 700% higher than after boosting by i.m. or s.c. injection. Challenge experiments showed that EPI also resulted in protection against mortality, weight loss and virus replication in the lungs of the mice [182].

In a phase I clinical trial, a trivalent influenza vaccine was administered by EPI using the PowderJect ND5.2 device and compared to conventional i.m. injection. The powdered vaccine was prepared by spray freeze-drying, and contained 45 µg haemagglutinin (HA)/ mg powder. Subjects received EPI on either one or two skin sites. Strong antibody responses were elicited using EPI, meeting the requirements of the CPMP. Results were comparable to i.m. injection. Local site reactions like erythema, petechiae, oedema and skin discoloration were prominent after EPI [58].

The immunogenicity of recombinant envelope protein gp20 (rgp120), a human immunodeficiency virus (HIV) component, was investigated, following either precipitation onto gold particles or formulation together with trehalose as powder particles. Both such formulations were administered to mice by EPI, and compared to conventional administration via i.m. injection. Higher antibody responses were achieved as a result of HIV rgp120 administration by EPI in comparison to i.m. injection. Trehalose-formulated rpg120 powder particles induced IgG_1 antibody responses, whereas rpg120 precipitated onto gold particles induced IgG_1, IgG_{2a} and IgG_{2b} subclass antibody responses and CTL responses. The type of vaccine formulation as well as the deposition of the particles (intra- or extracellular) may have an impact on the observed differences in immune responses [207]. Osorio *et al.* demonstrated that administration of hepatitis B surface antigen (HBsAg) in mice via EPI resulted in superior immune responses in comparison to i.m.-injected, non-adjuvanted HBsAg. Similar immune responses were obtained in comparison to alum-adjuvanted HBsAg injected i.m.   Adjuvantation of HBsAg with CpG DNA and

administration by EPI induced more efficient immune responses than a corresponding i.m. injection, and resulted in activation of T-helper cells [208]. Ballistic injectors have not gained regulatory approval for use in humans but are widely used in preclinical and clinical studies.

2.3   TECHNICAL AND REGULATORY CHALLENGES

Several technical challenges have to be overcome in order to bring a novel device targeting the intradermal layers of the skin to the level of clinical studies, and further to market release. Firstly, the device must reach the targeted region - the intradermal tissue with resident immunocompetent LCs. The potential for dose-sparing by intradermal delivery has to be determined case-by-case, for each individual vaccine and corresponding delivery device, so that adequate immunogenicity and sufficient protection is ensured. For optimal patient acceptance and widespread use, for example in mass vaccination programs, the device should be easy and intuitive to use, and should be effective for delivery to a variety of patient groups with different skin types (children, adults and people with different ethnical heritage). Furthermore, the device has to be competitive in terms of cost with conventional vaccination systems such as needles and syringes. In order to facilitate regulatory approval, it is advantageous if the device permits the use of standard off-the-shelf licensed vaccines. In this case, an application for marketing clearance may be made for the device under the regulations of the medical device directive, a pre-market notification (510(k)) or pre-market approval (PMA). In such a case, it must be proven that the vaccine is compatible with the injector, and that the use of the device in question will not change the characteristics of the marketed vaccine. In some cases it might be necessary to concentrate the vaccine so that it can be delivered in a reduced volume appropriate for intradermal injection (around 100 µl per dose). Such reformulations as well as the use of fractional doses of vaccines would require a licensing amendment. If the injector is intended for use with a specific vaccine formulation, and is therefore pre-filled or co-packaged with that product, a new drug application (NDA) or biological licensing application (BLA) is required for FDA clearance. Furthermore, it has to be defined if the injector is intended for self-administration, or use by a health care provider, and if the device is designed for single-use or can be reused.

2.3.1 Issues and challenges surrounding the stability of vaccines

Dry powder vaccine formulations can offer improved stability [15, 209, 210], opening up the possibility for independence from cold-chain transport and storage. However, approved vaccines are mostly provided as liquid formulations. Microinjection devices, liquid jet injectors and hollow microneedles can be used with approved liquid vaccine formulations, whereas a reformulation of the vaccine is required for solid microneedles and ballistic delivery of dry powders. Significant research has to be undertaken in order to stabilize vaccines coated on microneedles [147] or to develop dry powders for ballistic injection which are capable of achieving regulatory clearance.

2.4 CONCLUSION

Delivery systems targeting the skin have attracted growing attention during the last years. Needle-free delivery systems are associated with significant advantages, particularly with regard to safety issues and application in mass vaccination programs. Also, the potential for vaccine dose reduction by targeting the intradermal layers of the skin strengthens the position of intradermal vaccination devices and offers savings in delivery costs and coverage of a broad population with vaccines in limited supply. An effective targeting of immunocompetent cells in the epidermal layer of the skin has been made possible due to considerable progress in device development. Even though the potential of needle-free injections and the targeting of the epidermal layer of the skin is the focus of a lot of research groups, only a few delivery devices have progressed to clinical trials and are currently approved for commercial use.. These include devices which are compatible with existing liquid or lyophilized formulations, such as the liquid jet injector PharmaJet[®], the MicronJet[®] device, and the intradermal microinjection system BD Soluvia[®].

So far, there is no device approved for intradermal vaccination delivering a dry solid vaccine, although promising development in this field has been made by PMED and EPI techniques. Dry solid vaccine formulations offer considerable advantages, in terms of enhanced stability and the potential for cold chain independency. The ability to deliver such vaccines via an intradermal device may therefore be preferable to delivery of liquid vaccine formulations by conventional needles and syringes.

However, reformulation of existing vaccines might be required using solid injection systems.

Recent technologies like tattoo vaccination are not likely to surpass the experimental stage, as they are associated with a painful and complex vaccination procedure.

Microneedle arrays are still in a development process but encouraging data has been reported. Operational challenges like the reproducibility of the coating procedure and of antigen delivery must be overcome in order to gain regulatory approval for such systems.

In conclusion, while there has been considerable development of intradermal vaccination devices in the past years, there is still a need for further improvement to the design of devices for intradermal administration in order to fulfil their potential to be competitive with conventional needle and syringe forms of administration.

Acknowledgements

2.5 REFERENCES

[1]   Payette PJ, Davis HL. History of Vaccines and Positioning of Current Trends. Current Drug Targets - Infectious Disorders 2001;1(3):241.

[2]   Jenner E. Two cases of Small-Pox Infection communicated to the Foetus in Utero under peculiar circumstances, with additional remarks. Med Chir Trans 1809;1:271-7.

[3]   Jenner E. An Inquiry into the Causes and Effects of the Variolae Vaccinae, A disease discovered in some of the western counties of England, particularly Gloucestershire, and known by the name of the Cow Pox. In. London. Sampson Low 1798.

[4]   Levine MM. Can needle-free administration of vaccines become the norm in global immunization? Nature Medicine 2003;9(1):99-103.

[5]   Dowdle W. The principles of disease elimination and eradication. Bulletin of the World Health Organization 1998;76 Suppl 2:23-5.

[6]   Heymann DL, Aylward LB. Perspective – Global health: eradicating polio. N Eng J Med 2004;351:1275-7.

[7]   Lambert PH, Laurent PE. Intradermal vaccine delivery: Will new delivery systems transform vaccine administration? Vaccine 2008;26(26):3197-208.

[8]   WHO. Saftey of Injections:Global Facts and Figures. World Health Organization, Geneva: World Health Organization, 2004.

[9]   Mitragotri S. Immunization without needles. Nature Reviews Immunology 2005;5(12):905-16.

[10]   Banchereau J, Steinman RM. Dendritic cells and the control of immunity. Nature 1998;392(6673):245-52.

[11]   Mishra D, Mishra PK, Dubey V, Dabadghao S, Jain NK. Evaluation of uptake and generation of immune response by murine dendritic cells pulsed with hepatitis B surface antigen-loaded elastic liposomes. Vaccine 2007;25(39-40):6939-44.

[12]   Warger T, Schild H, Rechtsteiner G. Initiation of adaptive immune responses by transcutaneous immunization. Immunol Lett 2007;109(1):13-20.

[13]   Combadière B, Mahé B. Particle-based vaccines for transcutaneous vaccination. Comparative Immunology Microbiology and Infectious Diseases 2008;31(2-3):293-315.

[14]   Toebak MJ, Gibbs S, Bruynzeel DP, Scheper RJ, Rustemeyer T. Dendritic cells: biology of the skin. Contact Dermatitis 2009;60(1):2-20.

[15]   Amorij J-P, Hinrichs WLJ, Frijlink HW, Wilschut JC, Huckriede A. Needle-free influenza vaccination. Lancet Infectious Diseases 2010;10(10):699-711.

[16]   Stoitzner P, Sparber F, Tripp CH. Langerhans cells as targets for immunotherapy against skin cancer. Immunol Cell Biol 2010;88(4):431-7.

[17]   Auewarakul P, Kositanont U, Sornsathapornkul P, Tothong P, Kanyok R, Thongcharoen P. Antibody responses after dose-sparing intradermal influenza vaccination. Vaccine 2007;25(4):659-63.

[18]   Belshe RB, Newman FK, Cannon J, Duane C, Treanor J, Van Hoecke C, et al. Serum Antibody Responses after Intradermal Vaccination against Influenza. The New England Journal of Medicine 2004;351(22):2286-94.

[19]   Belshe RB, Newman FK, Wilkins K, Graham IL, Babusis E, Ewell M, et al. Comparative immunogenicity of trivalent influenza vaccine administered by intradermal or intramuscular route in healthy adults. Vaccine 2007;25(37-38):6755-63.

[20]   Brown H, Kasel JA, Freeman DM, Moise LD, Grose NP, Couch RB. The Immunizing Effect of Influenza A/New Jersey/76 (Hsw1N1) Virus Vaccine Administered Intradermally and Intramuscularly to Adults. J Infect Dis 1977 December 1, 1977;136(Supplement 3):S466-S71.

[21]   Bryan JP, Sjogren MH, Macarthy P, Cox E, Legters LJ, Perine PL. Persistence of antibody to hepatitis B surface antigen after low-dose, intradermal hepatitis B immunization and response to a booster dose. Vaccine 1992;10(1):33-8.

[22]   Carcaboso Á, Hernández R, Igartua M, Rosas J, Patarroyo M, Pedraz J. Enhancing Immunogenicity and Reducing Dose of Microparticulated Synthetic Vaccines: Single Intradermal Administration. Pharmaceutical Research 2004;21(1):121-6.

[23]   Halperin W, Weiss WI, Altman R, Diamond MA, Black KJ, Iaci AW, et al. A comparison of the intradermal and subcutaneous routes of influenza vaccination with A/New Jersey/76 (swine flu) and A/Victoria/75: report of a study and review of the literature. American Journal of Public Health 1979 December 1, 1979;69(12):1247-51.

[24]   Herbert FA, Larke RPB, Markstad EL. Comparison of Responses to Influenza A/New Jersey /76-A/Victoria/75 Virus Vaccine Administered Intradermally or Subcutaneously to Adults with Chronic Respiratory Disease. Journal of Infectious Diseases 1979 August 1, 1979;140(2):234-8.

[25]   Kenney RT, Frech SA, Muenz LR, Villar CP, Glenn GM. Dose sparing with intradermal injection of influenza vaccine. The New England Journal of Medicine 2004;351(22):2295-301.

[26]   Kurugöl Z, Erensoy S, Aksit S, Egemen A, Bilgiç A. Low-dose intradermal administration of recombinant hepatitis B vaccine in children: 5-year follow-up study. Vaccine 2001;19(28-29):3936-9.

[27]   Egemen A, Aksit S, Kurugöl Z, Erensoy S, Bilgiç A, Akilli M. Low-dose intradermal versus intramuscular administration of recombinant hepatitis B vaccine: a comparison of immunogenicity in infants and preschool children. Vaccine 1998;16(16):1511-5.

[28]   Pancharoen C, Mekmullica J, Thisyakorn U, Kasempimolporn S, Wilde H, Herzog C. Reduced-Dose Intradermal Vaccination against Hepatitis A with an Aluminum-Free Vaccine Is Immunogenic and Can Lower Costs. Clinical Infectious Diseases 2005;41(10):1537-40.

[29]   Playford EGM, Hogan PGP, Bansal ASDM, Kareena Harrison BN, Drummond DM, Looke DFMM, et al. Intradermal Recombinant Hepatitis B Vaccine for Healthcare Workers Who Fail to Respond to Intramuscular Vaccine. . Infect Control Hosp Epidemiol 2002;23(2):87-90.

[30]   Propst T, Propst A, Lhotta K, Vogel W, Konig P. Reinforced intradermal hepatitis B vaccination in hemodialysis patients is superior in antibody response to intramuscular or subcutaneous vaccination. American Journal of Kidney Diseases 1998;32(6):1041-5.

[31]   Redfield RR, Innis BL, Scott RM, Cannon HG, Bancroft WH. Clinical Evaluation of Low-Dose Intradermally Administered Hepatitis B Virus Vaccine. JAMA 1985 December 13, 1985;254(22):3203-6.

[32]   Warrell MJ, Suntharasamai P, Sinhaseni A, Phanfung R, Vincent-Falquet JC, Bunnag D, et al. An economical regimen of human diploid cell strain anti-rabies vaccine for post-exposure prophylaxis. Lancet 1983;322(8345):301-4.

[33]   Mitragotri S. Current status and future prospects of needle-free liquid jet injectors. Nat Rev Drug Discov 2006:543-8.

[34]   PATH. Intradermal delivery of vaccines: a review of the literature and the potential for development for use in low- and middle-income countries. Seattle: Program for Appropriate Technology in Health (PATH), 2009.

[35]   Leroux-Roels I, Vets E, Freese R, Seiberling M, Weber F, Salamand C, et al. Seasonal influenza vaccine delivered by intradermal microinjection: A randomised controlled safety and immunogenicity trial in adults. Vaccine 2008;26(51):6614-9.

[36]   Holland D, Booy R, De Looze F, Eizenberg P, McDonald J, Karrasch J, et al. Intradermal Influenza Vaccine Administered Using a New Microinjection System Produces Superior Immunogenicity in Elderly Adults: A Randomized Controlled Trial. J Infect Dis 2008;198(5):650-8.

[37]   Bernard KW, Mallonee J, Wright JC, Reid FL, Makintubee S, Parker RA, et al. Preexposure immunization with intradermal human diploid cell rabies vaccine. Risks and benefits of primary and booster vaccination. JAMA 1987;257(8):1059-63.

[38]   Chen W, Gluud C. Vaccines for preventing hepatitis B in health-care workers. Cochrane Database of Systematic Reviews 2005(4).

[39]   Sangaré L, Manhart L, Zehrung D, Wang CC. Intradermal hepatitis B vaccination: A systematic review and meta-analysis. Vaccine 2009;27(12):1777-86.

[40]   Mohammed AJ, AlAwaidy S, Bawikar S, Kurup PJ, Elamir E, Shaban MMA, et al. Fractional Doses of Inactivated Poliovirus Vaccine in Oman. The New England Journal of Medicine 2010;362(25):2351-9.

[41]   Resik S, Tejeda A, Mas Lago P, Diaz M, Carmenates A, Sarmiento L, et al. Randomized Controlled Clinical Trial of Fractional Doses of Inactivated Poliovirus Vaccine Administered Intradermally by Needle-Free Device in Cuba. Journal of Infectious Diseases 2010 May 1, 2010;201(9):1344-52.

[42]   Hickling JK, Jones KR, Friede M, Zehrung D, Chen D, Kristensen D. Intradermal delivery of vaccines: potential benefits and current challenges. Bulletin of the World Health Organization 2011;89:221-6.

[43]   Etchart N, Hennino A, Friede M, Dahel K, Dupouy M, Goujon-Henry C, et al. Safety and efficacy of transcutaneous vaccination using a patch with the live-attenuated measles vaccine in humans. Vaccine 2007;25(39-40):6891-9.

[44]   Kendall M. Engineering of needle-free physical methods to target epidermal cells for DNA vaccination. Vaccine 2006;24(21):4651-6.

[45]   WHO. WHO recommendations on rabies post-exposure treatment and the correct technique of intradermal immunization against rabies. WHO/EMS/ZOO/966.

[46]   Kim Y-C, Jarrahian C, Zehrung D, Mitragotri S, Prausnitz MR. Delivery systems for intradermal vaccination. Current Topics in Microbiology and Immunology 2012(351):77-112.

[47]   Kersten G, Hirschberg H. Needle-free vaccine delivery. Expert Opinion on Drug Delivery 2007;4(5):459-74.

[48]   Kersten G, Hirschberg H. Antigen delivery systems. Expert Rev Vaccines 2004;3(4):453-62.

[49]   O'Hagan DT, Rappuoli R. Novel Approaches to Vaccine Delivery. Pharmaceutical Research 2004;21(9):1519-30.

[50]   Glenn GM, Taylor DN, Li X, Frankel S, Montemarano A, Alving CR. Transcutaneous immunization: A human vaccine delivery strategy using a patch. Nature Medicine 2000;6(12):1403-6.

[51]   Glenn G, Kenney R, Plotkin SA. Mass Vaccination: Solutions in the Skin. Mass Vaccination: Global Aspects — Progress and Obstacles: Springer Berlin Heidelberg, 2006: 247-68.

[52]   Zhang L, Nolan E, Kreitschitz S, Rabussay DP. Enhanced delivery of naked DNA to the skin by non-invasive in vivo electroporation. Biochimica et Biophysica Acta 2002;1572(1):1-9.

[53]   Tezel A, Paliwal S, Shen Z, Mitragotri S. Low-frequency ultrasound as a transcutaneous immunization adjuvant. Vaccine 2005;23(29):3800-7.

[54]   Bramson J, Dayball K, Evelegh C, Wan YH, Page D, Smith A. Enabling topical immunization via microporation: a novel method for pain-free and needle-free delivery of adenovirus-based vaccines. Gene Ther 2003;10(3):251-60.

[55]   Choi MJ, Zhai H, Löffler H, Dreher F, Maibach HI. Effect of Tape Stripping on Percutaneous Penetration and Topical Vaccination. Exogenous Dermatology 2003;2(5):262-9.

[56]   Frerichs DM, Ellingsworth LR, Frech SA, Flyer DC, Villar CP, Yu J, et al. Controlled, single-step, stratum corneum disruption as a pretreatment for immunization via a patch. Vaccine 2008;26(22):2782-7.

[57]   Peachman KK, Rao M, Alving CR. Immunization with DNA through the skin. Methods 2003;31(3):232-42.

[58]   Dean HJ, Chen D. Epidermal powder immunization against influenza. Vaccine 2004;23(5):681-6.

[59]   EMA. ANNEX I: Summary of product characteristics. Available at http://wwwemaeuropaeu/docs/de_DE/document_library/EPAR_-_Summary_for_the_public/human/000957/WC500033848pdf Accessed: 28 April 2011.

[60]   Choi MJ, Maibach HI. Topical Vaccination of DNA Antigens: Topical Delivery of DNA Antigens. Skin Pharmacol Appl Skin Physiol 2003;16(5):271-82.

[61]   Laurent PE, Bonnet S, Alchas P, Regolini P, Mikszta JA, Pettis R, et al. Evaluation of the clinical performance of a new intradermal vaccine administration technique and associated delivery system. Vaccine 2007;25(52):8833-42.

[62]   Flynn PM, Shenep JL, Mao L, Crawford R, Williams BF, Williams BG. Influence of Needle Gauge in Mantoux Skin Testing. Chest 1994;106(5):1463–5.

[63]   Roth A, Sodemann M, Jensen H, Poulsen A, Gustafson P, Gomes J, et al. Vaccination technique, PPD reaction and BCG scarring in a cohort of children born in Guinea-Bissau 2000-2002. Vaccine 2005;23(30):3991-8.

[64]   Bricks LF. Percutaneous or intradermal BCG vaccine? J Pediatr (Rio J) 2004;80(2):93-8.

[65]   Laurent A, Mistretta F, Bottigioli D, Dahel K, Goujon C, Nicolas JF, et al. Echographic measurement of skin thickness in adults by high frequency ultrasound to assess the appropriate microneedle length for intradermal delivery of vaccines. Vaccine 2007;25(34):6423-30.

[66]   Arnou R, Icardi G, De Decker M, Ambrozaitis A, Kazek M-P, Weber F, et al. Intradermal influenza vaccine for older adults: A randomized controlled multicenter phase III study. Vaccine 2009;27(52):7304-12.

[67]   Alarcon JB, Hartley AW, Harvey NG, Mikszta JA. Preclinical Evaluation of Microneedle Technology for Intradermal Delivery of Influenza Vaccines. Clinincal and Vaccine Immunology 2007 April 1, 2007;14(4):375-81.

[68]   Mikszta JA, Dekker JP, III, Harvey NG, Dean CH, Brittingham JM, Huang J, et al. Microneedle-Based Intradermal Delivery of the Anthrax Recombinant Protective Antigen Vaccine. Infect Immun 2006;74(12):6806-10.

[69]   Van Damme P, Oosterhuis-Kafeja F, Van der Wielen M, Almagor Y, Sharon O, Levin Y. Safety and efficacy of a novel microneedle device for dose sparing intradermal influenza vaccination in healthy adults. Vaccine 2009;27(3):454-9.

[70]   Paccalin M, Weinberger B, Nicolas JF, Van Damme P, Mégard Y. The intradermal vaccination route - an attractive opportunity for influenza vaccination in the elderly. European Geriatric Medicine 2010;1(2):82-7.

[71]   Duggan ST. Intanza 15µg Intradermal Seasonal Influenza Vaccine in Older Adults (Aged 60 Years): Profile Report. Bio Drugs 2010;24:407-9.

[72]   van den Berg JH, Nuijen B, Beijnen JH, Vincent A, van Tinteren H, Kluge Jr, et al. Optimization of Intradermal Vaccination by DNA Tattooing in Human Skin. Hum Gene Ther 2009;20(3):181-9.

[73]   Ciernik IF, Krayenbühl BH, Carbone DP. Puncture-Mediated Gene Transfer to the Skin. Hum Gene Ther 1996;7(8):893-9.

[74]   Bins AD, Jorritsma A, Wolkers MC, Hung C-F, Wu TC, Schumacher TNM, et al. A rapid and potent DNA vaccination strategy defined by in vivo monitoring of antigen expression. Nature Medicine 2005;11(8):899-904.

[75]   Pokorná D, Poláková I, Kindlová M, Dusková M, Ludvíková V, Gabriel P, et al. Vaccination with human papillomavirus type 16-derived peptides using a tattoo device. Vaccine 2009;27(27):3519-29.

[76]   Pokorna D, Rubio I, Muller M. DNA-vaccination via tattooing induces stronger humoral and cellular immune responses than intramuscular delivery supported by molecular adjuvants. Genet Vaccines Ther 2008;6(1):4.

[77]   Quaak SGL, den Berg JHv, Oosterhuis K, Beijnen JH, Haanen JBAG, Nuijen B. DNA tattoo vaccination: Effect on plasmid purity and transfection efficiency of different topoisoforms. Journal of Controlled Release 2009;139(2):153-9.

[78]   McAllister DV, Wang PM, Davis SP, Park J-H, Canatella PJ, Allen MG, et al. Microfabricated needles for transdermal delivery of macromolecules and nanoparticles: Fabrication methods and transport studies. Proc Natl Acad Sci U S A 2003 November 25, 2003;100(24):13755-60.

[79]   Wang PM, Cornwell M, Hill J, Prausnitz MR. Precise Microinjection into Skin Using Hollow Microneedles. J Invest Dermatol 2006;126(5):1080-7.

[80]   Daugimont L, Baron N, Vandermeulen G, Pavselj N, Miklavcic D, Jullien M-C, et al. Hollow Microneedle Arrays for Intradermal Drug Delivery and DNA Electroporation. J Membr Biol 2010;236(1):117-25.

[81]   Prausnitz MR. Microneedles for transdermal drug delivery. Advanced Drug Delivery Reviews 2004;56(5):581-7.

[82]   Baxter J, Mitragotri S. Needle-free liquid jet injections: mechanisms and applications. Expert Rev Med Devices 2006;3(5):565-74.

[83]   Michinaka Y, Mitragotri S. Delivery of polymeric particles into skin using needle-free liquid jet injectors. Journal of Controlled Release 2011;In Press, Uncorrected Proof.

[84]   Benedek K, Walker E, Doshier LA, Stout R. Studies on the use of needle-free injection device on proteins. J Chromatogr A 2005;1079(1-2):397-407.

[85]   Kim Y-C, Quan F-S, Compans RW, Kang S-M, Prausnitz MR. Formulation of Microneedles Coated with Influenza Virus-like Particle Vaccine. AAPS PharmSciTech 2010.

[86]   Park J-H, Allen M, Prausnitz M. Polymer Microneedles for Controlled-Release Drug Delivery. Pharmaceutical Research 2006;23(5):1008-19.

[87]   Miyano T, Tobinaga Y, Kanno T, Matsuzaki Y, Takeda H, Wakui M, et al. Sugar Micro Needles as Transdermic Drug Delivery System. Biomedical Microdevices 2005;7(3):185-8.

[88]   Kolli C, Banga A. Characterization of Solid Maltose Microneedles and their Use for Transdermal Delivery. Pharmaceutical Research 2008;25(1):104-13.

[89]   Ito Y, Hagiwara E, Saeki A, Sugioka N, Takada K. Feasibility of microneedles for percutaneous absorption of insulin. Eur J Pharm Sci 2006;29(1):82-8.

[90]   Klein TM, Wolf ED, Wu R, Sanford JC. High-velocity microprojectiles for delivering nucleic acids into living cells. Nature 1987;327(6117):70-3.

[91]   Fuller DH, Loudon P, Schmaljohn C. Preclinical and clinical progress of particle-mediated DNA vaccines for infectious diseases. Methods 2006;40(1):86-97.

[92]   Bellhouse BJ SD, Greenford JC. Needleless syringe using supersonic gas flow for particle delivery. 1999.

[93]   Roberts LK, Barr LJ, Fuller DH, McMahon CW, Leese PT, Jones S. Clinical safety and efficacy of a powdered Hepatitis B nucleic acid vaccine delivered to the epidermis by a commercial prototype device. Vaccine 2005;23(40):4867-78.

[94]   Kendall MAF, Quinlan NJ, Thorpe SJ, Ainsworth RW, Bellhouse BJ. Measurements of the gas and particle flow within a converging-diverging nozzle for high speed powdered vaccine and drug delivery. Exp Fluids 2004;37(1):128-36.

[95]   Kendall MAF. The delivery of particulate vaccines and drugs to human skin with a practical, hand-held shock tube-based system. Shock Waves 2002;12(1):23-30.

[96]   Liu Y, Truong N, Kendall M, Bellhouse B. Characteristics of a micro-biolistic system for murine immunological studies. Biomedical Microdevices 2007;9(4):465-74.

[97]   Liu Y, Costigan G, Bellhouse BJ. Swirling effects on the performance of the micro-particle acceleration and penetration: parametric studies. Powder Technology 2008;183(2):189-95.

[98]   Liu Y. Utilization of the venturi effect to introduce micro-particles for epidermal vaccination. Med Eng Phys 2007;29(3):390-7.

[99]   Liu Y, Costigan G, Bellhouse BJ. Performance studies of a conical nozzle designed for the macromolecular skin delivery. Journal of Drug Targeting 2008;16(3):206-12.

[100]   Mantoux C. L'intradermo-reaction a la tuberculine et son interpretation clinique. Presse Medicale 1910;18(10-3).

[101]   Rubin BA. Pronged vaccinating and testing needle. 1965.

[102]   Kravitz H. A simplified technique for vaccination against smallpox. Pediatrics 1961;27(2):219-26.

[103]   Griffith AH, Kinsley BJ, Anderson DJ. A comparison between multiple puncture and intradermal methods of BCG vaccination. Tubercle 1963;44(3):372-7.

[104]   de La Rocque F, Cohen R, Vie Le Sage F, Bocquet A, Boucherat M, Levy Bruhl D. Enquête sur les pratiques actuelles et futures du vaccin contre la tuberculose auprès des pédiatres et généralistes en France. Archives de Pédiatrie 2005;12(11):1665-9.

[105]   Gupta J, Park SS, Bondy B, Felner EI, Prausnitz MR. Infusion pressure and pain during microneedle injection into skin of human subjects. Biomaterials 2011;32(28):6823-31.

[106]   Seidenari S, Pagnoni A, di Nardo AD, Giannetti A. Echographic Evaluation with Image Analysis of Normal Skin: Variations according to Age and Sex. Skin Pharmacol 1994;7(4):201-9.

[107]   Van Damme P, Arnou R, Kafeja F, Fiquet A, Richard P, Thomas S, et al. Evaluation of non-inferiority of intradermal versus adjuvanted seasonal influenza vaccine using two serological techniques: a randomised comparative study. BMC Infectious Diseases 2010;10(1):134.

[108]   Laurent PE, Bourhy H, Fantino M, Alchas P, Mikszta JA. Safety and efficacy of novel dermal and epidermal microneedle delivery systems for rabies vaccination in healthy adults. Vaccine 2010;28(36):5850-6.

[109]   FDA.   [cited   18th   October   2011];   Available   from: http://www.accessdata.fda.gov/SCRIPTs/cdrh/devicesatfda/index.cfm?db=pmn&id=K092746

[110]   Kim Y-C, Ouan F-S, Yoo DG, Compans RW, Kang SM, Prausnitz MR. Enhanced Memory Responses to Seasonal H1N1 Influenza Vaccination of the Skin with the Use of Vaccine-Coated Microneedles. Chicago, IL, ETATS-UNIS: University of Chicago Press, 2010.

[111]   Mikszta JA, Alarcon JB, Brittingham JM, Sutter DE, Pettis RJ, Harvey NG. Improved genetic immunization via micromechanical disruption of skin-barrier function and targeted epidermal delivery. Nature Medicine 2002;8(4):415-9.

[112]   Kaushik S, Hord AH, Denson DD, McAllister DV, Smitra S, Allen MG, et al. Lack of Pain Associated with Microfabricated Microneedles. Anesthesia and Analgesia 2000;92:502-4.

[113]   Gill H, Prausnitz M. Coating Formulations for Microneedles. Pharmaceutical Research 2007;24(7):1369-80.

[114]   Quan F-S, Kim Y-C, Compans RW, Prausnitz MR, Kang S-M. Dose sparing enabled by skin immunization with influenza virus-like particle vaccine using microneedles. J Control Release 2010;In Press, Accepted Manuscript.

[115]   Matriano JA, Cormier M, Johnson J, Young WA, Buttery M, Nyam K, et al. Macroflux® Microprojection Array Patch Technology: A New and Efficient Approach for Intracutaneous Immunization. Pharmaceutical Research 2002;19(1):63-70.

[116]   Cormier M, Johnson B, Ameri M, Nyam K, Libiran L, Zhang DD, et al. Transdermal delivery of desmopressin using a coated microneedle array patch system. Journal of Controlled Release 2004;97(3):503-11.

[117]   Kendall M, Rishworth S, Carter F, Mitchell T. Effects of Relative Humidity and Ambient Temperature on the Ballistic Delivery of Micro-Particles to Excised Porcine Skin. Journal of Investigative Dermatology 2004;122(3):739-46.

[118]   Hiraishi Y, Nandakumar S, Choi S-O, Lee JW, Kim Y-C, Posey JE, et al. Bacillus Calmette-Guérin vaccination using a microneedle patch. Vaccine 2011;29(14):2626-36.

[119]   Lee K, Lee CY, Jung H. Dissolving microneedles for transdermal drug administration prepared by stepwise controlled drawing of maltose. Biomaterials 2011;32(11):3134-40.

[120]   Ito Y, Kashiwara S, Fukushima K, Takada K. Two-layered dissolving microneedles for percutaneous delivery of sumatriptan in rats. Drug Development and Industrial Pharmacy 2011:1-7.

[121]   Martanto W, Davis S, Holiday N, Wang J, Gill H, Prausnitz M. Transdermal Delivery of Insulin Using Microneedles in Vivo. Pharmaceutical Research 2004;21(6):947-52.

[122]   Gill HS, Denson DD, Burris BA, Prausnitz MR. Effect of Microneedle Design on Pain in Human Volunteers. Clinical Journal of Pain 2008;24(7):585-94.

[123]   Davis SP, Martanto W, Allen MG, Prausnitz MR. Hollow metal microneedles for insulin delivery to diabetic rats. IEEE Trans Biomed Eng 2005;52(5):909-15.

[124]   Widera G, Johnson J, Kim L, Libiran L, Nyam K, Daddona PE, et al. Effect of delivery parameters on immunization to ovalbumin following intracutaneous administration by a coated microneedle array patch system. Vaccine 2006;24(10):1653-64.

[125]   Bal SM, Slütter B, Jiskoot W, Bouwstra JA. Small is beautiful: N-trimethyl chitosan-ovalbumin conjugates for microneedle-based transcutaneous immunisation. Vaccine 2011;29(23):4025-32.

[126]   Pearton M, Kang S-M, Song J-M, Kim Y-C, Quan F-S, Anstey A, et al. Influenza virus-like particles coated onto microneedles can elicit stimulatory effects on Langerhans cells in human skin. Vaccine 2010;28(37):6104-13.

[127]   Oh J-H, Park H-H, Do K-Y, Han M, Hyun D-H, Kim C-G, et al. Influence of the delivery systems using a microneedle array on the permeation of a hydrophilic molecule, calcein. Eur J Pharm Biopharm 2008;69(3):1040-5.

[128]   Lee JW, Park J-H, Prausnitz MR. Dissolving microneedles for transdermal drug delivery. Biomaterials 2008;29(13):2113-24.

[129]   Park J-H, Choi S-O, Seo S, Choy YB, Prausnitz MR. A microneedle roller for transdermal drug delivery. Eur J Pharm Biopharm 2010;In Press, Corrected Proof.

[130]   Lee JW, Choi S-O, Felner EI, Prausnitz MR. Dissolving Microneedle Patch for Transdermal Delivery of Human Growth Hormone. Small 2011;7(4):531-9.

[131]   Raphael AP, Prow TW, Crichton ML, Chen X, Fernando GJP, Kendall MAF. Targeted, Needle-Free Vaccinations in Skin using Multilayered, Densely-Packed Dissolving Microprojection Arrays. Small 2010;6(16):1785-93.

[132]   Migalska K, Morrow D, Garland M, Thakur R, Woolfson A, Donnelly R. Laser-Engineered Dissolving Microneedle Arrays for Transdermal Macromolecular Drug Delivery. Pharmaceutical Research 2011:1-12.

[133]   Ito Y, Yoshimitsu J-I, Shiroyama K, Sugioka N, Takada K. Self-dissolving microneedles for the percutaneous absorption of EPO in mice. J Drug Target 2006;14(5):255 - 61.

[134]   Park J-H, Allen MG, Prausnitz MR. Biodegradable polymer microneedles: Fabrication, mechanics and transdermal drug delivery. Journal of Controlled Release 2005;104(1):51-66.

[135]   Wu Y, Qiu Y, Zhang S, Qin G, Gao Y. Microneedle-based drug delivery: studies on delivery parameters and biocompatibility. Biomedical Microdevices 2008;10:601-10.

[136]   Chu LY, Choi S-O, Prausnitz MR. Fabrication of dissolving polymer microneedles for controlled drug encapsulation and delivery: Bubble and pedestal microneedle designs. J Pharm Sci 2010;99(10):4228-38.

[137]   Baek C, Han M, Min J, Prausnitz MR, Park J-H, Park J. Local transdermal delivery of phenylephrine to the anal sphincter muscle using microneedles. J Control Release 2011;In Press, Uncorrected Proof.

[138]   Ito Y, Shiroyama K, Yoshimitsu J, Ohashi Y, Sugioka N, Takada K. Pharmacokinetic and pharmacodynamic studies following percutaneous absorption of erythropoietin micropiles to rats. Journal of Controlled Release 2007;121(3):176-80.

[139]   McAllister DV, Henry S, Allen MG, Prausnitz MR. Microfabricated microneedles: a novel approach to transdermal drug delivery. Proc Int Symp Controlled Release Bioact Mater 1998;25th:30-1.

[140]   Andrianov AK, DeCollibus DP, Gillis HA, Henry HK, Marin A, Prausnitz MR, et al. Poly [di (carboxylatophenoxy) phosphazene] is a potent adjuvant for intradermal immunization. Proceedings of the National Academy of Sciences 2009;106(45):18936-41.

[141]   Ding Z, Verbaan FJ, Bivas-Benita M, Bungener L, Huckriede A, van den Berg DJ, et al. Microneedle arrays for the transcutaneous immunization of diphtheria and influenza in BALB/c mice. Journal of Controlled Release 2009;136(1):71-8.

[142]   Gill HS, Soderholm J, Prausnitz MR, Sallberg M. Cutaneous vaccination using microneedles coated with hepatitis C DNA vaccine. Gene Ther 2010;17(6):811-4.

[143]   Cosman F, Lane NE, Bolognese MA, Zanchetta JR, Garcia-Hernandez PA, Sees K, et al. Effect of transdermal teriparatide administration on bone mineral density in postmenopausal women. The Journal of Clinical Endocrinology & Metabolism 2010;95(1):151-8.

[144]   Mikszta JA, Sullivan VJ, Dean C, Waterston AM, Alarcon JB, Dekker JP, et al. Protective immunization against inhalational anthrax: a comparison of minimally invasive delivery platforms. Journal of Infectious Diseases 2005;191(2):278-88.

[145]   Ito Y, Murakami A, Maeda T, Sugioka N, Takada K. Evaluation of self-dissolving needles containing low molecular weight heparin (LMWH) in rats. Int J Pharm 2008;349(1-2):124-9.

[146]   Davis SP, Landis BJ, Adams ZH, Allen MG, Prausnitz MR. Insertion of microneedles into skin: measurement and prediction of insertion force and needle fracture force. Journal of Biomechanics 2004;37(8):1155-63.

[147]   Kim Y-C, Quan F-S, Yoo D-G, Compans RW, Kang S-M, Prausnitz MR. Improved influenza vaccination in the skin using vaccine coated microneedles. Vaccine 2009;27(49):6932-8.

[148]   McAllister DV, Allen MG, Prausnitz MR. Microfabricated microneedles for gene and drug delivery Annual Review of Biomedical Engineering 2000;2(1):289-313.

[149]   Zahn JD, Talbot NH, Liepmann D, Pisano AP. Microfabricated Polysilicon Microneedles for Minimally Invasive Biomedical Devices. Biomedical Microdevices 2000;2(4):295-303.

[150]   Zahn JD, deshmukh A, Pisano AP, Liepmann D. Continuous On-Chip Micropumping for Microneedle Enhanced Drug Delivery. Biomedical Microdevices 2004;6(3):183-90.

[151]   Sivamani RK, Stoeber B, Wu GC, Zhai H, Liepmann D, Maibach H. Clinical microneedle injection of methyl nicotinate: stratum corneum penetration. Skin Research and Technology 2005;11(2):152-6.

[152]   Sivamani RK, Stoeber B, Liepmann D, Maibach HI. Microneedle penetration and injection past the stratum corneum in humans. Journal of Dermatological Treatment 2009;20(3):156-9.

[153]   Sivamani RK, Liepmann D, Maibach HI. Microneedles and transdermal applications. Expert Opinion on Drug Delivery 2007;4(1):19-25.

[154]   Kim Y-C, Prausnitz M. Enabling skin vaccination using new delivery technologies. Drug Delivery and Translational Research 2011;1(1):7-12.

[155]   Burton S, Ng C-Y, Simmers R, Moeckly C, Brandwein D, Gilbert T, et al. Rapid Intradermal Delivery of Liquid Formulations Using a Hollow Microstructured Array. Pharmaceutical Research 2011;28(1):31-40.

[156]   Gupta J, Gill HS, Andrews SN, Prausnitz MR. Kinetics of skin resealing after insertion of microneedles in human subjects. Journal of Controlled Release 2011;154(2):148-55.

[157]   Kalluri H, Banga AK. Formation and closure of microchannels in skin following microporation. Pharmaceutical research 2011;28(1):82-94.

[158]   Bal SM, Ding Z, Kersten G, Jiskoot W, Bouwstra J. Microneedle-Based Transcutaneous Immunisation in Mice with N-Trimethyl Chitosan Adjuvanted Diphtheria Toxoid Formulations. Pharmaceutical Research 2010;27(9):1837-47.

[159]   Ding Z, Van Riet E, Romeijn S, Kersten G, Jiskoot W, Bouwstra J. Immune Modulation by Adjuvants Combined with Diphtheria Toxoid Administered Topically in BALB/c Mice After Microneedle Array Pretreatment. Pharmaceutical Research 2009;26(7):1635-43.

[160]   Bal SM, Caussin J, Pavel S, Bouwstra JA. In vivo assessment of safety of microneedle arrays in human skin. Eur J Pharm Sci 2008;35(3):193-202.

[161]   Ding Z, Bal S, Romeijn S, Kersten G, Jiskoot W, Bouwstra J. Transcutaneous Immunization Studies in Mice Using Diphtheria Toxoid-Loaded Vesicle Formulations and a Microneedle Array. Pharmaceutical Research 2011;28(1):145-58.

[162]   Harvey A, Kaestner S, Sutter D, Harvey N, Mikszta J, Pettis R. Microneedle-Based Intradermal Delivery Enables Rapid Lymphatic Uptake and Distribution of Protein Drugs. Pharmaceutical Research 2011;28(1):107-16.

[163]   Song J-M, Kim Y-C, Lipatov AS, Pearton M, Davis CT, Yoo D-G, et al. Microneedle Delivery of H5N1 Influenza Virus-Like Particles to the Skin Induces Long-Lasting B- and T-Cell Responses in Mice. Clininical and Vaccine Immunology 2010 September 1, 2010;17(9):1381-9.

[164]   Quan F-S, Kim Y-C, Vunnava A, Yoo D-G, Song J-M, Prausnitz MR, et al. Intradermal vaccination with influenza virus-like particles by using microneedles induces protection superior to that with intramuscular immunization. Journal of Virology 2010;84(15):7760-9.

[165]   Giudice EL, Campbell JD. Needle-free vaccine delivery. Advanced Drug Delivery Reviews 2006;58(1):68-89.

[166]   Baxter J, Mitragotri S. Jet-induced skin puncture and its impact on needle-free jet injections: Experimental studies and a predictive model. Journal of Controlled Release 2005;106(3):361-73.

[167]   Haar H-P. Transdermales Injektionssystem. EP application 0853952A1. July 1998.

[168]   Lell P. Needleless injection device with pyrotechnical drive. WO application 01/97880A2. December 2001.

[169]   Chase CCL, Daniels CS, Garcia R. Needle-free injection technology in swine: Progress toward vaccine efficacy and pork quality. J Swine Health Prod 2008;16(5):254-61.

[170]   Grosenbaugh D, Leard T, Pardo M. Comparison of the safety and efficacy of a recombinant feline leukemia virus (FeLV) vaccine delivered transdermally and an inactivated FeLV vaccine delivered subcutaneously. Vet Ther 2004; 5:258–62.

[171]   Schramm-Baxter J, Mitragotri S. Needle-free jet injections: dependence of jet penetration and dispersion in the skin on jet power. Journal of Controlled Release 2004;97(3):527-35.

[172]   Jackson LA, Austin G, Chen RT, Stout R, DeStefano F, Gorse GJ, et al. Safety and immunogenicity of varying dosages of trivalent inactivated influenza vaccine administered by needle-free jet injectors. Vaccine 2001;19(32):4703-9.

[173]   Cui Z, Baizer L, Mumper RJ. Intradermal immunization with novel plasmid DNA-coated nanoparticles via a needle-free injection device. J Biotechnol 2003;102(2):105-15.

[174]   Williams J, Fox-Leyva L, Christensen C, Fisher D, Schlicting E, Snowball M, et al. Hepatitis A vaccine administration: comparison between jet-injector and needle injection. Vaccine 2000;18(18):1939-43.

[175]   Lemon SM, Scott RM, Bancroft WH. Subcutaneous administration of inactivated hepatitis B vaccine by automatic jet injection. Journal of Medical Virology 1983;12(2):129-36.

[176]   Babiuk S, Baca-Estrada M, Babiuk LA, Ewen C, Foldvari M. Cutaneous vaccination: the skin as an immunologically active tissue and the challenge of antigen delivery. Journal of Controlled Release 2000;66(2-3):199-214.

[177]   Aguiar JC, Hedstrom RC, Rogers WO, Charoenvit Y, Sacci JB, Lanar DE, et al. Enhancement of the immune response in rabbits to a malaria DNA vaccine by immunization with a needle-free jet device. Vaccine 2001;20(1-2):275-80.

[178]   Sarno MJ, Blase E, Galindo N, Ramirez R, Schirmer CL, Trujillo-Juarez DF. Clinical immunogenicity of measles, mumps and rubella vaccine delivered by the Injex jet injector: comparison with standard syringe injection. Pediatr Infect Dis J 2000;19(9):839-42.

[179]   Gorres JP, Lager KM, Kong W-P, Royals M, Todd J-P, Vincent AL, et al. DNA Vaccination Elicits Protective Immune Responses against Pandemic and Classic Swine Influenza Viruses in Pigs. Clinincal and Vaccine Immunology 2011 September 14, 2011:CVI.05171-11.

[180]   FDA.   [cited   20th   October   2011];   Available   from: http://www.accessdata.fda.gov/scripts/cdrh/cfdocs/cfpmn/pmn.cfm?ID=36147

[181]   Burkoth TL, Bellhouse BJ, Hewson G, Longridge DJ, Muddle AG, Sarphie DF. Transdermal and transmucosal powdered drug delivery. Critical Reviews in Therapeutic Drug Carier Systems 1999;16(4):331-84.

[182]   Chen D, Endres RL, Erickson CA, Weis KF, McGregor MW, Kawaoka Y, et al. Epidermal immunization by a needle-free powder delivery technology: Immunogenicity of influenza vaccine and protection in mice. Nature Medicine 2000;6(10):1187-90.

[183]   Roy MJ, Wu MS, Barr LJ, Fuller JT, Tussey LG, Speller S, et al. Induction of antigen-specific CD8+ T cells, T helper cells, and protective levels of antibody in humans by particle-mediated administration of a hepatitis B virus DNA vaccine. Vaccine 2000;19(7-8):764-78.

[184]   Quinlan NJ, Kendall MAF, Bellhouse BJ, Ainsworth RW. Investigations of gas and particle dynamics in first generation needle-free drug delivery devices. Shock Waves 2001;10(6):395-404.

[185]   Liu Y, Kendall M. Numerical simulation of heat transfer from a transonic jet impinging on skin for needle-free powdered drug and vaccine delivery. Proceedings of the Institution of Mechanical Engineers, Part C: J Mech Eng Sci 2004;218(11):1373-83.

[186]   Liu Y, Mark AFK. Optimization of a jet-propelled particle injection system for the uniform transdermal delivery of drug/vaccine. Biotechnology and Bioengineering 2007;97(5):1300-8.

[187]   Kendall MAF. Needle-Free Vaccine Injection. Drug Delivery: Springer Berlin Heidelberg, 2010: 193-219.

[188]   Liu Y, Kendall M. Numerical analysis of gas and micro-particle interactions in a hand-held shock-tube device. Biomedical Microdevices 2006;8(4):341-51.

[189]   Chen D, Weis KF, Chu Q, Erickson C, Endres R, Lively CR, et al. Epidermal Powder Immunization Induces both Cytotoxic T-Lymphocyte and Antibody Responses to Protein Antigens of Influenza and Hepatitis B Viruses. Journal of Virology 2001;75(23):11630-40.

[190]   Dean HJ. Epidermal delivery of protein and DNA vaccines. Expert Opinion on Drug Delivery 2005;2(2):227-36.

[191]   Lesinski GB, Smithson SL, Srivastava N, Chen D, Widera G, Westerink MAJ. A DNA vaccine encoding a peptide mimic of Streptococcus pneumoniae serotype 4 capsular polysaccharide induces specific anti-carbohydrate antibodies in Balb/c mice. Vaccine 2001;19(13-14):1717-26.

[192]   Raju PA, McSloy N, Truong NK, Kendall MAF. Assessment of epidermal cell viability by near infrared multi-photon microscopy following ballistic delivery of gold micro-particles. Vaccine 2006;24(21):4644-7.

[193]   Tacket CO, Roy MJ, Widera G, Swain WF, Broome S, Edelman R. Phase 1 safety and immune response studies of a DNA vaccine encoding hepatitis B surface antigen delivered by a gene delivery device. Vaccine 1999;17(22):2826-9.

[194]   Lebre F, Borchard G, de Lima M, Borges O. Progress Towards a Needle-Free Hepatitis B Vaccine. Pharmaceutical Research 2010:1-27.

[195]   Eisenbraun MD, Fuller DH, Haynes JR. Examination of parameters affecting the elicitation of humoral immune responses by particle bombardment-mediated genetic immunization. DNA and Cell Biology 1993;12(9):791-7.

[196]   Rottinghaus ST, Poland GA, Jacobson RM, Barr LJ, Roy MJ. Hepatitis B DNA vaccine induces protective antibody responses in human non-responders to conventional vaccination. Vaccine 2003;21(31):4604-8.

[197]   Drape RJ, Macklin MD, Barr LJ, Jones S, Haynes JR, Dean HJ. Epidermal DNA vaccine for influenza is immunogenic in humans. Vaccine 2006;24(21):4475-81.

[198]   Schiffter H, Condliffe J, Vonhoff S. Spray-freeze-drying of nanosuspensions: the manufacture of insulin particles for needle-free ballistic powder delivery. Journal of the Royal Society Interface 2010:-.

[199]   Maa Y-F, Ameri M, Shu C, Payne LG, Chen D. Influenza vaccine powder formulation development: spray-freeze-drying and stability evaluation. Journal of Pharmaceutical Sciences 2004;93(7):1912-23.

[200]   Maa Y-F, Ameri M, Shu C, Zuleger CL, Che J, Osorio JE, et al. Hepatitis-B Surface Antigen (HBsAg) Powder Formulation: Process and Stability Assessment. Current Drug Delivery 2007;4:57-67.

[201]   Maa Y-F, Zhao L, Payne LG, Chen D. Stabilization of alum-adjuvanted vaccine dry powder formulations: Mechanism and application. Journal of Pharmaceutical Sciences 2002;92(2):319-32.

[202]   Sonner C, Maa Y-F, Lee G. Spray-freeze-drying for protein powder preparation: Particle characterization and a case study with trypsinogen stability. Journal of Pharmaceutical Sciences 2002;91(10):2122-39.

[203]   Rochelle C, Lee G. Dextran or hydroxyethyl starch in spray-freeze-dried trehalose/mannitol microparticles intended as ballistic particulate carriers for proteins. Journal of Pharmaceutical Sciences 2007;96(9):2296-309.

[204]   Hardy MP, Kendall MAF. Mucosal deformation from an impinging transonic gas jet and the ballistic impact of microparticles. Physics in Medicine and Biology 2005;50(19):4567.

[205]   Chen D, Erickson CA, Endres RL, Periwal SB, Chu Q, Shu C, et al. Adjuvantation of epidermal powder immunization. Vaccine 2001;19(20-22):2908-17.

[206]   Truong N, Liu Y, Kendall M. Gas and Particle Dynamics of a Contoured Shock Tube for Pre-clinical Microparticle Drug Delivery. Shock Waves 2006;15(3):149-64.

[207]   Chen D, Zuleger C, Chu Q, Maa YF, Osorio J, Payne LG. Epidermal Powder Immunization with a Recombinant HIV gp120 Targets Langerhans Cells and Induces Enhanced Immune Responses. AIDS Research and Human Retroviruses 2002;18(10):715-22.

[208]   Osorio JE, Zuleger CL, Burger M, Chu Q, Payne LG, Chen D. Immune responses to hepatitis B surface antigen following epidermal powder immunization. Immunology and Cell Biology 2003;81(1):52-8.

[209]   Abdul-Fattah A, Truong-Le V, Yee L, Pan E, Ao Y, Kalonia D, et al. Drying-Induced Variations in Physico-Chemical Properties of Amorphous Pharmaceuticals and Their Impact on Stability II: Stability of a Vaccine. Pharmaceutical Research 2007;24(4):715-27.

[210]   Amorij JP, Huckriede A, Wilschut J, Frijlink H, Hinrichs W. Development of Stable Influenza Vaccine Powder Formulations: Challenges and Possibilities. Pharmaceutical Research 2008;25(6):1256-73.

3   LIST OF FIGURES

4   LIST OF TABLES

PRESENTATIONS AND PUBLICATIONS ASSOCIATED WITH THIS THESIS

ARTICLES

Etzl EE, Winter G, Engert J
Toward intradermal vaccination: preparation of powder formulations by collapse freeze-drying. Pharmaceutical Development and Technology 2014;19(2):213-22.

Kis EE, Winter G, Myschik J
Devices for Intradermal Vaccination. Vaccine 2012;30(3):523-38

PATENTS

Winter G, Engert J, Etzl E, Lell P
Fixation of vaccine formulations on devices for epidermal immunisation by oily adjuvants. Europäische Patentanmeldung EP13 185 631.2, 23.09.2013

POSTER PRESENTATIONS

Kis EE, Deng Y, Lell P, Winter G, Myschik J
Intradermal ballistic delivery – New approaches to deliver powdered particles using a surrogate accelerator. AAPS Annual Meeting and Exposition, Washington D.C., USA, October 2011

Kis EE, Pott J, Winter G, Myschik J
Evaluation of a cryo-mill for the production of particles for intradermal ballistic delivery. AAPS Annual Meeting and Exposition, Washington D.C., USA, October 2011

Kis EE, Deng Y, Lell P, Winter G, Myschik J
Novel intradermal vaccination devices using ballistic delivery of powder particles. Forum Life Science 2011, Technische Universität München – Garching, March 23rd -24th, 2011

Kis EE, Winter G, Myschik J
Can collapse freeze-drying provide high density protein sugar particles for ballistic powder injection? 8th Central European Symposium on Pharmaceutical Technology (CESPT), Graz, Austria, September 2010

Kis EE, Lell P, Winter G, Myschik J
Evaluation of a surrogate apparatus for epidermal ballistic powder injection. 7th World Meeting on Pharmaceutics, Biopharmaceutics and Pharmaceutical Technology, Valletta, Malta, March 2010